SIMILARITY ANALYSIS OF TURBULENT BOUNDARY LAYERS

By

Luciano Castillo

A dissertation submitted to the
Faculty of the Graduate School of the
State University of New York at Buffalo
in partial fulfillment of the requirements
for the degree of
Doctor of Philosophy
February 1997

To my mother Carmen Cabrera and my father Luciano Castillo which are my examples of love and hard work

ACKNOWLEDGEMENTS

First I would like to express my appreciation to Dr. Nancy Woodruff, Dr. Charles Carr from The Office of Public Affairs and to Mr. Drexel Giney from the School of Engineering and Applied Science from which my fellowship for minority students came. Without this source it would have been impossible to conduct this research.

I would like to deeply thank my mentor Professor William K. George, Jr. for his unlimited support throught the entire investigation. Not only did he advise me and guide me in the proper direction, but he really cared for me like a son. He has become very special person to me. I am very PROUD to be his student and I will never forget this part of my life.

I would like to also especially thank the following faculty: Dr. D. Taulbee, Dr. C.Liu, Dr. C.Bloebaum, Dr. J. Felske, Dr. R. Mayne, and Dr. W. Rae for sharing their knowledge with me during many courses and conversations. Dr. W. Rae, in particular, was like a second advisor and always was willing to talk to me with the best intention to help. Also Dr. J. Sonnenmeier has been a great help since I arrived at the Turbulence Research Laboratory. The department secretaries, Ms. Eileen Graber, Ms. Kay Ward and Ms. Bonnie Boskat, provided help whenever I needed them. Mr. Scoot Woodword really assisted me with his great ability to solve problems, as did Mr Martin Wosnik and Asad Sardar; I thank them for their help.

I would like to thank my parents for always having been there for me and for really giving me their unconditional love. My mother has really made so many sacrifies for all her children and friends. My grandfathers, Francisco A. Castillo and Sixto Cabrera, taught me how to work very hard and to enjoy life. My very special friend, Jose Angel Feliciano, was a victim of drunk driving; your memory is alway with

me. My mother-in-law, Solmerina Aponte, really help us financially so many times, I really appreciated. I would like thank also our friends, Martin Higuera and especially Michael Peppers, who was always there for my family while I have been away.

And finally I want to thank the woman that since I first saw here in January 1, 1990 has made my live very different, **my beloved wife Zoraida**. Thank you so much for giving me four children: Bayrex, Yarey, Yetzia and my dear Khalil. You really brough a lot a happines to my life. **I really love you** and part of you is always with me.

ABSTRACT

A new theory for boundary layers and for pipe and channels flows is proposed based on similarity analyses of the inner and outer boundary layer equations in the limit as the Reynolds number goes to infinity. Using the scales obtained from the equations of motion, Near Asymptotics is used to determine the functions describing the flow in the overlap region at finite values of the Reynolds number.

It was found that for boundary layers the flow is characterized by two velocity scales in the overlap region (U_∞ and u_*), and not one as in classical theory. As a result, the functions for the mean velocity and Reynolds stress profiles are power law functions and not logarithmic. A clear distinction between boundary layer (inhomogeneous flows) and channel and pipe flows (homogeneous in streamwise direction) is made. Channel and pipe flows scale with a single velocity in inner and outer variables (u_*). Thus, the profiles in the overlap region are logarithmic as in the classical theory, but the coefficients are Reynolds number dependent.

In the case of boundary layers with pressure gradient, a new definition for equilibrium flows is obtained from the similarity of the outer equations. There is only one new parameter (Π) needed as long as the boundary layer is not near separation. From this new definition, many flows are indeed equilibrium flows, contrary to the traditional belief that equilibrium flows are difficult to achieve in experiments. In addition, the new theory works for non-equilibrium flows which are evolving equilibrium boundary layers. For boundary layers at separation the velocity and length scales are consistent with Stratford variables.

It will be shown that the present theory is consistent with experimental data available. The present theory provides a composite mean velocity profile for the entire boundary layer at finite Reynolds number; therefore, the boundary layer parameters

(displacement thickness, momentum thickness, and shape factors) can be determined. Since a composite profile for the boundary layers is known, the Reynolds shear stress can be obtained by integrating the boundary layer equations.

Contents

List of Figures

Chapter 1

Introduction

There are few problems in turbulence which have been more generally regarded as solved than the scaling laws for turbulent boundary layer flows. The classical analysis is based on the assumption that there are two regions where universal scaling exists which is independent of Reynolds number: one is near the wall (Law of the Wall) and the other is a velocity deficit region covering most of the flow. A small summary of the classical work will be given in this chapter, and the goal of this dissertation will be stated.

1.1 The Boundary Layer Equations

The equations of motion and boundary conditions for a pressure gradient turbulent boundary layer (with constant properties) at high Reynolds number are well-known to be given by (Tennekes and Lumley 1972)

$$U\frac{\partial U}{\partial x} + V\frac{\partial U}{\partial y} = -\frac{1}{\rho}\frac{dP_\infty}{dx} + \frac{\partial}{\partial y}\left[- < uv > +\nu\frac{\partial U}{\partial y}\right] \tag{1.1}$$

where $U \rightarrow U_\infty$ as $y \rightarrow \infty$ and $U = 0$ at $y = 0$. For fully developed pipe and channel flows, the inertia terms (left hand side of the equation) are zero due to the homogeneity in the streamwise direction. The viscous stresses are negligible over most of the flow. As a result the equations and boundary conditions appropriate to a turbulent boundary layer at high Reynolds number over this outer region are given by

$$U\frac{\partial U}{\partial x} + V\frac{\partial U}{\partial y} = -\frac{1}{\rho}\frac{dP_\infty}{dx} + \frac{\partial}{\partial y}\left[- < uv >\right] \tag{1.2}$$

where $U \rightarrow U_\infty$ as $y \rightarrow \infty$. For the zero pressure gradient boundary layer the pressure term vanishes identically.

Near the wall the viscous terms reappear, but the convection terms vanish identically in the limit of infinite Reynolds number, so the inner equation reduces to

$$0 = -\frac{1}{\rho}\frac{dP_\infty}{dx} + \frac{\partial}{\partial y}\left[\nu\frac{\partial U}{\partial y} - < uv >\right] \tag{1.3}$$

This can be integrated to yield

$$u_*^2 = -\frac{y}{\rho}\frac{dP_\infty}{dx} - < uv > +\nu\frac{\partial U}{\partial y} \tag{1.4}$$

where u_* is the friction velocity and $U = 0$ at $y = 0$. Note that the pressure gradient in inner variables has been retained for now, but in fact it also vanishes exactly (at least away from separation) in the limit of infinite Reynolds number to yield,

$$u_*^2 = - < uv > +\nu\frac{\partial U}{\partial y} \tag{1.5}$$

It is clear that in the limit of infinite Reynolds number, the total stress is constant across the inner layer (but only in this limit) even for boundary layers with pressure gradient, and hence its name "the Constant Stress Layer". It should be noted that the appearance of u_* in equation 1.4 and equation 1.5 does not imply that the wall

shear stress is an independent parameter (like ν or U_∞). It enters the problem only because it measures the forcing of the inner flow by the outer; or alternatively, it can be viewed as measuring the retarding effect of the inner flow on the outer. Thus u_* is a *dependent* parameter which must be determined by matching solutions of the inner and outer equations. It is also interesting to note that the inner layer occurs only because of the necessity of including viscosity in the problem so that the no-slip condition can be met. The outer layer, on the other hand, is dominated by inertia and the effects of viscosity enter only through the matching to the inner layer. Thus the outer flow is effectively governed by inviscid equations, *but with viscous-dominated inner boundary conditions set by the inner layer.*

The flow outside of the boundary layer is given governed by Euler's equation given by,

$$U_\infty \frac{dU_\infty}{dx} = -\frac{1}{\rho}\frac{dP_\infty}{dx} \tag{1.6}$$

Obviously this equation is trivially satisfied if there is not a pressure gradient and if U_∞ is a constant.

Equations 1.3– 1.5 also describe a turbulent fully developed channel flow driven entirely by the pressure gradient. Here the convection terms vanish everywhere because of the streamwise homogeneity (i.e., the flow is independent of x). Thus the inner equation are the same as the boundary layer *in the limit*, but the outer equations are different.

1.2 The Velocity Scaling Laws for the Zero Pressure Gradient

It has been customary to seek solutions to the governing equations which depend only on the streamwise coordinate through a local length scale $\delta(x)$, v. Monin and Yaglom 1971. Thus, for the mean velocity over a flat plate

$$U = U(y, \delta, U_\infty, u_*, \nu) \tag{1.7}$$

The dependence of u_* on the other parameters can be expressed from dimensional considerations as a friction law by

$$\frac{u_*}{U_\infty} = \sqrt{\frac{c_f}{2}} = g\left(\delta^+\right) \tag{1.8}$$

where

$$\delta^+ \equiv \frac{u_*\delta}{\nu} = \delta^+ \tag{1.9}$$

and

$$c_f \equiv \frac{\tau_w}{\frac{1}{2}\rho U_\infty^2} = 2\frac{u_*^2}{U_\infty^2} \tag{1.10}$$

Application of the Buckingham Pi theorem to the velocity itself yields a number of possibilities, *all of which describe the variation of the velocity across the entire boundary layer.* Among them are:

$$\frac{U}{u_*} = f_i\left(\frac{yu_*}{\nu}, \delta^+\right) \tag{1.11}$$

$$\frac{U - U_\infty}{U_\infty} = f_o\left(\frac{y}{\delta}, \delta^+\right) \tag{1.12}$$

$$\frac{U - U_\infty}{u_*} = F_o\left(\frac{y}{\delta}, \delta^+\right) \tag{1.13}$$

Note that since u_*/U_∞ and δ^+ (or $u_*\delta/\nu$) are related by equation 1.8, only the later need be retained in equations 1.11 – 1.13. (This fact seems to have escaped Monin and Yaglom 1971 who dismiss a separate dependence on u_*/U_∞, only on empirical grounds.)

In the limit as $\delta^+ \to \infty$, equation 1.11 becomes asymptotically independent of δ and U_∞ and thus can at most describe a limited region very close to the wall, i.e.,

$$\frac{U}{u_*} = f_{i\infty}\left[\frac{yu_*}{\nu}\right] \tag{1.14}$$

This is, of course, the familiar *Law of the Wall* expressed in inner variables as originally proposed by Prandtl (1932).

A similar limiting argument for f_o and F_o yields two quite different candidates for an outer profile; namely,

$$\frac{U - U_\infty}{U_\infty} = f_{o\infty}\left(\frac{y}{\delta}\right) \tag{1.15}$$

and

$$\frac{U - U_\infty}{u_*} = F_{o\infty}\left(\frac{y}{\delta}\right) \tag{1.16}$$

Both cannot, of course, be Reynolds number independent (and finite) in the limit if the ratio u_*/U_∞ continues to vary (as the Millikan/Clauser theory requires, see below).

The first form given by equation 1.15 has only been fleetingly considered by the fluid dynamics community, and discarded in favor of the second alternative. Millikan, following Von Karman for example, appears to have considered it briefly, noted that it leads to self-preserving power law solutions of the outer equations, and then dismissed these solutions as interpolation formulas. The second was proposed by Von Karman 1930 for boundary layers following a similar a similar proposal by Pannel and Stanton 1914 for channel and pipe flows. It has become the classical velocity deficit law.

Clauser (1954) (see also Hinze 1975) plotted only the highest and lowest Reynolds number data of Schultz-Grunow 1941 in deficit form and concluded that the collapse using equation 1.15 was not as satisfactory as that obtained using the deficit form of equation 1.16. There is no evidence that either of these conclusions has been refuted, or even questioned (even though there were numerous other Schultz-Grunow profiles at intermediate Reynolds numbers which showed a clear trend with increasing Reynolds number toward the highest).

1.3 Von Karman's Log Profile

Assuming the Boussinesq 1877,1896 eddy viscosity model, the Reynolds stress can be expressed in a similar form as a Newtonian viscous stress by,

$$\tau_t = -\rho\overline{uv} = \nu_t \frac{dU}{dy} \tag{1.17}$$

where ν_t is the eddy viscosity. Prandtl's 1925 mixing length hypothesis suggests a physical model for ν_t as,

$$\nu_t = \rho l^2 \Big|\frac{dU}{dy}\Big| \tag{1.18}$$

It follows that the turbulent shear stress is given by,

$$\tau_t = \rho l^2 \Big|\frac{dU}{dy}\Big|\frac{dU}{dy} \tag{1.19}$$

where l is the mixing length which has to be chosen. The goal now is to find a model for the mixing length l so that the Reynolds stress is known.

Von Karman assumed that the mixing length satisfies the following equation,

$$l = \kappa \Big|\frac{dU/dy}{d^2U/dy^2}\Big| \tag{1.20}$$

where the mixing length (l) is independent of the magnitude of the velocity and is function of the velocity distribution only. κ is presumed to be a universal constant which is the same for all turbulent flows and independent of Reynolds number. Using the previous results he showed that the turbulent shear stress is given as

$$\tau_t = \kappa^2 \frac{(dU/dy)^4}{(d^2U/dy^2)^2} \tag{1.21}$$

Now Von Karman 1930 assumed that the shear stress varied linearly. (Note that for fully developed flow in a channel or pipe, dP_∞/dx = constant. In the limit as Reynolds number goes to infinity, if the pressure term is retained in the inner boundary layer equation it is clear that turbulent stress distribution away from the wall is linear.) Then by combining equation 1.19 and equation 1.21 he showed that the relation between the stress at the wall and the turbulent stress reduces to,

$$\frac{\tau_w}{\rho}\frac{y}{h} = \kappa^2 \frac{(dU/dy)^4}{(d^2U/dy^2)^2} \tag{1.22}$$

where $\tau_w/\rho = u_*^2$ is the friction velocity. Integrating this equation twice and applying the corresponding boundary conditions at the center of channel and at the wall, it follows that

$$\frac{U_{max} - U}{u_*} = -\frac{1}{\kappa}\Big[ln\Big(1 - \sqrt{\frac{y}{h}}\Big) + \sqrt{\frac{y}{h}}\Big] \tag{1.23}$$

which is in fact the logarithmic profile, although not the one usually cited.

1.4 Prandtl's Velocity Distribution

Prandtl 1932 was able to derive a logarithmic function for the law of the wall by using two fundamental assumptions: First, the mixing length is proportional to the distance from the wall; therefore,

$$l = \kappa y \tag{1.24}$$

Second, instead of assuming the stress to vary linearly as Von Karman did, he assumed that a constant stress layer existed near the wall. (From equation 1.5 it is clear that there is indeed a constant stress layer even for boundary layers with pressure gradient. So Prandtl's assumption is better than Von Karman's assumption of a linear stress layer.) Equation 1.24 and equation 1.19, together with the constant stress layer assumption yield,

$$u_*^2 = \kappa^2 y^2 \Big[\frac{dU}{dy}\Big]^2 \tag{1.25}$$

Taking the square root of the above equation and integrating with respect to y, it is clear that a logarithmic function is derived and given as,

$$\frac{U}{u_*} = \frac{1}{\kappa} ln(y^+) + B_i \tag{1.26}$$

where $y^+ = yu_*/\nu$. This is the form of the log law usually cited.

1.5 Millikan's Asymptotic Matching for Channels

Millikan 1938 took a completely different approach and began with the proposed inner and outer scaling laws of equation 1.14 and equation 1.16, but for channels where $U_\infty = U_c$, the centerline velocity, and $\delta = R$, the channel half-width. He argued that in the limit as Reynolds number goes to infinity there must be an overlap region (or matched layer) if $y^+ \to \infty$ and $\overline{y} \to 0$ simultaneously such that both solutions inner and outer velocity profiles exist in a common region. (This procedure is known now as asymptotic matching, and it was the first example of it.) Then he matched the velocity derivatives in this limit and concluded that

$$y^+ \frac{f_i(y^+)}{dy^+} = \overline{y} \frac{f_o(\overline{y})}{d\overline{y}} = \kappa \tag{1.27}$$

where κ was a universal constant, the von Karman constant.

It follows immediately that the velocity profiles are logarithmic and given by,

$$f_i(y^+) = \frac{U}{u_*} = \frac{1}{\kappa} ln(y^+) + B_i \tag{1.28}$$

$$f_o(\overline{y}) = \frac{U - U_c}{u_*} = \frac{1}{\kappa} ln(\overline{y}) + B_o \tag{1.29}$$

By matching the velocities themselves he obtained a friction law as,

$$\frac{U_c}{u_*} = \frac{1}{\kappa} ln(\frac{hu_*}{\nu}) + (B_i - B_o) \tag{1.30}$$

where U_c is the centerline velocity and h is the width of channel. Note that B_i and B_o are also supposed to be constant, although in practice all the "constants" change with Reynolds number.

Note that these functions are obtained in the limit, and are based on the assumptions of a single velocity scale (u_*) and that an overlap exists. Also, note that the turbulence community uses these solutions to describe velocity profiles in an overlap region at finite Reynolds number.

1.6 Clauser's Equilibrium Boundary Layers

Clauser 1954, following Millikan 1938, matched the 'inner' scaling of equation 1.14 to the 'outer' scaling of equation 1.16 in the limit of infinite Reynolds number to obtain the familiar *inertial sublayer* profiles for boundary layers as

$$\frac{U}{u_*} = \frac{1}{\kappa} ln(y^+) + B_i \tag{1.31}$$

$$\frac{U - U_\infty}{u_*} = \frac{1}{\kappa} ln(\overline{y}) + B_o \tag{1.32}$$

and a friction law given by

$$\frac{U_\infty}{u_*} = \sqrt{\frac{2}{c_f}} = \frac{1}{\kappa} ln\delta^+ + (B_i - B_o) \tag{1.33}$$

where κ, B_i, and B_o are presumed to be universal constants. Note that in the limit as $\delta^+ \rightarrow \infty$, equation 1.33 requires that $u_*/U_\infty \rightarrow 0$ for finite values of the constants.

By substituting the inner and outer scaling laws into the defining integrals for the displacement and momentum thicknesses, Clauser 1954 showed that

$$\frac{\delta_*}{\delta} = A_1 \frac{u_*}{U_\infty} \tag{1.34}$$

$$\frac{\theta}{\delta} = A_1 \frac{u_*}{U_\infty} \left[1 - A_2 \frac{u_*}{U_\infty}\right] \tag{1.35}$$

where A_1 and A_2 should be universal constants which can be evaluated from integrals of the outer velocity profile function. It follows that the shape factor is given by the asymptotic relation

$$H = \frac{\delta_*}{\theta} = 1 - A_2 \frac{u_*}{U_\infty} \tag{1.36}$$

Thus as $\delta^+ \rightarrow \infty$ and $u_*/U_\infty \rightarrow 0$ (if it in fact does), $H \rightarrow 1$. Note that similar results are obtained for the pressure gradient boundary layer.

The underlying assumption of the above matching is that the inner and outer scaling laws used for the profiles, in fact, have a region of common validity (or overlap) in the limit as $\delta^+ \rightarrow \infty$. Long and Chen (1981) have remarked that it is indeed strange that the matched layer between one characterized by inertia and another characterized by viscosity does not depend on both inertia and viscosity, but only inertia (hence the term 'inertial sublayer', Tennekes and Lumley 1972). They further suggested that this might be a consequence of improperly matching two layers which did not overlap. The fact that the limiting ratio of the outer length scale δ to both of the commonly used integral length scales, δ_* and θ, is infinite lends considerable

weight to their concern. In particular, this implies that from the perspective of the outer flow, the boundary layer does not exist at all in the limit of infinite Reynolds number. If one imagines approaching this limit along a semi-infinite plate where the boundary layer continues to grow, the outer length scale increases faster than any dynamically significant integral length. This is particularly troubling since δ itself is unspecified by the theory and can not be related to physically measurable length scales except through the degenerate expressions above.

Clauser also extended the theory to include pressure gradient boundary layers. Using "quasi"-similarity considerations, he defined an equilibrium boundary layer as one which satisfied

$$\beta = \frac{\tilde{\delta}}{\rho u_*} \frac{dP_\infty}{dx} = const. \tag{1.37}$$

where $\tilde{\delta}$ is an empirical length scale. He kept the same velocity deficit law; i.e.,

$$\frac{U_\infty - U}{u_*} = f_o(\overline{y}) \tag{1.38}$$

and suggested that theses profiles are self-similar, which means all profiles collapse into a single curve.

Although, Clauser's analysis suggests $\tilde{\delta} = \delta$ (i.e., some observable thickness like δ_{99}), he was forced by his data to use $\tilde{\delta} = \delta_*$. Even so, the results were not spectacular, and Clauser tried with limited success to adjust the pressure gradient in his experiments such that the velocity profiles along the test section agreed with the deficit law given above for β=constant. We shall see later that the problem was that Clauser had adjusted the friction velocity u_* such that all profiles obeyed the log-law in the overlap region. This created erroneous shear stress estimates with the result that the Clauser pressure parameter β computed from them does not remains constant for a given flow, even if it really is.

Clauser's theory for equilibrium boundary layer has been questioned before. Among them: Townsend 1956a,b, 1961, 1976, Rotta 1962, Mellor and Gibson 1966 and Schofield 1980. In spite of the questions and doubts about Clauser equilibrium flows, his 1954 paper remains the key work up to now on boundary layers with pressure gradient.

1.7 Extension of Clauser's Idea

Townsend 1956a,b, 1961, 1976 and Rotta 1962 used the idea of self-preservation which is related to the full similarity considered later in this work. If all profiles are self-preserving, all profiles along the streamwise direction of the flow should collapse as a single curve. The physical reasoning is that in the limit as Reynolds number goes to infinity, the equations of motion should become invariant. This is the idea behind the Asymptotic Invariance Principle described in subsequent chapters. It is also what Clauser was trying to accomplish with his equilibrium boundary layers by forcing u_* to collapse the profiles in deficit form as a single curve.

In brief, Townsend and Rotta assumed that solutions of the following forms exist:

$$U(x,y) = U_\infty + U_{so}(x) f_o(\frac{y}{l_o}) \tag{1.39}$$

$$-\overline{u'v'} = U_{so}^2(x) r_o(\frac{y}{l_o}) \tag{1.40}$$

where U_{so} and l_o are velocity and length scales to be determined from the equations of motions only. Note that these self-preservation forms are very restrictive (as first noted by George 1989) since there is only a single velocity scale for velocity and Reynolds stress and there is no Reynolds number dependence in the functions. (This is quite unlike the kind of similarity proposed later in this work.) By ignoring terms

of order $(u_*/U_\infty)^2$, Townsend showed that the conditions resulting from this special kind of self-preservation analysis are:

$$\frac{u_*}{U_\infty} = const. \tag{1.41}$$

$$\frac{d\delta}{dx} = const. \tag{1.42}$$

with the corollary

$$\beta = \frac{\delta_*}{\rho u_*^2}\frac{dP_\infty}{dx} = const. \tag{1.43}$$

The third condition is the same as Clauser's, but the other two are very different. In particular, $d\delta/dx$=const implies that the boundary layer grows linearly. Thus, δ^+ increases, but u_*/U_∞ remains constant. No one before seems to have noticed the inconsistency with the logarithmic friction law, equation 1.33, which requires $u_*/U_\infty \rightarrow$ constant unless $\kappa \rightarrow \infty$.

Schofield 1981 tried to show that the equilibrium conditions given by Rotta 1962 were true. But as will be shown later, when the range of Reynolds number is limited, it is difficult to notice the variation with Reynolds number in the flow. For instance from the integral boundary layer parameters (i.e., δ_*/δ, θ/δ, and δ_*/θ) and c_f for zero the pressure gradient boundary layers examined later, most of the variation occurs in the range from $465 \leq R_\theta \leq 8,000$. For $R_\theta > 10,000$, the boundary layer seems to grow linearly; but if higher values for R_θ were considered the results will continue to exhibit a significant variation with R_θ. The same will be seem to be true for the pressure gradient boundary layer as well.

Rotta 1962 concluded that the Clauser flows were not in equilibrium because the similarity condition for linear growth rate and constant β were not satisfied. He suggested that the problem was that the Clauser experiment was performed on a smooth wall, and argued that in order to get equilibrium flows the surface roughness

would have to vary linearly in the test section. Therefore, he concluded that Clauser flows were only approximately in equilibrium.

Figure 1.1 shows the Reynolds number based on the boundary layer thickness (R_δ versus R_x of the moderate adverse pressure gradient of Clauser 1954. The data is compared with a linear fit to the experimental data and a quadratic fit. There is no doubt that the boundary layer thickness does not growth linearly, contrary to Schofield 1981, Townsend 1976, 1956a,b, 1961 and Rotta 1962. The same is true for the displacement and momentum thickness data in Figures 1.2 and 1.3 which is the same data that Schofield used to conclude that the boundary layer grows linearly. It is clear that the boundary layer does not growth linearly at finite values of Reynolds number, and it is at most a first order approximation to say that it does.

The second example is the Ludweig and Tillman 1949 data in favorable pressure gradient. Figures 1.4, 1.5 and 1.6 show the boundary layer thickness, displacement thickness and momentum thickness versus R_x respectively. The dashed line is the first order regression, and the line is the second order regression. Again it may appear that the boundary layer grows linearly, but careful analysis indicates otherwise. It is just due to the limited range in Reynolds number of the data (i.e., $1000 \simeq R_\theta \simeq 4000$), unlike the previous case where the variation in Reynolds number was relatively large ($8,031 \leq R_\theta \leq 31,017$).

The third example is the case where the flow moves from one equilibrium state to another. The data of Schubauer and Klebanoff 1947, first with mild favorable pressure gradient, then at strong adverse pressure gradient with eventual separation, is shown in Figure 1.7. This example illustrates very clearly that the flow does not grow linearly at all, even locally.

It is obvious then that the definitions given above by Townsend 1976, 1956a,b

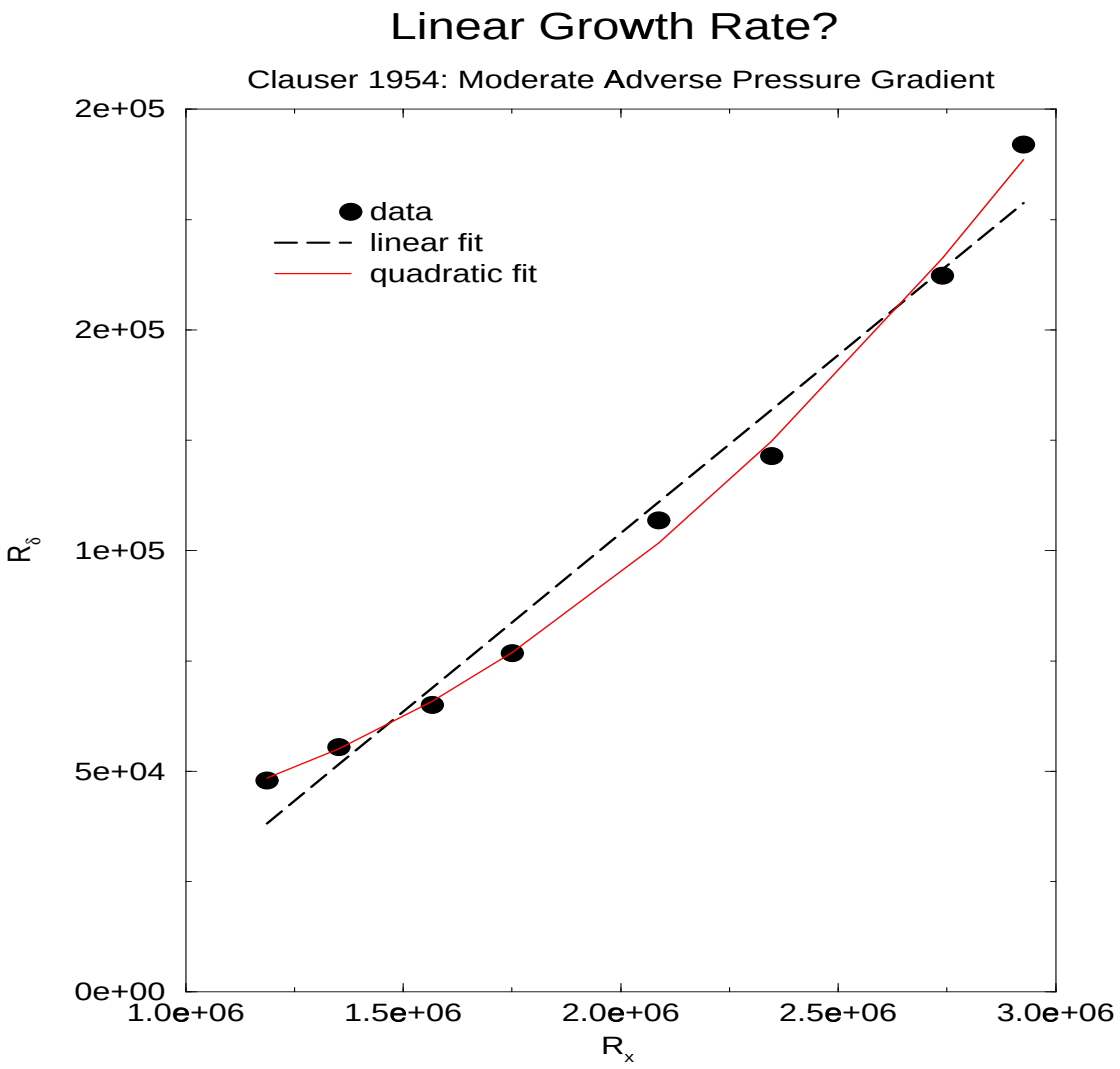

Figure 1.1: The Reynolds number based on the boundary layer thickness (R_δ) versus R_x of the moderate adverse pressure gradient of Clauser 1954.

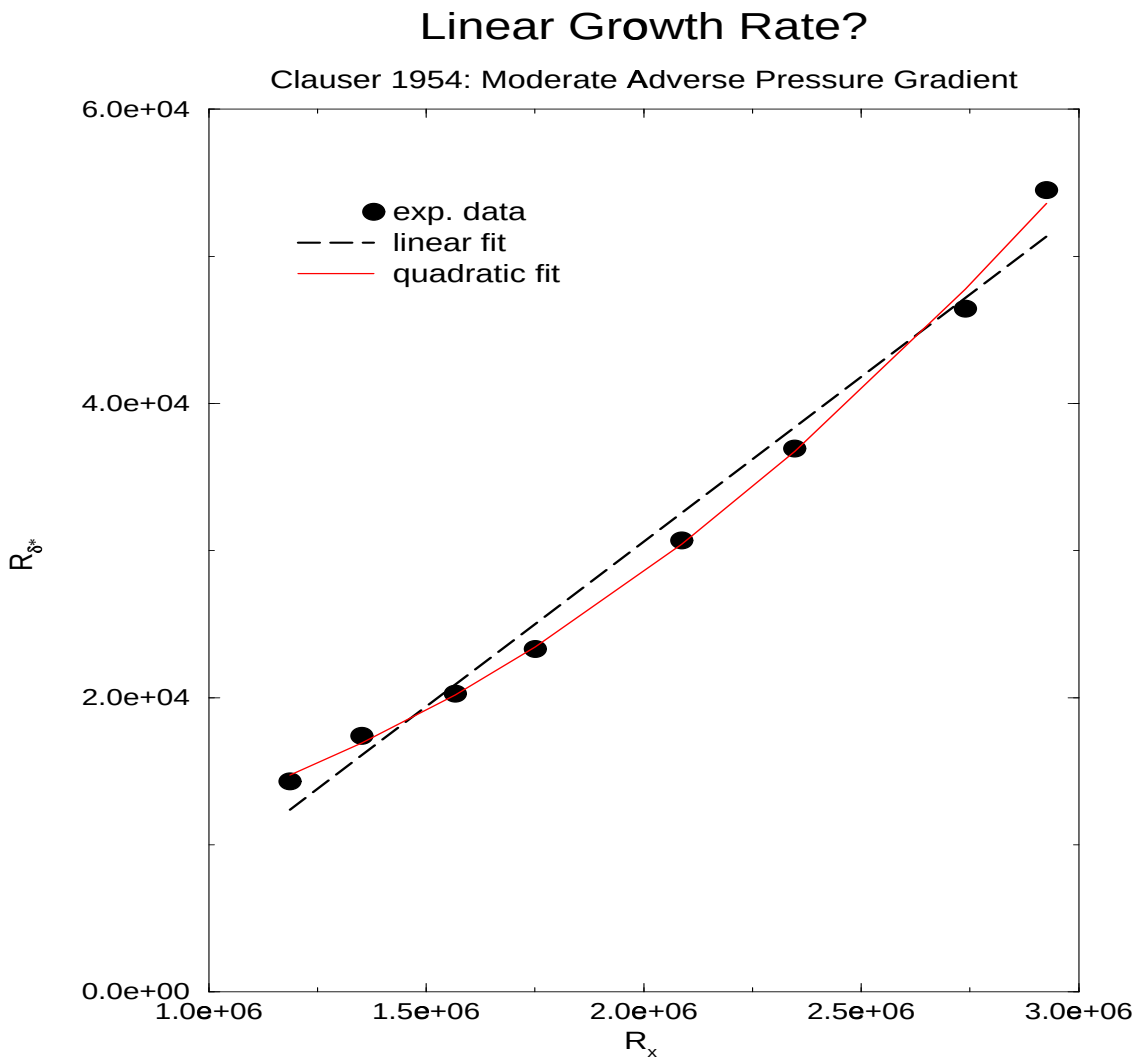

Figure 1.2: The Reynolds number based on displacement thickness (R_{δ_*}) versus R_x of the moderate adverse pressure gradient of Clauser 1954.

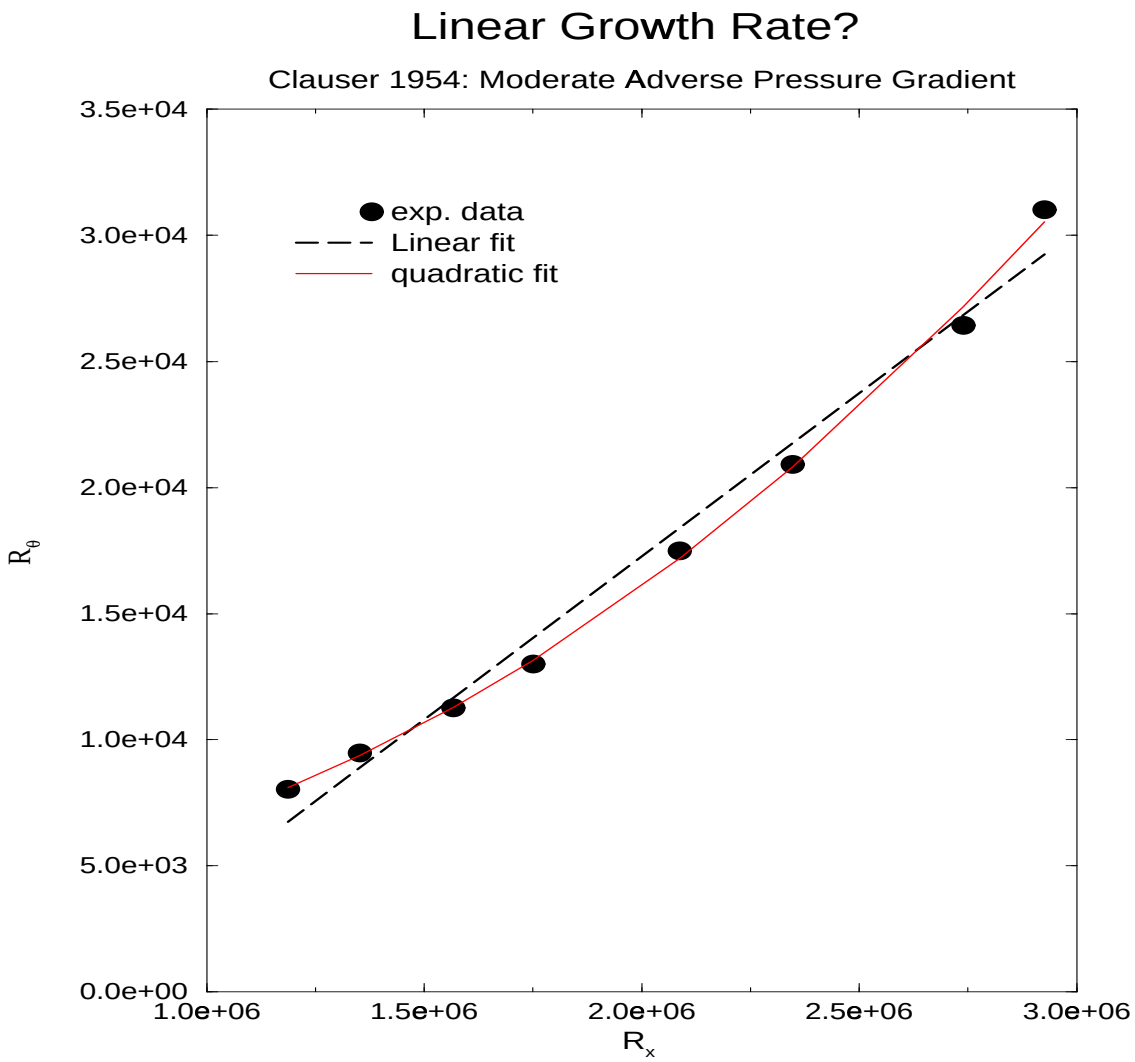

Figure 1.3: The Reynolds number based on momentum thickness (R_θ) versus R_x of the moderate adverse pressure gradient of Clauser 1954.

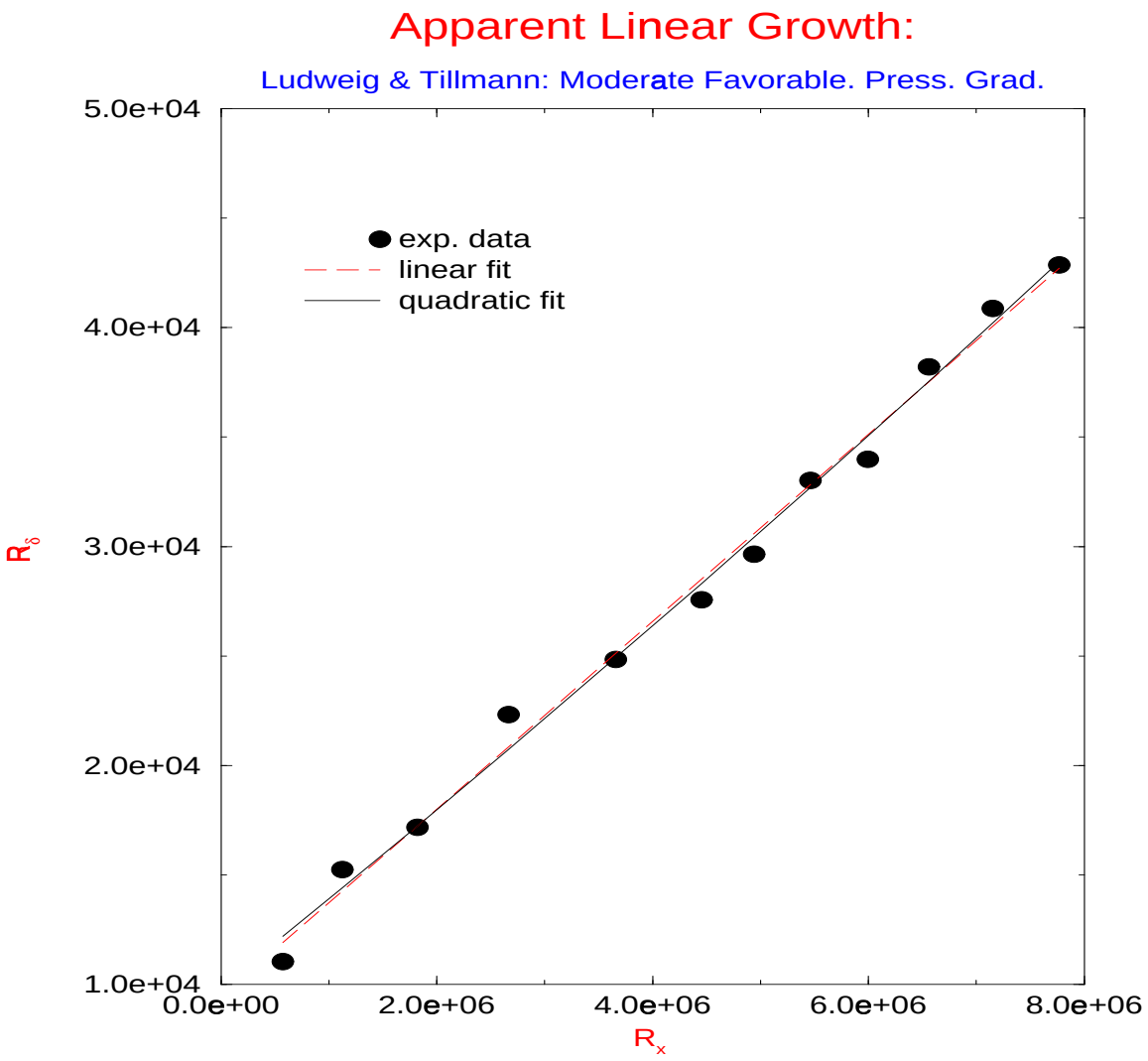

Figure 1.4: The Reynolds number based on the boundary layer thickness (R_δ) versus R_x of the moderate favorable pressure gradient of Ludweig and Tillman 1949.

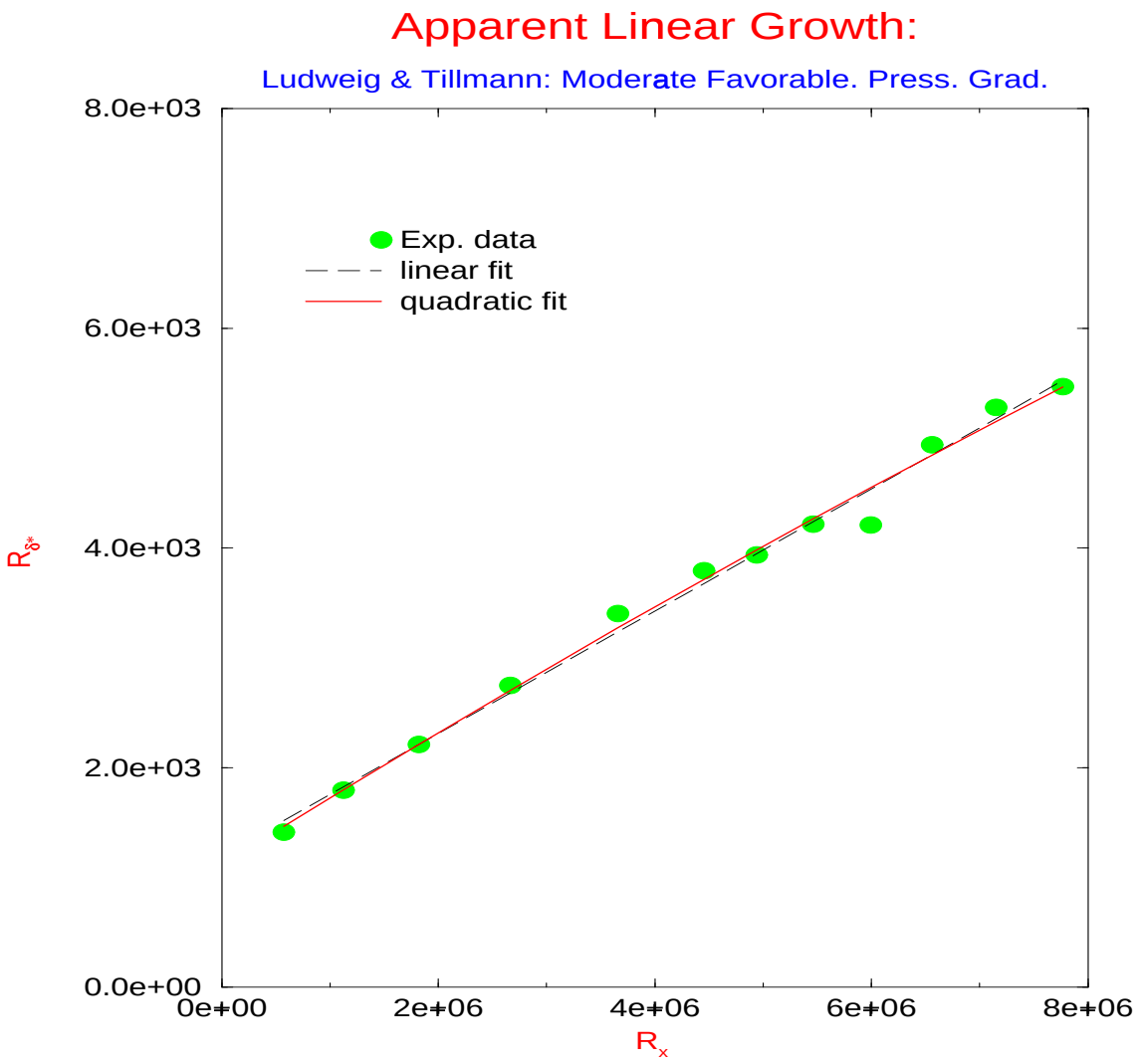

Figure 1.5: The Reynolds number based on displacement thickness (R_{δ_*}) versus R_x of the moderate favorable pressure gradient of Ludweig and Tillman 1949.

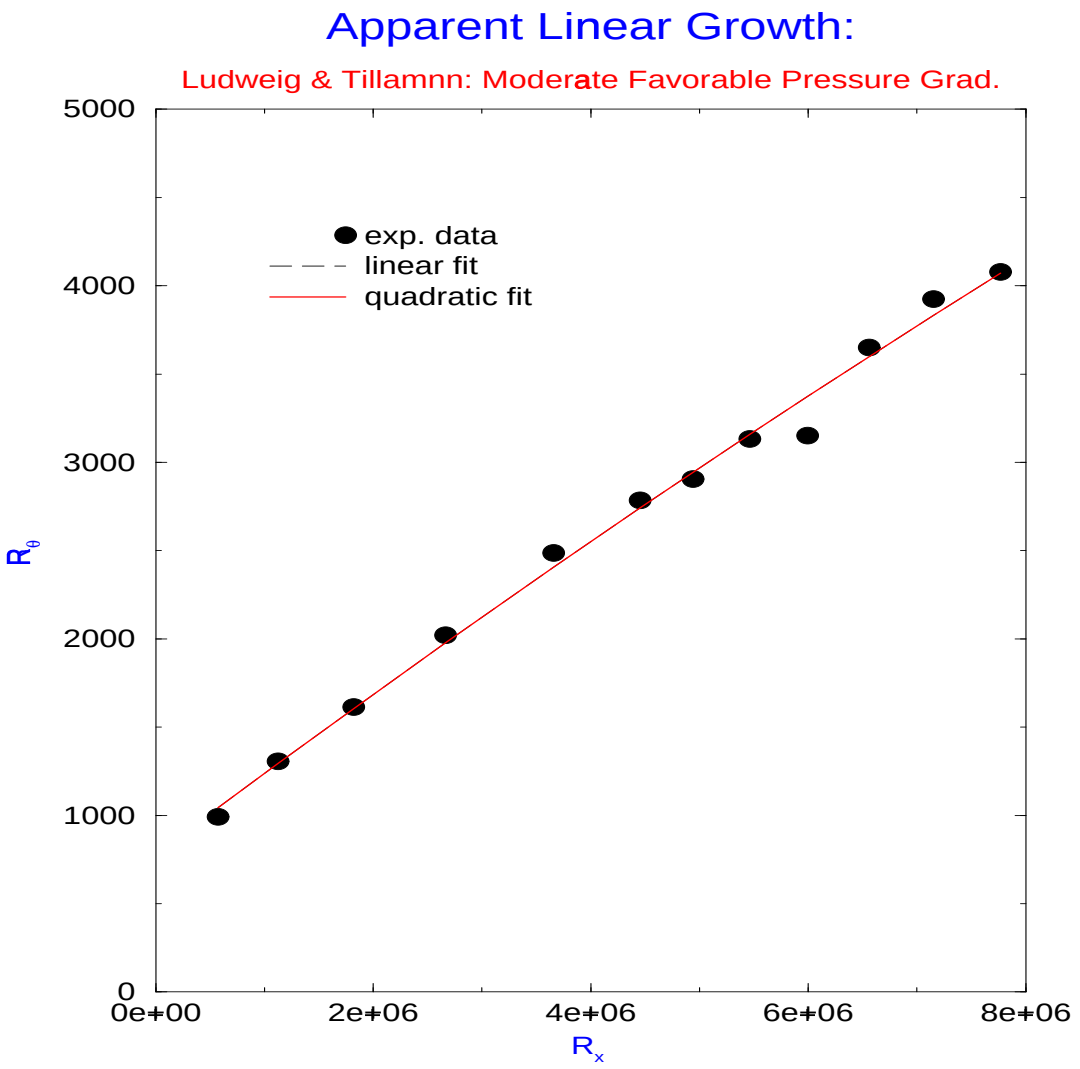

Figure 1.6: The Reynolds number based on momentum thickness (R_θ) versus R_x of the moderate favorable pressure gradient of Ludweig and Tillman 1949.

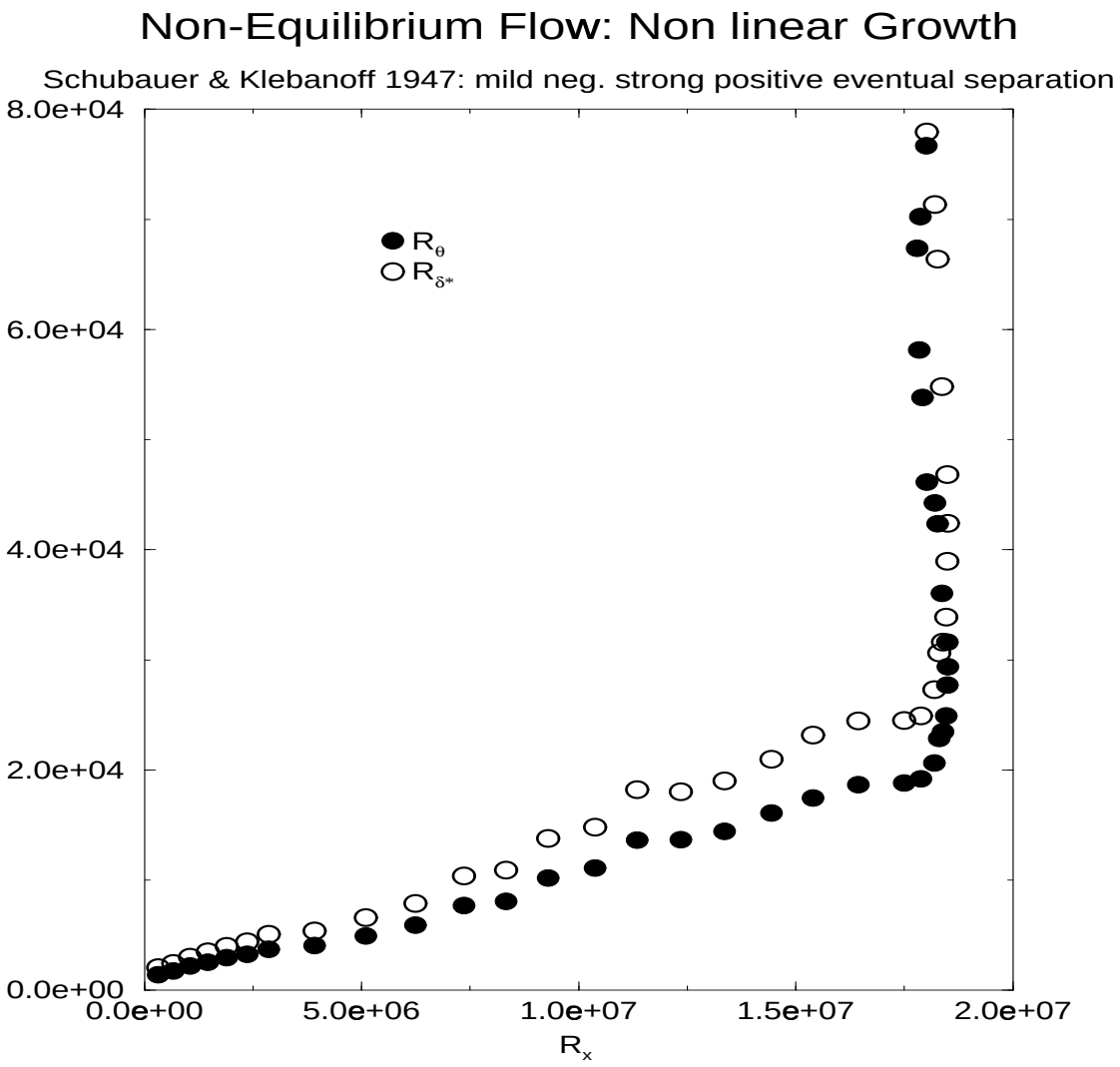

Figure 1.7: Moving Equilibrium Boundary layer: Schubauer and Klebanoff 1947

1961 and Rotta 1962 for both equilibrium and non-equilibrium flows are not quite right. The same data will be reconsidered later in Chapter 4 and shown to be in excellent agreement with the new theory for equilibrium boundary layers proposed here. In fact, it will be shown in chapter 4 that most flows that had been believed to be non-equilibrium are indeed equilibrium flows using the new definition. Thus equilibrium flows are not really very special or very difficult to achieve in experiments. In fact, quite the opposite will be seem to be the case: It is hard not to generate them.

1.8 Coles's Law of the Wake

The well known "Law of the Wake" proposed by Coles (1956) describes the outer flow of the incompressible turbulent boundary layer. It based on the assumption that a universal function, "the log law", exists in the matched layer or overlap region. In inner variables, the "law of the wall" is given as,

$$\frac{U}{u_*} = f(\frac{yu_*}{\nu}) = f(y^+) \tag{1.44}$$

and in outer variables "the deficit law" is given by,

$$\frac{U_\infty - U}{u_*} = g(\frac{y}{\delta}) = g(\overline{y}) \tag{1.45}$$

The functions f and g are given as (Tennekes and Lumley 1972),

$$f(y^+) = \frac{1}{\kappa}\ln(y^+) + C \tag{1.46}$$

and

$$g(\overline{y}) = \frac{1}{\kappa}\ln(\overline{y}) + B \tag{1.47}$$

where κ, C and B are supposed to be "universal constants" and determined empirically. Furthermore, note that these self-preservation solutions (eq. 1.44 and eq. 1.45)

are characterized by a single velocity scale u_* (i.e., the Reynolds stresses and velocity in inner and outer variables should all scale with the friction velocity u_* and the functions should be independent of Reynolds number,v. Townsend 1956). As result, the overlap layer is independent of Reynolds number in the classical theory (Tennekes and Lumley 1972).

Assuming all the above to be true, Coles formulated the "law of the wall-law of the wake" as (Coles 1956),

$$\frac{U}{u_*} = f(y^+) + \frac{\Pi}{\kappa} w(\overline{y}) \tag{1.48}$$

where Π is the profile parameter which is a constant equal to 0.55 for zero pressure gradient turbulent boundary layers, $w(\overline{y})$ is the "universal" wake function given in (Coles 1956) as

$$w(\overline{y}) = 2\sin^2(\frac{\pi}{2}\overline{y}) \tag{1.49}$$

However, there is significant amount of evidence indicating that the overlap region is Reynolds number dependent (Simpson 1970, Blackwelder and Haridonitis 1983, Smith 1994, Erm and Joubert 1991, Klewicki and Falco 1990). In fact Gad-el-Hak and Bandyopadhyay 1994 wrote an intense review showing the problems of the classical theory. For instance, the "universal constants" κ and C have been expressed as function of R_θ for $R_\theta < 6000$ (Simpson 1970). Also, the profile parameter Π is a function of R_θ for $R_\theta < 5000$ in Cebecci and Smith 1974. These are both indications that the boundary layer is dependent on Reynolds number.

The wake can be represented by multiplying equation 1.48 by u_*/U_∞ and subtracting the velocity normalized with U_∞ from the inner solution $f(y^+)$ to obtain,

$$w(\overline{y}) = \frac{U}{U_\infty} - [\frac{u_*}{U_\infty}]f(y^+) \tag{1.50}$$

The data of Purtell et al. 1981 (R_θ from 465 to 5100) and Smith and Walker 1959 (R_θ from 3000 to 50000) can be used to further emphasize the problem with the classical wake. In Figure 1.8, the wake is represented using equation 1.50 with the friction velocity u_* obtained from the viscous sublayer for the low Reynolds number data, since the velocity profile is linear in this region ($U^+ = y^+$). For the high R_θ the friction velocity is obtained from a fit to R_θ vs R_x, from which dR_θ/dRx is obtained and c_f is calculated.[1] Recognize that if the overlap layer is described by a logarithmic function the data should be zero in this region. Clearly, Figures 1.7 and 1.8 do not support the existence of a universal "log law" and "law of the wake" as the turbulence community has believed for more than 40 years. This point will be discussed in more detail in Chapter 3.

Contrary to the procedure used above, u_* is not usually directly determined but is instead obtained by assuming the existence of a universal function with known constants κ and B_i, and using the mean velocity profile (U) and the kinematic viscosity (ν) (Coles 1956). This is known as the Clauser method. In fact, Coles used this method in Coles 1956 to find not just u_*, but to find δ. Thus contrary to popular belief that the classical theory has only three universal parameters κ, B_o and B_i; it has two additional parameters δ and u_* which are adjusted for each profile. This probably explains why most of the flows in Coles 1968 do not satisfy the integral momentum equation.

Figure 1.9 shows the wake (equation 1.50) using the Clauser method value for u_*.

[1] It was shown in George et al. 1992, 1996 and later here that c_f was in good agreement with the measured c_f (using floating element) data of Smith and Walker 1959. In fact, the values of c_f calculated from dR_θ/dR_x were very close to c_f from the low Reynolds number data of Purtell et al. 1981 determined from the viscous sublayer by George et al. 1992.

Although, most of the Reynolds number dependence is removed, the overlap layer and the outer flow still show some Reynolds number dependence. Clearly as suggested by others, the universality of the law of the wall and law of the wake are indeed questionable. Part of the problem may have been that Coles 1956 only considered relatively high Reynolds number data in his analysis, in contrast with the present work where both low and high Reynolds number data are considered simultaneously. Again the use of a limited range of Reynolds number could have led to the conclusion that the overlap layer is independent of Reynolds number.

1.9 Clauser Theory and the Need for a New One

The extension by Clauser (1954), Hama 1954, Coles 1962 and others of Millikan's arguments to boundary layers with pressure gradients, roughness, compressibility and a law of the wake (Coles' wake) all assumed the existence of the log-law. An important reason for this has been the apparent agreement of experimental data with the theoretical results, but as seen in the preceding section there is clearly reason for concern. But there are theoretical objections as well.

There are a number of features of the Millikan/Clauser theory which, if not unsatisfying, are at least interesting. Among them:

- (i) The velocity profile disappears in the limit of infinite Reynolds number (i.e., $U/U_\infty = 1$);
- (ii) The outer length scale is not proportional to any integral length scale, and in fact blows up relative to them as the Reynolds number becomes infinite (i.e., δ/δ_* and $\delta/\theta \to \infty$); and

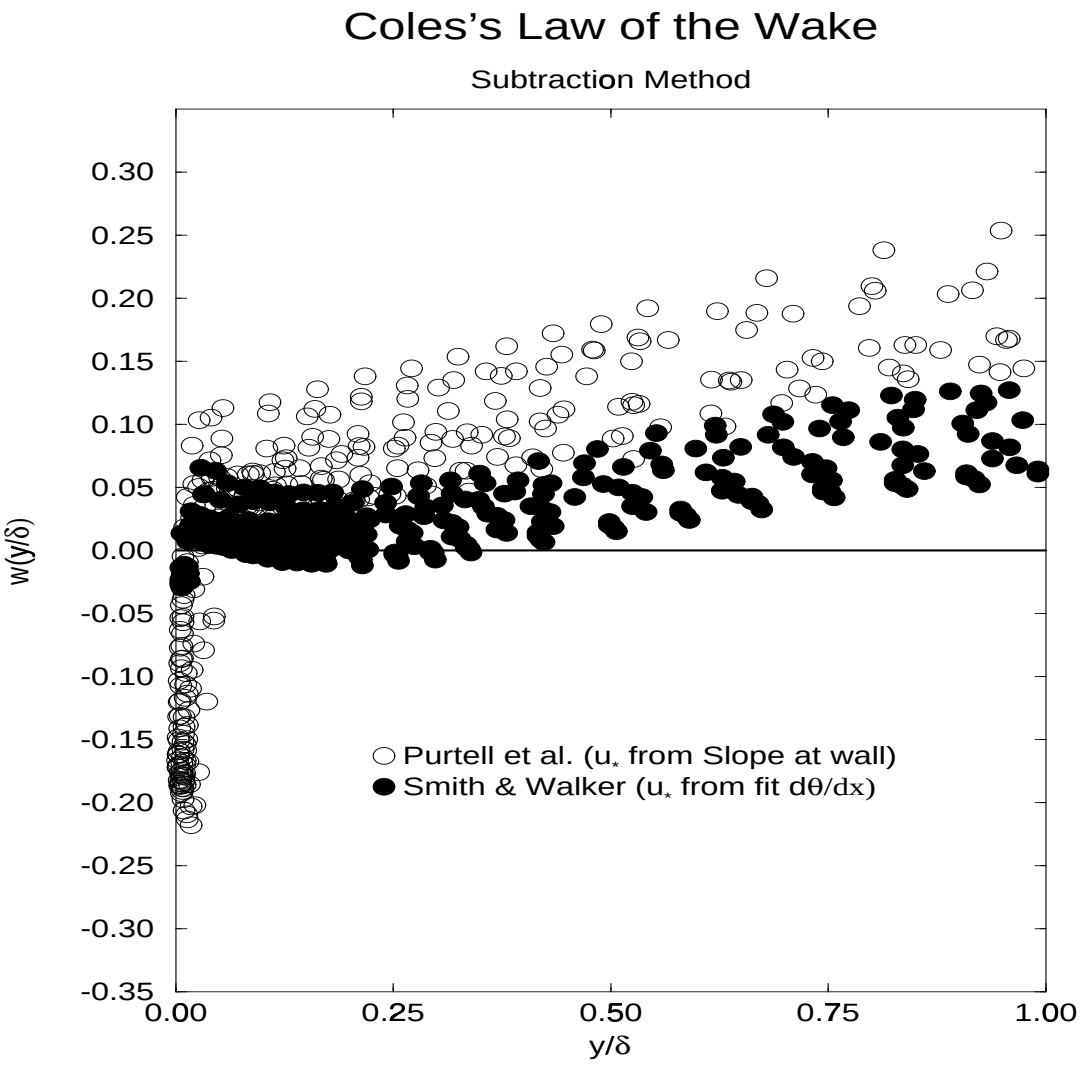

Figure 1.8: Coles's Wake (eq. 1.50): u_* from velocity gradient at the wall and from momentum integral equation.

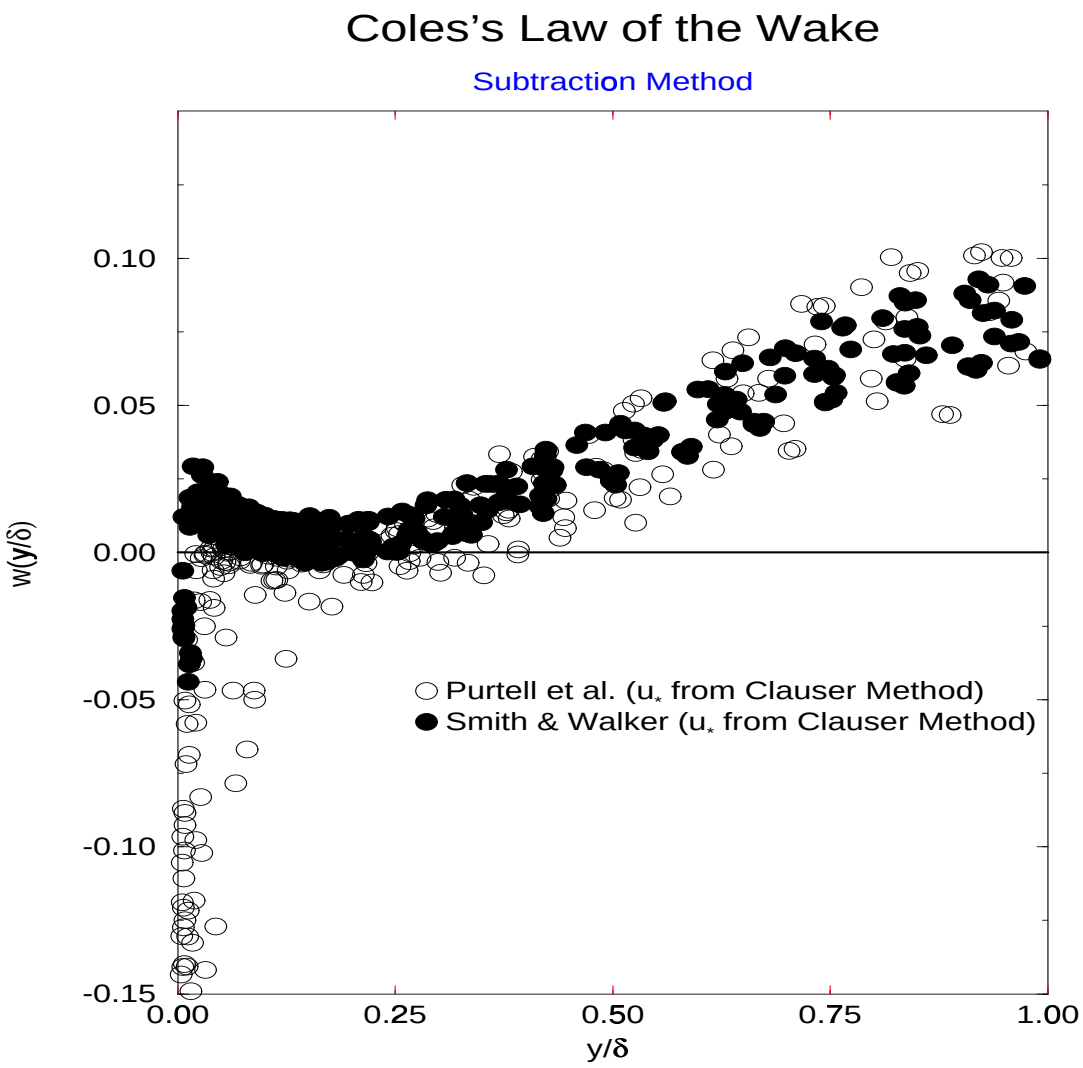

Figure 1.9: Coles's Wake (eq. 1.50): u_* from Clauser method

- (iii) The shape factor approaches unity in the infinite Reynolds number limit (i.e., $H = \delta_*/\theta \rightarrow 1$).

While these might be considered plausible if the limit is approached by increasing the free stream velocity or by decreasing the viscosity, they seem less reasonable if the limit is approached by simply increasing the streamwise distance (e.g., by proceeding along the surface). In addition, a practical objection can be raised because the logarithmic forms permit only empirical models for the streamwise development of the boundary layer parameters.

It might be argued that some free shear flows (like wakes) share these characteristics; however, this is of small comfort since the very essence of a boundary layer is the continuing loss of momentum to the wall. Experimentally, in addition to the problem discussed earlier, there are other reasons for concern, since no shape factors below about 1.25 have been reported, and boundary layer profiles seem to collapse as well with momentum and displacement thicknesses as with the boundary layer thickness determined from the profile (e.g., $\delta_{0.99}$). Nonetheless it has somehow been possible to live with these 'problems'. Clauser (1954) and Tennekes and Lumley (1972), for example, use the displacement thickness as the outer length scale in the analysis of equilibrium boundary layers, even though its use is inconsistent with the Millikan/Clauser analysis (see *(ii)* above). Acceptance of these ambiguities can in part be understood because of the relatively limited range of Reynolds numbers at which experiments have been performed, but in larger part it probably should be attributed to the absence of rational alternative theories. This is somewhat surprising since an even more fundamental objection can be raised to the classical theory: It begins with two scaling 'laws', only the inner one of which is derivable from the the equations of motion. The other, the velocity deficit law, depends entirely on

experimental data.

1.10 The Problem with the Data and any Theory

In view of the difficulty of carrying out the experiments, especially close to the wall and in determining the shear stress, it is unlikely that the data will speak unequivocally. Moreover, the experimental problem is complicated by the fact that the all important ratio, u_*/U_∞, decreases ever more slowly with increasing Reynolds number, regardless of what its limiting value is. Therefore experiments at higher Reynolds numbers will be primarily useful for sorting out what the limits are, and less useful for sorting differences in scaling. Experiments at relatively low Reynolds number will be more useful for the latter because the greater variation of u_*/U_∞ will make trends more evident. But even the low Reynolds number experiments will be of little value for establishing the scaling laws unless the shear stress is directly determined, and to an accuracy greater than the variation among experiments. Few experiments to-date satisfy these criteria.

The fact that with the present work (described in the following chapters) there are now two competing theories for the boundary layer makes a considerable difference because the data can usefully sort between them. With only one theory, the experimentalist (who is really at his best when sorting theories) is under considerable pressure to obtain results which confirm it, particularly if the theory has been believed to be correct. This has certainly been the case with the "log law" and its consequences. There is ample evidence in the abundant literature of "creative" data analysis to confirm the log results, especially with regard to choice of the appropriate value of the wall shear stress (e.g., Coles 1968, Fernholz et al. 1995). Coles (1968), for

example, not only uses equation 1.31 to determine the shear stress from the velocity profile data, but then uses equation 1.33 to determine the appropriate value of the boundary layer thickness δ. Thus both of these important parameters are allowed to "float", a reasonable approach only if the theory is known to be true and the constants universal. The fact that few experiments using the values determined in this manner satisfy the momentum integral equation is disturbing, to say the least.

Thus one of the major problems of the present study has been to recognize when data "contamination" has occurred, to attempt to "decontaminate" the data when possible, and to abandon it when that proved impossible. Because a certain element of subjectivity is necessary in this process, a careful attempt has been made to identify precisely what was done so that the reader can judge for himself whether the results here are reasonable. Final judgment can only await a new round of experiments in which the experimentalist is unconstrained by the need to agree with either theory. Fortunately a number of such experiments are in progress (eg., Princeton, IIT/Chicago, KTH/Stockhom, NASA/Langley).

The task of this dissertation is somewhat more complicated than simply showing that the new theory is consistent with the experimental data. Since there is an existing theory which has been more or less accepted as being correct, it is also necessary to demonstrate that the data are inconsistent with it. Or failing that, that the new theory works better. Fortunately the recent review of Gad-el-Hak and Bandyopadhyay 1994 considerably simplifies this endeavor. Their work is a comprehensive review of the experimental contributions over the past 30 years; in particular, the failure to achieve Reynolds number independence of either the outer scaling for the mean velocity deficit, or of the turbulence quantities outside of the linear sublayer. Therefore their effort will not be repeated here, and attention will be focused on showing that

the data are at least as consistent with the new theory as with the old. In fact, it will be possible to show that some of the alleged 'problems' with the data disappear when viewed from the perspective of the new theory .

1.11 Objective of the Present Work

This work reconsiders first the theoretical foundations of the laws on which the Clauser/Millikan analysis is based, and shows one of them (the velocity deficit law) to be inconsistent with similarity of the outer equations of motion (in the case of boundary layer with and without pressure gradient). Then it examines the consequences of an alternative formulation of the outer scaling law which *is* consistent with similarity in the limit of infinite Reynolds number. When combined with the Law of the Wall, this new deficit law is shown to lead to velocity and friction laws which are power laws, a consequence of two velocity scales in the overlap region. On the other hand, pipe and channel flows will be shown here to be described by logarithmic functions with coefficients that vary with Reynolds number, a consequence of a single velocity scale for this flow (i.e., the velocity in both inner and outer variables scales with u_*).

In Chapter 2, similarity analysis is applied to the equations of motion for a boundary layer with zero pressure gradient, and the velocity and length scales are determined from the equations of motion only. Then a Near Asymptotics Method is used in order to find the functions describing the velocity profiles in the overlap region. The advantage of this approach is that it is performed at finite Reynolds number so the Reynolds number dependence of the boundary layer is captured, contrary to the classical theory which is done in the limit and fails to capture the Reynolds number dependence. The comparison of the zero pressure gradient theory with the

experimental data is given in chapter 3.

The similarity analysis and results for the turbulent boundary layer with pressure gradient in outer variables is given chapter 4. The similarity analysis for the same flow in inner variables is given in chapter 5, and the overlap relationships are derived there also. In chapter 6, the theory is applied to pipe and channel flows. Finally, Chapter 7 contains a summary and the conclusions of this work.

Chapter 2

The Zero Pressure Gradient

In this chapter the theoretical foundations will be given for the zero pressure gradient (e.g., $U_\infty = constant$) turbulent boundary layer[1] The objective is to develop a theory that will yield the scales and the functionalities for wall bounded flows in the near the wall region. The scales are determined from the equations of motion in the limit as Reynolds number goes to infinity using an Asymptotic Invariance Principle.

2.1 The Asymptotic Invariance Principle

For reasons that will become clear below, the traditional approach to the boundary layer equations has been to abandon the possibility of full similarity, and seek instead local similarity solutions of the type described earlier. As a consequence, the local similarity solutions obtained were not necessarily similarity solutions of either equation 1.1, equation 1.2 or equation 1.3, since no effort was made to insure that they were. Instead investigators attempted to establish their validity by experiment alone, dismissing as unimportant terms in the mean momentum equations which were

[1] Chapters 2 and 3 follow closely George, Castillo and Knecht 1996.

inconsistent and and ignoring the higher order moment equations altogether.

An alternative approach (which does not seem to have been previously attempted) is to seek full similarity solutions of the inner and outer equations separately. Since these equations (equations 1.2 and 1.3) are themselves exactly valid only in the limit of infinite Reynolds number, then their full similarity solutions will also be exactly valid only in this limit. Seen another way, since the equations themselves have neglected terms which are Reynolds number dependent and lose these terms only in the infinite Reynolds number limit; solutions to these full equations will likewise be Reynolds number dependent and lose this dependence only at infinite Reynolds number. This idea will be referred to as the *Asymptotic Invariance Principle*. (This term appears to have first been used by Knecht 1990, but with a slightly different meaning.)

The *Asymptotic Invariance Principle* can be applied to turbulent free shear flows, as well as boundary layer flows. Similarity solutions for free shear flows (when they exist) are, in fact, infinite Reynolds number solutions because the equations from which they are derived are strictly valid only at infinite Reynolds number (c.f., George 1989). The difference in application here is that for the boundary layer there will be two different scaling laws to be applied to the complete solution — one which reduces to a full similarity solution of the *outer* equations at infinite Reynolds number, and another which reduces to a full similarity solution of the *inner* equations in the same limit. For finite Reynolds numbers, the Reynolds number dependence of the equations themselves, however weak, dictates that the solutions can not be similarity solutions anywhere. But, as noted above, this is no different than for free shear flows which only asymptotically show Reynolds number independence.

In the following sections, the Asymptotic Invariance Principle will be applied to some of the single point equations governing the zero pressure gradient turbulent

boundary layer. In particular, solutions will be sought which reduce to full similarity solutions of the equations in the limit of infinite Reynolds number, first for the inner equations and then for the outer. The form of these solutions will determine the appropriate scaling laws for *finite* as well as infinite Reynolds number, since alternative scaling laws could not be independent of the Reynolds number in the limit. Once the method has been established by application to the equations governing the mean momentum, then the same principle will be applied to equations governing the Reynolds stress equations and the statistical quantities appearing in them. There is, of course, no reason why the Asymptotic Invariance Principle can not be applied to equations governing any statistical quantity, including multi-point equations, and some inferences will be made as to what the results of such application might be.

2.2 Full Similarity of the Inner Equations

In keeping with the Asymptotic Invariance Principle set forth above, solutions are sought which reduce to similarity solutions of the inner equations and boundary conditions in the limit of infinite Reynolds number (i.e., $\delta^+ \to \infty$). Solutions will be sought of the form

$$U = U_{si}(x) f_{i\infty}(y^+) \tag{2.1}$$

$$-\overline{uv} = R_{si}(x) r_{i\infty}(y^+) \tag{2.2}$$

where

$$y^+ \equiv \frac{y}{\eta} \tag{2.3}$$

and the length scale $\eta = \eta(x)$ remains to be determined. Note that the subscript $i\infty$ is used to distinguish the scaled velocity and Reynolds stress profiles, $f_i(y^+, \delta^+)$ and

$r_i(y^+, \delta^+)$, which will be used later, from their limiting forms used here. Obviously f_i and r_i are dependent on δ^+, while $f_{i\infty}$ and $r_{i\infty}$ are not.

Substitution into equation 1.4 and clearing terms yields to leading order in δ^+,

$$\left[\frac{u_*^2}{U_{si}^2}\right] = \left[\frac{R_{si}}{U_{si}^2}\right] r_{i\infty} + \left[\frac{\nu}{\eta U_{si}}\right] {f_{i\infty}}' \tag{2.4}$$

A similarity solution exists only if η, U_{si}, and R_{si} can be determined so that all the terms in brackets have the same x-dependence; i.e.,

$$\left[\frac{u_*^2}{U_{si}^2}\right] \sim \left[\frac{R_{si}}{U_{si}^2}\right] \sim \left[\frac{\nu}{\eta U_{si}}\right] \tag{2.5}$$

Since there are three scaling functions to be determined, but only two independent constraints, there is some arbitrariness in their determination. A convenient choice for η is

$$\eta = \nu / U_{si} \tag{2.6}$$

from which it follows immediately that similarity solutions are possible only if the inner Reynolds stress scale is given by

$$R_{si} = U_{si}^2 \tag{2.7}$$

It is now also obvious that the inner velocity scale must be the friction velocity so that

$$U_{si} \equiv u_* \tag{2.8}$$

It follows that

$$\eta = \nu / u_* \tag{2.9}$$

$$R_{si} = u_*^2 \tag{2.10}$$

Thus, the integrated inner equation at infinite Reynolds number (i.e., $\delta^+ \to \infty$) reduces to

$$1 = r_{i\infty} + {f_{i\infty}}' \tag{2.11}$$

For finite values of δ^+. this is equation is only approximately valid because of the neglected mean convection terms.

The similarity variables derived above are the usual choices for the inner layer, and thus the *Law*[2] *of the Wall* is consistent with full similarity of the inner equations, *in the limit of infinite Reynolds number*. For any finite (but large Reynolds number) solutions for the inner layer will retain a Reynolds number dependence (as discovered from the Pi-theorem in deriving equation 1.11) since the governing equations themselves do so. It is obvious then that it is equation 1.11 which reduces to the proper limiting form to be a similarity solution for the inner layer, and thus it must be the real Law of the Wall for finite Reynolds numbers. At finite Reynolds numbers however, it also describes the velocity profile over the entire layer. These ideas are not incompatible since in inner variables the outer layer can never be reached in the limit of infinite Reynolds number (i.e., as $\delta^+ \to \infty$, $y^+ \to \infty$ for finite values of y).

2.3 Full Similarity of the Outer Equations

In accordance with the Asymptotic Invariance Principle, solutions will be sought which reduce to similarity solutions of the outer momentum equation and boundary conditions in the limit of infinite Reynolds number. It is important to remember that no scaling laws will be assumed at the outset, but rather will be derived from the conditions for similarity of the equations.

For the outer equations, solutions are sought which are of the form

$$U - U_\infty = U_{so}(x) f_{o\infty}(\overline{y}) \tag{2.12}$$

$$-\overline{uv} = R_{so}(x) r_{o\infty}(\overline{y}) \tag{2.13}$$

[2]The word 'law' is formally incorrect since the result has been derived, and no longer depends on experimental results alone to establish its validity.

where

$$\overline{y} = y/\delta(x) \tag{2.14}$$

and U_{so}, R_{so}, and δ are functions only of x. Note that extra arguments could have been included in the functional dependence of $f_{o\infty}$ and $r_{o\infty}$ to account for the effect of upstream conditions, etc. The velocity has been written as a deficit to avoid the necessity of accounting for its variation across the inner layer. This is, of course, not possible with the Reynolds stress since it vanishes outside the boundary layer. As in the previous section, the ∞ has been added to the subscript to distinguish $f_{o\infty}$ and $r_{o\infty}$ from the the δ^+-dependent profiles scaled with U_{so} and R_{so} used later. The V-component of velocity has been eliminated by integrating the continuity equation from the wall, thus introducing a contribution from the inner layer which vanishes identically at infinite Reynolds number.

Substitution into equation 1.2 and clearing terms yields

$$\begin{aligned} &\left[\left(\frac{U_\infty}{U_{so}}\right)\frac{\delta}{U_{so}}\frac{dU_{so}}{dx}\right] f_{o\infty}\left[\frac{\delta}{U_{so}}\frac{dU_{so}}{dx}\right] f_{o\infty}^2 - \left[\frac{U_\infty}{U_{so}}\frac{d\delta}{dx}\right]\overline{y} f_{o\infty}{}' \\ -\ &\left\{\frac{d\delta}{dx} + \left[\frac{\delta}{U_{so}}\frac{dU_{so}}{dx}\right]\right\} f_{o\infty}{}' \int_0^{\overline{y}} f_{o\infty}(\xi)d\xi = \left[\frac{R_{so}}{U_{so}^2}\right] r_{o\infty}{}' \end{aligned} \tag{2.15}$$

For a similarity solution to be possible, the bracketed terms must all have the same $x-$dependence (or be identically zero). Therefore, it is clear that full similarity is possible only if

$$\left(\frac{U_\infty}{U_{so}}\right)\frac{\delta}{U_{so}}\frac{dU_{so}}{dx} \sim \frac{\delta}{U_{so}}\frac{dU_{so}}{dx} \sim \left(\frac{U_\infty}{U_{so}}\right)\frac{d\delta}{dx} \sim \frac{d\delta}{dx} \sim \frac{R_{so}}{U_{so}^2} \tag{2.16}$$

It follows immediately that

$$U_{so} = U_\infty \tag{2.17}$$

and

$$R_{so} = U_\infty^2 \frac{d\delta}{dx} \tag{2.18}$$

are the only choices, at least to within a constant of proportionality. Thus, the proper velocity scale for the velocity deficit law must be U_∞, and not u_* as suggested by Von Karman (1930) and widely utilized since (eg., Clauser 1954, Coles 1956, 1962).

Since U_∞ is presumed constant, the limiting form of the outer equation governing the mean flow reduces to

$$-\overline{y} f_{o\infty}{}' - f_{o\infty}{}' \int_0^{\overline{y}} f_{o\infty}(\xi) d\xi = \left[\frac{R_{so}}{U_{so}^2 d\delta/dx} \right] r_{o\infty}{}' \tag{2.19}$$

This equation will not receive further attention in this paper since it is not possible to close it without a turbulence model. It is important to note, however, that it has served an extremely important role since it has determined the outer scaling parameters according to the AIP, and hence the real deficit law.

The analysis above makes it clear that of the possible candidates for an outer scaling law for the velocity, only the profile represented by equation 1.12 is Reynolds number invariant in the limit. Therefore this must be the appropriate scaling for finite Reynolds numbers as well. (This is, of course, the whole idea behind the Asymptotic Invariance Principle.)

The old deficit profile, equation 1.13, can not be Reynolds number invariant in the limit (unless u_*/U_∞ is non-zero in the limit), since $F_o = (u_*/U_\infty) f_o$. In fact, since f_o is Reynolds number invariant in the limit, it is clear why F_o vanishes in this limit if $u_*/U_\infty \to 0$ (as required in the Clauser/Millikan theory). This is precisely objection (i) registered in the Introduction.

The Reynolds stress scale, on the other hand, is *not* U_∞^2, but an entirely different scale depending on the growth rate of the boundary layer, $d\delta/dx$. In effect, $d\delta/dx$ is acting as a Reynolds number dependent correlation coefficient, just as for free shear flows (George 1989). This will be shown later to be related to the fact that as the Reynolds number increases, less and less of the energy is dissipated at the scales at

which the Reynolds stress is adding energy to the flow so they become effectively inviscid (v. George 1995). It will also be shown below that R_{so} can be determined by matching the outer Reynolds stress to the inner Reynolds stress. The need for such a matching is intuitively obvious, since the only non-zero boundary condition on the Reynolds stress in the outer flow is that imposed by the inner.

Millikan (1938) and others have objected to the type of similarity analysis employed here as leading to unphysical results for the boundary layer. Certainly there is nothing unphysical about the velocity deficit law using U_∞ in and of itself, and a case for such a deficit law could have been made, even with the data available at the time (as was suggested earlier). Thus the fundamental basis for this objection must have been the condition on the Reynolds stress. However, this would have been a problem only if it were also required or *assumed at the outset* that $R_{so} = U_{so}^2$, for then it would have also been necessary that $d\delta/dx = constant$. Since the boundary layer was believed not to grow linearly, Millikan (and many before and after him as well) was forced to conclude that full self-preservation (in the assumed sense) was not possible, and therefore had to settle for a *locally* self-preserving solution.

George (1989), however, pointed out that (contrary to the conventional wisdom of self-preservation presented in texts) there is no reason *a priori* to insist that $R_{so} = U_{so}^2$. If this arbitrary requirement is relaxed, then there is no longer the requirement for linear growth, and both equation 2.18 and similarity become tenable. In fact, these conditions require that the outer flow be governed by two velocity scales, U_∞ and a second governing the Reynolds stress which is determined by the boundary conditions imposed on the Reynolds stress by the inner layer. It will be shown below that the inner and outer Reynolds stresses can overlap asymptotically only if

$$R_{so} \sim U_\infty^2 \frac{d\delta}{dx} \sim u_*^2 \tag{2.20}$$

which resembles closely the momentum integral equation, both a surprising and gratifying result. More will be said on this relationship later.

That the outer (and inner) equations admit to similarity solutions (in the sense of George 1989) should come as no surprise to the experimentalists who have long recognized their ability to collapse the outer mean velocity data with only U_∞ and δ. Hinze 1976 and Schlichting 1968, for example, show profiles normalized by U/U_∞ and plotted as a function of y/δ. Even the fact that the outer Reynolds stress scales with u_* (but only to first order) is in accord with common practice, since it is assumed in the old theory — but in a way which could not account for the observed weak dependence on Reynolds number. Thus one can speculate that Millikan's conclusions might have been quite different had he (and several generations after him) not been locked-in to the too restrictive idea of self-preservation (i.e., single length and velocity scales).

2.4 Scaling of the Other Turbulence Quantities

For the inner layer, there is only one velocity scale, u_*, which enters the *single point* equations; therefore all *single point* statistical quantities must scale with it. This is, of course, the conventional wisdom, but with an important difference: *The inner layer does not include the overlap layer* — the region between the inner and outer regions — which is Reynolds number dependent. This is contrary to the conventional wisdom of including the overlap layer as part of the wall layer. But since the inner and outer scales are different, the dependent variables in the overlap layer must be expected to be functions of both, *and thus Reynolds number dependent.* (Note that different considerations must be applied to the multi-point equations since conditions

at a point can depend on those at another, and in particular those at a distance.)

From the preceding analysis, it is apparent that the outer layer at finite Reynolds numbers is governed by not one, but two velocity scales. In particular, the mean velocity and its gradients scale with U_∞, while the Reynolds shear stress scales with $U_\infty^2 d\delta/dx \sim u_*^2$. Therefore it is not immediately obvious how the remaining turbulence quantities should scale. In particular, do they scale with U_∞ or u_*, or both? If the latter, then quantities scaled in the traditional way with only one of them will exhibit a Reynolds number dependence and will not collapse. (Note that if the ratio of velocity scales, u_*/U_∞, is asymptotically constant, this Reynolds number dependence would appear to reduce with increasing distance downstream and could lead to the erroneous conclusion that certain quantities scaled with only one of them take longer to reach equilibrium than others.)

In view of the possible similarity of the outer equations for the mean flow, it is reasonable to inquire whether the equations for other turbulence quantities also admit to fully similar solutions. For the outer part of the boundary layer at high Reynolds number, the equation for $< u^2 >$ can be written (Tennekes and Lumley 1972) as

$$\begin{aligned} U\frac{\partial < u^2 >}{\partial x} + V\frac{\partial < u^2 >}{\partial y} &= 2 < p\frac{\partial u}{\partial x} > \\ &+ \frac{\partial}{\partial y}\left\{- < u^2 v >\right\} - 2 < uv > \frac{\partial U}{\partial y} - 2\epsilon_u \end{aligned} \quad (2.21)$$

where ϵ_u is the energy dissipation rate for $< u^2 >$ and the viscous transport term has been neglected.

By considering similarity forms for the new moments like

$$\frac{1}{2} < u^2 > = K_u(x)k(\overline{y}) \quad (2.22)$$

$$< p\frac{\partial u}{\partial x} > = P_u(x)p_u(\overline{y}) \quad (2.23)$$

$$-\frac{1}{2} < u^2 v > = T_{u^2 v}(x) t(\overline{y}) \tag{2.24}$$

$$\epsilon_u = D_u(x) d(\overline{y}) \tag{2.25}$$

and using $R_s = U_\infty^2 d\delta/dx$, it is easy to show that similarity of the $< u^2 >$-equation is possible only if

$$K_u \sim U_\infty^2 \tag{2.26}$$

$$P_u \sim \frac{U_\infty^3}{\delta}\frac{d\delta}{dx} \sim \frac{U_\infty u_*^2}{\delta} \tag{2.27}$$

$$T_{u^2 v} \sim U_\infty^3 \frac{d\delta}{dx} \sim U_\infty u_*^2 \tag{2.28}$$

$$D_u \sim \frac{U_\infty^3}{\delta}\frac{d\delta}{dx} \sim \frac{U_\infty u_*^2}{\delta} \tag{2.29}$$

All of these are somewhat surprising: The first (even though a second moment like the Reynolds stress) because the factor of $d\delta/dx$ is absent; the second, third and fourth because it is present. The mixed forms using u_* and U_∞ instead of $d\delta/dx$ should be especially useful for scaling experimental data at low to moderate Reynolds numbers where u_*/U_∞ shows considerable variation.

Similar equations can be written for the $< v^2 >$ and $< w^2 >$; i.e.,

$$U\frac{\partial < v^2 >}{\partial x} + V\frac{\partial < v^2 >}{\partial y} = 2 < p\frac{\partial v}{\partial y} > + \frac{\partial}{\partial y}\Big\{- < v^3 > -2 < pv > \Big\} - 2\epsilon_v \tag{2.30}$$

and

$$U\frac{\partial < w^2 >}{\partial x} + V\frac{\partial < w^2 >}{\partial y} = 2 < p\frac{\partial w}{\partial z} > + \frac{\partial}{\partial y}\Big\{- < w^2 v > \Big\} - 2\epsilon_w \tag{2.31}$$

When each of the terms in these equations is expressed in similarity variables, the resulting similarity conditions are:

$$D_v \sim P_v \sim \frac{U_\infty K_v}{\delta}\frac{d\delta}{dx} \tag{2.32}$$

$$D_w \sim P_w \sim \frac{U_\infty K_w}{\delta}\frac{d\delta}{dx} \tag{2.33}$$

$$T_{v^3} \sim \frac{U_\infty K_v}{\delta}\frac{d\delta}{dx} \tag{2.34}$$

$$T_{w^2 v} \sim \frac{U_\infty K_w}{\delta}\frac{d\delta}{dx} \tag{2.35}$$

There is an additional equation which must be accounted for; namely that the sum of the pressure strain-rate terms in the component energy equations be zero (from continuity). Thus, in similarity variables,

$$P_u(x)p_u(\overline{y}) + P_v(x)p_v(\overline{y}) + P_w(x)p_w(\overline{y}) = 0 \tag{2.36}$$

This can be true for all $\overline{y}$ only if

$$P_u \sim P_v \sim P_w \tag{2.37}$$

An immediate consequence is that

$$D_u \sim D_v \sim D_w \sim D_s \sim \frac{U_\infty^3}{\delta}\frac{d\delta}{dx} \sim \frac{U_\infty u_*^2}{\delta} \tag{2.38}$$

where D_s is the scale for the entire dissipation, and

$$K_u \sim K_v \sim K_w \sim U_\infty^2 \tag{2.39}$$

Thus all of the Reynolds *normal* stresses scale with U_∞^2, and not with u_*^2 like the Reynolds *shear* stress.

The remaining equation for the Reynolds shear stress is given by

$$\begin{aligned} U\frac{\partial < uv >}{\partial x} + V\frac{\partial < uv >}{\partial y} &= < p\left(\frac{\partial u}{\partial y} + \frac{\partial v}{\partial x}\right) > \\ &+ \frac{\partial}{\partial y}\left\{- < uv^2 >\right\} - < v^2 > \frac{\partial U}{\partial y} \end{aligned} \tag{2.40}$$

This does not introduce any new similarity functions, but it does impose a surprising constraint on the ones which exist already, namely,

$$K_v \sim R_{so}\frac{d\delta}{dx} \sim U_\infty^2(\frac{d\delta}{dx})^2 \tag{2.41}$$

There is an apparent contradiction between equation 2.41 and equation 2.39. It must be recalled, however, that that R_{so} is only *asymptotically* equal to u_*^2 (from the matching), so the outer Reynolds stress scale evolves to this value with increasing Reynolds number. Obviously, the two conditions together require that in the limit of infinite Reynolds number,

$$\frac{d\delta}{dx} \sim \frac{u_*^2}{U_\infty^2} \sim constant \tag{2.42}$$

It is in, indeed, somewhat surprising that similarity of the turbulence moments in the outer flow is possible only if the asymptotic growth rate ($d\delta/dx$) of the boundary layer is constant. If this constant is indeed zero, as argued later, then it is clear that similarity of the outer moments is approached only at very high Reynolds numbers since u_*/U_∞ approaches its asymptotic value very slowly. The full implications of this will be considered in more detail in section 2.13.

From equations 2.38 and 2.29 it follows that

$$D_s \sim \frac{U_\infty^3}{\delta} \tag{2.43}$$

The relations given by equations 2.39 and 2.43 were assumed without proof in the George 1989 analysis of free shear flows. The additional constraint imposed by equation 2.37 was not derived, however, and arises from the additional information provided by the pressure strain-rate terms.

Before leaving this section it should be noted that conditions for similarity of the turbulence moments also give a clue as to when, if ever, this asymptotic state might

be achieved. Similarity solutions of the Reynolds stress equations are possible only when $D_s(x) \sim U_s^3/\delta$ where $U_s = U_\infty$ for the boundary layer. There are only two possibilities for this to occur (George 1995):

- i) Either the local Reynolds number of the flow is constant so that the effect of viscosity on the energy containing eddies (and those producing the Reynolds stress as well) does not vary with downstream distance; or

- ii) The local turbulence Reynolds number is high enough so that the Reynolds stresses are effectively inviscid and the relation $\epsilon \sim q^3/L$ is approximately valid (for a *physical* length $L \sim \delta$).

Unlike some flows (like the axisymmetric jet or plane wake) where the local Reynolds number is constant, for the boundary layer it continues to increase with downstream distance. Therefore the only possibility for similarity at the level of the Reynolds stresses is (ii). Thus similarity in the outer boundary layer at the level of the second order moments can occur only when the *turbulence* Reynolds number is large enough.

Since the local Reynolds number for the boundary layer continues to increase with increasing downstream distance, the similarity state will eventually be reached. The higher the unit Reynolds number of the flow (U_∞/ν), the smaller the value of x at which similarity of the second order moments will be realized. (Section 2.8 below will attempt to establish approximate bounds where each part of the boundary layer can be Reynolds number independent.) It is worth noting that there appears to be nothing in the equations to indicate whether the similarity state achieved in the outer part of the boundary layer is independent of upstream effects.

2.5 The Overlap Layer: An Application of Near-Asymptotics

It is obvious that since both the outer and inner profiles are non-dimensional profiles with different scales and the ratio of the scales is Reynolds number dependent, then any region between the two similarity regimes cannot be Reynolds number independent, except possibly in the limit. The actual mean velocity profile at any Reynolds number, however, is the average of the instantaneous solutions to the Navier-Stokes equations and boundary conditions. And this profile, whether determined from a real flow, DNS simulation, or not at all, exists, at least in principle, and is valid everywhere regardless of how it is scaled. Therefore both scaled forms of this solution, $f_i(y^+, \delta^+)$ and $f_o(\overline{y}, \delta^+)$ (equations 1.11 and 1.12 respectively), represent the velocity everywhere, at least as long as the Reynolds number is finite. In fact, the parameter δ^+ uniquely labels the fanning out of the inner scaled profiles in the outer region and the outer scaled profiles near the wall (e.g., Figures 1, 2 and 3 of Chapter 3).

Thus, f_i and f_o are quite unlike their limiting forms, $f_{i\infty}$ and $f_{o\infty}$, which are infinite Reynolds number solutions only for the inner and outer equations respectively. If f_i and f_o are considered instead of $f_{i\infty}$ and $f_{o\infty}$ (as is usually done), the problem of determining whether an overlap region exists is quite different from the usual asymptotic matching where infinite Reynolds number inner and outer solutions are extended and matched in an overlap region if one exists. Therefore, the objective here is *not* to see if f_i and f_o overlap and match them if they do. Rather, it is to see *whether the fact that these scaled finite Reynolds number solutions (to the whole flow) degenerate at infinite Reynolds number in different ways can be used to determine their functional forms in the common region they describe in the limit.* The methodology

outlined below (termed *Near-Asymptotics*) is believed to be new, but is necessary because the traditional approach cannot account for the possibility of the matching parameter tending to zero, as might be the case.

The fact that analytical forms for these Reynolds number dependent solutions are not available and are only known *in principal* turns out not to be a significant handicap. There are several pieces of information about the two profiles which can be utilized without further assumptions. They are:

- First, since both inner and outer forms of the velocity profile must describe the flow everywhere as long as the ratio of length scales, $\delta^+ = \delta/\eta = \delta^+$, is finite, it follows from equations 1.11 and 1.12 that

$$1 + f_o(\overline{y}, \delta^+) = g(\delta^+) f_i(y^+, \delta^+) \tag{2.44}$$

  where $g(\delta^+) = u_*/U_\infty$ is defined by equation 1.8.

- Second, for finite values of δ^+, the velocity derivatives from both inner and outer forms of the velocity must also be the same everywhere. It is easy to show that this requires that

$$\frac{\overline{y}}{1 + f_o} \frac{df_o}{d\overline{y}} = \frac{y^+}{f_i} \frac{df_i}{dy^+} \tag{2.45}$$

  for all values of δ^+ and y.

- Third, in the limit, both f_o and f_i must become asymptotically independent of δ^+. Thus $f_o(\overline{y}, \delta^+) \to f_{o\infty}(\overline{y})$ only, and $f_i(y^+, \delta^+) \to f_{i\infty}(y^+)$ only as $\delta^+ \to \infty$ or otherwise the velocity scales have been incorrectly chosen. (This is, in fact, the *Asymptotic Invariance Principle*.)

Now the problem is that *in the limit* as $\delta^+ \to \infty$, the outer form fails to account for the behavior close to the wall while the inner fails to describe the behavior away

from it. The question then is: In this limit (as well as for all finite values approaching it) does there exist an "overlap" region where equation 2.44 is still valid? Since both δ and η are increasing with streamwise distance along the surface, this "overlap" region will not only increase in extent when measured in either inner or outer coordinates, it will move farther from the wall in actual physical variables. (Note that this is quite different from pipe and channel flows in which the overlap layer remains at fixed distance from the wall for all x because of the streamwise homogeneity, as long as the external parameters are fixed.)

The question of whether there is a common region of validity can be investigated by examining how rapidly f_o and f_i are changing with δ^+. From the Taylor expansion about a fixed value of δ^+,

$$\frac{f_i(y^+;\delta^+ + \Delta\delta^+) - f_i(y^+;\delta^+)}{\Delta\delta^+ f_i(y^+;\delta^+)} \approx \frac{1}{f_i(y^+;\delta^+)} \frac{\partial f_i(y^+;\delta^+)}{\partial \delta^+}\Big|_{y^+} \equiv S_i(\delta^+, y^+) \qquad (2.46)$$

and

$$\frac{f_o(\overline{y};\delta^+ + \Delta\delta^+) - f_o(\overline{y};\delta^+)}{\Delta\delta^+ f_o(\overline{y};\delta^+)} \approx \frac{1}{f_o(\overline{y};\delta^+)} \frac{\partial f_o(\overline{y};\delta^+)}{\partial \delta^+}\Big|_{\overline{y}} \equiv S_o(\delta^+, \overline{y}) \qquad (2.47)$$

Thus S_i and S_o are measures of the Reynolds number dependencies of f_i and f_o respectively. Both vanish identically in the limit as $\delta^+ \to \infty$. If ${y^+}_{max}$ denotes a location where outer flow effects begin to be strongly felt on the inner scaled profile, then for $y^+ < {y^+}_{max}$, S_i should be much less than unity (or else the inner scaling is not very useful). Similarly, if $\overline{y}_{min}$ measures the location where viscous effects begin to be strongly felt (e.g., as the linear velocity region near the wall is approached), then S_o should be small for $\overline{y} > \overline{y}_{min}$. Obviously either S_i or S_o should increase as these limits are approached. Outside these limits, one or the other should increase dramatically.

The quantities S_i and S_o can, in fact, be used to provide a formal definition of an

"overlap" region where both scaling laws are valid. Since S_i will increase drastically for large values of y for given δ^+ and S_o will increase for small values of y, an "overlap" region exists only if there exists a region for which both S_i and S_o remain small simultaneously. In the following paragraphs, this condition will be used in conjunction with equation 2.44 to derive the functional form of the velocity in the overlap region *at finite Reynolds number*, hence the term 'Near-Asymptotics'. Obviously there is a very close relation between the idea of Near-Asymptotics and Intermediate Asymptotics (Barenblatt 1978), the difference being that the former is carried out at finite Reynolds number.

Because of the movement of the matched layer away from the wall with increasing x, it is convenient and necessary to introduce an intermediate variable $\tilde{y}$ which can be fixed in the overlap region all the way to the limit, regardless of what is happening in physical space (v. Cole and Kevorkian 1981). A definition of $\tilde{y}$ which accomplishes this is given by

$$\tilde{y} = y^+ \delta^{+-n} \tag{2.48}$$

or

$$y^+ = \tilde{y}\delta^{+n} \tag{2.49}$$

Since $\overline{y} = y^+/\delta^+$, it follows that

$$\overline{y} = \tilde{y}\delta^{+n-1} \tag{2.50}$$

For all values of n satisfying $0 < n < 1$, $\tilde{y}$ can remain fixed in the limit as $\delta^+ \to \infty$ while $\overline{y} \to 0$ and $y^+ \to \infty$. Substituting these into equation 2.44 yields the matching condition on the velocity in terms of the intermediate variable as

$$1 + f_o(\tilde{y}\delta^{+n-1}, \delta^+) = g(\delta^+) f_i(\tilde{y}\delta^{+n}, \delta^+) \tag{2.51}$$

Now equation 2.51 can be differentiated with respect to δ^+ *for fixed* $\tilde{y}$ to yield

equations which explicitly include S_i and S_o. The result is

$$\frac{\partial(1+f_o)}{\partial\overline{y}}\Big|_{\delta^+}\frac{\partial\overline{y}}{\partial\delta^+}\Big|_{\tilde{y}}+\frac{\partial(1+f_o)}{\partial\delta^+}\Big|_{\overline{y}}=\frac{dg}{d\delta^+}f_i+g\left\{\frac{\partial f_i}{\partial y^+}\Big|_{\delta^+}\frac{\partial y^+}{\partial\delta^+}\Big|_{\tilde{y}}+\frac{\partial f_i}{\partial\delta^+}\Big|_{y^+}\right\} \tag{2.52}$$

Carrying out the indicated differentiation of y^+ and $\overline{y}$ by δ^+ (for fixed $\tilde{y}$), and multiplying by $\delta^+/(1+f_o)$ yields (after some rearranging)

$$(n-1)\frac{\overline{y}}{(1+f_o)}\frac{\partial(1+f_o)}{\partial\overline{y}}\Big|_{\delta^+}-n\frac{y^+}{f_i}\frac{\partial f_i}{\partial y^+}\Big|_{\delta^+}=\frac{\delta^+}{g}\frac{dg}{d\delta^+}+\delta^+\left\{\frac{1}{f_i}\frac{\partial f_i}{\partial\delta^+}\Big|_{y^+}-\frac{1}{1+f_o}\frac{\partial(1+f_o)}{\partial\delta^+}\Big|_{\overline{y}}\right\} \tag{2.53}$$

It follows immediately from equation 2.45 that

$$\frac{\overline{y}}{1+f_o}\frac{\partial(1+f_o)}{\partial\overline{y}}\Big|_{\delta^+}=-\frac{\delta^+}{g}\frac{dg}{d\delta^+}-\delta^+\left\{\frac{1}{f_i}\frac{\partial f_i}{\partial\delta^+}\Big|_{y^+}-\frac{1}{1+f_o}\frac{\partial(1+f_o)}{\partial\delta^+}\Big|_{\overline{y}}\right\} \tag{2.54}$$

Equation 2.54 can be rewritten as

$$\frac{\overline{y}}{1+f_o}\frac{\partial(1+f_o)}{\partial\overline{y}}\Big|_{\delta^+}=\gamma(\delta^+)-\delta^+(S_i-S_o) \tag{2.55}$$

where $\gamma=\gamma(\delta^+)$ is defined by

$$\gamma(\delta^+)\equiv-\frac{\delta^+}{g}\frac{dg}{d\delta^+} \tag{2.56}$$

Note that the first term on the right hand side 2.55 is at most a function of δ^+ alone, while the second term contains all of the residual y-dependence.

Now it is clear that if both

$$\delta^+|S_o|<<\gamma \tag{2.57}$$

and

$$\delta^+|S_i|<<\gamma \tag{2.58}$$

then the first term on the right-hand side of equation 2.54 dominates. If $\gamma\to 0$, then the inequalities are still satisfied as long as the left hand side does so more rapidly than γ. Note that a much weaker condition can be applied which yields the same

result; namely that both inner and outer scaled profiles have the same dependence on δ^+, i.e., $S_i = S_o$ in the overlap range so γ is the only term remaining. (The author is grateful to Professor R. Karlsson of KTH/Stockholm for pointing this out.) If these inequalities are satisfied over some range in y, then to leading order, equation 2.54 can be written as

$$\frac{\overline{y}}{1+f_o^{(1)}}\frac{\partial(1+f_o^{(1)})}{\partial\overline{y}}\Big|_{\delta^+} = \gamma(\delta^+) \tag{2.59}$$

The solution to equation 2.59 can be denoted as $f_o^{(1)}$ since it represents a first order approximation to f_o. It is *not*, however, simply the same as $f_{o\infty}$ because of the δ^+ dependence of γ, but reduces to it in the limit. Thus, by regrouping into the leading term all of the y-independent contributions, the method applied here has yielded a more general result than the customary expansion about infinite Reynolds number. (It is also easy to see why the usual matching of infinite Reynolds number inner and outer solutions will not work since the limiting value of γ might be zero.)

From equations 2.45 and 2.59, it follows that

$$\frac{y^+}{f_i^{(1)}}\frac{\partial f_i^{(1)}}{\partial y^+}\Big|_{\delta^+} = \gamma(\delta^+) \tag{2.60}$$

An interesting feature of these first order solutions is that the inequalities given by equations 2.57 and 2.58 determine the limits of validity of both equations 2.59 and 2.60 since either S_o or S_i will be large outside the overlap region. Clearly the extent of this region will increase as the Reynolds number (or δ^+) increases.

Equations 2.59 and 2.60 can be readily integrated to yield (to leading order)

$$1+f_o^{(1)}(\overline{y},\delta^+) = C_o(\delta^+)\overline{y}^{\gamma(\delta^+)} \tag{2.61}$$

$$f_i^{(1)}(y^+,\delta^+) = C_i(\delta^+)y^{+\gamma(\delta^+)} \tag{2.62}$$

In the remainder of this paper, the superscript '(1)' will be dropped; however it is these first order solutions that are being referred to unless otherwise stated. (Note that some

earlier versions of this theory included additive constants which were believed to be zero only on experimental grounds. The derivation here makes it clear that these constants are indeed zero.)

The relation between u_* and U_∞ follows immediately from equation 2.44; i.e.,

$$\sqrt{\frac{c_f}{2}} = \frac{u_*}{U_\infty} = g(\delta^+) = \frac{C_o(\delta^+)}{C_i(\delta^+)}\delta^{+-\gamma(\delta^+)} \tag{2.63}$$

Thus the friction law is also a power law entirely determined by the velocity parameters for the overlap region. However, equation 2.56 must also be satisfied. Substituting equation 2.63 into equation 2.56 implies that γ, C_o, and C_i are constrained by

$$ln\delta^+ \frac{d\gamma}{d\delta^+} = \frac{d}{d\delta^+} ln\left[\frac{C_o}{C_i}\right] \tag{2.64}$$

Equation 2.64 is exactly the criterion for the neglected terms in equation 2.54 to vanish identically (i.e., $S_i - S_o \equiv 0$). Therefore the solution represented by equations 2.61 – 2.64 is, indeed, the first order solution for the velocity profile in the overlap layer at *finite*, but large, Reynolds number. Clearly when y^+ is too big or $\overline{y}$ is too small for a given value of δ^+, the inequalities of equation 2.57 and 2.58 cannot be satisfied. Since all the derivatives with respect to δ^+ must vanish as $\delta^+ \to \infty$ (the A.I.P.), the inner range of the outer overlap solution is unbounded in the limit, as is the outer range of the inner.

Thus the velocity profile in the overlap layer is a power law with coefficients and exponent which depend only on Reynolds number, δ^+. The functions $C_i(\delta^+)$, $C_o(\delta^+)$ and $\gamma(\delta^+)$ must be determined either empirically or from a closure model for the turbulence. However they are determined, the results must be consistent with equation 2.64.

Equations 2.61 and 2.62 must be asymptotically independent of Reynolds number, since f_i and f_o are. Therefore the coefficients and exponent must be asymptotically

constant; i.e.

$$\begin{aligned} \gamma(\delta^+) &\rightarrow \gamma_\infty \\ C_o(\delta^+) &\rightarrow C_{o\infty} \\ C_i(\delta^+) &\rightarrow C_{i\infty} \end{aligned}$$

as $\delta^+ \rightarrow \infty$. These conditions are powerful physical constraints and together with equation 2.64 will be seen to rule out some functional forms for γ, like that suggested by Barenblatt 1993 for example (see below). Therefore it is important to note that they are a direct consequence of the AIP and the assumption that scaling laws should correspond to similarity solutions of the equations of motion.

It is convenient to write the solution to equation 2.64 as

$$\frac{C_o}{C_i} = \exp[(\gamma - \gamma_\infty)\ln\delta^+ + h] \tag{2.65}$$

where $h = h(\delta^+)$ remains to be determined, but must satisfy

$$\gamma - \gamma_\infty = -\delta^+\frac{dh}{d\delta^+} = -\frac{dh}{d\ln\delta^+} \tag{2.66}$$

It is easy to show the conditions that both $C_{o\infty}$ and $C_{i\infty}$ be finite and non-zero require that:

Either

- C_o, C_i and γ remain constant always;

or

- (i) $\gamma \rightarrow \gamma_\infty$ faster than $1/\ln\delta^+$

and

- (ii) $h(\delta^+) \rightarrow h_\infty = constant.$

It follows immediately that

$$\frac{C_{o\infty}}{C_{i\infty}} = exp[h_\infty] \tag{2.67}$$

Note that condition (i) together with equation 2.66 requires that $dh/d\ln\delta^+ \rightarrow 0$ faster than $1/\ln\delta^+$.

Condition (ii) rules out solutions of the form suggested by Barenblatt 1993 who proposed power law profiles with $\gamma = a/\ln\delta^+$ for which $h = \ln b - a\ln\ln\delta^+$ where $\ln b$ is the integration constant. Obviously this h is unbounded in the limit as $\delta^+ \rightarrow \infty$. Substitution into equation 2.65 yields $C_o/C_i = b(e/\ln\delta^+)^A$. Thus, either $C_o \rightarrow 0$ or $C_i \rightarrow \infty$ or both. Both of these are unacceptable alternatives in that they are inconsistent with similarity of even the mean velocity. [3]

In Chapter 3 it will be found on empirical grounds that the variation of $\gamma - \gamma_\infty$ and C_o/C_i with δ^+ is described to an very good approximation by

$$h - h_\infty = \frac{A}{(\ln\delta^+)^\alpha} \tag{2.68}$$

where $\alpha \approx 0.46$. This can easily be shown to satisfy the constraints above.

Before leaving this section it is reassuring to note that in flows where the inner and outer velocity scales are the same (as for the channel flow of Appendix I), the procedure utilized above leads to the familiar logarithmic profiles with coefficients which are Reynolds number dependent, but asymptotically constant. The possibility of Reynolds number dependent parameters for the log law in pipe and channel flows is certainly contrary to the prevailing wisdom, but consistent with widespread speculation in the experimental community over many decades. Finally, both the power

[3]Barenblatt's form does produce a logarithmic drag law which is desirable for channel flow, but not necessarily for a boundary layer. A logarithmic drag law can be obtained for channel flow in another way as shown in Appendix I.

law profile proposed here and the log profile have recently been shown by Oberlack (1996) to be consistent with a Lie group analysis of the governing equations for parallel shear flow. The AIP and Near-Asymptotic analysis used here has supplied the information missing from the Lie group analysis; namely, *where* at least two of the particular analytical solutions apply.

2.6 A New Friction Law

The relation between u_*/U_∞ and δ^+ has already been established by equation 2.63. This can be rewritten as

$$\frac{u_*}{U_\infty} = \frac{C_o}{C_i}\delta^{+-\gamma} = \frac{C_o}{C_i}e^{-\gamma \ln \delta^+} \tag{2.69}$$

The asymptotic behavior of u_*/U_∞ obviously is determined by both γ and the ratio C_o/C_i, which are themselves interrelated by equation 2.64.

The advantage of this form of the solution is easily seen by substituting equations 2.65 and 2.66 into equation 2.69 to obtain

$$\frac{u_*}{U_\infty} = \exp[-\gamma_\infty \ln \delta^+ + h] \tag{2.70}$$

Thus u_*/U_∞ is entirely determined by γ_∞ and $h(\delta^+)$. It is easy to see from the above conditions on γ and $h(\delta^+)$ that if $\gamma_\infty \neq 0$, then $u_*/U_\infty \to 0$. On the other hand, if $\gamma_\infty \equiv 0$, then $u_*/U_\infty \to const.$ Either possibility, is consistent with similarity of the mean and turbulence quantities considered earlier. However, an energy dissipation argument will be presented in section 2.13 which suggests that the limiting value of γ must be finite. This conclusion will be seen to be consistent with the data analysis of Chapter 3 where the best estimate is $\gamma_\infty = 0.036$, but there is considerable uncertainty.

The friction laws written above all use u_* on both sides of the equation. This can be cast in an alternative form by eliminating the dependence of the right-hand side of equation 2.63 on u_*; i.e.,

$$\frac{u_*}{U_\infty} = \left(\frac{C_o}{C_i}\right)^{1/1+\gamma} \left(\frac{U_\infty \delta}{\nu}\right)^{-\gamma/(1+\gamma)} \tag{2.71}$$

or

$$c_f = 2\left(\frac{C_o}{C_i}\right)^{2/(1+\gamma)} \left(\frac{U_\infty \delta}{\nu}\right)^{-2\gamma/(1+\gamma)} \tag{2.72}$$

Unfortunately, because C_o/C_i is itself a function of Reynolds number, this form is less useful than it might appear to be. In sections 2.11 and 3.10 the relation of R_δ to R_θ and R_{δ_*} will be determined so that the friction law can be expressed in terms of any of the convenient Reynolds numbers.

2.7 The Reynolds Stress in the Overlap Layer

By following the same procedure as for the velocity, the outer and inner Reynolds stress profile functions for the overlap region can be obtained. For example, the Reynolds shear stress is given by,

$$r_o(\overline{y};\delta^+) = D_o(\delta^+)\overline{y}^{\beta(\delta^+)} \tag{2.73}$$

$$r_i(y^+;\delta^+) = D_i(\delta^+)y^{+\beta(\delta^+)} \tag{2.74}$$

where a solution is possible only if

$$\frac{R_{so}}{R_{si}} = \frac{D_i}{D_o}\delta^{+\beta} \tag{2.75}$$

and

$$ln\delta^+ \frac{d\beta}{d\delta^+} = \frac{d}{d\delta^+} ln\left[\frac{D_o}{D_i}\right] \tag{2.76}$$

Unlike the velocity, however, more information about the Reynolds stress is available from the averaged momentum equation for the overlap layer since both equations 1.2 and 1.4 reduce to

$$\frac{\partial}{\partial y}\left(-<uv>\right)=0 \tag{2.77}$$

in the limit of infinite Reynolds number. Thus,

$$\beta R_{so} D_o \overline{y}^{\beta-1} \rightarrow 0 \tag{2.78}$$

and

$$\beta R_{si} D_i y^{+\beta-1} \rightarrow 0 \tag{2.79}$$

Since both D_o and D_i must remain finite and be asymptotically constant (if the Reynolds stress itself is non-zero), these conditions can be met only if

$$\beta \rightarrow 0 \tag{2.80}$$

From equation 2.11 for large values of y^+, the Reynolds stress in inner variables in the matched layer is given to first order (exact in the limit) by

$$r_i \rightarrow 1 \tag{2.81}$$

Since $R_{si} = u_*^2$, this can be consistent with equation 2.74 only if $D_i \rightarrow 1$ as $\delta^+ \rightarrow \infty$. It follows immediately that

$$R_{so} \rightarrow \frac{D_i}{D_o} u_*^2 \tag{2.82}$$

in the infinite Reynolds number limit, just as suggested in Section 2.3.

Some insight into the behavior of $D_o(\delta^+)$ and $D_i(\delta^+)$ can be obtained by introducing the momentum integral equation defined by

$$\frac{d\theta}{dx} = \frac{u_*^2}{U_\infty^2} \tag{2.83}$$

Using this, equation 2.82 and the similarity relation for R_{so} from equation 2.18 yields

$$\frac{D_o(\delta^+)}{D_i(\delta^+)} = \frac{d\theta/dx}{d\delta/dx} \tag{2.84}$$

The relationship between θ and δ will be explored in more detail below, and it will be shown that θ/δ is asymptotically constant. Thus the scale for the outer Reynolds stress is asymptotically proportional to u_*^2 as noted earlier, and the outer layer is indeed governed by two velocity scales. Note that for *finite* Reynolds numbers, both D_o and D_i are Reynolds number dependent. Hence, u_*^2 *alone* should not be able to perfectly collapse the Reynolds stress in either the overlap or outer layers, except possibly in the limit of infinite Reynolds number. This has been observed by numerous experimenters (e.g., Klewicki and Falco[4] who show persistent Reynolds number trends in the Reynolds stress measurements).

The interrelation of the Reynolds stress and velocity parameters can be examined by considering the production term $- < uv > \partial U/\partial y$. Since this must be the same whether expressed in inner or outer variables, it follows that

$$C_o D_o U_\infty^2 \frac{d\delta}{dx} \sim C_i D_i u_*^2 \tag{2.85}$$

or asymptotically, $D_o = C_i(D_i/C_o)$. C_o and D_i achieve a nearly constant value for relatively low values of R_θ while C_i only approaches a constant value for much higher Reynolds numbers. Obviously the outer Reynolds stress parameter follows the inner velocity, thus emphasizing the role of the boundary condition provided by the Reynolds stress on the outer flow by the inner.

[4]submitted for publication

2.8 The Effect of Reynolds Number

The overlap layer identified in the preceding sections can be related directly to the averaged equations for the mean flow and the Reynolds stresses. Of particular interest is the question of how large the Reynolds number must be before the boundary layer begins to show the characteristics of the asymptotic state.

The averaged momentum equation from about $y^+ > 10$ out to $\overline{y} < 0.1$ is given approximately by

$$0 = -\frac{\partial < uv >}{\partial y} \tag{2.86}$$

It has no explicit Reynolds number dependence; and the Reynolds shear stress is effectively constant throughout this region. Unfortunately many low Reynolds number experiments do not have a region where this is even approximately true because the convection terms are not truly negligible. Hence it is unreasonable to expect these experimental profiles to display any of the characteristics of the overlap described above, except possibly in combination with the characteristics of the other regions. (For example, the composite velocity profile of section 2.10 can be used to obtain the Reynolds stress by integrating the complete momentum equation from the wall.)

Even when there is a region of reasonably constant Reynolds stress, however, this is not the entire story because of the Reynolds number dependence of $- < uv >$ itself. Recall that the parameters D_i, D_o, and β (and the velocity parameters C_o, C_i and γ as well) were only asymptotically constant, and only in the limit did $\beta \to 0$. The origin of this weak Reynolds number dependence can be seen by considering the Reynolds transport equations. For this "constant shear stress region", the viscous diffusion and mean convection terms are negligible (as in the mean momentum equation), so the

equations reduce approximately to (Tennekes and Lumley 1972),

$$0 = -(< p\frac{\partial u_i}{\partial x_k} > + < p\frac{\partial u_k}{\partial x_i} >) - \left[< u_i u_2 > \frac{\partial U_k}{\partial x_2} + < u_k u_2 > \frac{\partial U_i}{\partial x_2} \right] - \frac{\partial < u_i u_k u_2 >}{\partial x_2} - \epsilon_{ik} \tag{2.87}$$

where $U_i = U\delta_{i1}$. Thus viscosity does not appear directly in any of the single point equations governing this region, nor does it appear in those governing the outer boundary layer.

In spite of the above, however, viscosity can be shown to play a crucial role in at least a portion of the constant stress layer, even at infinite Reynolds number. The reason is that the scales of motion at which the dissipation, ϵ_{ik}, actually takes place depend on the *local* turbulence Reynolds number, $R_t = q^4/\nu\epsilon$. For $R_t > 1000$ approximately, the energy dissipation is nearly completely controlled by the large energetic scales of motion. These are effectively inviscid, but control the energy transfer through non-linear interactions (the energy cascade) to the much smaller viscous scales where the actual dissipation occurs (v. Tennekes and Lumley 1972). When this is the case, the dissipation is nearly isotropic so $\epsilon_{ik} \approx 2\epsilon\delta_{ik}$. Moreover, ϵ can be approximated by the infinite Reynolds number relation: $\epsilon \sim q^3/L$ where L is a scale characteristic of the energy-containing eddies. The coefficient has a weak Reynolds number dependence, but is asymptotically constant. Thus, the Reynolds stress equations are effectively inviscid, but only exactly so in the limit. And in this limit the Reynolds shear stress has no dissipation at all, i.e., $\epsilon_{12} = 0$. (Note that these are nearly the same conditions required to observe a $k^{-5/3}$-range in the energy spectrum.)

At very low turbulence Reynolds number, however, the dissipative and energy-containing ranges nearly overlap, and so the latter (which also produce the Reynolds shear stress) feel directly the influence of viscosity. In this limit, the energy and

dissipative scales are about the same, so the dissipation is more reasonably estimated by $\epsilon \sim \nu q^2/L^2$, where the constant of proportionality is of order 10. The dissipation tensor, ϵ_{ik} is anisotropic and ϵ_{12}, in particular, is non-zero (Launder 1993). (Hanjalic and Launder 1972, for example, take $\epsilon_{12} = - < u_1 u_2 > /q^2\epsilon$.)

For turbulence Reynolds numbers between these two limits, the dissipation will show characteristics of both limits, gradually making a transition from $\epsilon \sim \nu q^2/L^2$ to $\epsilon \sim q^3/L$ as R_t increases. Thus the Reynolds stresses themselves will feel this directly through their balance equations, and will consequently show a Reynolds number dependence. Obviously, in order to establish when (if at all) parts of the flow become Reynolds number independent, it is necessary to determine how the local turbulence Reynolds number varies downstream and across flow.

Over the outer boundary layer (which is most of it), $L \approx 3\theta$ and $q \approx 0.1U_\infty$. So when $U_\infty\theta/\nu > 3,000$, the dissipation in the outer flow is effectively inviscid. Above this value the mean and turbulence quantities in the outer flow should show little Reynolds number dependence, and this is indeed the case — when they are scaled properly! This outer region can, of course, not be entirely Reynolds number independent, except in the limit, and this residual dependence manifests itself in the overlap layer in the slow variations of γ, for example.

The near wall region is considerably more interesting since in it the scales governing the energy-containing eddies are constrained by the proximity of the wall. Hence, the turbulence Reynolds number, R_t, depends on the distance from the wall, y. In fact, $R_t \sim y^+$ with a coefficient of about 3; so, in effect, y^+ is the turbulence Reynolds number. Because of this, two things are immediately obvious:

- First, since a fixed value of y^+ does not move away from the wall as fast as δ, then as the Reynolds number increases more and more of the boundary layer

(in outer variables) will become effectively inviscid and will be governed by the inviscid dissipation relation. And correspondingly, the mean and turbulence quantities in the overlap layer will become Reynolds number independent, albeit very slowly. Clearly these limiting values cannot be reached until the entire overlap layer is governed by the infinite Reynolds number dissipation relation and its coefficient has reached the limiting value. Obviously this can happen only when there is a substantial range satisfying $y^+ > 300$ and for which the mean convection terms are negligible, typically $\overline{y} < 0.1$. Thus the asymptotic limits are realized only when $300\nu/u_* << 0.1\delta$ or $u_*\delta/\nu >> 3000$, which corresponds approximately to $U_\infty\theta/\nu >> 10,000$. This is above the range of the available data which end at about $50,000$. Therefore the overlap layer, to the extent that it is identifiable at all, should (and does, as will be seen in Part II) display a Reynolds number dependence, not only in C_o, C_i, and γ, but correspondingly in the behavior of $< u^2 >$, $< uv >$, etc.

- Second, there will always be a *MESOLAYER* [5], below about $y^+ \approx 300$ in which the dissipation can *never* assume the character of a high Reynolds number flow, no matter how high the Reynolds number for the boundary layer becomes. This is because the dissipation (and Reynolds stress as well) can never become independent of viscosity — even though the mean momentum equation itself is inviscid above $y^+ \approx 10$! This fact is well-known to turbulence modellers (v. Hanjalic and Launder 1972), but the consequences for similarity theory and asymptotic analyses do not seem to have been noticed previously. It is particularly important for experimentalists who have routinely tried to apply

[5] This appropriates a term from Long 1976 (see also Long and Chen 1982) who argued strongly for its existence, but from entirely different physical and scaling arguments which we find untenable. Nonetheless, despite the skepticism which greeted his ideas, Long's instincts were correct.

asymptotic formulas to this region, wrongly believing the mesolayer to be the overlap region.

Thus the constant stress layer is really four separate regions, each having their own unique character. The overlap layer ($y^+ > 300$, $\overline{y} < 0.1$) obtained in the preceding section which is nearly inviscid; a 'mesolayer' ($10 < y^+ < 300$) in which the viscous stresses are negligible, but in which viscosity acts directly on the turbulence scales producing the Reynolds stresses; a buffer layer ($5 < y^+ < 10$) where the Reynolds stress and viscous stress both act directly on the mean flow; and the real viscous sublayer, the linear region near the wall ($y^+ < 5$) where the viscous stresses dominate. And of these four regions, the overlap layer will be the *last* to appear as the flow develops or as the Reynolds number is increased. Thus it will be the most difficult to identify at the modest Reynolds numbers of laboratory experiments. Identification will be easier if the properties of the mesolayer are known, and accordingly a model for it is presented in the next section.

2.9 A Mesolayer Model

It was Long 1976 (see Long and Chen 1982) who first argued for the existence of a mesolayer — but on very different physical grounds. He did not consider the turbulence energy equation, but instead only the mean momentum equation. From it he argued that some residual viscous stress must be retained in addition to the Reynolds stress, and used this to define a meso-length scale which varied as the square root of the flow Reynolds number. All subsequent deductions were based on matching four flow regions, one of which was characterized by this new length scale. The suspicions that a new layer involving viscosity and inertia was needed between

the overlap and viscous layers has proven to be quite insightful. The arguments, however, can not be justified since there is simply no physical basis for arguing that the viscous stress must be important *in the equations for the mean flow*. In fact it is negligible outside of $y^+ \approx 10$. It was argued in the preceding section that viscosity enters the dynamics of the mesolayer only through its effect on the energy cascade, and that is reflected in the nature of the dissipation, and in turn in the component Reynolds stress equations.

It is easy to show that no new length scale is necessary to account for this dissipation effect. The whole reason for the existence of this mesolayer is that the local turbulence Reynolds number near the wall can never be large enough for the dissipation to become inviscid. Near the bottom of the constant stress layer, the scales of the energy-containing eddies and those at which the energy is dissipated will be nearly the same size, and in this limit $\epsilon \sim \nu q^2/L^2$ where L is typically about equal to y, the distance from the wall. At the outer part of the constant stress layer, the required scale separation will have been achieved — if the flow Reynolds number is high enough — so the dissipation is nearly inviscid and thus $\epsilon \sim q^3/y$. The essence of the mesolayer is that neither of these limits applies and a transition from one to the other is occurring. Thus in the mesolayer, $\nu q^2/y^2 \sim q^3/y$, and it follows immediately the length scale for the mesolayer is just proportional to $y \sim \nu/q \approx \nu/u_*$. But this just says that the mesolayer length scale is proportional to the viscous one. It does show clearly, however, that the mesolayer is bounded by relatively fixed values of y^+ as argued earlier, the slight variation being due to the fact the ratio q/u_* has a weak Reynolds number dependence (for a given of y^+). and is constant only in the limit.

In the mesolayer, the nature of the dissipation is changing with distance from the wall as the local Reynolds number, y^+, increases. And it is this evolution from low

to high Reynolds number dissipation which provides a clue for building a model for at least part of the mesolayer. Note that the analysis below is a *physical model* based on an assumed form of the dissipation, and is therefore quite distinct from the AIP and Near-Asymptotics approach described earlier. It will be shown, however, to be consistent with the latter, and to lend considerable insight into it.

Since it is the dissipation itself which creates the mesolayer, it is reasonable to begin by assuming a form for how the dissipation changes with Reynolds number, and then pursuing its logical consequences. A simple model incorporating both the high and low Reynolds number dissipation limits is

$$\epsilon = c_1 \frac{q^3}{L} + c_2 \nu \frac{q^2}{L^2} \tag{2.88}$$

For very high values of qL/ν the first term dominates, but the second overwhelms it when $qL/\nu << c_2/c_1$. Variations on this idea have appeared in numerous low Reynolds number turbulence models (c.f. Hanjalic and Launder 1973, Reynolds 1976, Rodi 1993). Since only the near wall region is of interest, it is appropriate to take $L = y$, as done by many single equation turbulence modellers for the near wall region.

As long as $y^+ > 30$, the kinetic energy equation for the turbulence reduces to simply a balance between production and dissipation, the turbulence transport terms being negligible; i.e.,

$$- < uv > \frac{\partial U}{\partial y} = \epsilon \tag{2.89}$$

The turbulence transport terms are certainly not negligible in the region $10 < y^+ < 30$ which is also part of the mesolayer, so any success of the model in this region must be regarded as fortuitous. (The authors are grateful to Drs. M.M. Gibson and W.P. Jones of the Imperial College of London for helpful discussion about this region.)

Now consistent with the single equation turbulence model is the assumption that the Reynolds stress can be modelled with an eddy viscosity acting on the mean

velocity gradient; i.e.,

$$- < uv >= \nu_t \frac{dU}{dy} \tag{2.90}$$

The usual choice of turbulence modellers is (Rodi 1993)

$$\nu_t = c_3^2 \frac{q^4}{\epsilon} \tag{2.91}$$

Substituting the dissipation and Reynolds stress models into the energy balance of equation 2.89, dividing by q^4/ϵ, and taking the square root yields

$$\frac{\partial U}{\partial y} = \left(\frac{c_1}{c_3}\right) \frac{q}{y} + \left(\frac{c_2}{c_3}\right) \frac{\nu}{y^2} \tag{2.92}$$

or in inner variables,

$$\frac{du^+}{dy^+} = \left(\frac{c_1}{c_3}\right) \left(\frac{q}{u_*}\right) y^{+-1} + \left(\frac{c_2}{c_3}\right) y^{+-2} \tag{2.93}$$

Obviously it is the factor q/u_* which determines whether the first term on the right hand side integrates to a logarithm or a power law (or something else).

It is easy to show that in the overlap region (just as for the Reynolds shear stress considered earlier), $q^2/u_*^2 = C_k(\delta^+)y^{+\alpha}$. [6] The overlap velocity power law can be recovered in the limit of large y^+ if $\alpha = 2\gamma$, which is, in fact, consistent with the eddy viscosity and dissipation modeling assumptions above. Substitution into equation 2.93 and integration yields immediately,

$$u^+ = C_i y^{+\gamma} + C_{mi} y^{+-1} \tag{2.94}$$

The integration constant has been taken as identically zero to correspond to the previously derived overlap layer as $y^+ \to \infty$, and the other parameters have been collected into $C_i(\delta^+)$ and C_{mi}. The second term is unaffected by the behavior of

[6] This is a consequence of the fact that the inner and outer scales are different. Pipe and channel flows, however, show a logarithmic dependence for all quantities.

q/u_*; hence there is reason to hope that it may be the same for all wall-bounded flows. (Note that equation 2.94 can be derived using only the overlap characteristics without reference to an eddy viscosity model.)

Thus the additional contribution of the mesolayer to the velocity profile (in inner variables) is $C_{mi}y^{+^{-1}}$. The parameter C_{mi} must be negative and should be nearly constant. It will be seen later in Chapter 3 that that because of the relative values of C_i and C_{mi} there is no region where the second term dominates, at least where the assumptions are valid. Therefore there will be no $y^{+^{-1}}$-layer, only a modified power law region. Moreover, because of this, the first term in equation 2.94 will be clearly visible only when the second is negligible. Since this is not the case for many of the low and moderate Reynolds number experiments, it will not be possible to even identify the parameters C_i, C_o, and γ for most of the data *without first accounting for the mesolayer contribution.* (Note that similar considerations for a channel or pipe flow yield a similar term added to the log profile.)

Equation 2.94 can be expressed in outer variables as

$$\frac{U}{U_\infty} = C_o\overline{y}^{\gamma} + C_{mo}\overline{y}^{-1} \tag{2.95}$$

where

$$C_{mo} = C_{mi}\delta^{+^{-1}}\frac{u_*}{U_m} = C_{mi}\frac{C_o}{C_i}\delta^{+^{-(1+\gamma)}} \tag{2.96}$$

Obviously if C_{mi} is constant, C_{mo} is not.

Since the constant stress layer for much of the data under consideration extends to only values of y^+ of a few hundred, inclusion of the mesolayer profile into the data analysis significantly modifies the conclusions about where the power law overlap region is located, as well as the values deduced for the parameters C_o, C_i, and γ. Both the inner and outer expressions will be utilized in the Chapter 3 to analyze the velocity profile data.

Before leaving this section it is interesting to note that equation 2.93 offers another insight as why the familiar log profile has survived so long. Suppose there were a region in the boundary layer for which production were not only approximately equal to the dissipation, but for which the ratio q/u_* were also approximately constant. If this region were at sufficiently large values of y^+ for the second term to be relatively small, then to a first approximation $du^+/dy^+ \sim 1/y^+$. Thus the profile corresponds exactly to that originally deduced by Prandtl (1932) from an viscosity hypothesis. These assumptions above are satisfied only over a narrow region for boundary layer flows ($50 < y^+ < 150$), but this is exactly the region where the log law is known to work best in boundary layer flows (Bradshaw and Huang 1995). (It will be seen later in Chapter 3 that the overlap plus mesolayer profile derived above and the old log law are nearly indistinguishable over this range.) In fact, these same authors note the seemingly paradoxical facts that the log profile is remarkably 'resilient', but its range of validity does not seem to increase with increasing Reynolds number like a proper overlap solution (or like pipe or channel flow). All of these observations are consistent with the interpretation that the boundary layer 'log region' is in fact just a portion of the mesolayer. Thus von Karman's log law is preserved, but only as an approximation over a limited range to the mesolayer. Clauser's identification of this region with Millikan's matched layer is, however, clearly incorrect.

2.10 A Composite Velocity Profile

It is possible to use the information obtained in the preceding sections to form a composite velocity profile which is valid over the entire boundary layer. This is accomplished by expressing the inner profile in outer variables, adding it to the outer

profile and subtracting the common part (Van Dyke 1964), which is the profile for the overlap region. Alternatively, the outer profile could be expressed in inner variables, etc.

The composite velocity profile in outer variables is given by

$$\frac{U}{U_\infty} = \left[1 + f_o(\overline{y}, \delta^+)\right] + \frac{u_*}{U_\infty}\left[f_i(\overline{y}\delta^+, \delta^+) - C_i\left(\overline{y}\delta^+\right)^\gamma\right] \tag{2.97}$$

Recall that f_o, f_i, C_i and γ are all functions of δ^+, as is u_*/U_∞. The mesolayer contribution has been considered to be part of the inner solution, but could have been included with the common part since it is known.

The composite velocity solution has the following properties:

- As $\delta^+ = \delta/\eta \to \infty$, $U/U_\infty \to 1 + f_o(\overline{y})$. Thus there is a boundary layer profile even in the limit of infinite Reynolds number and it corresponds to the outer scaling law. This can be contrasted with the Millikan approach for which $U/U_\infty \to 1$, a limit remarkably like no boundary layer at all, even in its own variables.

- As $\overline{y} \to 0$, $U/U_\infty \to (u_*/U_\infty) f_i(\overline{y}\delta^+)$ for all δ/η. This is because the small $\overline{y}$ behavior of $[1 + F(\overline{y})]$ is cancelled out by the last term leaving only the inner solution.

- As $\overline{y}\delta^+ \to \infty$, $U/U_\infty \to 1 + f_o$. This is because the large $\overline{y}\delta^+$ behavior of f_i is cancelled by the last term.

- In the matched layer, only the power law profile remains.

It is an interesting exercise to substitute the composite solution into the full boundary layer equation given by equation 1.1. As expected, it reduces to equation 1.2 for infinite Reynolds number and to equation 1.4 as the wall is approached. This can be

contrasted with the substitution of the Millikan/Clauser log law plus wake function (v. Coles 1956) in which the outer equation vanishes identically in the limit of infinite Reynolds number.

An alternative composite solution can be obtained by multiplying the inner and outer solutions together and dividing by the common part; i.e.,

$$\frac{U}{U_\infty} = \frac{[1 + f_o(\overline{y}, \delta^+)] f_i(\overline{y}\delta^+, \delta^+)}{C_o \overline{y}^\gamma} \tag{2.98}$$

For the zero pressure-gradient boundary layer, this composite solution is nearly indistinguishable from equation 2.97 when plotted against the experimental data.

2.11 The Displacement and Momentum Thicknesses

The displacement thickness, δ_*, is defined by

$$U_\infty \delta_* \equiv \int_0^\infty (U_\infty - U) dy \tag{2.99}$$

This can be expressed using equation 2.97 as

$$\frac{\delta_*}{\delta} = -I_1 - I_2 {R_\delta}^{-1} \tag{2.100}$$

or

$$\frac{\delta}{\delta_*} = -\frac{1}{I_1}(1 + \frac{I_2}{R_{\delta_*}}) \tag{2.101}$$

where

$$I_1 \equiv \int_0^\infty f_o(\overline{y}, \delta^+) d\overline{y} \tag{2.102}$$

$$I_2 \equiv \int_0^\infty \left[f_i(y^+, \delta^+) - C_i {y^+}^\gamma \right] dy^+ \tag{2.103}$$

and the Reynolds numbers R_δ and R_{δ_*} are defined by

$$R_\delta = \frac{U_\infty \delta}{\nu} \tag{2.104}$$

and

$$R_{\delta_*} = \frac{U_\infty \delta_*}{\nu} \tag{2.105}$$

The integrals I_1 and I_2 are functions only of the Reynolds number and become asymptotically constant.

The momentum thickness, θ, is defined by

$$U_\infty^2 \theta \equiv \int_0^\infty U(U_\infty - U)dy \tag{2.106}$$

Again using equation 2.97, the result is

$$\frac{\theta}{\delta} = -(I_1 + I_3) - {R_\delta}^{-1}\left[I_2 + 2I_4 + I_5\frac{u_*}{U_\infty}\right] \tag{2.107}$$

or

$$\frac{\delta}{\theta} = -\frac{1}{I_1 + I_3}\left\{1 + R_\theta^{-1}\left[I_2 + 2I_4 + I_5\frac{u_*}{U_\infty}\right]\right\} \tag{2.108}$$

where

$$R_\theta = \frac{U_\infty \theta}{\nu} \tag{2.109}$$

and

$$I_3 \equiv \int_0^\infty \left[f_o(\overline{y}, \delta^+)\right]^2 d\overline{y} \tag{2.110}$$

$$I_4 \equiv \int_0^\infty \left[f_i(y^+, \delta^+) - C_i {y^+}^\gamma\right] f_o(y^+/\delta^+, \delta^+)dy^+ \tag{2.111}$$

$$I_5 \equiv \int_0^\infty \left[f_i(y^+, \delta^+) - C_i {y^+}^\gamma\right]^2 dy^+ \tag{2.112}$$

Since u_*/U_∞ varies in the limit as $(U_\infty \delta/\nu)^{-\gamma/(1+\gamma)}$ and $\gamma \geq 0$, all terms but the first vanish in the limit of infinite Reynolds number. Thus, as for the displacement thickness, the momentum thickness is also asymptotically proportional to the outer

length scale, but with a different constant of proportionality. It will be seen in Chapter 3 that this limit is approached very slowly, and the limiting value is achieved at Reynolds numbers well above those at which experiments have been performed.

The shape factor can be computed by taking the ratio of equations 2.100 and 2.107. The result is

$$\begin{aligned} H &\equiv \delta_*/\theta \\ &= \frac{I_1 + I_2 R_\delta^{-1}}{(I_1 + I_3) + R_\delta^{-1}(I_2 + 2I_4 + I_5 u_*/U_\infty)} \end{aligned} \tag{2.113}$$

For large values of Reynolds number, the asymptotic shape factor is easily seen to be given by

$$H \to \frac{I_1}{I_1 + I_3} \tag{2.114}$$

Note that since $f_o \leq 1$ always, it follows from their definitions that $I_1 < 0$, $I_3 > 0$ and $|I_1| > I_3$. Therefore the asymptotic shape factor is greater than unity, in contrast to the old result, but consistent with all experimental observations.

It is obvious from equations 2.100 and 2.107 that both the displacement and momentum boundary layer thicknesses are asymptotically proportional to the outer length scale (or boundary layer thickness) used in the analysis. Note that it does not matter precisely how this outer length scale is determined experimentally, as long as the choice is consistent and depends on the velocity profile in the outer region of the flow (e.g., $\delta_{0.99}$ or $\delta_{0.95}$). This is quite different from the Millikan/Clauser theory (with finite κ) where the displacement and momentum thicknesses vanish relative to the unspecified outer length scale.

2.12 Streamwise Dependence of the Boundary Layer

The friction coefficient can be written entirely in terms of R_θ by using equations 2.108 and 2.72; i.e.,

$$c_f = 2(\frac{C_o}{C_i})^{2/(1+\gamma)}[\left(\frac{-1}{I_1+I_3}\right)(R_\theta + I_2 + 2I_4)]^{-2\gamma/(1+\gamma)} \tag{2.115}$$

where the term involving $I_5 u_*/U_\infty$ has been neglected. Also, I_2 and I_4 are much less than R_θ, so that

$$c_f \approx 2(\frac{C_o}{C_i})^{2/(1+\gamma)}[\left(\frac{-1}{I_1+I_3}\right)(R_\theta)]^{-2\gamma/(1+\gamma)} \tag{2.116}$$

The integral of equation 1.1 across the entire boundary yields the momentum integral equation for a zero-pressure gradient boundary layer as

$$\frac{d\theta}{dx} = \frac{1}{2}c_f \tag{2.117}$$

Thus the x-dependence of θ can be obtained by integrating

$$\{\left(\frac{-1}{I_1+I_3}\right)\left(\frac{C_i}{C_o}\right)^{1/\gamma}[1 + R_\theta^{-1}(I_2+2I_4)]\}^{2\gamma/(1+\gamma)} R_\theta^{2\gamma/(1+\gamma)} dR_\theta = dR_x \tag{2.118}$$

where $R_x \equiv U_\infty x/\nu$.

If the values of C_i, C_o, γ and the I's can be evaluated as functions of R_θ, equation 2.118 can be integrated numerically to yield the variation of R_θ as a function of $R_x - R_{x_o}$ where R_{x_o} is a virtual origin which will be determined by how the boundary layer is generated. This will be carried out in Chapter 3 using empirical relations for the parameters. The x-dependence of H, and the other boundary layer parameters can be similarly determined by substituting the results of the integration into the appropriate equations.

It is interesting to note that if γ can be considered to be constant over some range of Reynolds numbers, then equation 2.118 can be integrated analytically to obtain

$$R_\theta = \left(\frac{C_o}{C_i}\right)^{2/(1+3\gamma)}\{\left(\frac{1+3\gamma}{1+\gamma}\right)\left[\frac{-1}{I_1+I_3}\right](R_x - R_{x_l})\}^{(1+\gamma)/(1+3\gamma)} \tag{2.119}$$

where x_l is the virtual origin for the section of the flow under consideration. Thus the boundary layer thickness is proportional to $x^{(1+\gamma)/(1+3\gamma)}$. For example, if $\gamma \to 1/10$, $\theta \to x^{11/14}$. If $\gamma \to 0$, the asymptotic growth is linear; and the smaller γ becomes the closer the power approaches unity. Because of the slow approach of γ to its limiting value, a most important experimental clue that the present analysis is correct will be whether the exponent, $(1+\gamma)/(1+3\gamma)$, increases toward unity as data points are added from distances farther from the leading edge, especially if data from points close to leading edge are successively dropped.

2.13 The Asymptotic Behavior of u_*/U_∞ and γ

It is interesting to examine the relation between the asymptotic value of γ and u_*/U_∞. Since γ must be asymptotically independent of δ^+, the only possible values for γ_∞ are either a finite constant, or zero. For the former, $u_*/U_\infty \to 0$, while for the latter the limiting value is finite and non-zero. Note that both of these satisfy the condition from Section 2.4 for similarity of the Reynolds stress equations in the outer layer (i.e., $d\delta/dx \sim constant$), although a zero value for the boundary layer growth rate certainly is not easy to interpret in this context.

A zero limit for γ itself can be considered by using Equation 2.70 to obtain

$$\frac{u_*}{U_\infty} = \exp[h] \tag{2.120}$$

Recall that if $\gamma \to 0$ faster than $1/\ln \delta^+$ and $h \to const$ as required, this insures a finite asymptotic value of u_*/U_∞. Hence there is no question about whether the turbulence moments in the *outer* layer approach a state of asymptotic similarity; they do, since the limiting value of both $d\theta/dx$ and $d\delta/dx$ is finite. A finite and non-zero limiting value for u_*/U_∞ is certainly contrary to traditional thinking, and would have

important implications for the engineer.

So there would seem to be a strong argument for $\gamma \rightarrow 0$. But this presents another problem. In the overlap region in the limit of infinite Reynolds number, the production of turbulence energy is exactly balanced by the rate of dissipation. Thus, in inner variables, $\epsilon^+ = P^+ = \gamma C_i y^{+\gamma-1}$ since $< -uv >= u_*^2$ in this limit. If there is indeed an energy dissipation law (Frisch 1995) which demands that the *local* rate of dissipation be finite and non-zero in the limit of infinite Reynolds number, then γ_∞ must also be finite and non-zero since C_i must be finite and non-zero for similarity as noted earlier. In fact, the data shown in Chapter 3 are most consistent with a non-zero value of γ_∞, but the experimental evidence is not conclusive.

The consequences on the ratio, u_*/U_∞, of a non-zero value of γ_∞ are easily seen from equation 2.70 using the fact that $h \rightarrow \ln C_{o\infty}/C_{i\infty}$. Clearly $u_*/U_\infty \rightarrow (C_{o\infty}/C_{i\infty})\delta^{+-\gamma_\infty}$, which obviously goes to zero in the limit as $\delta^+ \rightarrow \infty$. Thus this limit is consistent with all of the requirements imposed by the similarity theory.

Regardless of what the limiting values are, they will not be achieved until both inner and outer parameters become Reynolds number independent. Hence this limiting value will not be reached before $R_\theta > 10^5$, and perhaps much later. Unfortunately this is already beyond the limit of all experiments to-date.

There is another interesting aspect of a finite and non-zero limit for u_*/U_∞, however unlikely it may be. If both u_* and U_∞ are the same in the limit, shouldn't an asymptotic theory based on either alone (like the Millikan/Clauser theory) be correct? An asymptotic approach of γ to zero (or even a small value), indeed makes it possible to recover the logarithmic relations of the classical theory as a limiting case. It is easy to show, however, that the limit is not very useful. The profiles of

equations 2.61 and 2.62 can be expanded for small values of γ as

$$f_i(y^+;\delta^+) = C_i e^{\gamma ln y^+} \approx C_i(1 + \gamma ln y^+ + \ldots) \tag{2.121}$$

and

$$f_o(\overline{y};\delta^+) = C_o e^{\gamma ln \overline{y}} \approx C_o(1 + \gamma ln \overline{y} + \ldots) \tag{2.122}$$

Thus the asymptotic boundary layer profiles would appear logarithmic to leading order, even for finite values of γ. (The authors are grateful to Prof. Prosperetti of Johns Hopkins University for pointing this out.)

From these "log" profiles and the asymptotic friction value of equation 2.63 it follows that the effective von Karman/Millikan "constants" of equations 1.31 and 1.32 are given by

$$1/\kappa \equiv \gamma_\infty C_{i\infty} \tag{2.123}$$

$$B_i \equiv C_{i\infty} \tag{2.124}$$

and

$$B_o \equiv C_{i\infty}(1 - \frac{1}{C_{o\infty}}) \tag{2.125}$$

Thus the Millikan/Clauser result appears to have been recovered in the limit as $R_\theta \rightarrow \infty$, *except for the fact that* κ *will blow up if* $\gamma \rightarrow 0$.

This unseemly behavior of κ is not a consequence of either theory by itself, but of the requirement that u_*/U_∞ be a non-zero constant. In fact, if the Millikan/Clauser scaling arguments are applied to the turbulence moment equations, then it is easy to show that similarity of the Reynolds stress equations is possible only if $d\delta/dx = constant$ and $u_*/U_\infty = constant$. And the only possibility of satisfying equation 1.33 with a finite value of u_*/U_∞ is for κ to increase without bound, exactly as derived here. Therefore, either the old theory is not the limit of the new (if $u_*/U_\infty \rightarrow 0$),

or it is but with an infinite von Karman constant (if the limiting value of u_*/U_∞ is finite).

Before leaving this section it is useful to consider again why the mean velocity profile could have been accepted for so long by experimentalists as logarithmic. There are two reasons, the first of which was considered earlier in Section 2.9; namely that the "log" profile identified in many boundary layer experiments was probably not the overlap region of Millikan/Clauser (or the present analysis), but instead part of the *Mesolayer*. The second reason is that it is very difficult to tell a logarithm from a weak power using experimental data alone since one can always be expanded in terms of the other. Suppose for the moment that it is indeed the overlap region which is being examined and that the present theory is correct, but that an experimenter believed the log theory to be correct with a constant and finite value of κ. The values for C_i and γ at $R_\theta = 50,000$, the limits of experimental data, will be estimated later in Chapter 3 to be about 12 and 0.09 respectively. These yield a value of $1/\kappa = 1.1$ which is nowhere close to the generally accepted value of about 2.5, believed to be the asymptotic value for both boundary layers and pipes. Over the range of most experiments, however, $R_\theta \sim 10^3$, γ varies between about 1/5 to 1/7 while C_i ranges from 9 to 10. Using $\gamma = 1/6$ and $C_i = 10$ yields about an estimate of $1/\kappa \approx 1.7$. However, the expansion above converges rather slowly and terms above first order are not negligible (nor were they in the calculation above). To third order in $\gamma \ln y^+$, the effective value of κ is given by

$$\frac{1}{\kappa} \approx \gamma C_i[1 + \frac{1}{2}\gamma \ln y^+ + \frac{1}{6}(\gamma \ln y^+)^2 + \frac{1}{24}(\gamma \ln y^+)^3] \tag{2.126}$$

Now the presence of y^+ in this expansion is interesting since it is well-known that attempts to fit the log law at modest Reynolds numbers depend on where the point of tangency is chosen. If κ is evaluated by fitting a log profile which is tangent

to the data at $y^+ = 100$ (as suggested by Bradshaw 1993), using the above values in the expansion yields an estimate of $1/\kappa \approx 2.5$ or $\kappa \approx 0.4$, which is the value usually assumed. Most often in practice, the experimenter picks his point to obtain the "right" value of κ (hence its *universal* value), and accepts whatever value of the other universal (but highly variable!) *constant* which comes out. In view of this and equation 2.126, the seemingly paradoxical variability of B_i and constancy of κ is not at all surprising since the 'right' point of tangency can always be found.

As noted above, there is considerable debate in the literature about the value of B_i with cited values ranging from 4 to 12 From equation 2.124 it is equal to C_i. C_i will be seen later to vary from about 7 to 10 over the range of the low Reynolds number experiments. This is higher than the value of 4.9 suggested by Coles 1968, but well in the range of recent experiments, some of which also show much higher values and a Reynolds number dependence (Nagib and Hites 1995). There is no consensus value for the outer 'constant' B_o, and it is seldom reported at all. Perhaps equation 2.125 suggests a reason for this in that it is quite small since C_o is never very far from unity. Hence estimates for it would vary widely since the errors might be larger than its value.

In summary, at least some of the general satisfaction with the log law over the range of most experiments can be explained with the new theory. Even the sensitivity noted by experimentalists to the choice of the point of tangency can be explained because of the $\ln y^+$-terms in the expansion of κ for finite values of γ. The power law profiles (and the parameters in them) resulting from the present theory, if correct, should be much less sensitive to the actual range of the data used, especially if the limits imposed by the mesolayer are honored.

Chapter 3

Comparison of Theory with data for ZPGBL

The results from the zero pressure gradient theory (previous chapter) will be presented in great detail and compared with the data.

3.1 The Velocity Deficit Region

Since there is usually little doubt as to the proper value of U_∞ in any given experiment, there is no data manipulation which can be done, particularly if a directly determined length scale (e.g., like δ_{99}) is used. Unfortunately, as will be seen below, there can be considerable doubt as to the value of u_*, and this presents serious problems to any evaluation of the data. The question of what is the proper value of u_* will be deferred until the next section, except to note that it will often be seen to be in dispute.

Figure 3.1 shows plots of the data of Purtell et al. 1981 ($465 < R_\theta < 5,100$) in the outer variables of equations 1.12 and 1.13 in both linear-linear (leftmost) and semilog (rightmost) plots. For the U_∞-scaling shown at the topmost, the collapse is excellent

far away from the wall at all Reynolds numbers, and the point of departure from the "asymptote" moves closer to the wall with increasing Reynolds numbers. As noted above, this is the expected behavior for an asymptotic outer solution. However, when the Purtell et al. data are plotted in the usual outer variables using u_* determined from the velocity gradient near the wall (middle figures), there is an obvious tendency for the collapse to come apart away from the single point where it must collapse because of the outside boundary condition. That this happens in the heart of the outer flow where an outer scaling law should work best is at the very least disconcerting from the perspective of the old theory. Absent almost completely is the expected splitting off toward the wall with increasing Reynolds number. The bottom figures of Figure 3.1 show the same data, but using values of u_* chosen to collapse the log layer. (These are in fact the values cited in the paper of Purtell et al.) Even though the data is forced to match at a single point in the "log" region, the same trends are clearly present.

Figure 3.2 shows the velocity data of Smith and Walker 1959 ($3000 < R_\theta < 50,000$) plotted in deficit form. The shear stresses used in the bottom figures were determined to make the "log" region collapse (the Clauser method discussed below) so that the collapse in the traditional scaling is "optimized". Moreover, the variation of u_*/U_∞ is much less than for the Purtell et al. data because of the higher Reynolds number range. Clauser 1954 plotted only the highest and lowest Reynolds number data of the somewhat less extensive data of Schultz-Grunow 1941 for the U_∞ scaling and concluded the absence of collapse ruled it out as as suitable scaling law. The u_* data was plotted only as a shaded area and deemed acceptable. Certainly if it were expected that the entire velocity profile should be Reynolds number independent, then Clauser's conclusion is reasonable. On the other hand, if it had been expected that

the outer layer is only asymptotically independent of Reynolds number, then the U_∞ scaling might have merited further consideration, particularly since as the Reynolds number increases the remainder of the Schultz-Grunow profiles, like the Smith/Walker profiles, are clearly moving toward that of the highest Reynolds number, and the region of collapse is moving toward the wall.

That the old outer scaling in previous works was deemed acceptable is probably due to the moderate Reynolds number range of the data, the choice of u_* to force the "log region" to overlap, the indirect determination of δ, and the mixed (inner and outer) nature of the variables used (i.e., u_* and δ). In spite of this, the outer data normalized by u_* do not appear to be consistent with the asymptotic nature of an outer scaling law. This is closely related to the observations of Gad-el-Hak and Bandyopadhyay 1994 who noted the failure of the "law of the wake " to reach an asymptotic state.

Thus, contrary to previous interpretations, the data would seem to indicate a preference for the new formulation of the velocity deficit law using U_∞ (equation 1.12). Further evidence for the new deficit law is shown in Figure 3.3 using the recent data of Klewicki 1989. The more limited Reynolds number range of this data ($1,000 < R_\theta < 5,000$) makes the Reynolds number independent range appear to be even larger than in the other two data sets. It was noted earlier that at these low Reynolds numbers u_*/U_∞ is varying quite rapidly so the success of the U_∞-scaling is quite impressive.

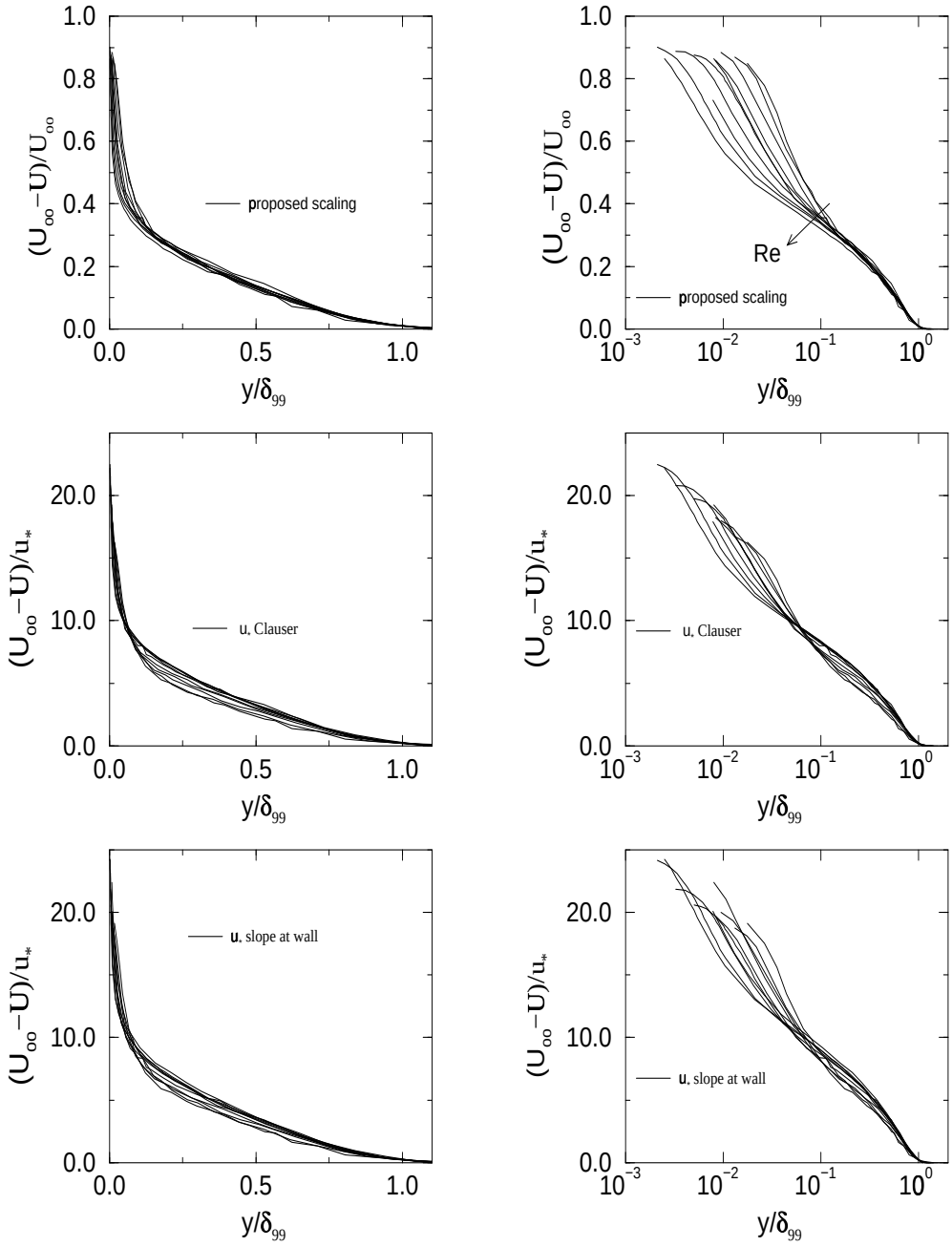

Figure 3.1: Velocity deficit data of Purtell et al. 1981 (linear-linear and semi-log). Top, proposed scaling with U_∞; Middle, old scaling with u_* from Clauser method; Bottom, old scaling with u_* from velocity gradient near wall.

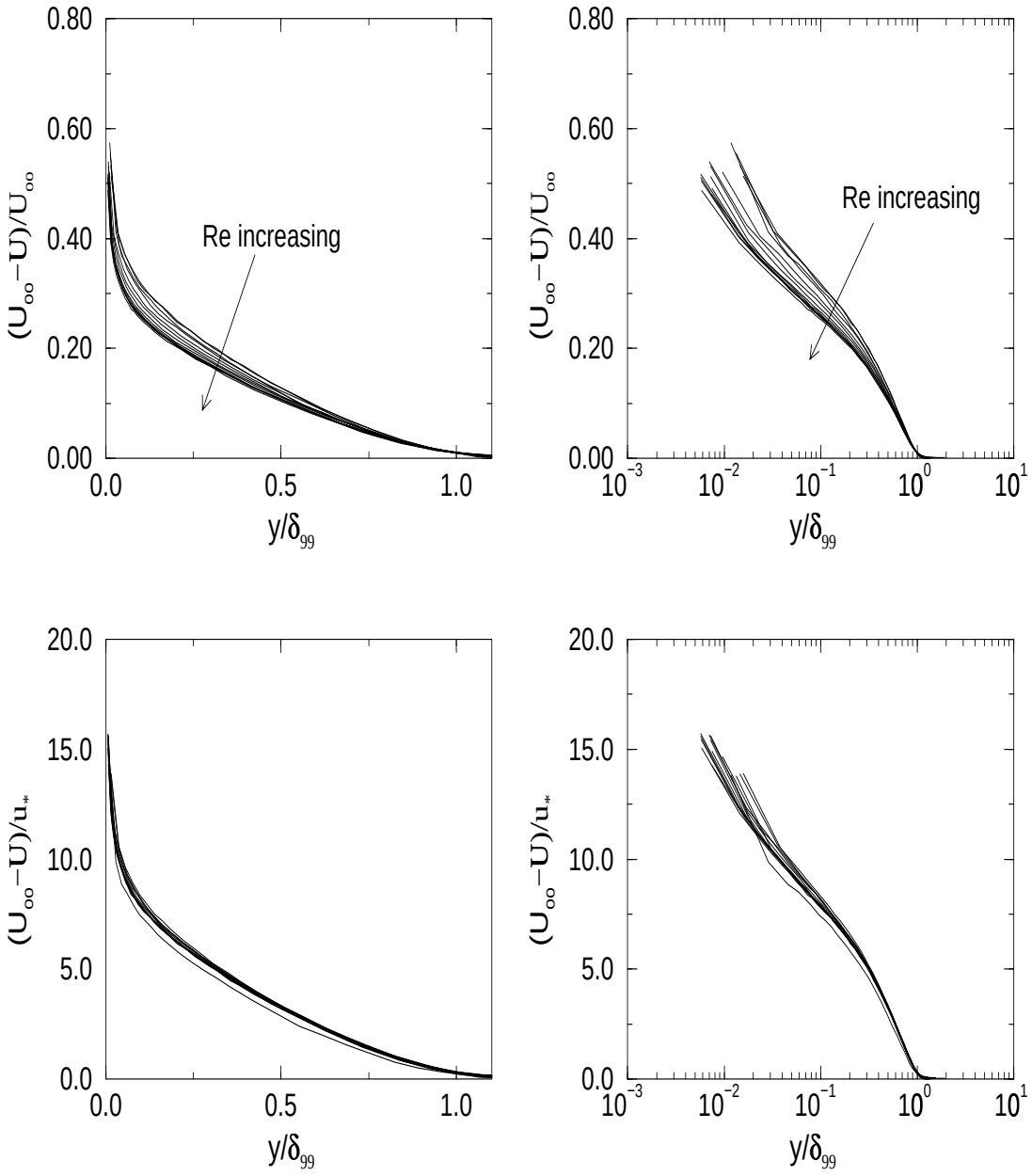

Figure 3.2: Velocity deficit data of Smith/Walker (1954) using U_∞(top) and u_* from Clauser method (bottom).

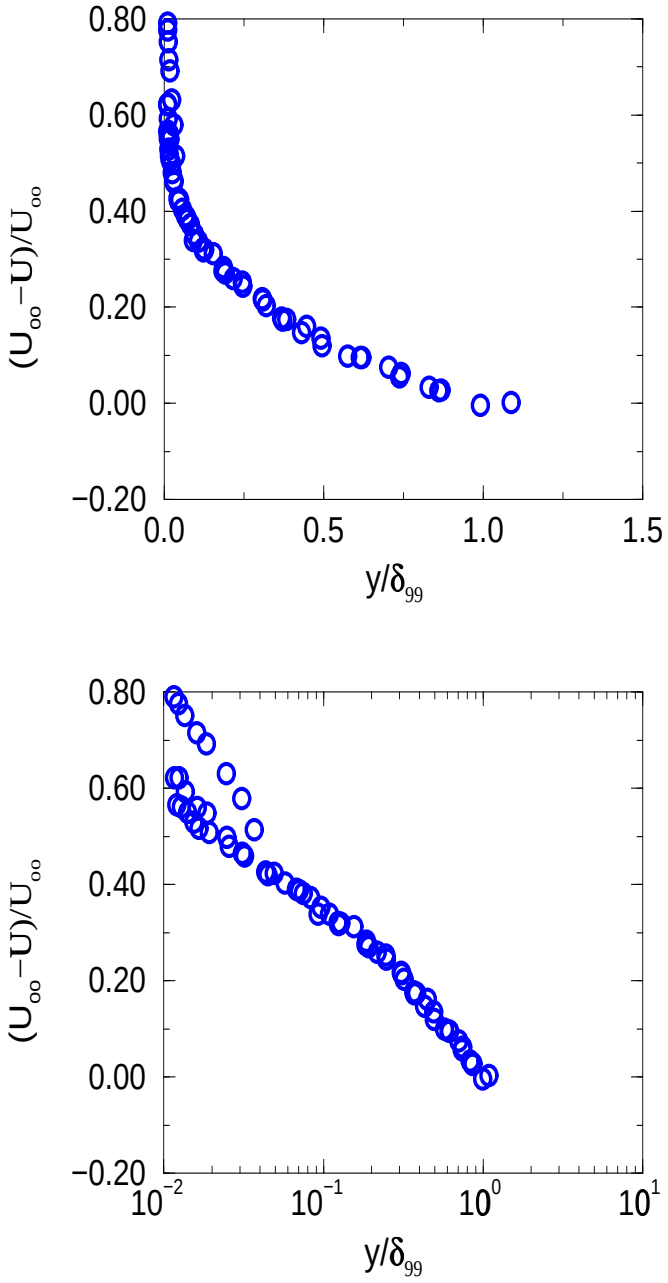

Figure 3.3: Velocity deficit data of Klewicki (1988) using U_∞ (R_θ=1010, 2870, 4850).

3.2 The Near Wall Region

The near wall region can not be addressed without first deciding what values of u_* to use for a given data set. Unfortunately, direct measurements of τ_w have, for the most part, not been very satisfactory for a variety of reasons, not the least of which being that the results did not confirm the Millikan/Clauser theory. Therefore it has been common practice (since Clauser 1954) to choose values for u_* which are consistent with the "universal" log law results for the matched layer, by which is usually meant the constants chosen from the more abundant pipe and channel flow data. Coles (1968) notes that the results obtained in this way are seldom consistent with the momentum integral equation. Nonetheless, in spite of the fact the measurement errors tend to cancel when the integrals are computed from the velocity profiles and therefore should be more accurate than the profiles themselves, the friction results calculated from them have been usually discarded in favor of the Clauser method. Typical of such results is Figure 3.4 which shows the data of Purtell et al. 1981 in inner variables using the wall stress determined from the Clauser method (bottom) and from the velocity gradient near the wall (top). Note the excellent collapse in the "log" region of the former, but also recognize that the data should collapse best in this region because u_* has been chosen to insure that it does — in fact the choice of the tangency point for the log is obvious from the figure. More interesting, however, is what has happened to the measurements in the linear layer for small values of $y^+ < 8$ or so where the data do not collapse at all.

This problem with the inner scaling has been noted before (e.g., Kline et al. 1967), and it seems to have been customary to opt for the method which collapses the "log layer", and rationalize the problems this presents by assuming the measurements near the wall to be in error. While certainly all measurement sets are subject to

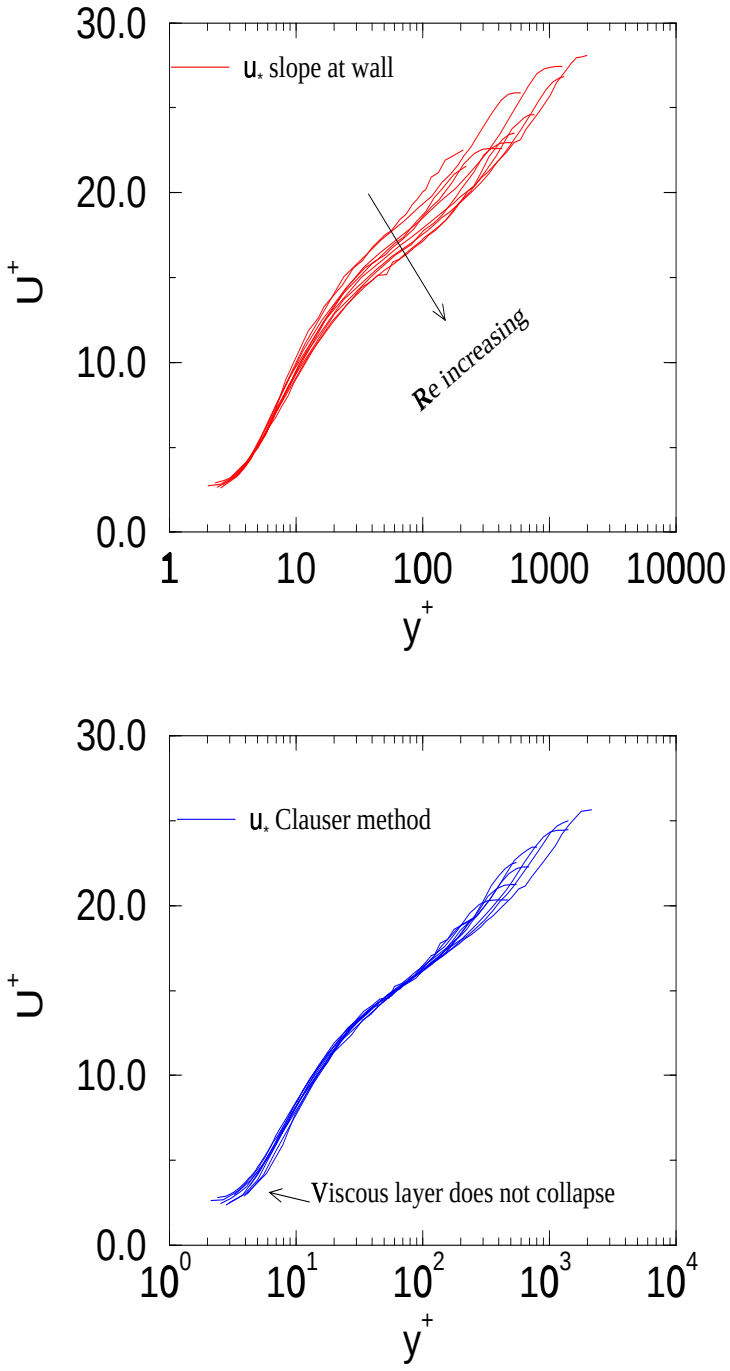

Figure 3.4: Inner scaling of Purtell et al. (1981) data: Top, u_* from velocity gradient; Bottom, u_* determined from Clauser method.

inaccuracies near the wall, the choice represents more an expression of faith in the log law than a consequence of careful error analysis. In fact, curiously, measurements in the linear regions of pipes and channels seem to have been routinely made over the past 50 or so years with little difficulty as long as the ratio of wire diameter to distance to the wall was greater than about 100 (e.g., Monin and Yaglom 1972, vol. I, Figure 3.25). Perry and Abell 1975 measure to within $0.4mm$ with $4\mu m$ hot-wires in a pipe flow before noticing effects of wall proximity. By the same criterion, the data for Purtell et al. should be expected to be valid to values of y^+ from 2 to 5 for eight of the 11 data sets. Thus, either hot-wires have behaved very differently in boundary layers than in pipes, or the experimenters have been unwilling to accept the answers the wires were providing.

The values of u_* from the velocity gradient were made using a linear fit for the data in the region $3 < y^+ < 6$ and points closer to the wall were ignored since they were clearly contaminated by near wall effects on the wires. (It will be seen below that there is evidence that the shear stress has been underestimated by about 20% by this method, but with relative errors which are nearly Reynolds number independent.) The data show clearly that the linear region both exists and the data in it collapse nearly perfectly. Moreover the extent of the linear region appears to be greater than for pipes and channels, but decreases with increasing Reynolds number. As expected from the new theory, the data outside the linear layer does not perfectly collapse in inner variables, but shows the Reynolds number dependence which must be present if the inner and outer scale velocities are different.

Similar profiles for the near wall region were published by Blackwelder and Haritonidis 1983 who documented the difference between the shear stress inferred from

the velocity gradient near the wall and from a fit to the "log" region. (These systematic differences were typically 15% and are tabulated in Table I of their paper.) Their plot of the velocity profile (normalized using the shear stress determined from the linear region) is strikingly similar to that of the Purtell data plotted in Figure 3.4. Of special interest is the fact that the very near wall data show clearly the onset of the near wall measurement errors well inside the linear region, except for the highest Reynolds numbers.

In the absence of direct force measurements, the fact that the velocity profile near the wall collapses in both these data sets using the wall shear stress inferred from the gradient suggests strongly that both the mean velocity and the shear stress have been reasonably estimated, at least at the lower Reynolds numbers. A similar inference cannot be made using a value of the stress which collapses a "log" region, since (as pointed out above) it is based on the assumptions that such a region exists and that the constants describing it are Reynolds number independent. Clearly the second of these is incorrect if the profiles normalized using the shear stress inferred from the velocity gradient are correct, and the first may be wrong as well.

The first important inference which can be seen from these figures is that the data collapse (if a cross-over can be called 'collapse') in the "log" region only if the shear stress is calculated from a method which forces it to by assuming such a layer exists, and then only by compromising the collapse in the linear region. On the other hand, when the measured shear stress is used, the profiles collapse well very close to the wall, but not in the "log" layer. The lack of collapse in the linear layer when the "Clauser method" is used is particularly serious since there are no adjustable constants or Reynolds number dependencies here; the measurements must yield $u^+ = y^+$ if they are to be believed.

A second important inference from the figures is that when the data are normalized by a "proper" shear stress, the point of departure from the linear region moves closer to the wall with increasing Reynolds number toward what might be a limiting value. This is clear evidence that if there is an intermediate layer outside the linear region, then it is only asymptotically independent of Reynolds number. The apparent Reynolds number dependence of the extent of the near-linear region is consistent with the new theory presented earlier since *only the linear region of the flow is Reynolds number independent in inner variables*. Once the mesolayer and overlap region are entered, neither u_* nor U_∞ completely collapse the data until the influence of the inner region has disappeared and the outer flow has been reached. Many (v. Gad-el-Hak and Bandyopadhyay 1993) have noted similar trends for the turbulence moment data near the wall, especially $< u^2 >$ and $< -uv >$.

3.3 The Overlap Layer and the Mesolayer Region

Figure 3.5 shows log-log (leftmost) and semilog (rightmost) plots in inner variables (using the velocity gradient at the wall to obtain the shear stress) for a few of the many cases which were considered. It is easy to argue from the log-log plots that there is evidence in all the data of an extensive power law region ranging from approximately $y^+ > 50$ to $\overline{y} < 0.2$. However, as noted in sections 2.8 and 2.9, great care must be used before inferring that this is the overlap region, especially at these low Reynolds numbers. It will be seen later that indeed it is not. The semilog plots show for comparison the same data in the traditional semi-log plot in inner variables along with the the traditional log profile ($1/\kappa = 2.44$, $B = 5.0$). Obviously an argument for a log region can also be made, although perhaps not the traditional one. Figure 3.6

shows the log-law using u_* from the Clauser method (leftmost) and from the velocity gradient at the wall (rightmost). Note the apparent collapse in the inertial sublayer whereas, the viscous sublayer is Reynolds number dependent even though it is well known that this region is describe $U^+ = y^+$. On the other hand, when u_* from the velocity gradient is used the viscous region is indeed linear and the overlap region shows Reynolds number dependence, consistence with the present theory.

Spalart 1988 recognized the difficulty of determining functional dependencies from velocity profile plots and suggested plotting y^+du^+/dy^+ versus y^+ since a constant region of the former would indicate a logarithmic variation of U. In view of the possibility of a power law region, a more useful plot is y^+du^+/dy^+ versus u^+ since it yields a constant value if the relation is logarithmic and a linearly varying region if a power law. (Note that it does not matter if outer variables are used instead of inner.) Figure 3.7 shows profiles of ydU/dy versus U using the data of of Purtell et al. 1981 in both inner and outer variables. While the data are subject to interpretation because of the large scatter, there is some evidence of the power law region in each set, and certainly considerably more evidence than for a log region. Also evident is the Reynolds number dependence of the slope and intercept, consistent with the theory and the observations above.

There are several complicating factors in using any of the type of plots above to determine whether there is a power law region (or for that matter, a log region). The first is that if there is a mesolayer region in which the power law is modified (as argued earlier), then any data inside $y^+ = 300$ approximately must be excluded. This eliminates all of the Purtell et al. data. The second is that the data outside $\overline{y} \approx 0.1$ (or $y^+ \approx 0.1\delta^+$) must be eliminated since the convection terms are becoming important. Thus, none of the velocity data below about $R_\theta = 10,000$ can be used

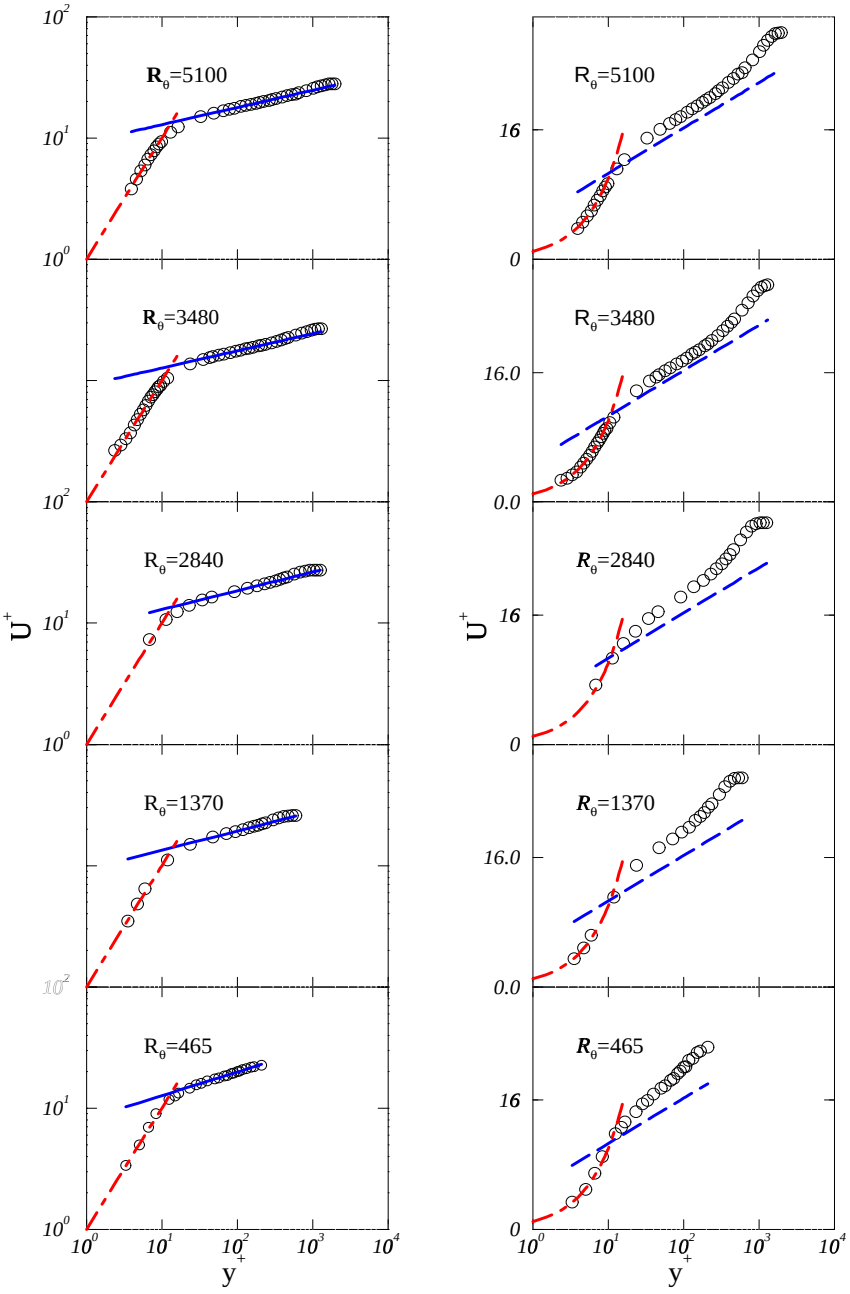

Figure 3.5: Velocity profiles in inner variables: Data from Purtell et al. (1981) using u_* from velocity gradient. Right: log-law; (long dashed line) Left: power law (line) with $U^+ = y^+$ (dot-dashed line).

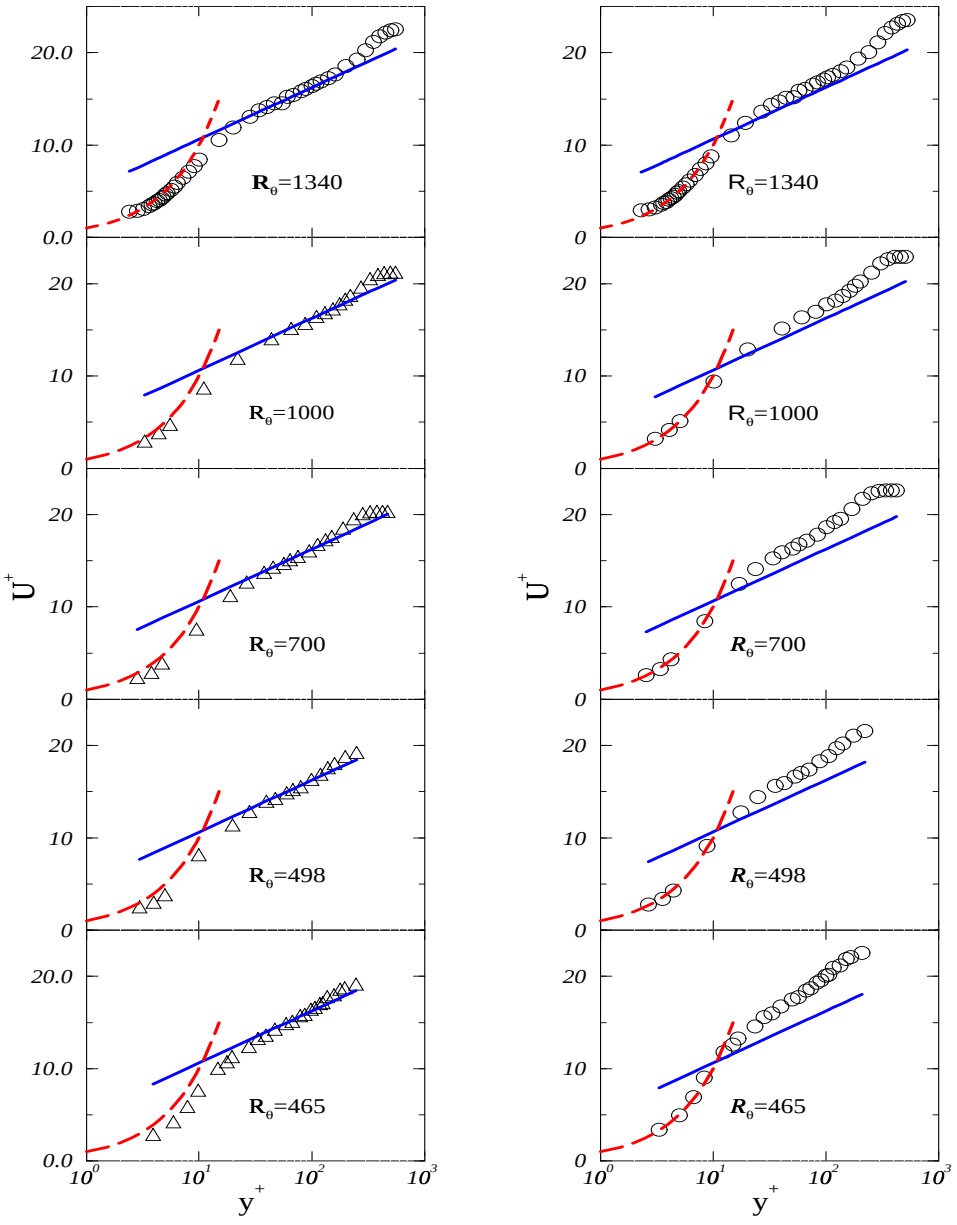

Figure 3.6: Log-law in inner variables using u_* from the Clauser method (leftmost) and from the velocity gradient at the wall (rightmost).

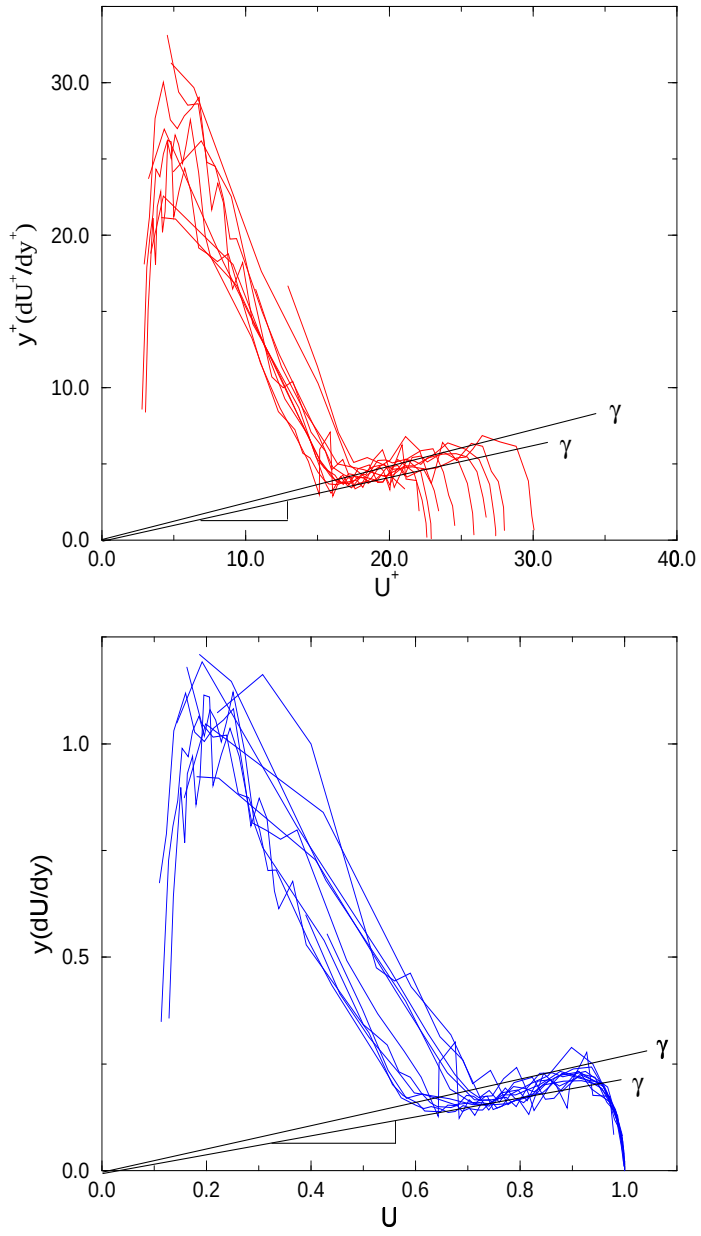

Figure 3.7: Velocity derivative profiles in inner variables (top) and outer variables (bottom).

— and that is most of the available data. Fortunately, by constructing a composite solution for the entire profile and applying it to all the data at once, it is possible to solve for the parameters of the individual pieces, even though they describe regions which are not clearly visible since they are simultaneously influenced by different physics.

3.4 Optimization of Velocity Parameters:

The value of the velocity parameters, γ, C_o and C_i proved to be strongly interrelated, hence the scatter in the data when each profile was considered individually. Therefore the final optimization of the velocity coefficients was determined including equation 3.9 (the γ function) and the corresponding solutions for C_o/C_i, u_*/U_∞,and the function for C_o (equation 3.7) together with all the velocity profiles (using the semi-empirical composite profiles described in section 3.9) in outer variables simultaneously.

The objective function to be optimized is the sum of the relative errors of all velocity profiles in outer variables from R_θ = 465 to 48,292 (data of Purtell et al. 1981 and Smith/Walker 1959), and is given below as

$$Objective\ Function: \sum_{R_\theta=465}^{48,292} Rel.\ error\Big[ABS(\frac{\overline{U}}{Fco} - 1)\Big] \tag{3.1}$$

where $\overline{U}$ is the mean velocity data dimensionalized with the free stream velocity (U_∞) and F_{co} is the composite velocity profile in outer variables. Note that the sum represents the summation of the relative error from a lower limit (in this case R_θ = 465) and an upper limit (R_θ=48,292). The optimization is carried out in such a way that the following *constraints* on selected individual profiles are satisfied

simultaneously:

$$\Big[ABS(\frac{\overline{U}}{F_{CO}} - 1)\Big]_{R_\theta=700} = 0 \tag{3.2}$$

$$\Big[ABS(\frac{\overline{U}}{F_{CO}} - 1)\Big]_{R_\theta=1000} = 0 \tag{3.3}$$

$$\Big[ABS(\frac{\overline{U}}{F_{CO}} - 1)\Big]_{R_\theta=2840} = 0 \tag{3.4}$$

$$\Big[ABS(\frac{\overline{U}}{F_{CO}} - 1)\Big]_{R_\theta=26,512} = 0 \tag{3.5}$$

These equality constraints ensure that no limited range of Reynolds number can dominate the optimization.

The Smith/Walker data in the very near wall region were limited because of the high Reynolds number and the resulting thin sublayer. Therefore it was necessary to input directly some estimate of the c_f. The values used for these profiles (only) were those obtained from the momentum integral as described in section 3.6. The additional constraint for the skin friction is then given as,

$$\sum_{R_\theta=3,000}^{48,292} Rel.error\Big[ABS(\frac{c_{f_{d\theta/dx}}}{c_{fthr}} - 1)\Big]_{(Smith/Walker)} = 0 \tag{3.6}$$

The constants A, α, B, $C_{o\infty}$, γ_∞, C_{oA} and C_{oB} were calculated such that *all the constraints were satisfied simultaneously.* C_{oA} and C_{oB} are the coefficients for the C_o expression given as,

$$C_o = C_{o\infty} + C_{oA}exp(-C_{oB}\delta^+) \tag{3.7}$$

The optimal values obtained for the design variables are given as $C_{o\infty} = 0.897$, $C_{i\infty} = 55$, $\gamma_\infty = 0.0362$, $A = 2.90$, $\alpha = 0.46$, $C_{oA} = 0.244$ and $C_{oB} = 0.0059$. One of the advantages of this optimization is that *the solutions for the velocity coefficients are generated directly.* As result, more accurate velocity profiles are expected than for previous optimizations, in which values for the velocity parameters were generated for every profile. Then a curve fit to this data was needed it to smooth the scatter.

The actual values of the parameters γ, C_o and C_i and C_o/C_i are shown in Figure 3.8 by the solid lines. There was remarkable consistency in the estimates of both γ and C_o for all of the methods utilized, especially when the role of the mesolayer was accounted for. The mesolayer parameter itself was found to be approximately constant at $C_{mi} = -37$.

The values of γ, C_o, C_o/C_i and C_i are plotted in Figure 3.8 as functions of δ^+. Note for future reference that the relation between δ^+ and R_θ is given by

$$R_\theta = \frac{U_\infty}{u_*}\frac{\theta}{\delta}\delta^+ \tag{3.8}$$

since $\delta^+ = u_*\delta/\nu$. The conversion from one to the other can either be done using the data, or the theoretical relations for u_*/U_∞ and θ/δ determined below (These will be shown later in Figure 3.18 after the development of the relationships in section 3.9.).

The values of γ shown in Figure 3.8 drop rapidly over the same range for which C_o shows most of its variation ($R_\theta < 1000$), and then ever more slowly. Whether γ would continue to drop beyond $R_\theta > 50,000$ can not be determined from the data, which are consistent with both non-zero and zero asymptotic values of γ.

The suggestion of Barenblatt (1993) that $\gamma = a/\ln\delta^+$ does provide a reasonable fit to the data for γ; however, the $C_o/C_i = b(e/\ln\delta^+)^a$ — which results from the constraint equation — does not. As noted earlier, this failure can most likely be attributed to the facts that $\gamma \to 0$ is inconsistent with the requirement for finite energy dissipation, and that $C_o/C_i \to 0$ does not satisfy the similarity of the mean reynolds stress squations.

A modified form of Barenblatt's assumption, however, which is consistent with both the Navier-Stokes equations and similarity is

$$\gamma - \gamma_\infty = \frac{-\alpha A}{(\ln\delta^+)^{1+\alpha}} \tag{3.9}$$

where $\alpha > 0$ is a necessary condition. Of all the forms tried for which solutions to the constraint equation could be found, this provided the best fit to all the parameters, and it was used in the final optimization shown in the next section.

Of the forms of the empirical fit to γ used above, equation 3.9 is particularly useful since as noted earlier $h(\delta^+)$ can be determined from it. From equation 2.66 it follows that

$$h = \frac{A}{(\ln \delta^+)^\alpha} + h_\infty \tag{3.10}$$

from which C_o/C_i is given from equation 2.65 by

$$\frac{C_o}{C_i} = \frac{C_{o\infty}}{C_{i\infty}} \exp[(1+\alpha)A/(\ln \delta^+)^\alpha] \tag{3.11}$$

It follows immediately from equation 2.70 that

$$\frac{u_*}{U_\infty} = \frac{C_{o\infty}}{C_{i\infty}} \delta^{+-\gamma_\infty} \exp[(1+\alpha)A/(\ln \delta^+)^\alpha)] \tag{3.12}$$

It should be noted that equation 3.9 is the only empirical equation that enters the entire theoretical formulation, aside from the interpolations used to construct the composite profile. Most importantly, it enters at the very end of the analysis, and not at the beginning as in the classical theory (the assumed velocity deficit law).

The theory states that the asymptotic value of C_o should be constant. This indeed appears to be the case as shown in Figure 3.8, and the asymptotic value of C_o is reached quite early. The range over which the exponential decay term is important will be seen later to correspond closely to the range in which the wake function (defined as the outer scaled profile minus the power law) is strongly Reynolds number dependent. This behavior is consistent with the Reynolds number arguments put forth earlier for when the outer flow can begin to be Reynolds number independent.

The velocity coefficient C_i can be determined either from the inner velocity profile data, or from the friction coefficient by substituting the data for c_f and the values of γ

and C_o determined above into equation 2.71. Unfortunately it is impossible to avoid confronting the problem of the shear stress. As is clear from the discussion in the preceding and following sections, there are serious questions about precisely what c_f (especially for the low Reynolds number) should be, and those uncertainties directly affect the plots of the velocity data in inner variables. Two different approaches were used: The first attempted to directly obtain the wall shear stress from the data using either a direct estimation of τ_w from the velocity gradient at the wall (Purtell et al. data), or from the momentum integral (Smith/Walker data). The second, the results of which are presented in Figure 3.8, used optimization methods which did not depend on any measurement of the shear stress at all but used the theoretical friction law to determine it. One advantage of this approach is that the friction measurements can be used as an independent measure of the success of the theory, since the choice of parameters is independent of them.

Combining the C_o function (equation 3.7) with equation 3.11 leads immediately to an explicit relation for C_i. (Note that C_o could have been assumed constant for all but the lowest Reynolds numbers without significantly changing the results; see Figure 3.7.) These parameters were used in the remainder of this chapter for calculating all the velocity profiles, shear stress and integral boundary layer parameters presented later.

3.5 The Mesolayer and Overlap Profiles:

Figures 3.9 and 3.10 show twenty of the Purtell et al. and Smith/Walker profiles in outer variables, with the mesolayer profile of equation 2.95 using only the parameters determined above and equations 3.9 – 3.12 with equation 3.7. The two vertical dashed

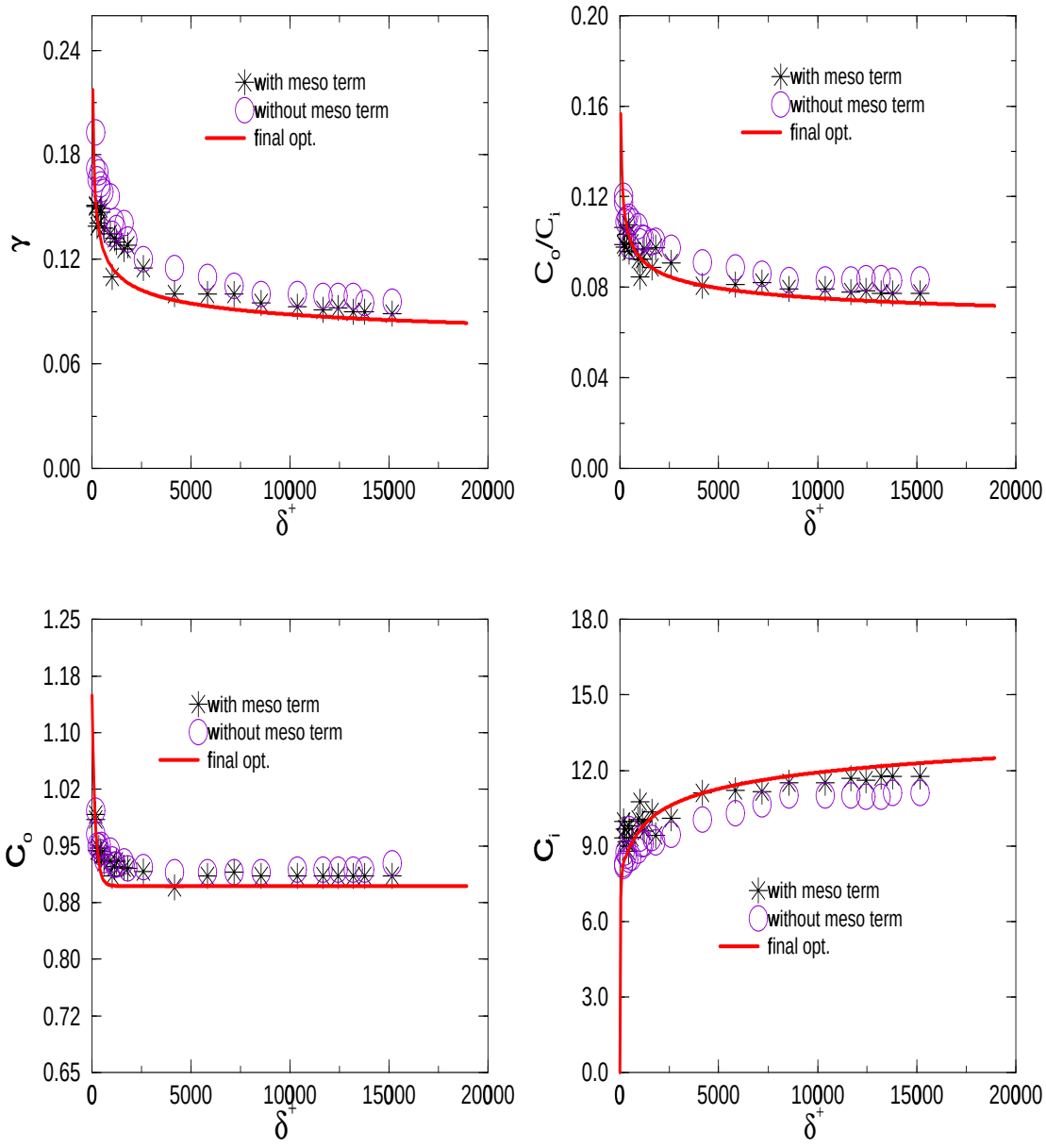

Figure 3.8: Overlap parameters as function of δ^+ using different methods of analysis.

lines on each plot mark the limits of the mesolayer ($30 < y^+ < 300$). Note that for two lowest Reynolds numbers ($Re = 465$ up to about $Re = 1340$), the entire outer region is contained within the boundaries of the mesolayer, which indicates that the convection terms are not making any contribution into the outer flow yet. The outer flow develops quickly, however, for $R_\theta > 1340$, but it is only for $R_\theta > 10,000$ that the overlap region begins to emerge. The overlap region goes from the upper extent of the mesolayer to $\overline{y} = 0.1$ approximately, the latter denoted by the light dotted vertical line on the plots for $R_\theta = 13,037$ and higher. Aside from the Smith/Walker data closest to the wall (which are probably in error since they were taken with Pitot tubes and were not corrected), the theoretical relationship provides an excellent description of the flow from well below the expected limits ($y^+ > 30$) to well outside it for all Reynolds numbers. Especially gratifying is the ability of the mesolayer term to capture the low Reynolds number behavior. The entire sequence of profiles from very low to very high Reynolds number is confirmation of the arguments put forth in Section 2.8.

In spite of the apparent success outlined above, there is still some reason for concern. The Smith/Walker mean velocity data was taken by Pitot tubes for which the measured mean velocity is known to be in error due to turbulence and velocity gradient effects. While hot-wires have a smaller error due to the fluctuating cross-flow, they have other problems which become important as the wall is approached (particularly with calibration at low velocities and heat loss to the wall). In addition, as noted in Chapter 2, a residual dependence of the flow on upstream conditions can not be ruled out from the Reynolds averaged equations. In view of this, the actual values reported need to be refined by further experimentation which takes account of all the factors influencing their determination.

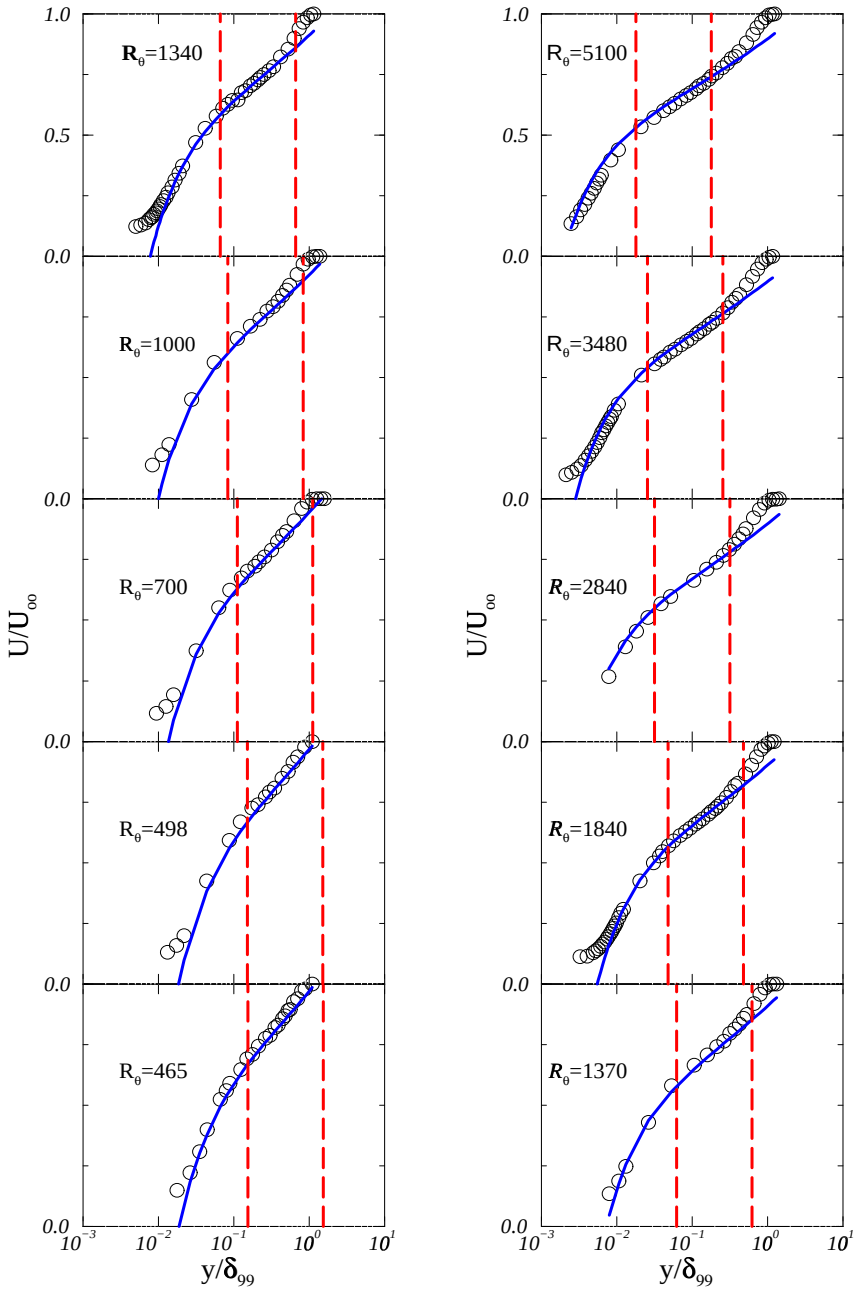

Figure 3.9: Velocity profiles in outer variables together with overlap plus mesolayer theoretical profile, data of Purtell et al. (1981). Dashed vertical lines show the boundaries of mesolayer ($30 < y^+ < 300$).

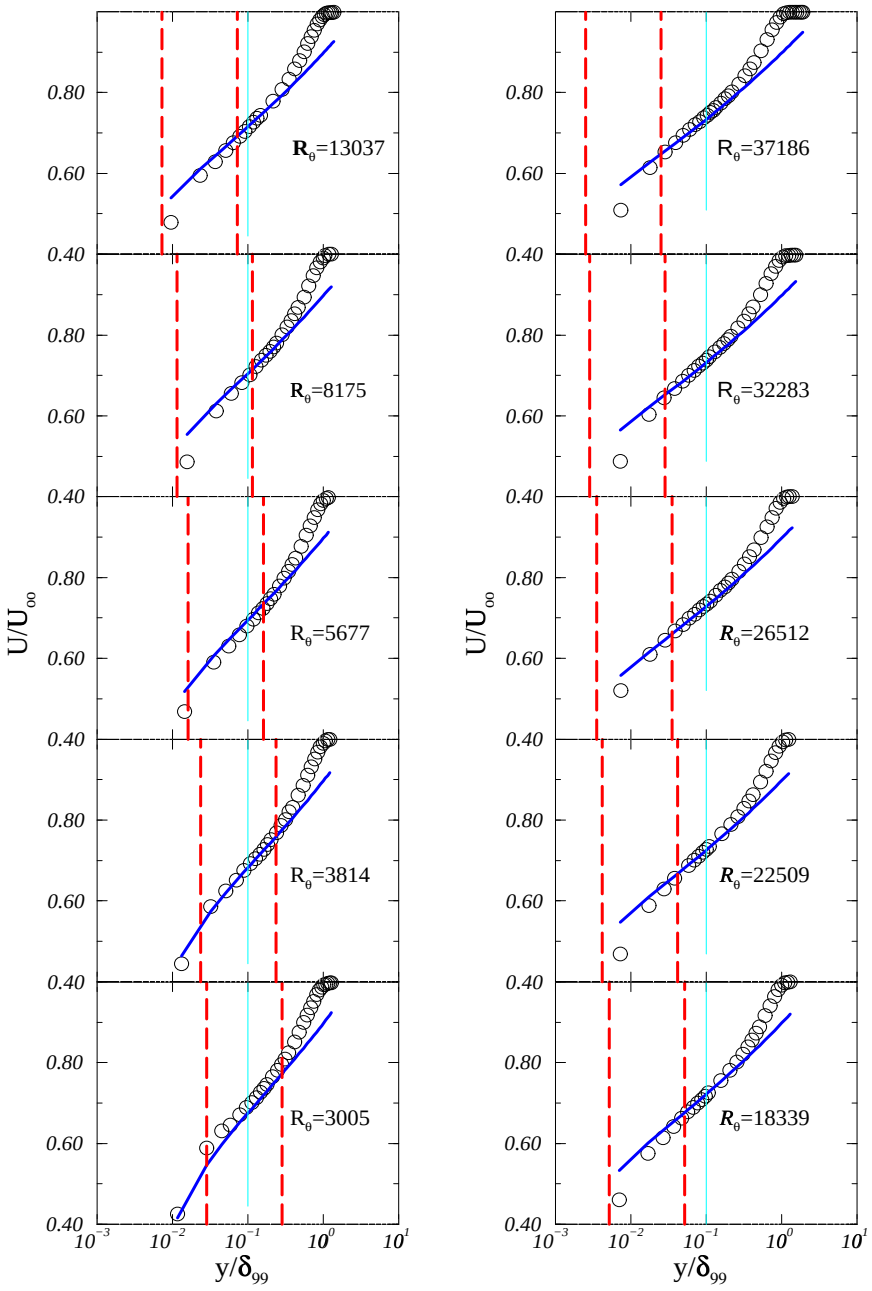

Figure 3.10: Velocity profiles in outer variables together with overlap plus mesolayer theoretical profile, data of Smith/Walker (1959). Dashed vertical lines show the boundaries of mesolayer ($30 < y^+ < 300$), while light solid line marks the outer bound of the overlap region ($\overline{y}$=0.1).

3.6 The Data for the Friction Coefficient

The theoretical friction law is uniquely determined by the ratio C_o/C_i and by γ. But these are all determined by equation 2.70 once the function h is specified. As noted above, there is considerable confusion and disagreement about the shear stress, so in the final optimization above, none of the data (for the low Reynolds number data) were considered reliable and only the theoretical values were used. Thus the theoretical friction law depends only on the empirical choice of the $h - function$ and the parameters determined from the velocity profiles.

Figure 3.11 shows u_*/U_∞ versus R_θ in linear–linear (leftmost) and semilog (rightmost) plots. The theoretical results using equations 3.8, 3.12, and the constants determined above are shown by the solid lines. The experimental data in the upper plots are from the floating element data of Smith/Walker 1959, the force balance data of Schultz-Grunow 1941, and the shear stress computed from the momentum integral data of Wieghardt and Tillman 1944 by Coles 1968. In addition, the data obtained by Spalart 1988 from a DNS simulation of boundary layers at low Reynolds numbers is also included. The agreement between the theoretical result and the experiments is especially remarkable since *NONE* of the data was used in the determination of empirical constants. Interestingly, both sets of data using direct measurement have previously been widely disregarded since they did not agree with the results obtained by applying the Clauser method to the velocity profile data of the same experiments.

The bottom figures of Figure 3.11 show several other data sets which are more or less in agreement with the theory. There is considerable scatter in the results, especially when the velocity gradient estimates from the Purtell et al. data and the Blackwelder/Haridonitis data are considered which are consistently about 15% to 20% low. These low values are due to using values of the velocity to estimate the gradient

above $y^+ = 3$ where the Reynolds stress is already beginning to rapidly appear. Similar behavior of plane wall jet data has been noted by Abrahamsson 1996 using the velocity profile data of Karlsson et al. 1993. These data were of sufficient quality that the differences in shear stress estimates from the gradient could be expressly accounted for by using a Taylor expansion for the velocity at the wall (see below), proving that the percent error was indeed Reynolds number independent.

Particular attention must be paid to the extensive data of Smith/Walker, both because of its quantity and the fact that three different methods were used — direct force measurements using a floating element, calculation from the momentum integral using $d\theta/dx$, and the Clauser method — and, perhaps as important, the data have been conveniently tabulated in the report so there is no uncertainty as to what they really are. The c_f deduced from the Smith/Walker momentum thickness data represents $2d\theta/dx$ (actually $2dR_\theta/dR_x$) obtained from fits to the measured values of R_θ and R_x. The values shown are not those presented by Smith/Walker who fitted a curve to $logR_\theta/logR_x$ as a polynomial in R_x, and obtained results closer to the Clauser method than to their floating element results for the lowest Reynolds numbers. The values shown were obtained by fitting $R_\theta/R_x^{1.167}$ as a polynomial in R_x. (The factor of 1.167 was chosen to correspond approximately to the value of γ over the range of the data and the drag law which would result from it using equation 2.118.) Both of these relations predict nearly the same values of c_f over the highest range of the data, but they diverge for smaller values of R_θ. There is a substantial difference in the extrapolations of these relations to values of $R_\theta < 10^4$: The log-derived curves bend up rather rapidly like the bulk of the data reported using the Clauser method, while the alternative fit yields a curve which passes directly through the lowest Reynolds number velocity gradient estimates of Purtell et al. The obvious

conclusion is: Extrapolations of fits to outside the range of the actual data should not be used since almost any desired result can be obtained. It should be noted that the Clauser method results are also in close agreement with the theory, but only over a limited range in Reynolds number. This is not surprising, since as pointed out in section 2.9, the von Karman/Prandt log profile (with its mixing length origins) is in fact a first approximation to the mesolayer/overlap result around $y^+ = 100$ which is the point most often used in the determination. (In fact, the "effective" value of the von Karman constant from the parameters obtained above is almost exactly 0.42 at $R_\theta = 10^4$.) Unfortunately for very large and very small Reynolds number, the variation of C_i and γ with Reynolds number seriously erodes the accuracy of the approximation, so the friction estimates from this method are not reliable.

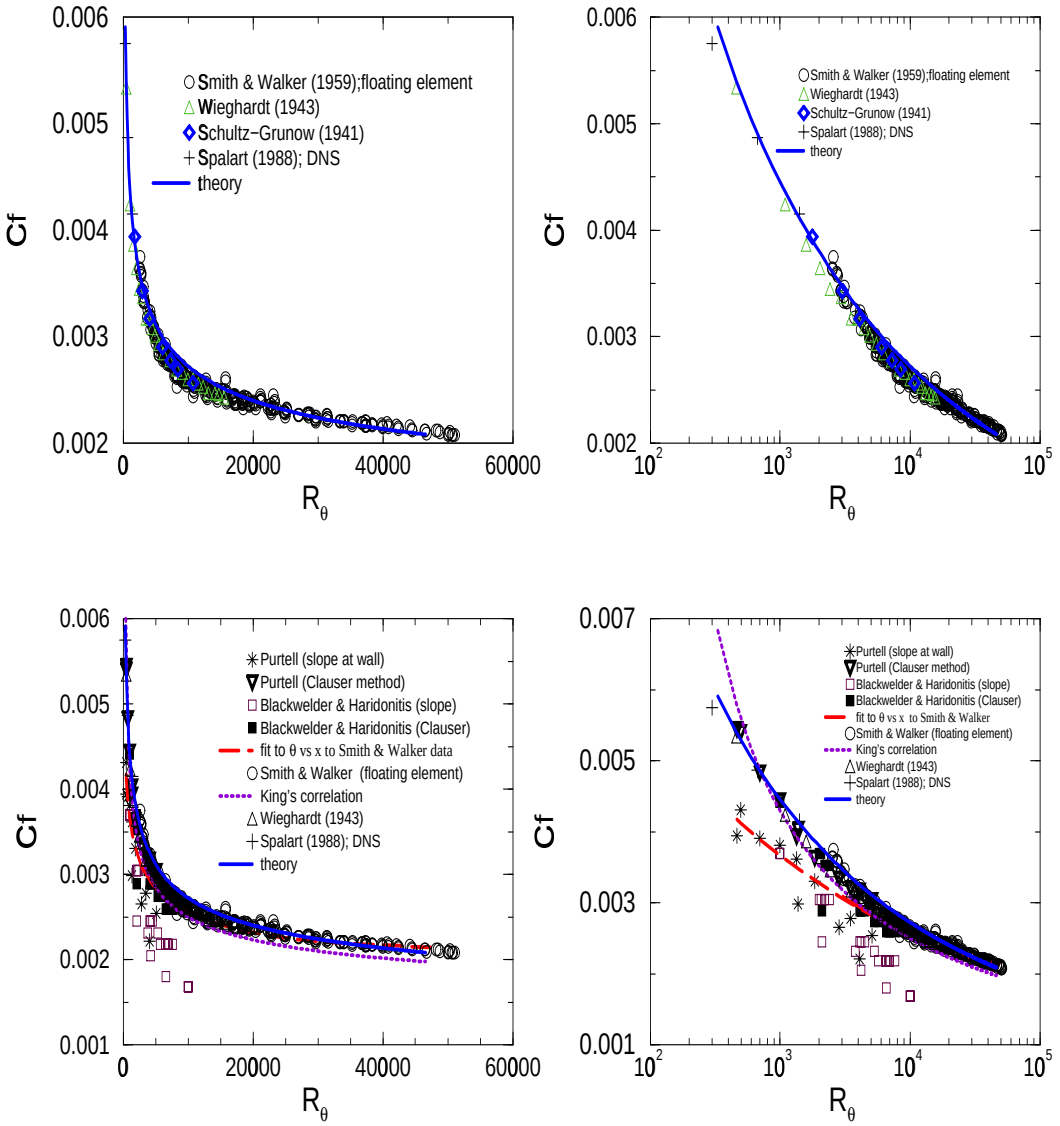

Figure 3.11: The skin friction coefficient as function of R_θ. (Left: linear-linear, Right: semi-log)

3.7 Empirical Velocity Profiles for the Wake and Buffer Regions.

A velocity profile valid over the entire flow can be obtained using equation 2.97 if empirical relations are introduced to account for the variation of $f_o(\overline{y}, \delta^+)$ outside the overlap layer and $f_i(y^+, \delta^+)$ inside it, This is exactly analogous to the use of the van Driest equation for the mixing length, the arctan profile for the Law of the Wall, or Coles Wake Function for the outer layer. All seek to use an empirical relation to splice together the various regions of the flow so that a continuous profile is obtained.

The part of the inner layer between the linear region and the inertial sublayer and the old log layer has often been referred to as the buffer layer. The same terminology will be used here to refer to the region of adjustment from linear to the meso/overlap region. A useful expression which makes this transition smoothly and in good agreement with the Purtell et al. data is given by

$$f_i(y^+) = y^+ exp(-dy^{+5}) + (C_i y^{+\gamma} + \frac{C_{mi}}{y^+})[1 - exp(-dy^{+5})] \tag{3.13}$$

The y^{+5}-dependence of the exponentials allows not only the no-slip condition to be satisfied at the wall, but also the boundary conditions on the first four velocity derivatives if the damping parameter d is chosen as

$$d = c_4/C_{mi} \tag{3.14}$$

where c_4 is the coefficient of the fourth order term in an expansion of the velocity at the wall (i.e., $u^+ = y^+ + c_4 y^{+4} + \cdots$). For the curves shown in this paper $d = 0.00002$ and the mesolayer constant was $C_{mi} = -37$, corresponding to $c_4 = -0.00074$. The value for c_4 is very difficult to determine with any accuracy, but was estimated from the data of Purtell et al.

3.8 The New Law of the Wake

In this section a new wake function which describes the outer flow will be proposed. For that portion of the boundary layer outside the log layer, Coles 1956 defined a "wake function" to account for the difference between the actual velocity profile and the log behavior. Similarly, a wake function can be defined here for the outer flow by subtracting the overlap solution in outer variables from the velocity normalized by U_∞. The resulting wake function is given by

$$w(\overline{y}, \delta^+) = \frac{U}{U_\infty} - C_o \overline{y}^\gamma \tag{3.15}$$

(Note that the term "wake" is probably not a great choice given our new understanding of this region, since θ is not constant, but continues to increase with x.)

The topmost plot of Figure 3.12 shows the velocity profile data of Purtell et al. and Smith/Walker plotted as $U/U_\infty - C_o\overline{y}^\gamma$ versus $\overline{y}$. The overlap region (or power law layer) manifests itself as the region for which the velocity difference, $U/U_\infty - C_o\overline{y}^\gamma$ is zero. The sharp drop for small $\overline{y}$ occurs in the viscous sublayer, while the region for $\overline{y} > 0.1$ approximately is the 'wake'. Two features are evident: Clearly there is an asymptotic wake function for $R_\theta > 3000$. Second, as the Reynolds number is reduced below this value, the wake begins to disappear, and is completely gone by $R_\theta = 500$ or so. This phenomenon was noted in Figures 3.9, and has also been observed by others using the "log" formulation (eg. Murlis and Bradshaw 1982). It is due to the effects of viscosity on the outer flow discussed in section 2.8, and particularly the failure of the dissipation to achieve a q^3/L form at these Reynolds numbers.

The bottommost plot of Figure 3.12 shows that simply dividing the data plotted above by the factor $1 - C_o$ collapses all the profiles for all Reynolds numbers between $Re = 465$ and $Re = 48,292$ on a single curve, at least for all values $\overline{y} \leq 1$ (to within

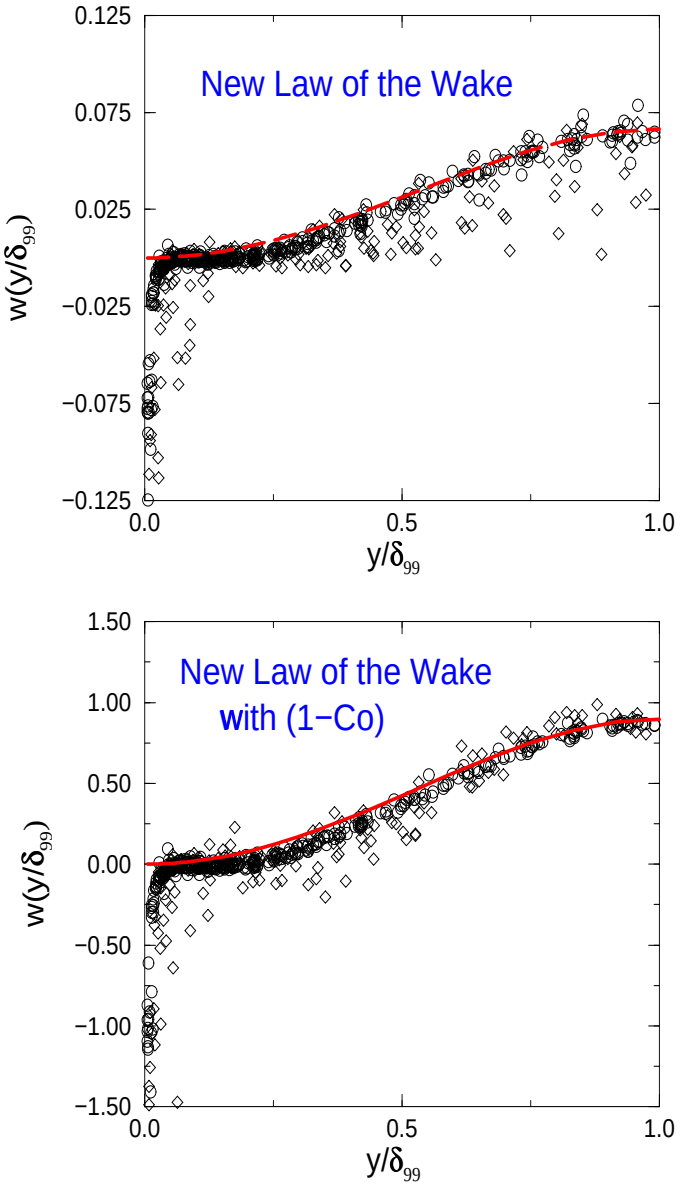

Figure 3.12: New law of the wake representation: $w(\overline{y}) = \overline{U} - C_o\overline{y}^{\gamma}$; $\diamond$ Purtell et al. (1981) and $\circ$ Smith/Walker (1959). The bottom graph is the wake normalized by $(1 - C_o)$, and top one without it. The long dashed line is the new wake function given by $w(\overline{y}) = (1 - C_o)\overline{y}\,\sin(B\overline{y})$ where B=2.026. The line in the bottom figure is the same function without the $(1 - C_o)$ term, since the data has been normalized by $(1 - C_o)$.

the scatter of the data). The large scatter for the lowest Reynolds number data is because both the wake and the factor $1 - C_o$ are very close to zero. There is no theoretical justification for this factor, although its use can be motivated by noting that it provides exactly the amount necessary to adjust the contribution of the power law to unity at $\overline{y} = 1$. The previously noted increase toward unity of C_o for small values of R_θ insures that the wake vanishes in this limit.

The success of the simple scaling factor above in collapsing the wake to a single curve means that a single empirical expression to describe this region is possible. Ideally a closed form solution to the outer similarity equation for the mean flow would be available, say one based on an eddy viscosity, for example. In the absence of that, a simple (and easily integrable) expression for the wake function which accounts for the observed behavior is given by

$$w(\overline{y}) = (1 - C_o)\overline{y} \sin B\overline{y} \tag{3.16}$$

The parameter B and the upper limit of applicability of this relation, say y_m can even be chosen to insure that $U/U_\infty = 1$ and $dU/dy = 0$ at $\overline{y} = y_m$. The disadvantage of this choice is that B depends on Reynolds number. An excellent compromise choice for all Reynolds numbers and $\overline{y} \leq 1$ is $B = 2.03$. The wake profile of equation 3.16 with this value for B is plotted together with the data in the bottom figure of Figure 3.12.

Substitution of equation 3.16 yields the complete outer velocity profile as

$$\frac{U}{U_\infty} = C_o \overline{y}^\gamma + (1 - C_o)\overline{y} \sin B\overline{y} \tag{3.17}$$

3.9 The Composite Velocity Profile

The profiles from the inner flow and outer flow from previous sections can be used to construct an analytical function for the entire velocity profile which captures the Reynolds number dependence of the flow. The result is (in outer variables)

$$\begin{aligned}\frac{U}{U_\infty} &= F_{co}(\overline{y};\delta^+) = (1-C_o)\overline{y}\sin B\overline{y} \\ &+\frac{u_*}{U_\infty}\{\overline{y}\delta^+ exp[-d(\overline{y}\delta^+)^5] + [C_i(\overline{y}\delta^+)^\gamma + C_{mi}(\overline{y}\delta^+)^{-1}] \\ &[1-exp\{-d(\overline{y}\delta^+)^5\}] - C_i {y^+}^\gamma\} \end{aligned} \tag{3.18}$$

where u_*/U_∞ is given by the friction law.

Note that $d = c_4/C_{mi} = 2.0E-05$ and $C_{mi} = -37$. Thus the entire velocity profile is described from $0 \le \overline{y} \le 1$, or for all values of y out to $y = \delta_{99}$.

Alternatively; the composite velocity can be written in inner variables as

$$\begin{aligned}\frac{U}{u_*} = F_{ci}(y^+;\delta^+) &= \Big[C_i {y^+}^\gamma + \frac{C_{mi}}{y^+}\Big]\Big[1-exp(-d{y^+}^5)\Big] \\ &+y^+ exp(-d{y^+}^5) + \frac{U_\infty}{u_*}(1-C_o)y^+ sin(\frac{B}{\delta^+}y^+) \end{aligned} \tag{3.19}$$

Figures 3.13 through 3.16 show the velocity data of Purtell et al. and Smith/Walker in outer variables, and the composite velocity of equation 3.18 using parameter values obtained in the preceding section. Note that the roll-off for small values of $\overline{y}$ in the Smith/Walker data (Figures 3.15 and 3.16) is due to their inability to measure close to the wall, which for some data sets is outside where the buffer region and mesolayer are located, hence the deviation from the composite solution for the first data point. Also, there is a slight underestimate (about 5%) around $y^+ = 10$ which probably represents a shortcoming of the exponential interpolation formula from the viscous

sublayer to the the mesolayer. Figure 3.17 is the velocity data of Purtell et al. 1981 in inner variables using equation 3.19.

Overall, the agreement of the composite profile must be considered quite good over the entire Reynolds number range, and throughout the entire boundary layer. And this agreement was assumed in the final regression which determined the parameters. It is rather remarkable that a theory with only four parameters and a single empirical function (h) can describe the entire boundary layer, including the shear stress, over more than two decades in Reynolds number. Recall that the old theory uses only three parameters, BUT it did not include the mesolayer parameter, AND most importantly, it treated both the shear stress and boundary layer thickness as variables to be determined for the best fit to each profile. No such juggling is necessary here, and the results would seem to provide a strong indication that both the theory and empirical interpolations are consistent with the data.

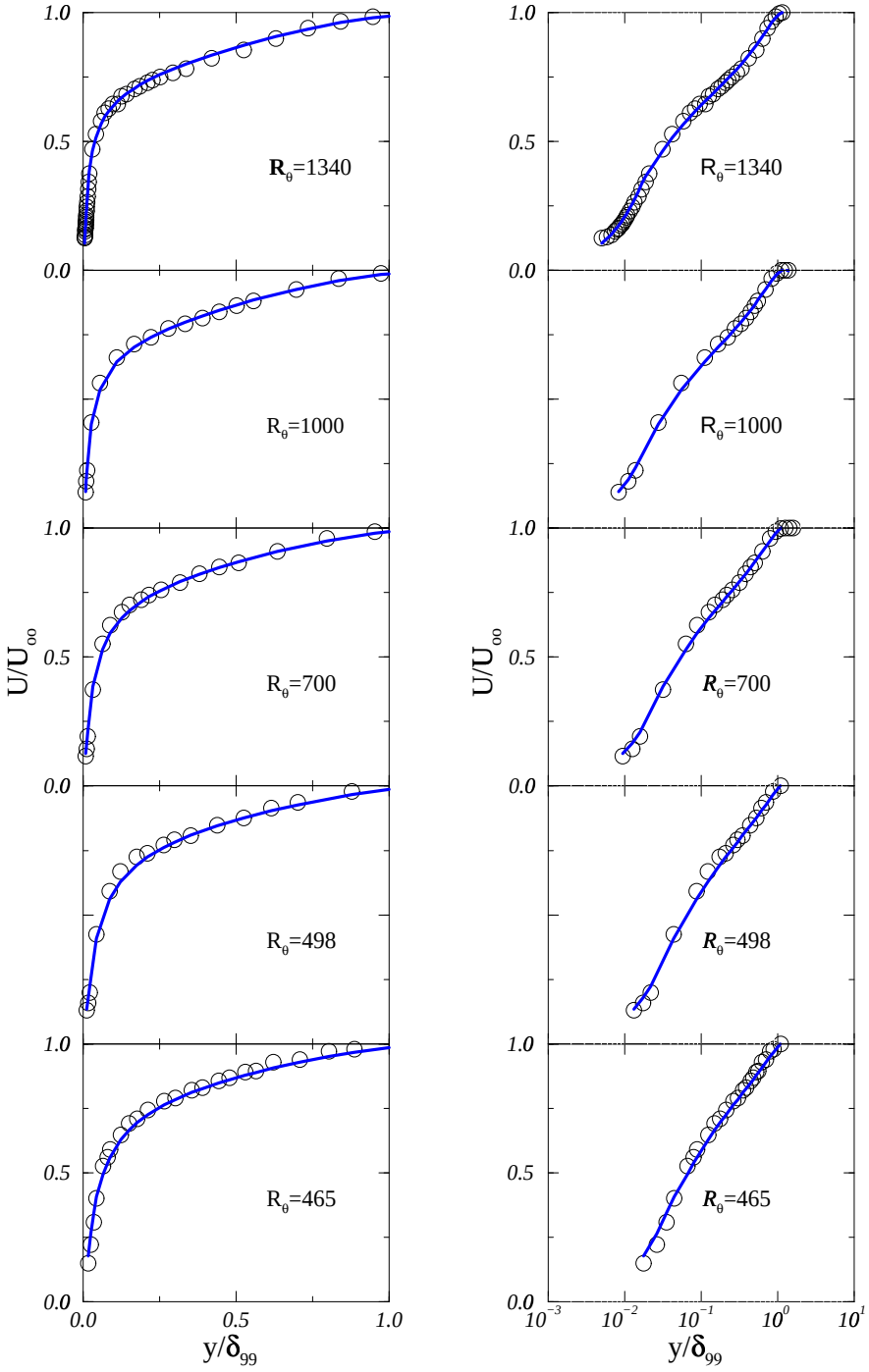

Figure 3.13: Purtell et al. (1981) data in outer variables with the theoretical profile.

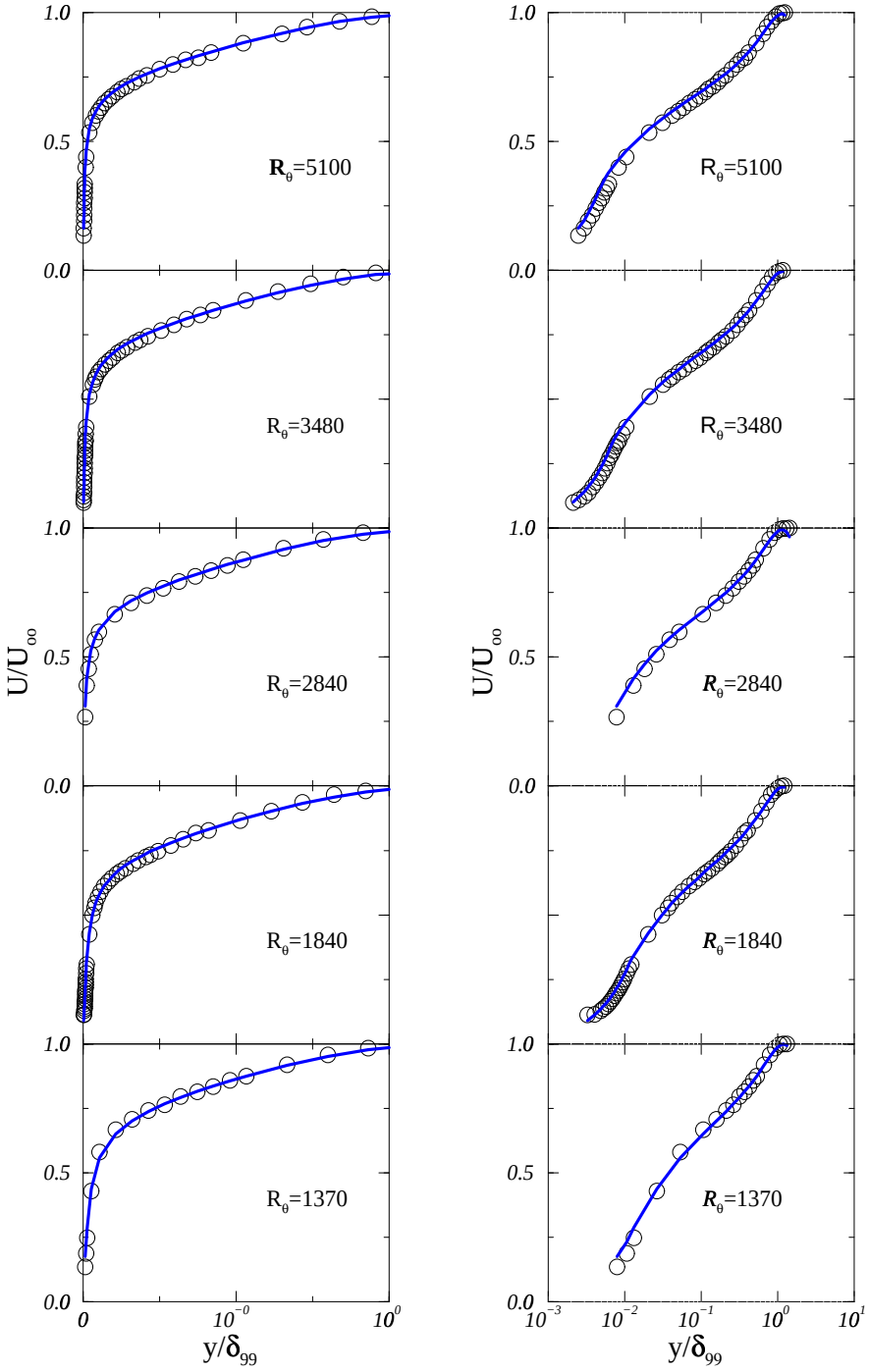

Figure 3.14: Purtell et al.(1981) data in outer variables with the theoretical profile.

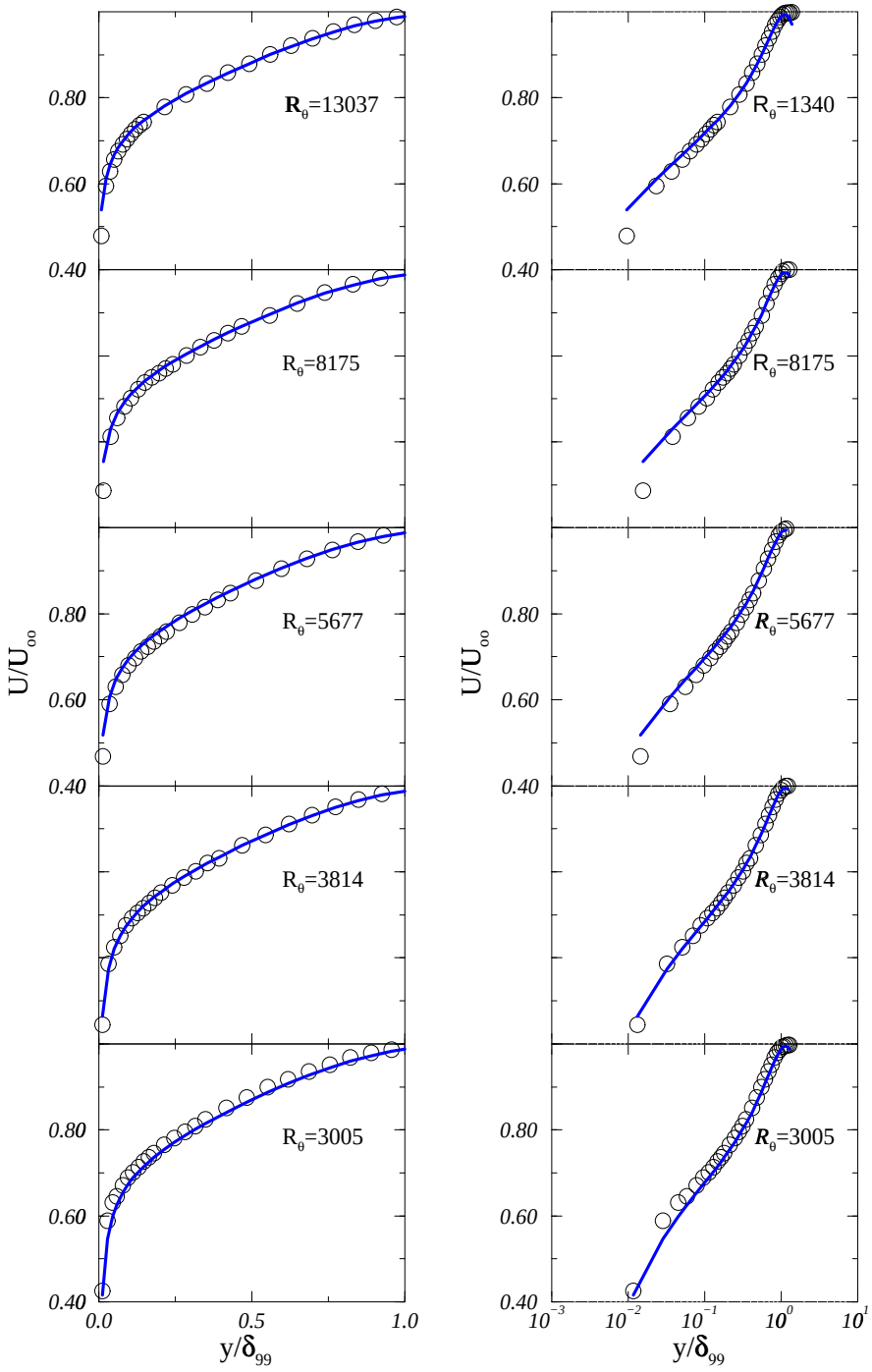

Figure 3.15: Smith/Walker (1959) data in outer variables with the theoretical profile.

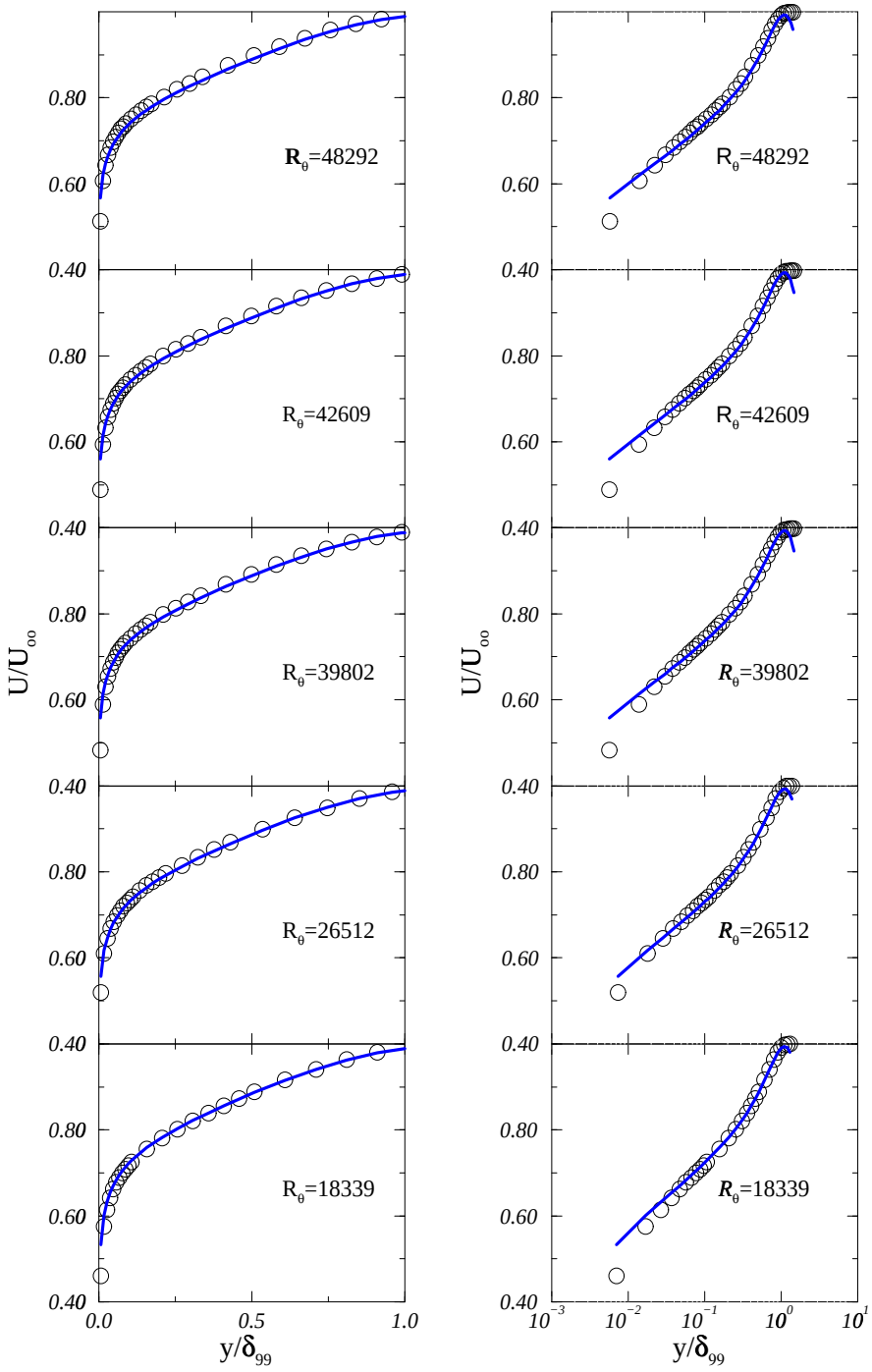

Figure 3.16: Smith/Walker (1959) data in outer variables with the theoretical profile.

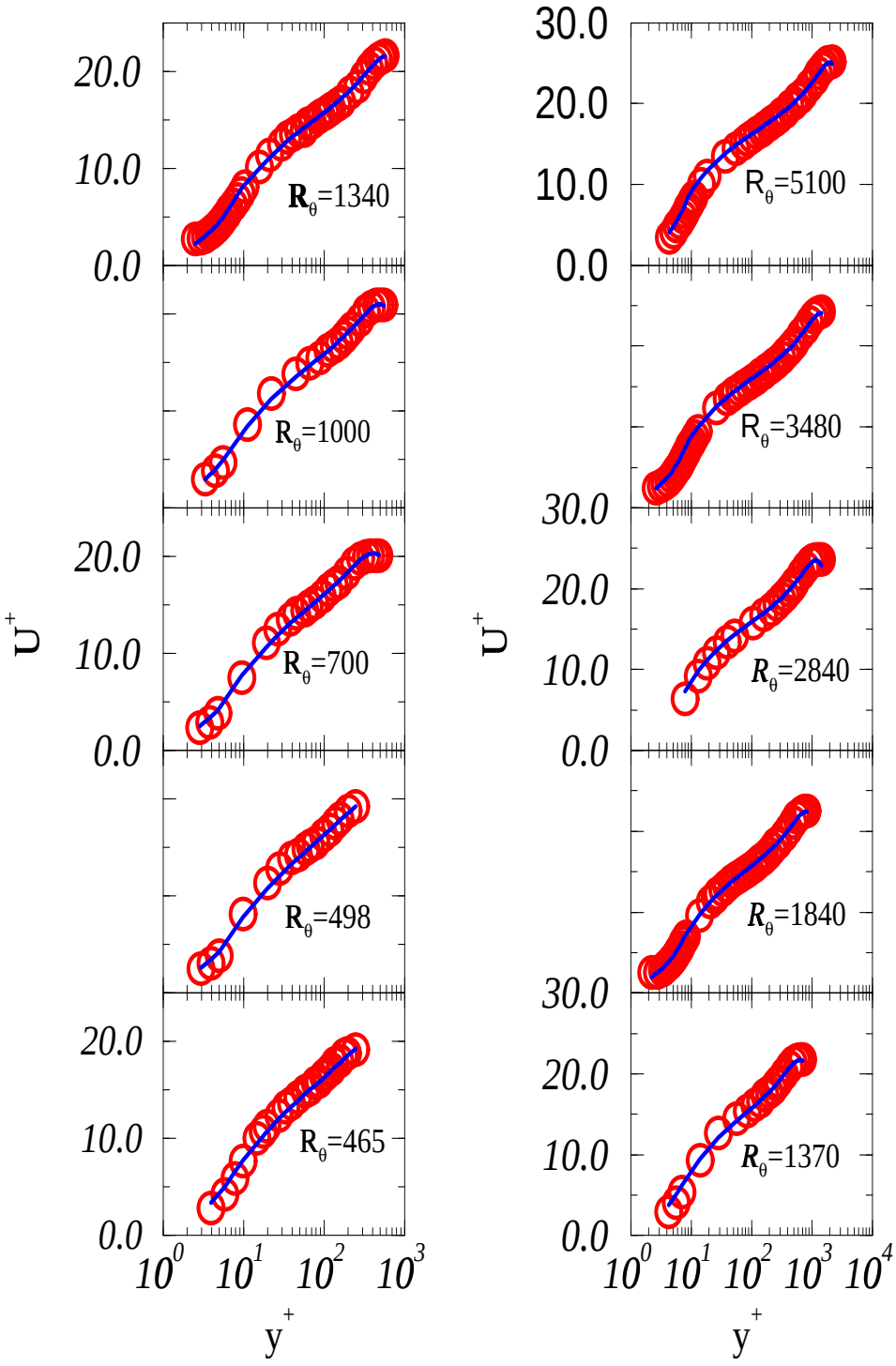

Figure 3.17: Purtell et al. (1981) data in inner variables with the theoretical profile.

3.10 Integral Boundary Layer Parameters

Figure 3.18 shows δ_*/δ, θ/δ, and the shape factor δ_*/θ versus both δ^+ (leftmost) and R_θ (rightmost). The data are from Smith/Walker (1959), Purtell et al. (1981), and Wieghardt (1943). The solid line indicates the theoretical values obtained by integrating numerically the theoretical profiles shown in Figures 3.13 - 3.16. As before, δ is taken to be δ_{99}. Clearly the data and theory are in good agreement. This is not surprising in view of the excellent agreement between the theoretical and experimental velocity profiles. The consistency of the results should restore some credibility to the much-maligned δ_{99} as a reasonable length scale. Note, however, the failure of the data from different experiments to perfectly overlap, indicating perhaps some residual effect of initial conditions which is also present in the c_f data.

It is convenient to have analytical formulas for the integral thicknesses, and this is possible. The empirical profiles given by equations 3.13 and 3.17 can be substituted directly into the integrals arising from the displacement and momentum integral thicknesses, equations 2.102, 2.103, 2.110, 2.111, and 2.112. The major contribution except for the lowest Reynolds number flows is due to the leading terms so that

$$\frac{\delta_*}{\delta} \approx -I_1 \tag{3.20}$$

$$\frac{\theta}{\delta} \approx -I_1 - I_3 \tag{3.21}$$

I_1 and I_3 can easily be integrated analytically to obtain

$$-I_1 = 1 - \frac{C_o}{1+\gamma} - (1-C_o)I_6 \tag{3.22}$$

$$I_3 = 1 - \frac{2C_o}{1+\gamma} + \frac{C_o^2}{1+2\gamma} + (1-C_o)^2[I_7 - 2I_6] \tag{3.23}$$

where

$$I_6 = \frac{\sin B - BcosB}{B^2} \tag{3.24}$$

$$I_7 = \frac{1}{6} - \frac{\sin 2B}{4B} - \frac{\cos 2B}{4B^2} + \frac{\sin 2B}{8B^3} \tag{3.25}$$

Using $B = 2.03$ implies that $I_6 = 0.436$, $I_7 = 0.289$. Since the contribution of a finite value of γ to the last term of equation 3.21 is very small, an excellent approximation can be obtained by setting $\gamma = 0$ (but in this term only). These values and the last approximation yield

$$-I_1 = 1 - \frac{C_o}{1+\gamma} + 0.436(1 - C_o) \tag{3.26}$$

$$I_3 \approx [1 - 0.582(1 - C_o)^2] - \frac{2C_o}{1+\gamma} + \frac{C_o^2}{1+\gamma} \tag{3.27}$$

from which δ_*/δ and θ/δ can easily be computed for any value of δ^+. The results are are in near perfect agreement with both the data and the theoretical curve shown in Figure 16 for $\delta^+ > 2000$ or $R_\theta > 3000$ approximately. Below these values, the neglected terms from the inner region cause both δ_* and θ to be underestimated.

The asymptotic values of I_1 and I_3 can readily be estimated using the asymptotic values for γ and C_o obtained above. The result is $I_{1\infty} = -0.0894$ and $I_{3\infty} = 0.0128$. It follows immediately that asymptotically

$$\frac{\delta_*}{\delta} \rightarrow 0.0894 \tag{3.28}$$

$$\frac{\theta}{\delta} \rightarrow 0.0767 \tag{3.29}$$

$$H \rightarrow 1.17 \quad . \tag{3.30}$$

The asymptotic values are well below those values of the data in Figure 3.18 indicating again that the asymptotic boundary layer is reached only at much higher Reynolds numbers than for which data is available. Interestingly, the asymptotic value of H is very close to those obtained by Kempf (1932) (see also Smith and Walker 1959) at Reynolds numbers more than an order of magnitude above that of the data utilized here.

One advantage of having analytical expressions for δ_*/δ and θ/δ (or I_1 and I_3) is that δ^+ can be computed for given values of R_{δ_*} or R_θ. This was done to produce Figure 3.19 using equations 3.8, 3.20, 3.21 and the final approximate forms for I_1 and I_3 derived above. Also shown for comparison are the results from the profile integration. As expected the agreement is excellent above $\delta^+ > 2000$ and $R_\theta = 3000$.

Finally, Figure 3.20 shows R_θ versus R_x from a numerical integration of equation 2.118 using equation 2.70 with the constants determined earlier. Also shown in the figure are the data of Smith and Walker. No attempt has been made to adjust for virtual origin in x by choosing a non-zero value for R_o. Obviously, the agreement is excellent over the the entire range of the data. Thus, unlike in other theories, momentum appears to be conserved.

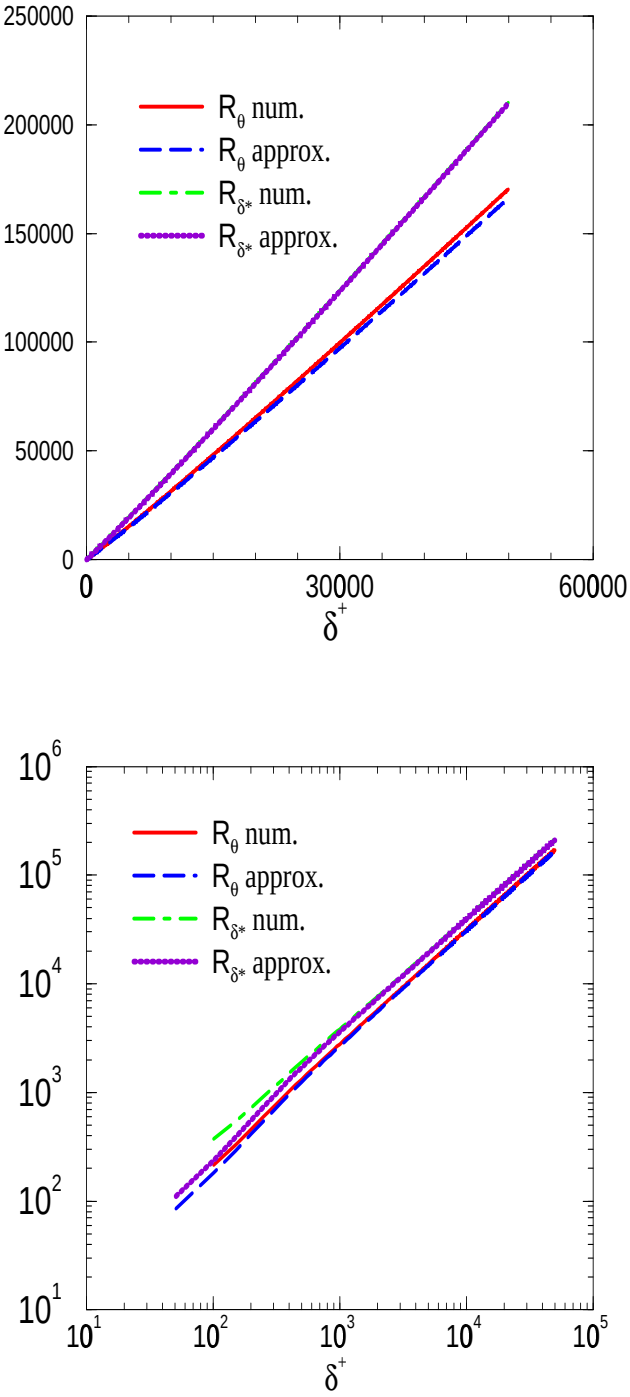

Figure 3.18: Variation of $R_{\delta*}$ and R_θ as function of δ^+ using numerical integration of composite profile and analytical approximations. (topmost: linear-linear; bottom-most: log-log)

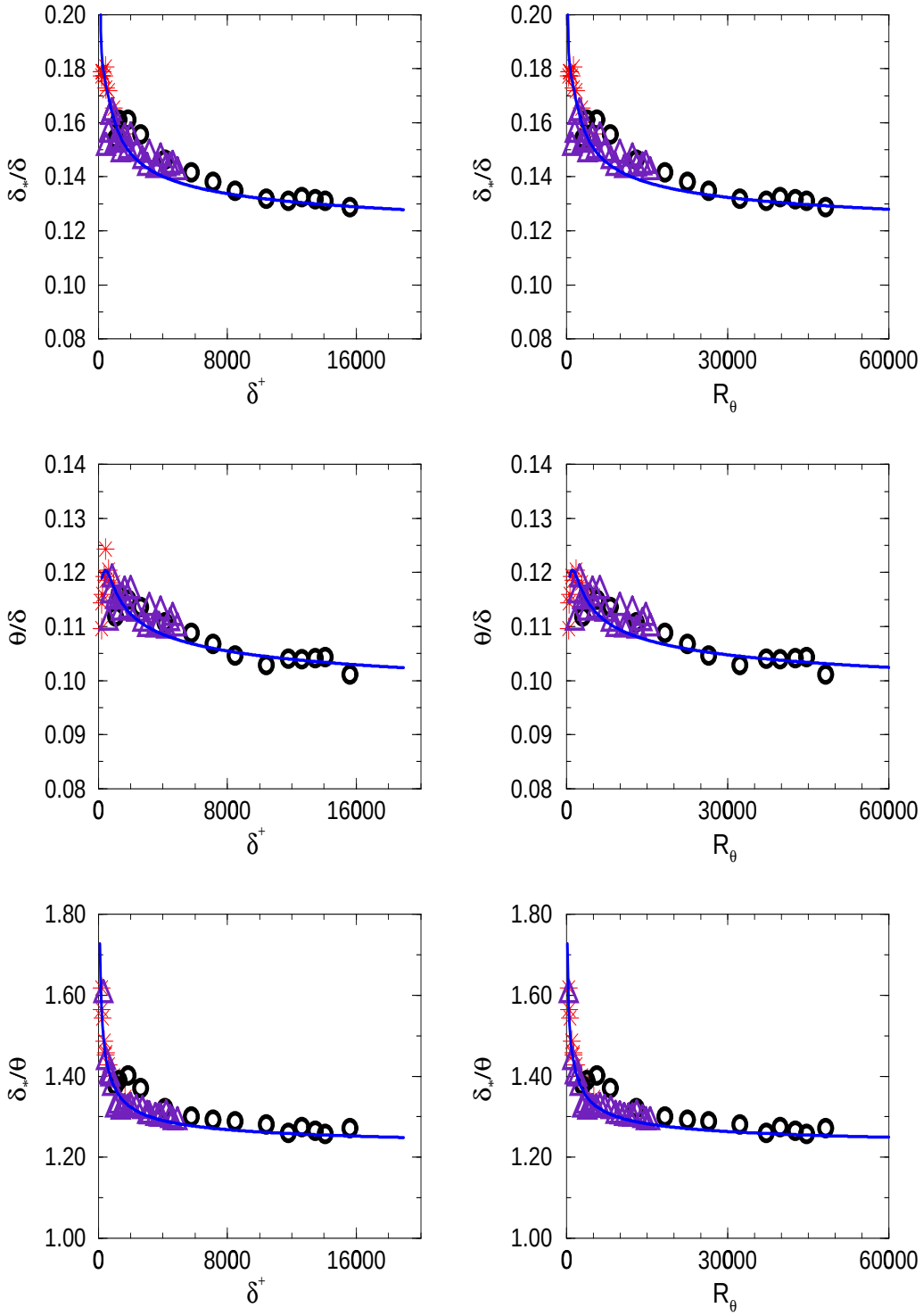

Figure 3.19: Boundary layer integral parameters; ∘ Smith/Walker (1954), ∗ Purtell et al. (1981), △ Wieghardt (1943); line (*theory*).

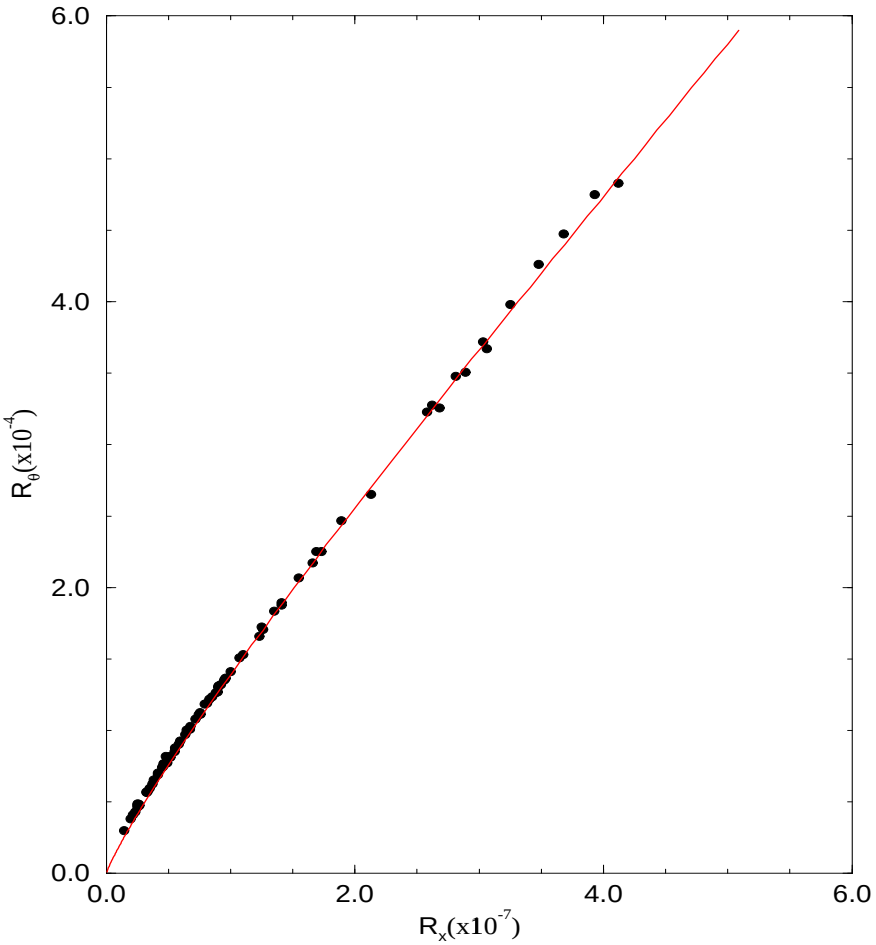

Figure 3.20: The x-dependence of the boundary layer. Smith/Walker data (1959), line (theory).

3.11 The Turbulence Quantities

There have been numerous papers written on the failure of the classical scaling laws to collapse the moments of fluctuating quantities in the wall region (by which is usually meant the "log" region as well as the buffer layer between it and the linear layer). Among the most troublesome quantities are the variances of the streamwise fluctuating velocities and the Reynolds stress (eg., Klewicki and Falco 1993, Bradshaw 1990, Spalart 1988). More recently problems with the behavior of two-point correlations in the wall region have been noted by Blackwelder 1993. Klewicki and Falco conclude:

- "In general, inner variable normalizations of statistical profiles derived from the u and v fluctuations and the uv shear product do not produce invariant curves in the inner and near-wall regions of the boundary layer over the given R_θ range ($1000 < R_\theta < 5000$)."

- "Both the peak value and the y^+ position of the peak value of the u'/u_*, v'/u_*, and $< uv > /u_*^2$ profiles increased with increasing R_θ."

- "The present measurements support the hypothesis that for y^+ less than about 50 and with inner variable normalization, the statistical characteristics of single point spanwise vorticity measurements are invariant over the given R_θ range."

All of these observations for the single-point statistics are consistent with the theory put forth here. The reason quite simply is that the mesolayer and overlap layers can not be considered to be Reynolds number independent in either inner or outer variables for any *finite* Reynolds number. As a consequence, any measurements outside the viscous sublayer — roughly the linear region — and inside the deficit region, should be expected to display Reynolds number dependencies, whatever the

quantity measured. For some quantities, like the mean velocity and vorticity, the Reynolds number dependence of the overlap range is hardly perceptible; for others, like the Reynolds stresses it is obvious. Since the velocity scale ratio, u_*/U_∞, varies more rapidly as the Reynolds number is reduced, these effects will be more pronounced at lower Reynolds numbers.

The theory put forth here has suggested that similarity of the turbulence quantities in the outer layer occurs only at Reynolds numbers high enough for the dissipation and Reynolds stresses to be effectively inviscid. While it is difficult to quantify this, it is generally assumed in turbulence that this occurs only when the turbulence Reynolds number, ul/ν, is on the order of 10^4 or larger (c.f. Batchelor 1953). Since $u \sim u_*$ and $l \sim \theta$, this requires values of R_θ of 10^5 or larger for these conditions to be met. This is well beyond the range of any experiments to-date. The theory does suggest, however, some alternatives which might work before this is reached. These different scalings for the turbulence quantities in the outer layer follow directly from the transformed equations and depend on both u_* and U_∞. The normal stresses, for example, scale as U_∞^2, while the Reynolds shear stress scales (to first order) with u_*^2. Note that nothing should be expected to collapse in the overlap region since it depends on both u_* and U_∞. However the fact that u_*/U_∞ varies more slowly with increasing R_θ might lead to the erroneous conclusion that an asymptote is being approached.

Figure 21 shows the rms streamwise fluctuating velocity measurements of Purtell et al. 1981 normalized by U_∞. It is clear that the collapse is remarkable for $\overline{y} > 0.5$ for all Reynolds numbers, and the region of collapse moves towards the wall with increasing Reynolds numbers (just as for the mean velocity profiles above). The same data normalized with u_* appears in the paper of Purtell et al 1981 and there is little evidence of even a trend toward collapse in the outer part of the flow. A similar

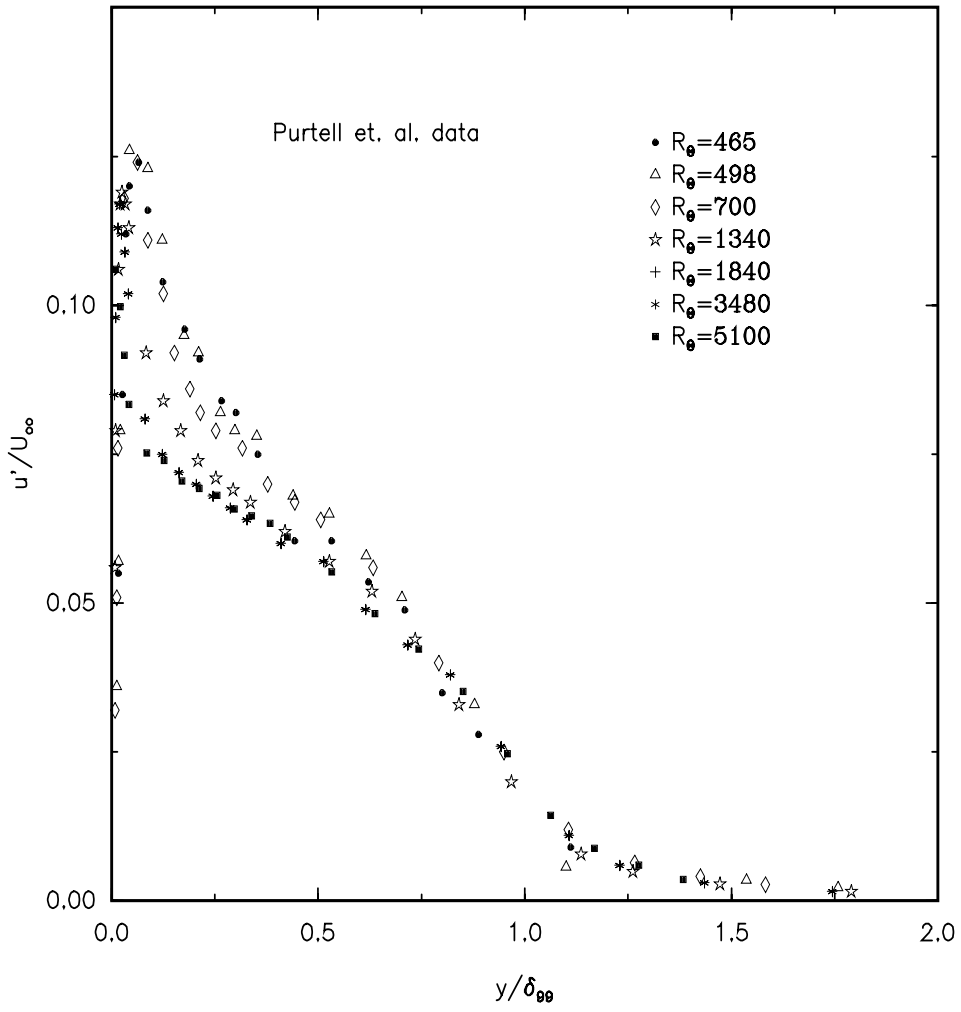

Figure 3.21: Turbulence intensity scaled with U_∞, data of Purtell et al. (1981).

failure of the u_* scaling for the normal Reynolds stresses in the outer part of the flow was noted by Smith 1994. Even more significantly, Smith (1994) shows that the production ($- < uv > dU/dy$) collapses in the outer region about the same when normalized by either $u_*^2 U_\infty/\delta$ or U_∞^3/δ. consistent with the fact that the outer layer is governed by two velocity scales and similarity is possible only in the limit when their ratio is constant.

Balint et al. 1991 show several attempts to collapse measurements of the mean square vorticity components over the outer layer, none of which are very successful. Most interesting though is that when the outer rms vorticity components were scaled with u_*^2/ν the order of the curves was reversed from when they were scaled with U_∞/δ. Thus the proper scaling (if there is one at all) is some combination of these. If the assumption of locally homogeneous turbulence is made, then the mean square vorticity is given by (v. George and Hussein 1991),

$$< \omega_i \omega_i >= \epsilon/\nu \tag{3.31}$$

where ϵ is the rate of dissipation of turbulence energy. Thus the vorticity in the outer layer should scale with the dissipation. From equations 2.29, 2.32 and 2.33 it follows that the dissipation scales as

$$D_s \sim U_\infty^3 \frac{d\delta}{dx} \sim U_\infty u_*^2 \tag{3.32}$$

Thus the rms vorticity in the outer region should scale as

$$< \omega_i \omega_i >^{1/2} \sim (u_*^2 U_\infty/\nu\delta)^{1/2} \tag{3.33}$$

Figure 22 shows a plot of the vorticity measurements of Klewicki and Falco 1990 using the outer scaling of equation 3.33. The values of wall shear stress used were those provided in the paper, and were quite close to the values computed from the

friction law determined herein. The lack of collapse of the lowest Reynolds number data might be associated with the disappearance of the wake function noted above. In particular, the Reynolds number dependent constant D_o in equation 2.82 may be sufficiently different from its asymptotic value at this low Reynolds number so that u_*^2 alone is not the right parameter. Alternatively, it may represent a problem with the flow or the measurements (background vorticity or noise) since a constant subtracted from this data set yields curves much like those for the velocity deficit. Of course, u_* itself may simply be in error; or the proposed theory incorrect.

The two point velocity correlation measurements in the wall region of Blackwelder (1993) provide further substantiation for the ideas presented here. Briefly, it is observed that for small values of separation in horizontal planes, the two point correlations appear to collapse in wall variables, while for large separations they do not. Moreover, at large separations the magnitudes of the correlations still show a strong Reynolds number dependence, even when re-scaled with the usual outer variables, u_* and δ. In particular, the amount of correlation at large separations increases with Reynolds number. This behavior can easily be understood in the context of the new theory presented here. The large separations are primarily the "foot-print" of the outer boundary layer motions and so should scale in outer variables. If both inner and outer velocity scales were the same, then no Reynolds number dependence of the amplitude would be possible and the shape of the correlation at large separations should be Reynolds number independent. If, on the other hand, the outer velocity scale for the energy is not u_*^2, but U_∞^2 as suggested earlier, then the shape of the velocity correlation functions at large separations should exhibit the Reynolds number dependence observed.

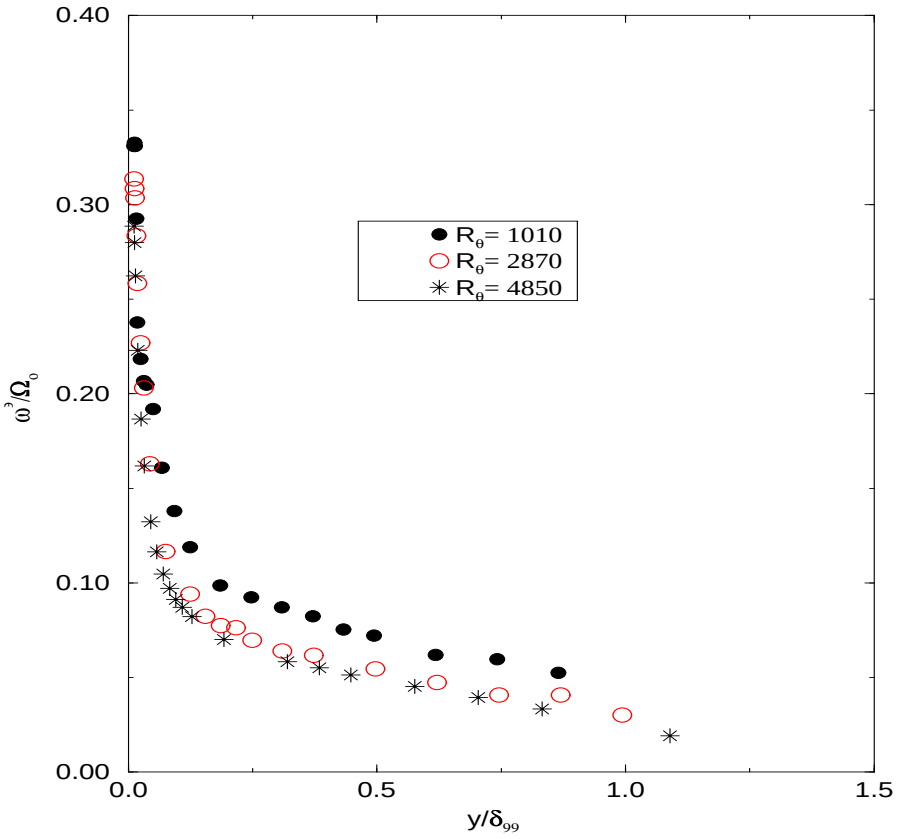

Figure 3.22: The rms of vorticity fluctuations scaled with Ω_o, data of Klewicki (1988).

The pressure fluctuations on the wall and near it have presented somewhat of a dilemma for the conventional theories because they do not scale in inner parameters, u_* and ν, alone. From the perspective of the theory presented here, these represent interesting examples of single point statistics which should not be expected to scale in local variables. This is because the pressure fluctuations are not governed by the same equations as the quantities for which the scaling arguments were derived. In fact, they are governed by a Poisson equation, the solution of which involves both an integral over the entire flow, and one over the wall (Batchelor 1967). Both of these integrals involve two points, the one under consideration, and the integration variable. Thus, only a two-point similarity analysis will suffice, and the considerations above are immediately applicable with the result that both inner and outer scales govern these quantities. Bradshaw 1967 hypothesized the existence of "inactive turbulent motions" and the "splat effect", the former recognizing that large energetic scales from outside the wall layer contribute to pressure fluctuations, and the latter accounting for the effect of the wall through the kinematic boundary condition. The idea of inactive motions is especially interesting because it anticipates the fact that the kinetic energy and Reynolds stress scale differently in the outer flow than in the inner. All these ideas follow naturally from the two point similarity considerations and the AIP, so unlike the classical approach, no new hypotheses need to be invoked to explain them.

Finally, the two point statistics also provide evidence for the mesolayer arguments put forth earlier. The one-dimensional velocity spectral measurements of Folz et al. (1996) show clearly the emergence of the $k^{-5/3}$ range for values of y^+ greater than a few hundred. Similar observations at much lower Reynolds number have been made by a number of investigators (eg., Perry et al. 1985, Smith 1994).

Chapter 4

PGBL: The Outer Region

The methodology utilized in chapter 2 will be applied to the outer boundary layers equations with pressure gradient in order to determine the length, velocity and Reynolds stress scales in outer variables.[1] A new definition of the *Equilibrium Boundary Layer* will be shown to fall naturally out of the equations. Many flows previously not believed to be in equilibrium will be seen to be so according to the new definition.[2]

4.1 Full Similarity of the Outer Equations

In accordance with the Asymptotic Invariance Principle, solutions will be sought which reduce to similarity solutions of the outer momentum equation and boundary conditions in the limit of infinite Reynolds number. It is important to remember that unlike the analysis of Clauser 1956 or Townsend 1956 (see also Tennekes and Lumley 1972), no scaling laws will be assumed at the outset. Rather scaling parameters will be derived from the conditions for similarity of the equations thus insuring that the

[1] The similarity analysis for boundary layer with pressure gradient in inner variables will be given in the next chapter.

[2] Chapters 4 and 5 extend the work of George and Castillo 1993.

scaled profiles are invariant in the limit. The outer equations and boundary conditions appropriate to a turbulent boundary layer at high Reynolds number with pressure gradient are given by

$$U\frac{\partial U}{\partial x}+V\frac{\partial U}{\partial y}=-\frac{1}{\rho}\frac{dP_\infty}{dx}+\frac{\partial}{\partial y}\left[-<uv>\right] \tag{4.1}$$

where $U\rightarrow U_\infty$ and $-<uv>\rightarrow 0$ as $y\rightarrow\infty$.

For the outer equations, solutions are sought which are of the form

$$U-U_\infty = U_{so}(x)f_{op\infty}(\overline{y};\Lambda) \tag{4.2}$$

$$-\overline{uv} = R_{so}(x)r_{op\infty}(\overline{y};\Lambda) \tag{4.3}$$

where

$$\overline{y}=y/\delta \tag{4.4}$$

and U_{so}, R_{so}, and δ are functions only of x. The parameter Λ accounts for the free stream pressure gradient and will be defined later. In the limit as $\delta^+\rightarrow\infty$ the outer boundary layer equations are independent of Reynolds number; therefore, the velocity and Reynolds stress scales for the outer region must also be independent of Reynolds number. This is the Asymptotic Invariance Principle (AIP). The velocity has been written as a deficit to avoid the necessity of accounting for its variation across the inner layer. This is, of course, not possible with the Reynolds stress since it vanishes outside the boundary layer. The subscript $op\infty$ is used to distinguish the infinite Reynolds number solutions from the finite Reynolds number profiles used later which are scaled the same way.

Substitution into equation 4.1 and clearing terms yields

$$\begin{aligned}\left[\left(\frac{\delta}{U_{so}}\frac{dU_\infty}{dx}\right)\right. &+ \left.\left(\frac{U_\infty}{U_{so}}\right)\frac{\delta}{U_{so}}\frac{dU_{so}}{dx}\right]f_{o\infty}+\left[\frac{\delta}{U_{so}}\frac{dU_{so}}{dx}\right]f_{o\infty}^2-\left[\left(\frac{U_\infty}{U_{so}}\frac{d\delta}{dx}\right)+\right.\\ \left.\left(\frac{\delta}{U_{so}}\frac{dU_{so}}{dx}\right)\right]\overline{y}f'_{o\infty} &- \left[\left(\frac{d\delta}{dx}\right)+\left(\frac{\delta}{U_{so}}\frac{dU_{so}}{dx}\right)\right]f'_{o\infty}\int_0^{\overline{y}}f_{o\infty}(\tilde{y})d\tilde{y}=\left[\frac{R_{so}}{U_{so}^2}\right]r'_{o\infty}\end{aligned} \tag{4.5}$$

where the term involving dP_∞/dx has been cancelled by the $U_\infty dU_\infty/dx$ term arising from the $U\partial U/\partial x$ by using Euler's equation for the external flow.

For a similarity solution to be possible, the bracketed terms must all have the same x-dependence; i.e.,

$$\begin{aligned} \frac{\delta}{U_{so}}\frac{dU_{so}}{dx} &\sim \frac{\delta}{U_{so}}\frac{dU_\infty}{dx} \sim \left(\frac{U_\infty}{U_{so}}\right)\frac{\delta}{U_{so}}\frac{dU_{so}}{dx} \\ &\sim \frac{d\delta}{dx} \sim \left(\frac{U_\infty}{U_{so}}\right)\frac{d\delta}{dx} \sim \frac{R_{so}}{U_{so}^2} \end{aligned} \tag{4.6}$$

It is clear that just as for the zero pressure gradient boundary layer, full similarity is possible only if

$$U_{so} \sim U_\infty \tag{4.7}$$

$$R_{so} \sim U_\infty^2 \frac{d\delta}{dx} \tag{4.8}$$

Thus, the outer equations do admit to full similarity solutions (in the limit of infinite Reynolds number), but the velocity scale for the velocity deficit law must be U_∞, and not u_* as used by previous investigators (e.g., Clauser 1954, Coles 1962).

There are several additional independent constraints given by

$$\frac{d\delta}{dx} \sim \frac{\delta}{U_\infty}\frac{dU_\infty}{dx} \tag{4.9}$$

or, equivalently,

$$\frac{d\delta}{dx} \sim \frac{\delta}{\rho U_\infty^2}\frac{dP_\infty}{dx} \tag{4.10}$$

The first of these has the surprising consequence that

$$\delta \sim U_\infty^n \tag{4.11}$$

where n can, to this point at least, be any exponent. The second can be rewritten to yield

$$\Lambda \equiv \frac{\delta}{\rho U_\infty^2 d\delta/dx}\frac{dP_\infty}{dx} \sim constant \tag{4.12}$$

or equivalently

$$\Lambda \equiv -\frac{\delta}{U_\infty d\delta/dx}\frac{dU_\infty}{dx} \sim constant \tag{4.13}$$

Since the outer and inner scaled Reynolds stress must yield the same value of $- < uv >$, and since the inner Reynolds stress scales with u_*^2 (see Chapter 5); it follows in the limit of infinite Reynolds numbers that,

$$R_{so} \sim U_\infty^2 d\delta/dx \sim u_*^2 \tag{4.14}$$

just as for the zero pressure gradient boundary layer. Therefore, the similarity condition of equation 4.8 reduces as before to

$$\frac{d\delta}{dx} \sim \frac{u_*^2}{U_\infty} \tag{4.15}$$

from which it follows that,

$$\Lambda = \frac{\delta}{\rho U_\infty^2}\frac{1}{d\delta/dx}\frac{dP_\infty}{dx} \sim \frac{\delta}{\rho u_*^2}\frac{dP_\infty}{dx} \tag{4.16}$$

Thus, asymptotically $\Lambda \sim \beta$ where $\beta = (\delta_*/\rho u_*^2)dP_\infty/dx$ is the Clauser parameter discussed in Chapter 1. In the old theory (Clauser 1954) $\beta = constant$ was a necessary condition for an equilibrium boundary layer. Since in the present theory $\delta \sim \delta_* \sim \theta$ asymptotically, Clauser's criteria is an asymptotic limit of the condition 4.13. The direct deduction here can be contrasted with the Clauser's analysis which led to a parameter based on δ, but he was forced by his experiments to use δ_*. This is a particularly serious problem for his analysis since he had earlier deduced that $\delta_*/\delta \sim u_*/U_\infty$. All of these problems were a consequence of Clauser's arbitrary selection of a deficit law instead of letting the equations themselves dictate one. The Clauser definition of an *Equilibrium Boundary Layer* is a natural consequence of the similarity analysis presented here with no empirical input required. Of course to apply it, the

wall shear stress must be correctly determined, a considerable problem as will be seen later.

Since, for equilibrium flows $\Lambda = const$ it follows that by integrating equation 4.9 that,

$$U_\infty \sim \delta^{-\Lambda} \tag{4.17}$$

Thus, not only is there a power law relation between the boundary layer thicknesses and the imposed *free stream* velocity, *the power exponent is the parameter* Λ*!* Since it is the free stream velocity, U_∞ (or dP_∞/dx), which is usually specified, this is a remarkably restrictive constraint on δ, and as a consequence will provide a powerful test and confirmation of the new theory. Note that the inverse relation, $\delta \sim U_\infty^{-1/\Lambda}$, does not present a problem for $\Lambda = 0$ since it simply implies that the relationship is undefined as it must be since $U_\infty =$ constant in this case.

4.2 The Momentum Integral Equation

The momentum integral for a boundary layer with pressure gradient can be reduced to

$$\frac{d\theta}{dx} - (2+H)\frac{\theta}{\rho U_\infty^2}\frac{dP_\infty}{dx} = \left(\frac{u_*}{U_\infty}\right)^2 \tag{4.18}$$

where $H \equiv \delta_*/\theta$ is the shape factor. This can be rewritten for the equilibrium boundary layers defined above as

$$\frac{d\theta}{dx}\Big[1 - \Lambda\Big(\frac{\delta_*}{\delta} + 2\frac{\theta}{\delta}\Big)\Big(\frac{d\delta/dx}{d\theta/dx}\Big)\Big] = \left(\frac{u_*}{U_\infty}\right)^2 \tag{4.19}$$

From the similarity conditions of the preceding section, the term in square brackets on the left hand side is asymptotically constant since the ratios δ_*/δ, θ/δ and $(d\delta/dx)/(d\theta/dx)$ are (see chapter 2).

4.3 Comparison of the new outer scaling with experimental data

As in boundary layer with zero pressure gradient, one of the greatest difficulties in analyzing the data specially in inner variables is the friction velocity u_*. As mentioned before, most values from c_f are from Clauser method, and very few flows reported in Coles 1968 satisfy the momentum integral equation.

It was shown from the equation of motion that an equilibrium boundary layer is one where

$$\Lambda = \frac{\delta}{\rho U_\infty^2} \frac{1}{d\delta/dx} \frac{dP_\infty}{dx} = const. \tag{4.20}$$

and

$$U_\infty \sim \delta^{-\Lambda} \tag{4.21}$$

Also, $\delta \sim \delta_* \sim \theta$ asymptotically. Therefore, at least asymptotically

$$\Lambda \sim \Lambda_{\delta_*} \sim \Lambda_\theta \tag{4.22}$$

where

$$\Lambda_{\delta_*} = \frac{\delta_*}{\rho U_\infty^2} \frac{1}{d\delta_*/dx} \frac{dP_\infty}{dx} = const. \tag{4.23}$$

$$\Lambda_\theta = \frac{\theta}{\rho U_\infty^2} \frac{1}{d\theta/dx} \frac{dP_\infty}{dx} = const. \tag{4.24}$$

Thus asymptotically at least,

$$U_\infty \sim \delta^{-\Lambda} \sim {\delta_*}^{-\Lambda_{\delta_*}} \sim \theta^{-\Lambda_\theta} \tag{4.25}$$

In addition to equilibrium flows it will be shown that the present theory works for moving equilibrium flows which are flows at a given equilibrium condition, then the flow is changed to new equilibrium.

4.3.1 Favorable Pressure Gradient (FPG): $\Lambda < 0$

Figure 4.1 shows a log-log of U_∞ (ft/sec) vs. δ, δ_*, θ (ft.) for the Moderate FPG data of Ludweig and Tillmann 1949. The slope is constant and nearly the same for all length scales. This data set has been considered a near equilibrium flow based on Clauser's definition (Coles 1968); however in terms of the new definition the flow is actually in full equilibrium since Λ is constant, as are Λ_{δ_*} and Λ_θ.

The velocity profiles in outer variables for the above experiments are shown in Figures 4.2 and 4.3. The first one is scaled with u_* (using the Clauser method explained earlier in this chapter) and the second one scaled with U_∞. Even though the friction velocity u_* was chosen (by the authors) to collapse the data in the overlap region in inner variables it fails to do so when plotted in old deficit form as in Figure 4.2. (Note that these curves look better when δ is treated as a variable as in Coles 1968 instead of as physical length scale.) In addition, note how the supposed constant value for equilibrium boundary layer parameter, β, (according to Clauser 1956) varies for every given data set. On the other hand note the excellent collapse when the same data is scaled with U_∞ in Figure 4.3, 4.4, and 4.5 with the length scales δ, δ_* and θ respectively.

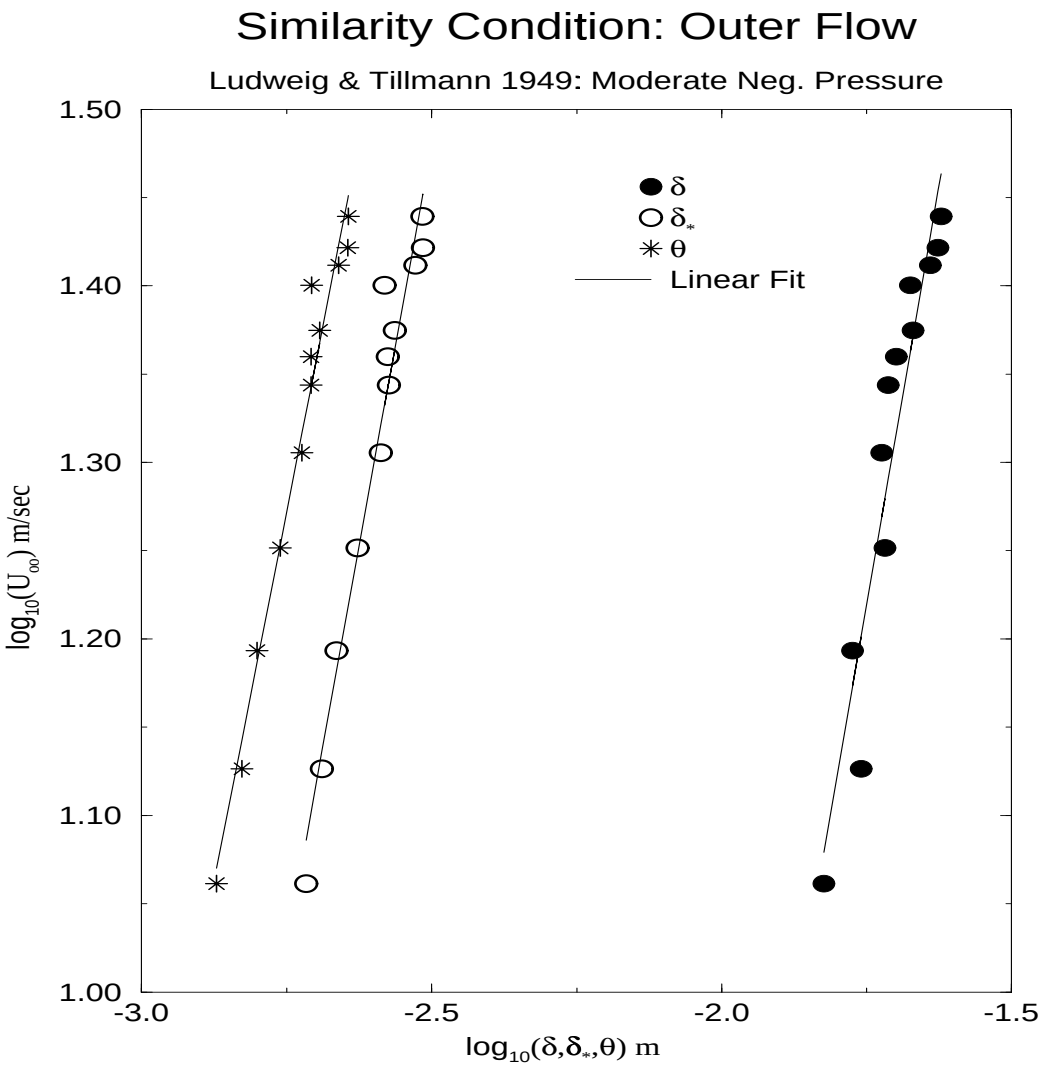

Figure 4.1: The log-log plot of U_∞ (ft/sec) vs. δ, δ_*, θ for the Ludweig and Tillmann 1949 data at moderate negative pressure gradient

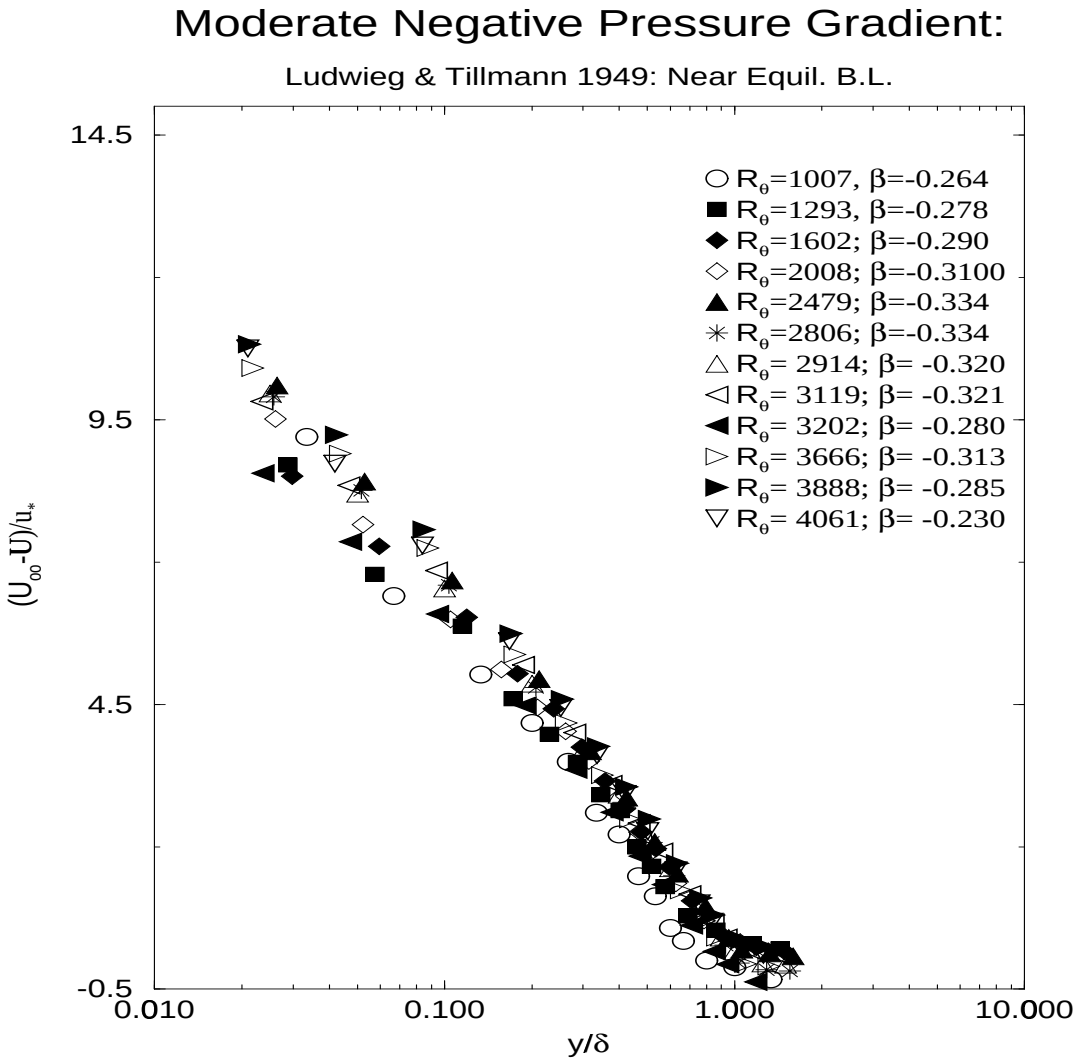

Figure 4.2: The velocity profiles in outer variables scaled with $U_{so} = u_*$ using the Clauser method) and δ for the Ludweig and Tillman 1949 data at moderate favorable Pressure gradient.

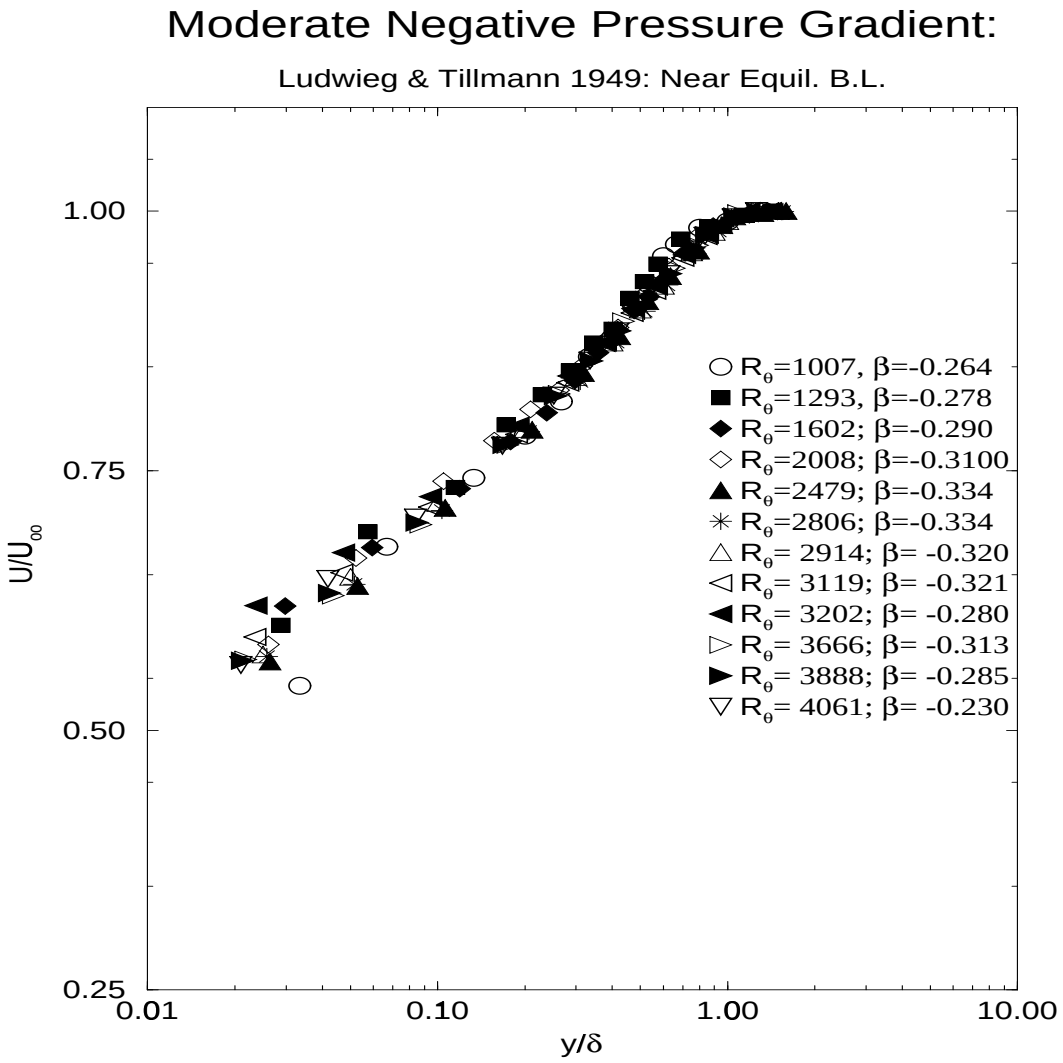

Figure 4.3: The velocity profiles in outer variables scaled with $U_{so} = U_\infty$ and δ for the Ludweig and Tillman 1949 data at moderate favorable pressure gradient.

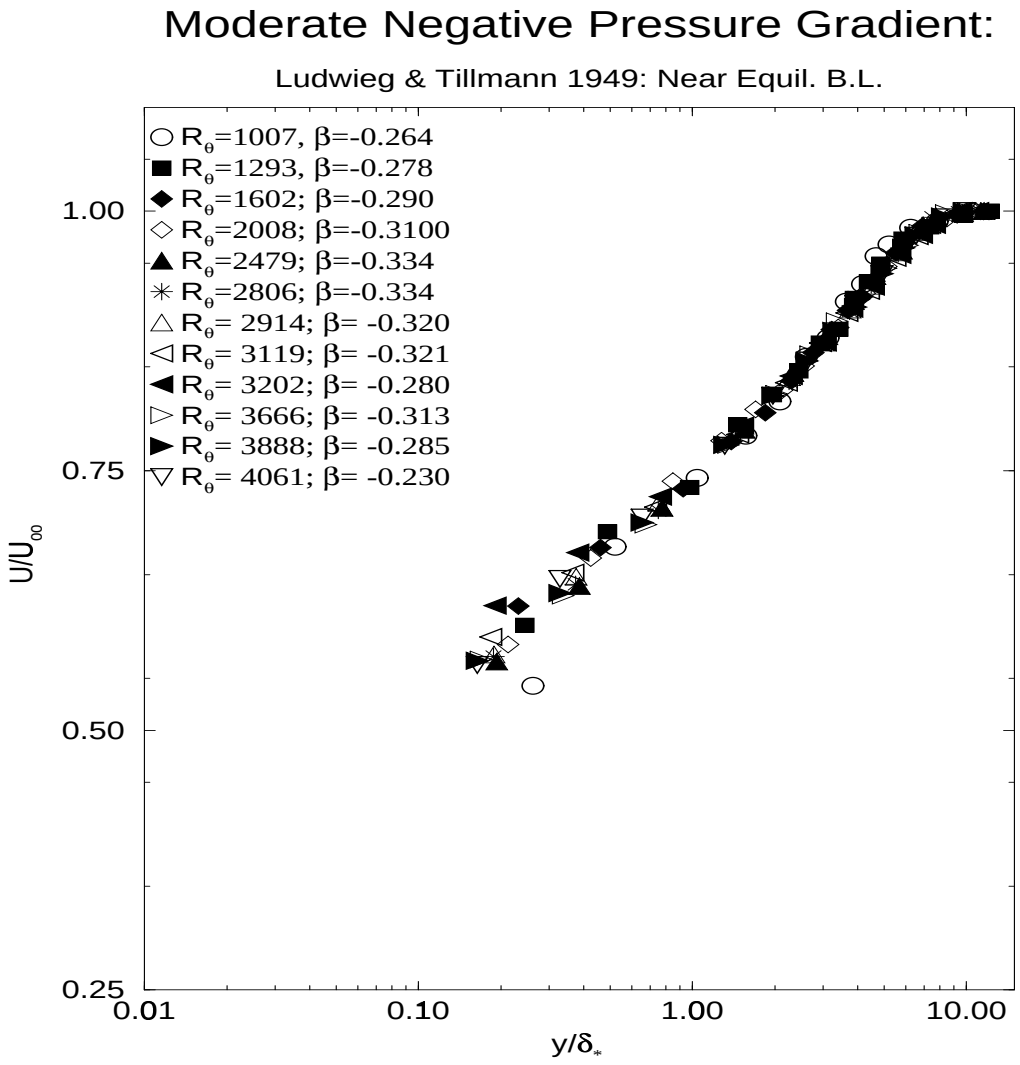

Figure 4.4: The velocity profiles in outer variables scaled with $U_{so} = U_\infty$ and δ_* for the Ludweig and Tillman 1949 data at moderate favorable pressure gradient

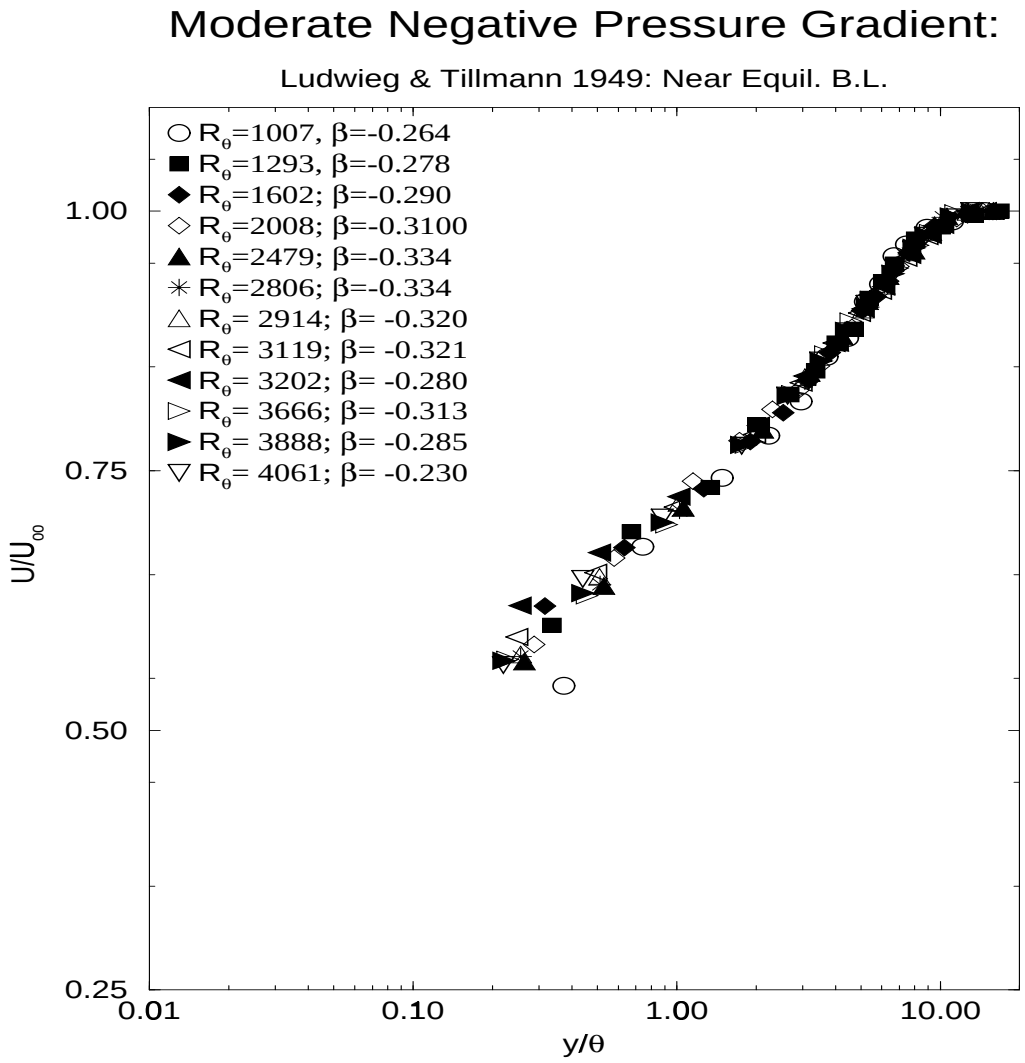

Figure 4.5: The velocity profiles in outer variables scaled with $U_{so} = U_\infty$ and θ for the Ludweig and Tillman 1949 data at moderate favorable pressure gradient.

4.3.2 Adverse Pressure Gradient (APG): $\Lambda > 0$

Figure 4.6 shows a log-log plot of U_∞ (ft/sec) vs. δ, δ_* and θ (ft.) for the data of Kline et al. 1967 in a Mild FPG flow. This figure illustrates the similarity condition for equation 4.21. If an equilibrium boundary layer exists, the data for log U_∞ versus log δ should be linear in a log-log plot with slope given by $-\Lambda$. Clearly there is a near constant slope for all three plots. Moreover, Λ_δ, $\Lambda_\delta*$ and Λ_θ are nearly proportional to each other. Obviously,

$$\frac{1}{\theta}\frac{d\theta}{dx} \sim \frac{1}{\delta}\frac{d\delta}{dx} \sim \frac{1}{\delta_*}\frac{d\delta_*}{dx} \tag{4.26}$$

even though θ/δ and δ_*/δ are far from their asymptotic values. This particular data has not been previously considered to be an equilibrium flow in terms of Clauser's definition, but obviously is by the criteria applied here. Unfortunately the velocity profile data for this fine experiment appear to have been lost (W.C. Reynolds, private communication to W.K. George).

The data of Bradshaw 1965 for U_∞ versus δ, δ_* and θ is shown in Figure 4.7. This data is considered to be a Mild Adverse Pressure Gradient, and R_θ varies from 10,061 to 22,578. The velocity profiles scaled with U_∞ and δ, δ_* and θ as outer length scales are shown in Figures 4.8 through 4.10. Figure 4.11 shows a similar plot for the Moderate Adverse Pressure Gradient of the same author where R_θ varies from 14,492 to 36,669. The velocity profiles for the Moderate APG are shown in Figures 4.12 to 4.14. Note the excellent collapse for both experiments in the new outer variables, regardless of which outer length scale is used. The single exception is most upstream profile of the Moderate FPG, which perhaps indicates that the flow has not yet reached equilibrium.

Figure 4.15 presents Clauser's own data for the Moderate APG showing U_∞ vs δ, δ_* and θ in a log-log plot. Clearly this flows has perfect linear behavior indicating that

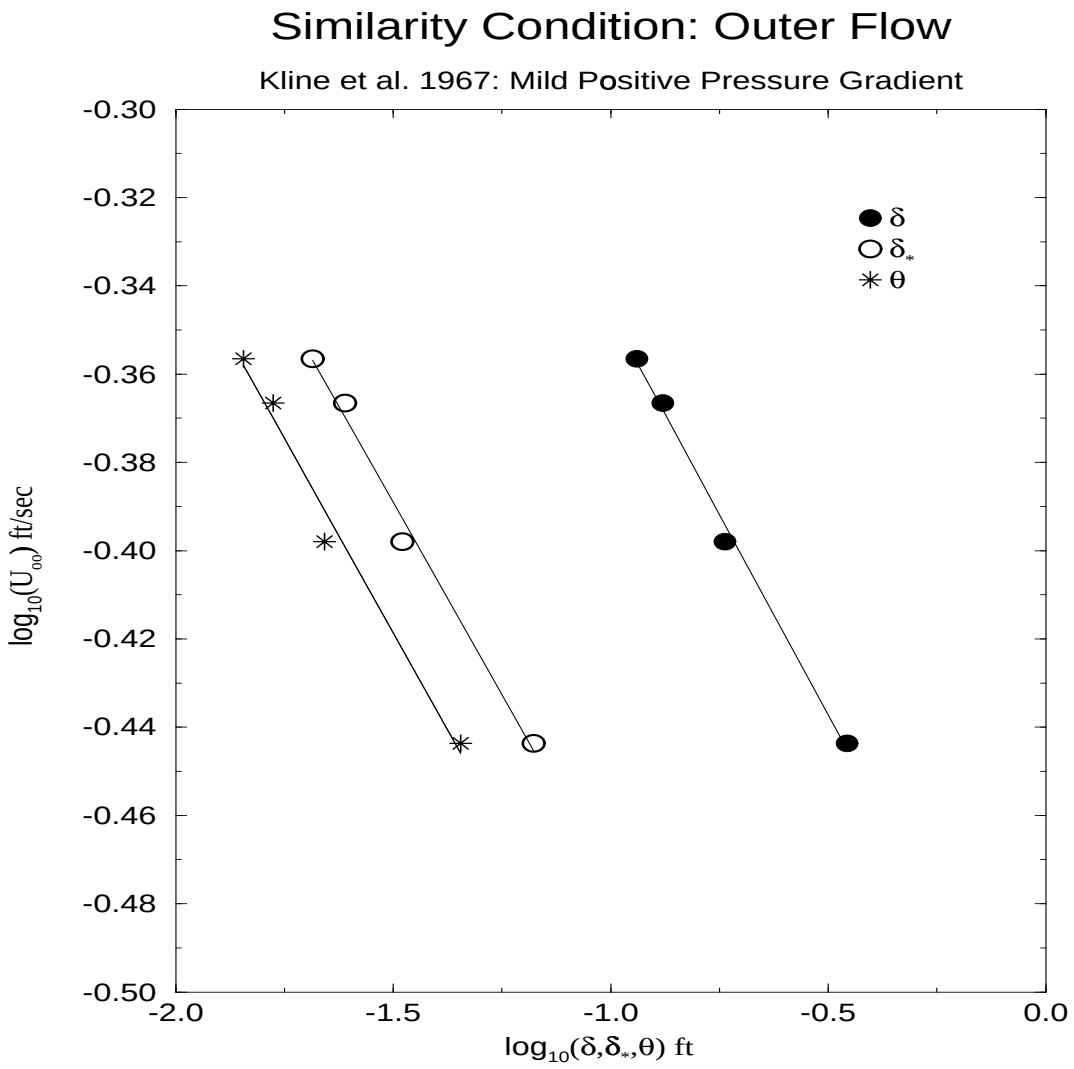

Figure 4.6: The log-log plot of U_∞ (ft/sec) vs. δ, δ_*, θ for the Kline et al. 1967 data at mild adverse pressure gradient.

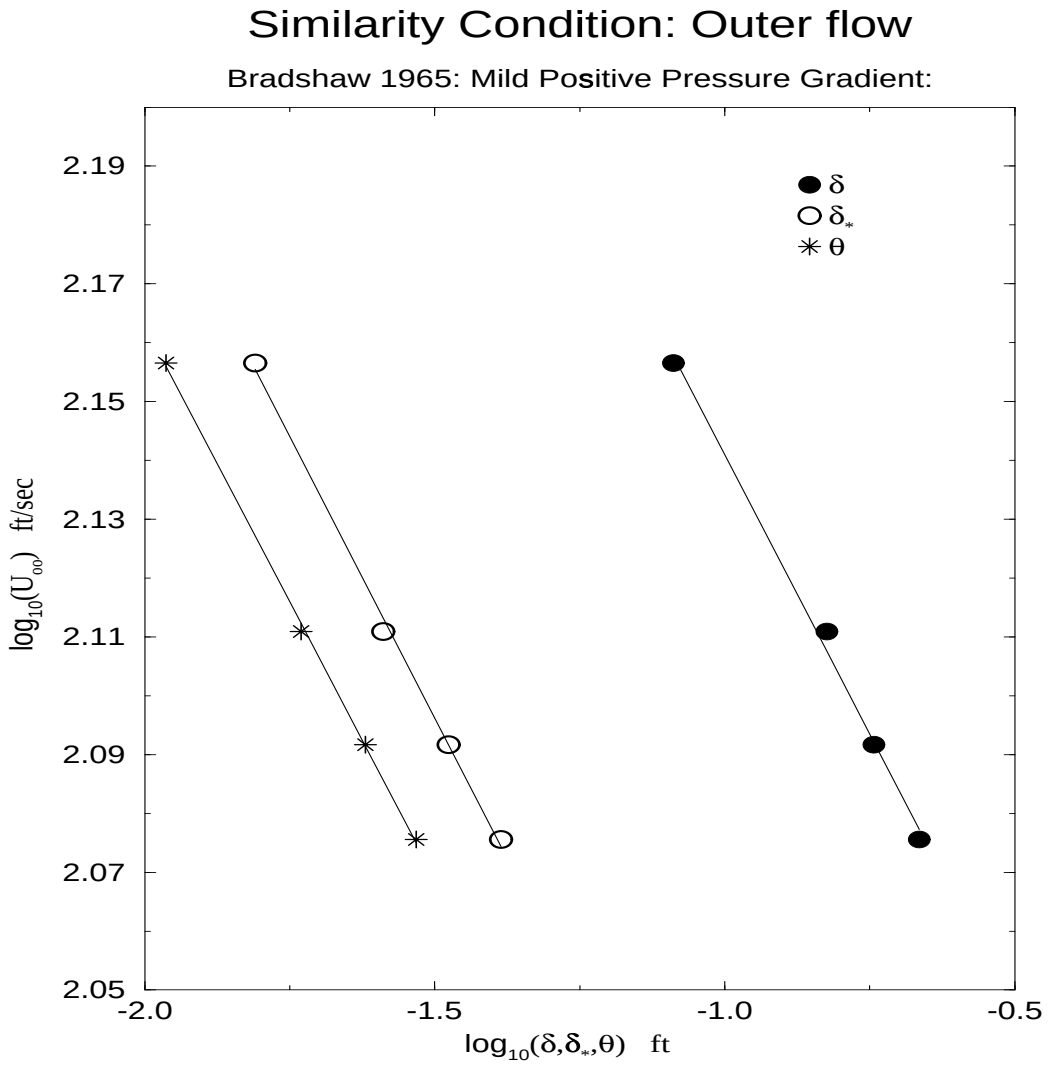

Figure 4.7: The log-log plot of U_∞ (ft/sec) vs. δ, δ_*, θ for the Bradshaw 1965 data at mild adverse pressure gradient.

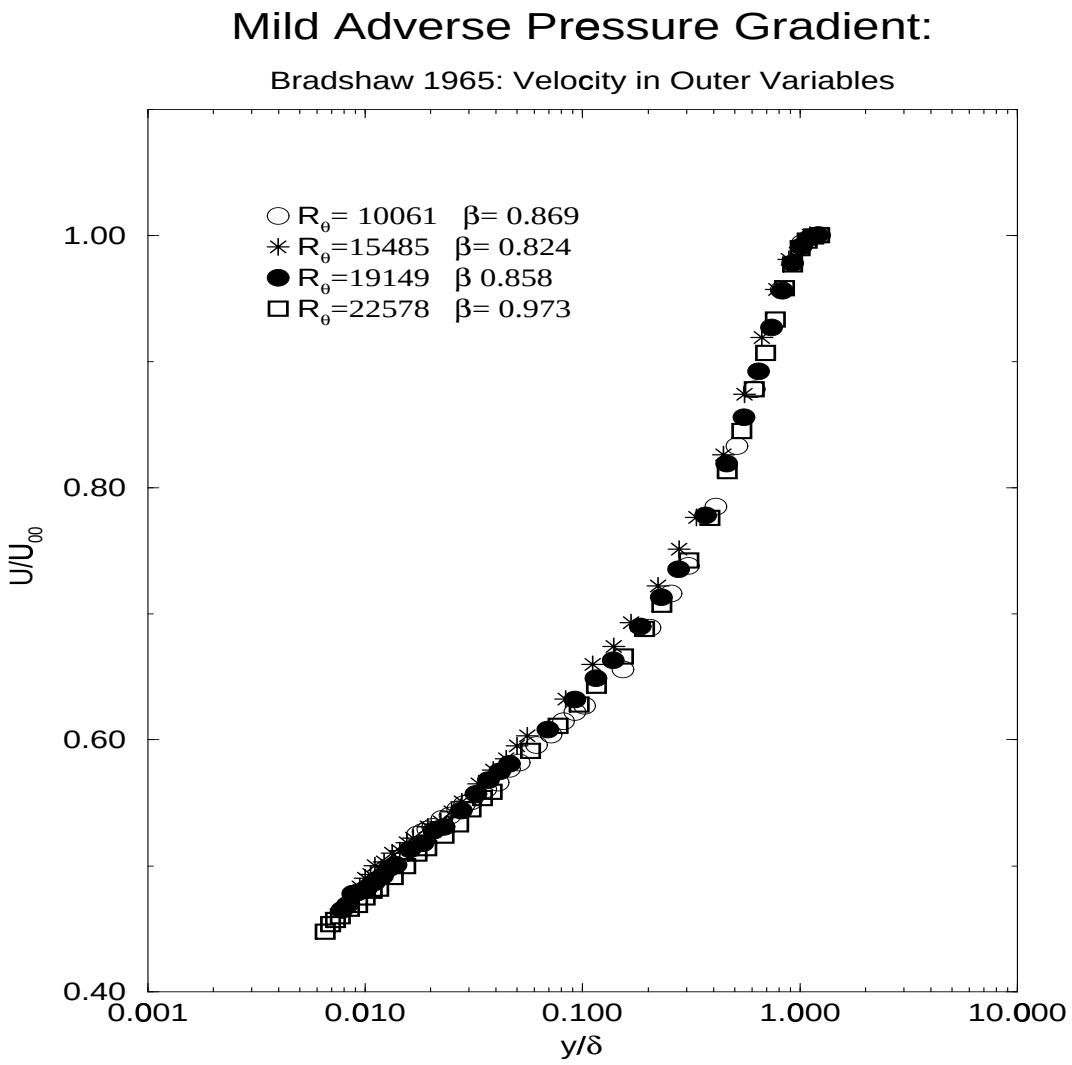

Figure 4.8: The velocity profiles in outer variables scaled with $U_{so} = U_\infty$ and δ for the Bradshaw 1965 data at mild adverse pressure gradient.

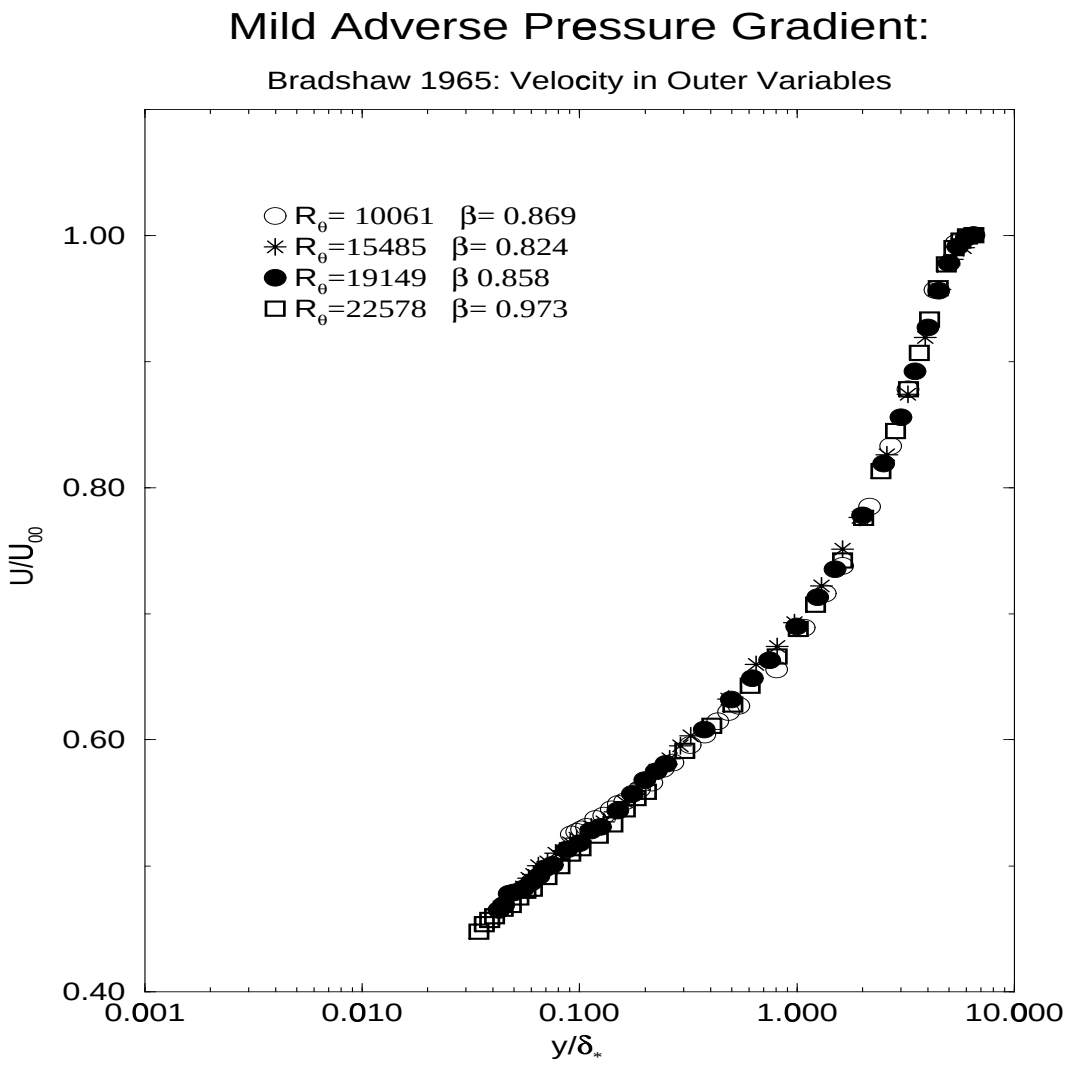

Figure 4.9: The velocity profiles in outer variables scaled with $U_{so} = U_\infty$ and δ_* for the Bradshaw 1965 data a mild adverse pressure gradient.

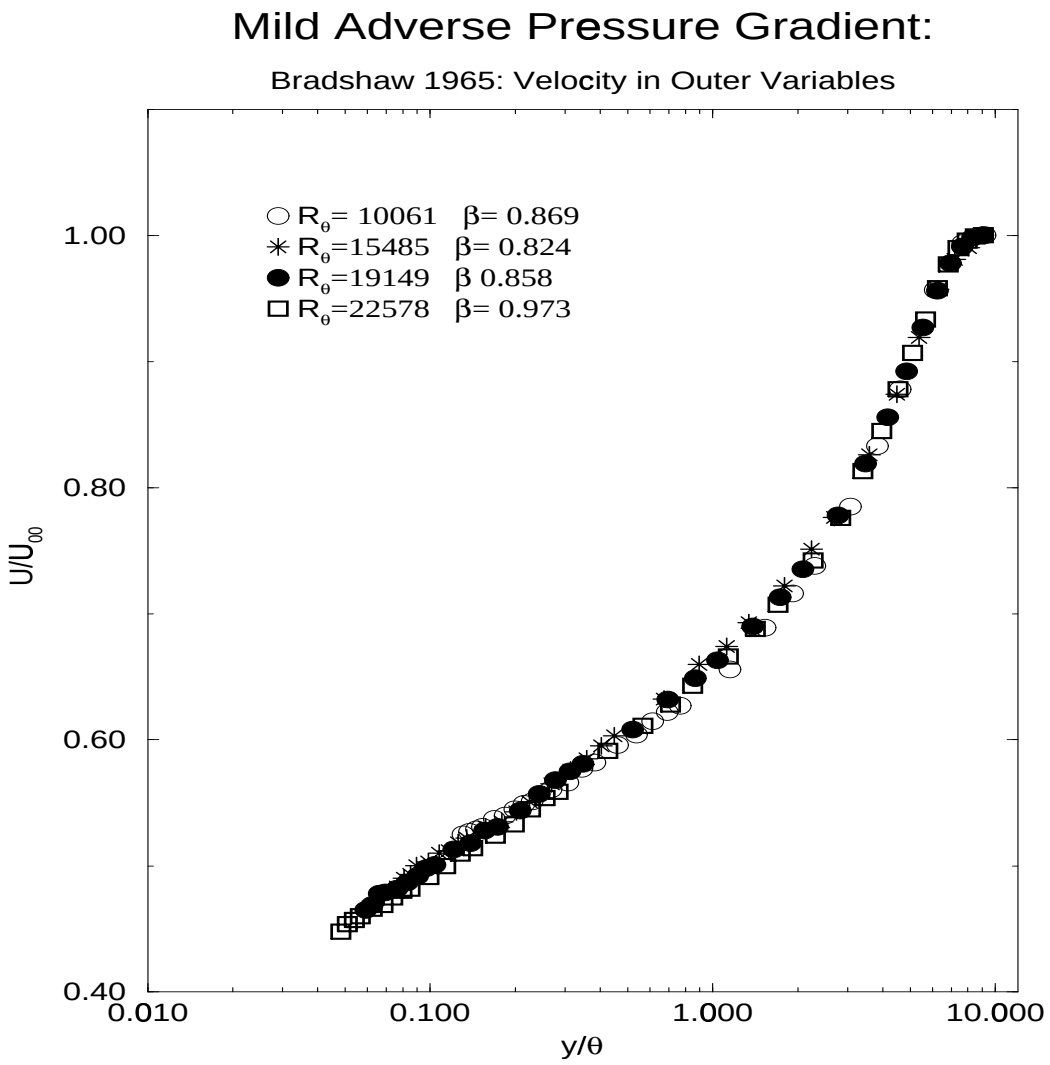

Figure 4.10: The velocity profiles in outer variables scaled with $U_{so} = U_\infty$ and θ for the Bradshaw 1965 data at mild adverse pressure gradient

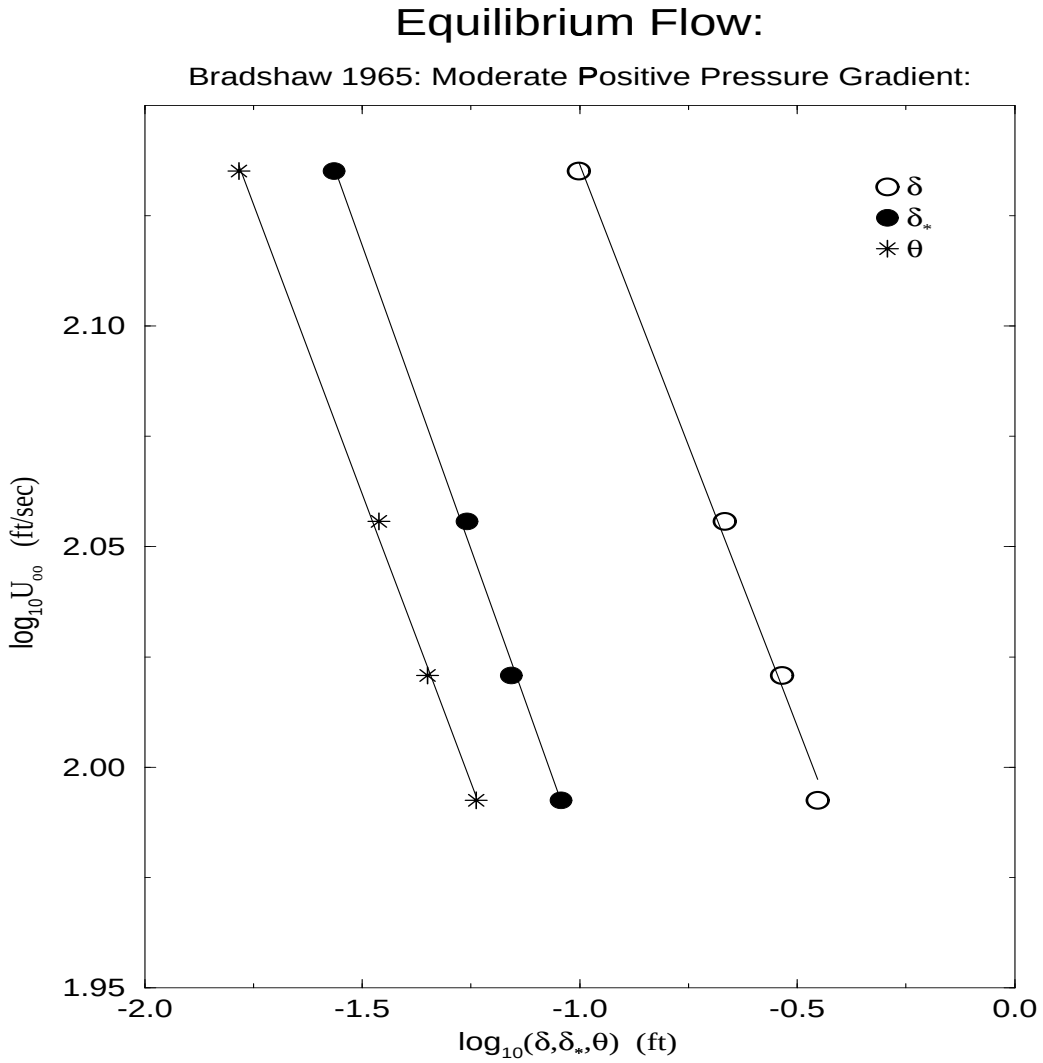

Figure 4.11: The log-log plot of U_∞ (ft/sec) vs. δ, δ_*, δ_* for the Bradshaw 1965 data at moderate adverse pressure gradient.

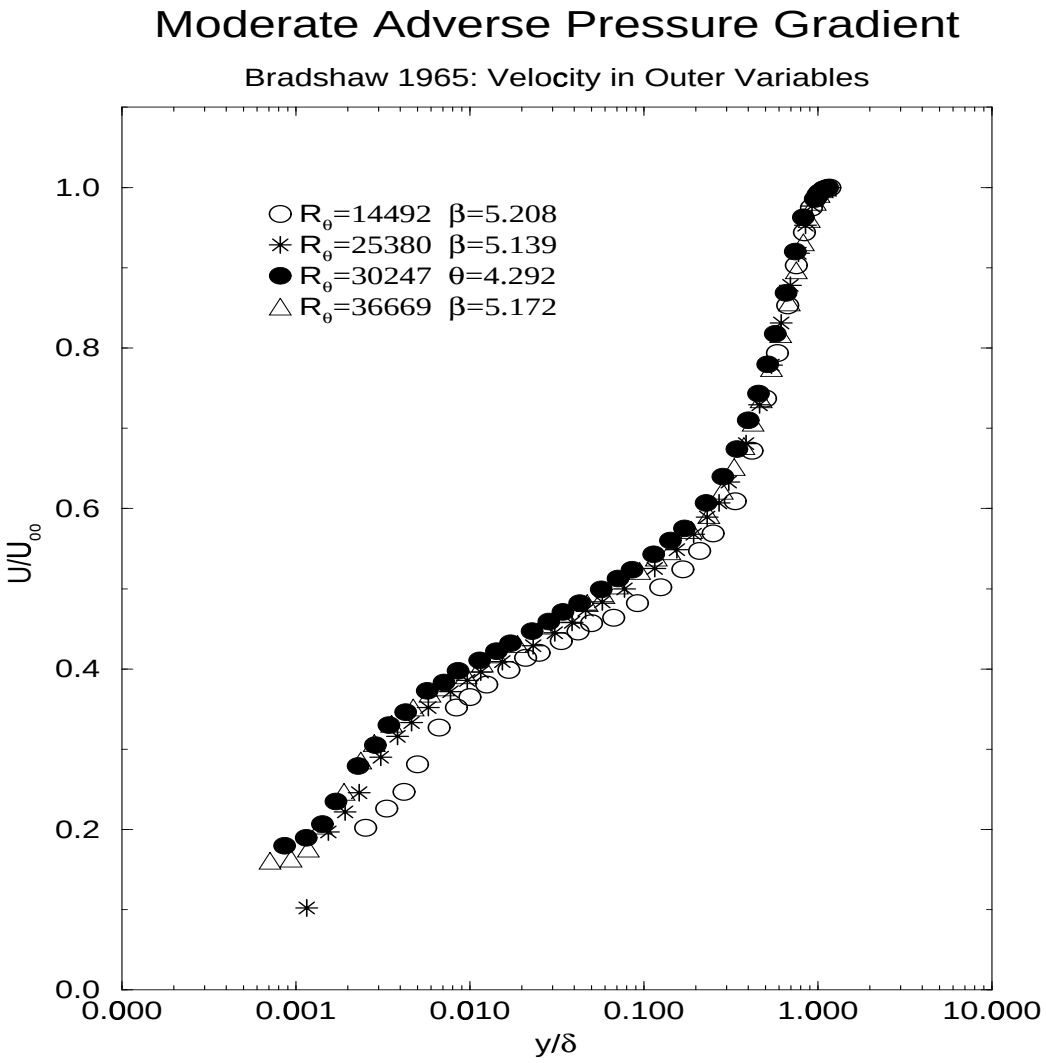

Figure 4.12: The velocity profiles in outer variables scaled with $U_{so} = U_\infty$ and δ for Bradshaw 1965 data at moderate adverse pressure gradient.

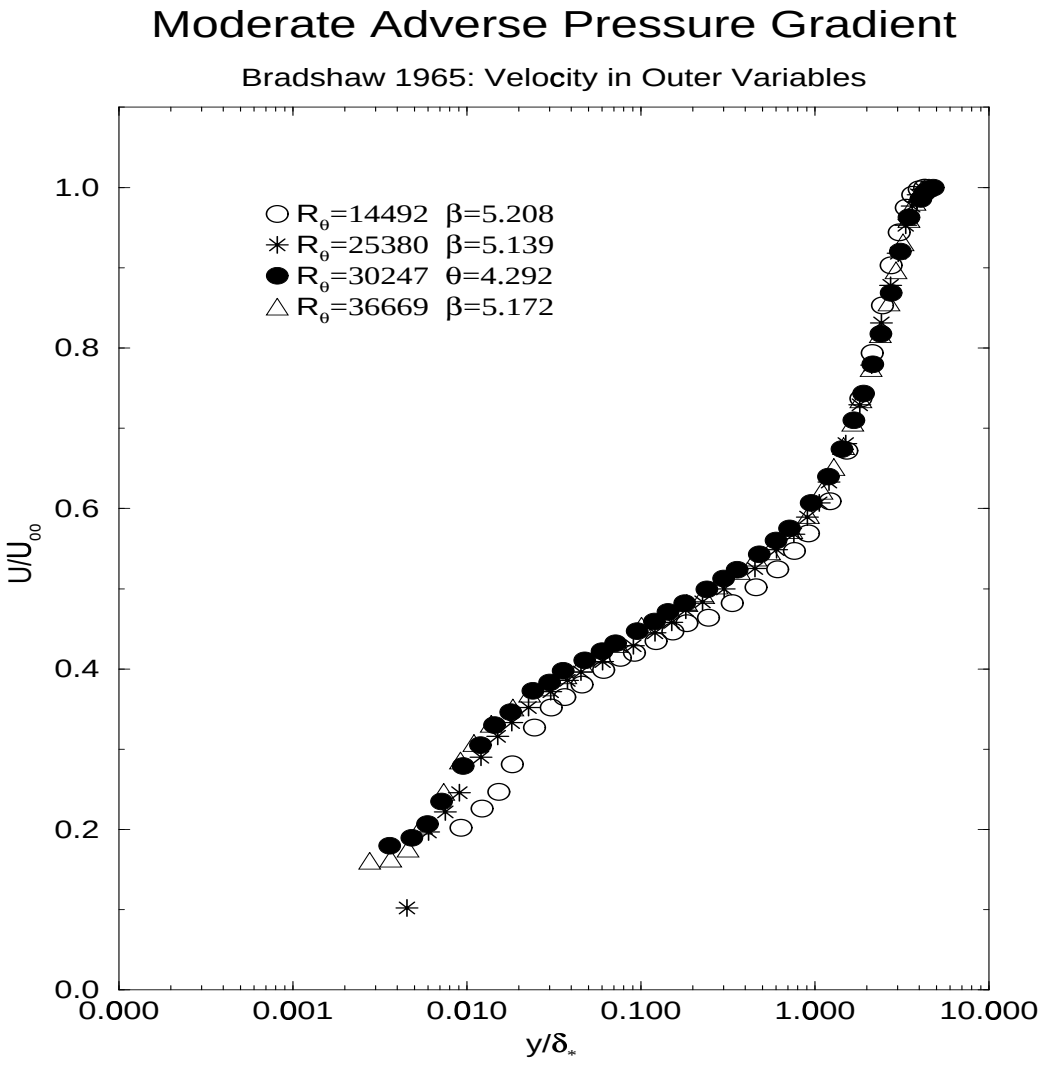

Figure 4.13: The velocity profiles in outer variables scaled with $U_{so} = U_\infty$ and δ_* for the Bradshaw 1965 at moderate adverse pressure gradient.

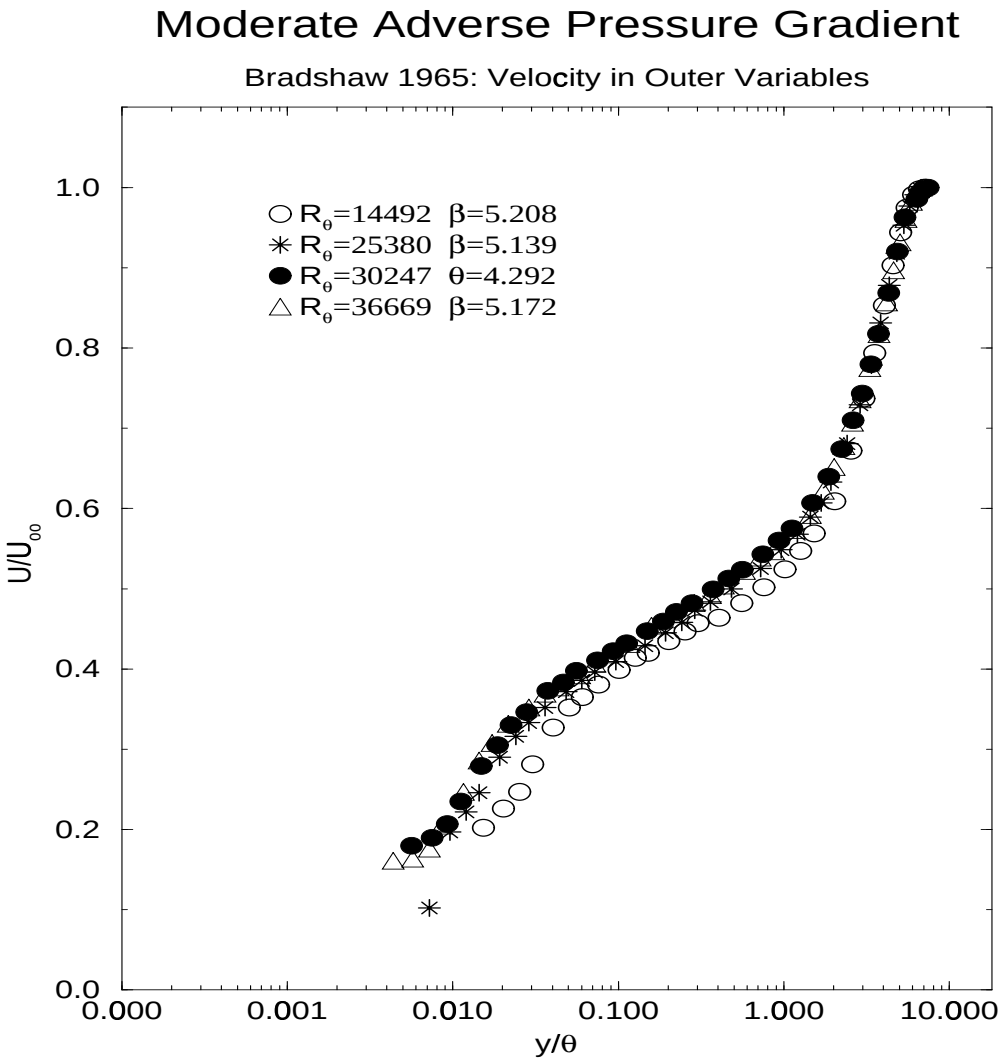

Figure 4.14: The velocity profiles in outer variables scaled with $U_{so} = U_\infty$ and θ for the Bradshaw 1965 data at moderate adverse pressure gradient.

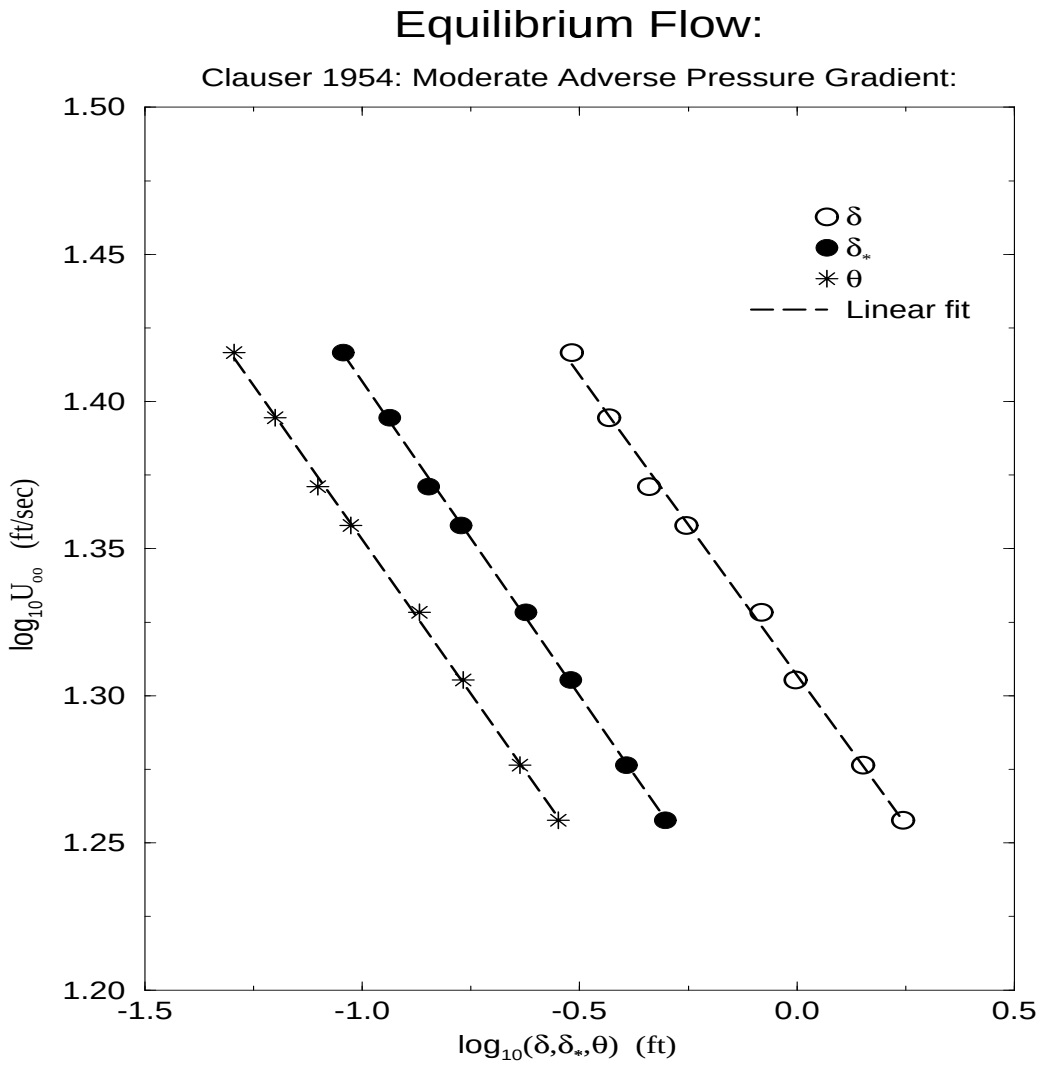

Figure 4.15: The log-log plot of U_∞ (ft/sec) vs. δ, δ_*, δ_* for the Clauser 1954 data at moderate adverse pressure gradient.

the new similarity condition for equilibrium flows is satisfied. The velocity profile in outer variables from Clauser data scaled with u_* (deficit law) is shown in Figure 4.16, and the same data but scaled with $U_{so} = U_\infty$ and δ, δ_* and θ are shown in Figures 4.16 to 4.19. The collapse for all three is is so good it is amazing that it has not been previously noted, especially by the experimenters themself. Figure 4.20 shows that the same is true for Clauser's Mild APG as well. The velocity profiles have not been plotted in this case, but the proposed scaling works as well for them as for the others.

According to Clauser's definition for equilibrium flows, β=const and the velocity deficit distribution in the the streamwise direction should be invariant with Reynolds number; in other words all profiles should collapse as a single curve. Notice how the values of β tabulated in the figures vary with Reynolds number. Clearly these flows have chose not to satisfy Clauser's definition of equilibrium flows, at least for the values of shear stress determined by him. On the other hand, when the same data is plotted using the new scale, not only do the data collapse better, *but by the new definition of equilibrium boundary layers (Λ = constant), Clauser's data are found to be in equilibrium.* Moreover the proposed outer scaling is considerally more succesful than the old, even though the stress was obtained to make the old work. This is the same data set criticized by Rotta 1962 as mentioned in Chapter 1. Obviously no such criticism is warranted.

An example of a very strong adverse pressure gradient proceeding toward separation is given by the airfoil data of Newman 1951. The log U_∞ versus log (δ, δ_* and θ) plot is shown in Figure 4.21 Because the lower points in the vertical axis are reaching a new equilibrium, the slopes are not constant. Obviously, however,there is a linear region and therefore this flow of Newman 1951 can also be considered to be in equilibrium since Λ=constant (at least over most of it). The lines have been fitted

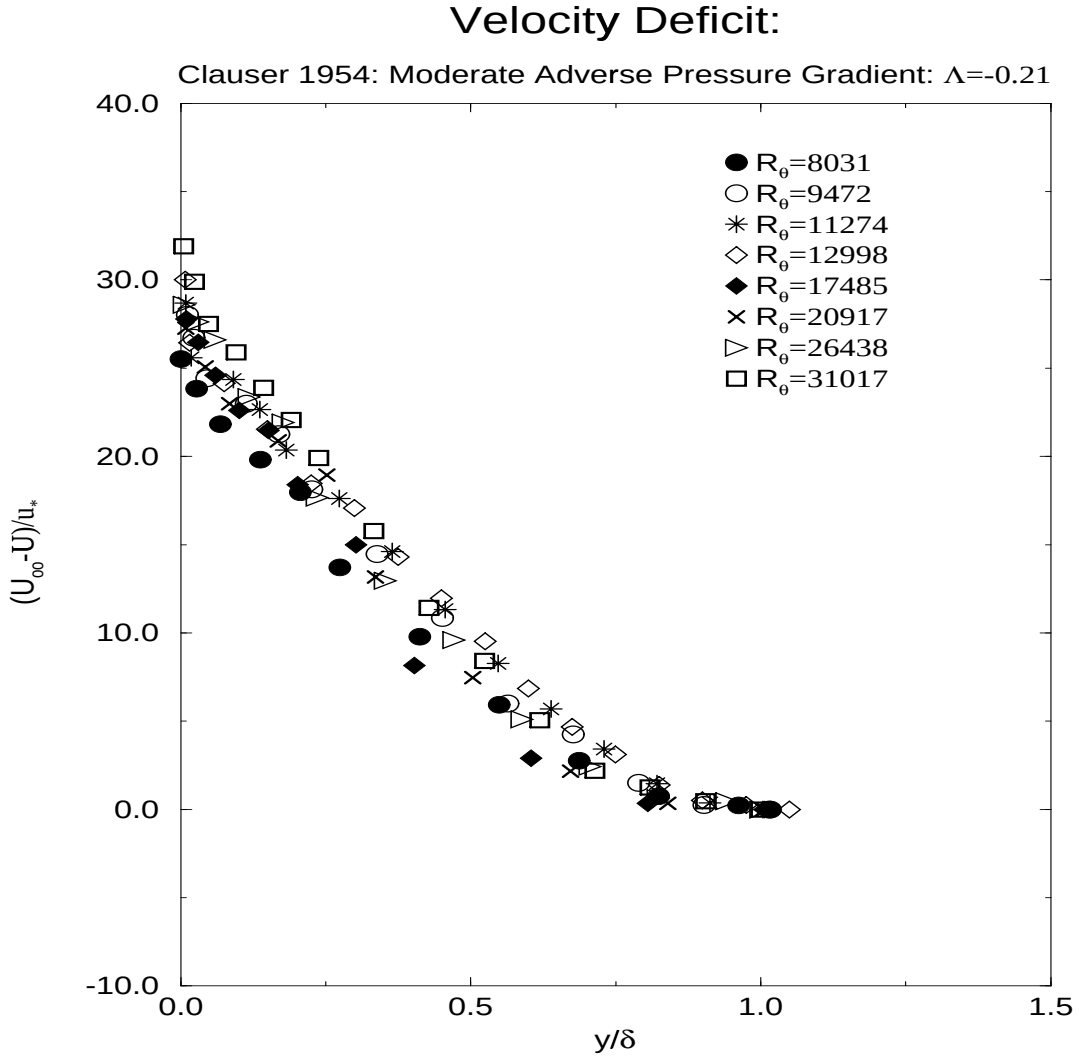

Figure 4.16: The velocity profiles in outer variables scaled with $U_{so} = U_*$ and δ for the Clauser 1954 data at moderate adverse pressure gradient.

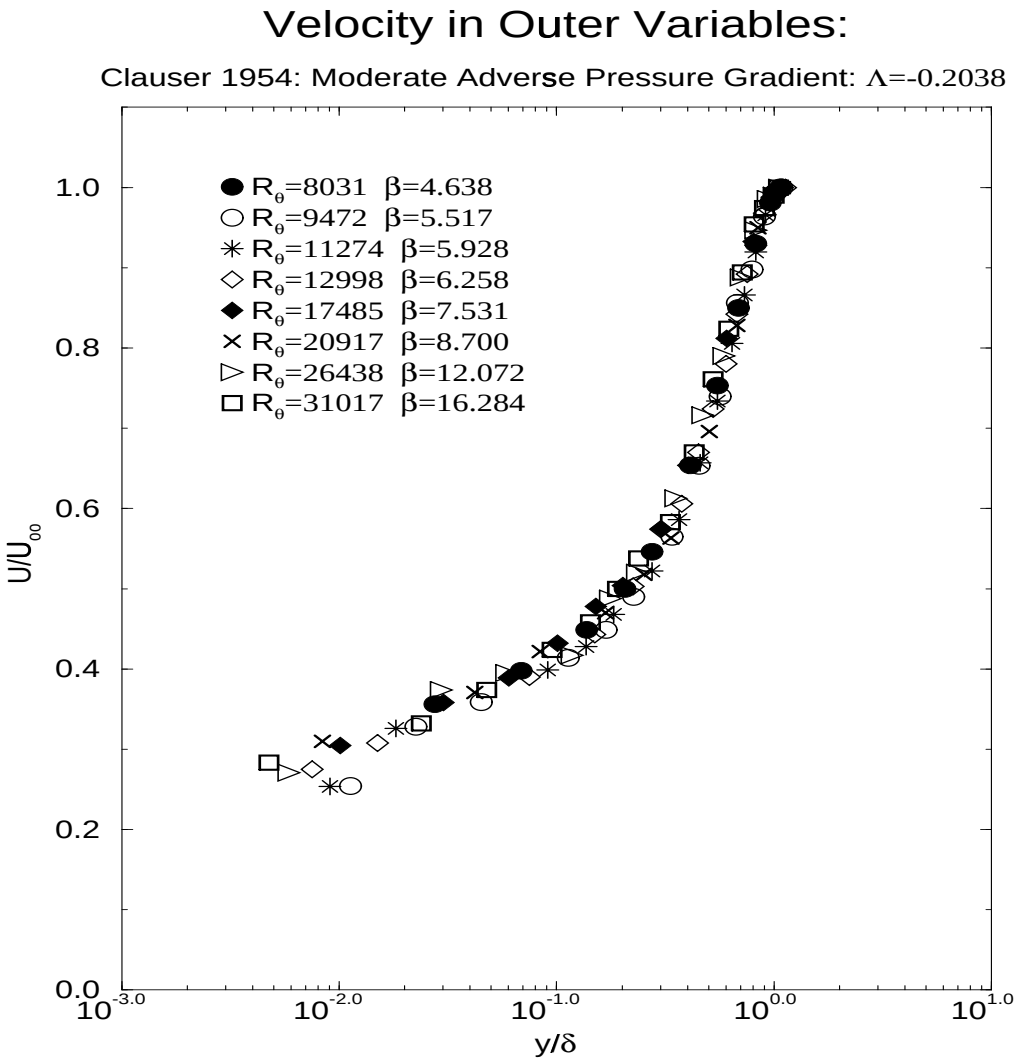

Figure 4.17: The velocity profiles in outer variables scaled with $U_{so} = U_\infty$ and δ for the Clauser 1954 data at moderate adverse pressure gradient.

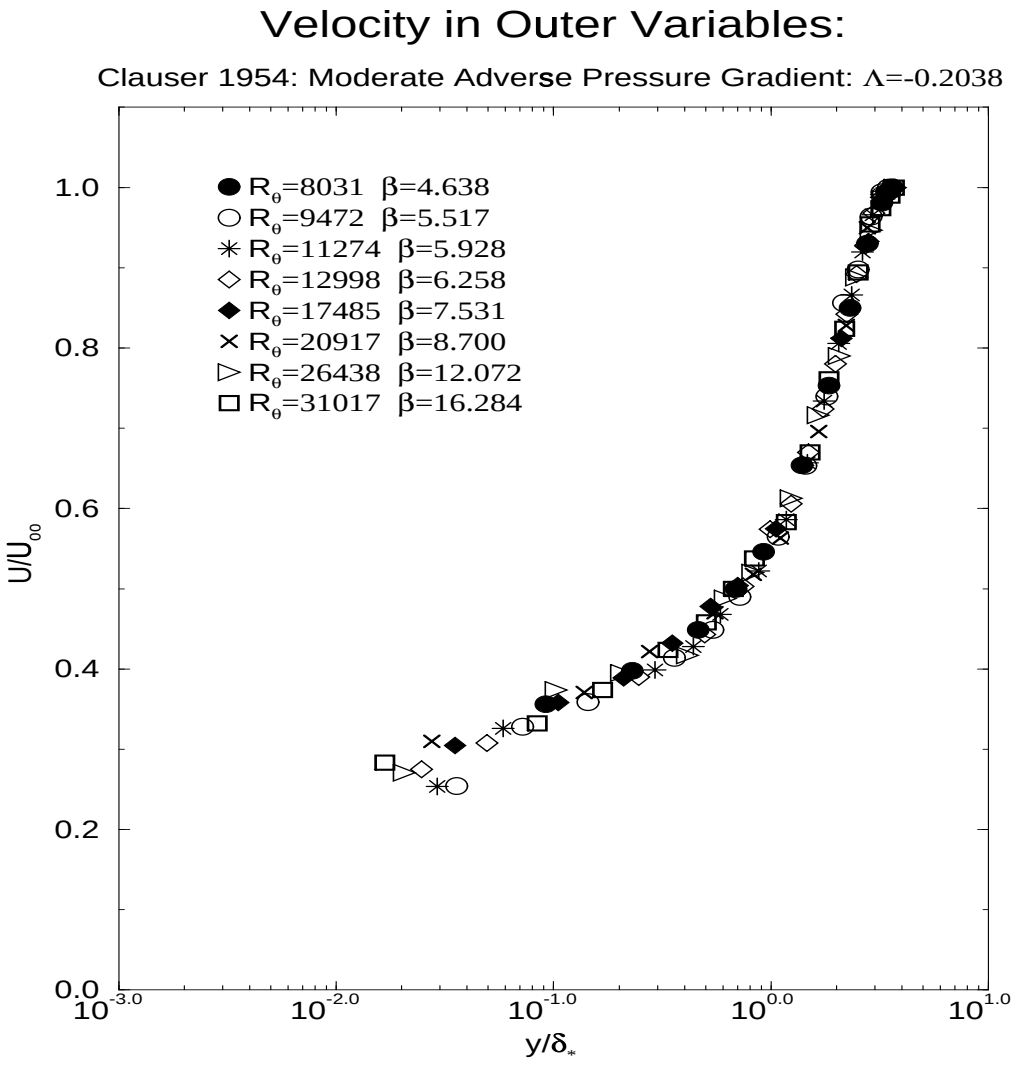

Figure 4.18: The velocity profiles in outer variables scaled with $U_{so} = U_\infty$ and δ_* for the Clauser 1954 data at moderate adverse pressure gradient.

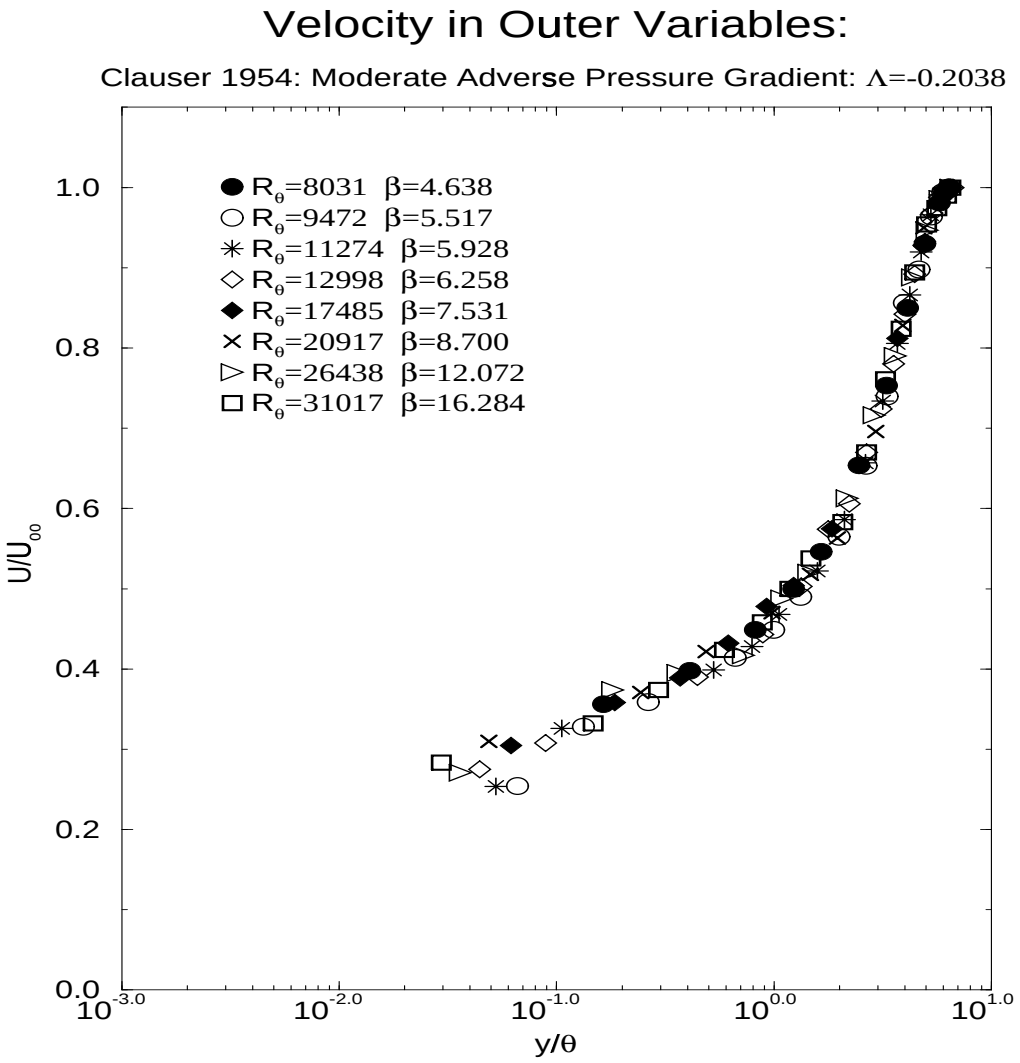

Figure 4.19: The velocity profiles in outer variables scaled with $U_{so} = U_\infty$ and θ for the Clauser 1954 data at moderate adverse pressure gradient.

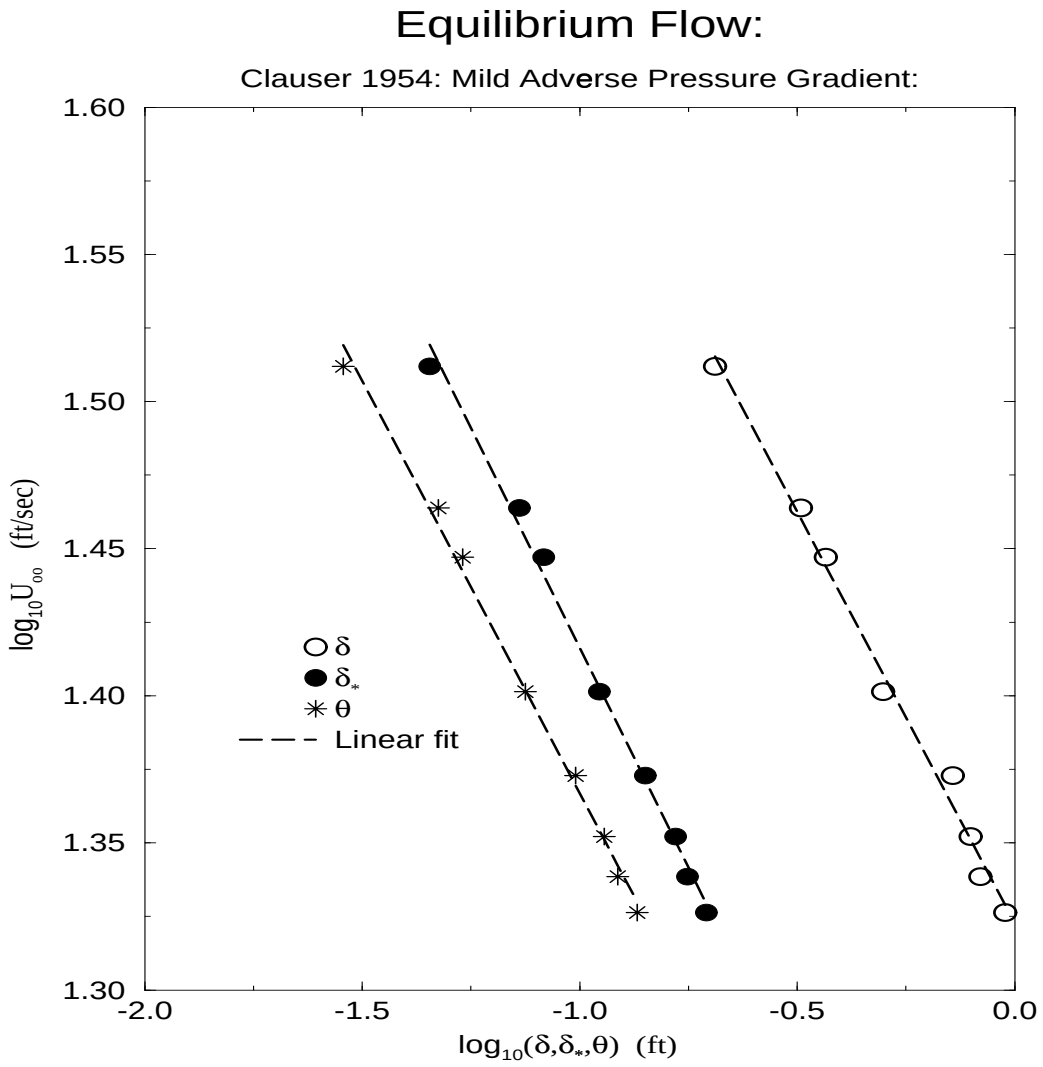

Figure 4.20: The log-log plot of U_∞ (ft/sec) vs. δ, δ_*, δ_* for the Clauser 1954 data at mild adverse pressure gradient.

by ignoring the first data point and the last two, since the flow clearly seems to be evolving in these regions. The data vary in R_θ from 5,510 to 26,829 which is large enough to observe a Reynolds number dependence in $\Lambda/\Lambda_{\delta*}$ and Λ/Λ_θ, unlike the earlier data set in which the Reynolds number range was more limited. The value for $\Lambda = -0.22$ does not vary with Reynolds number, by contrast with the cited values of the Clauser parameter β ($3.23 \leq \beta \leq 182.$), which led to the previous (and obviously erroneous) conclusion that this flow was not an equilibrium flow.

Figure 4.22 shows the velocity profile of Newman 1951 in outer variables using the traditional scale (u_* from Clauser method). Note that even though u_* was determined so that the data collapse in the "log" region in inner variables, it does not collapse at all in these outer variables, except at the outermost part of the flow where it must because of the boundary condition on $U - U_\infty$. The same data set of Newman 1951 is plotted in Figure 4.23, but scaled with U_∞. Note how the region of collapse of the profiles moves closer to the wall as the Reynolds number increases. This behavior is very consistent with the new theory and the previous results for the zero pressure gradient boundary layer. On the other hand, note how the region of collapse of the u_* scaled profiles moves away from the wall (opposite direction to Figure 4.23). The reason is quite clear: since u_* is decreasing in the adverse pressure gradient (and vanishes at separation), the deficit law using the traditional scale continues to increase without bound. No such problems occur in the present theory since the data will move to an asymptotic state in which all data collapse as single curve.

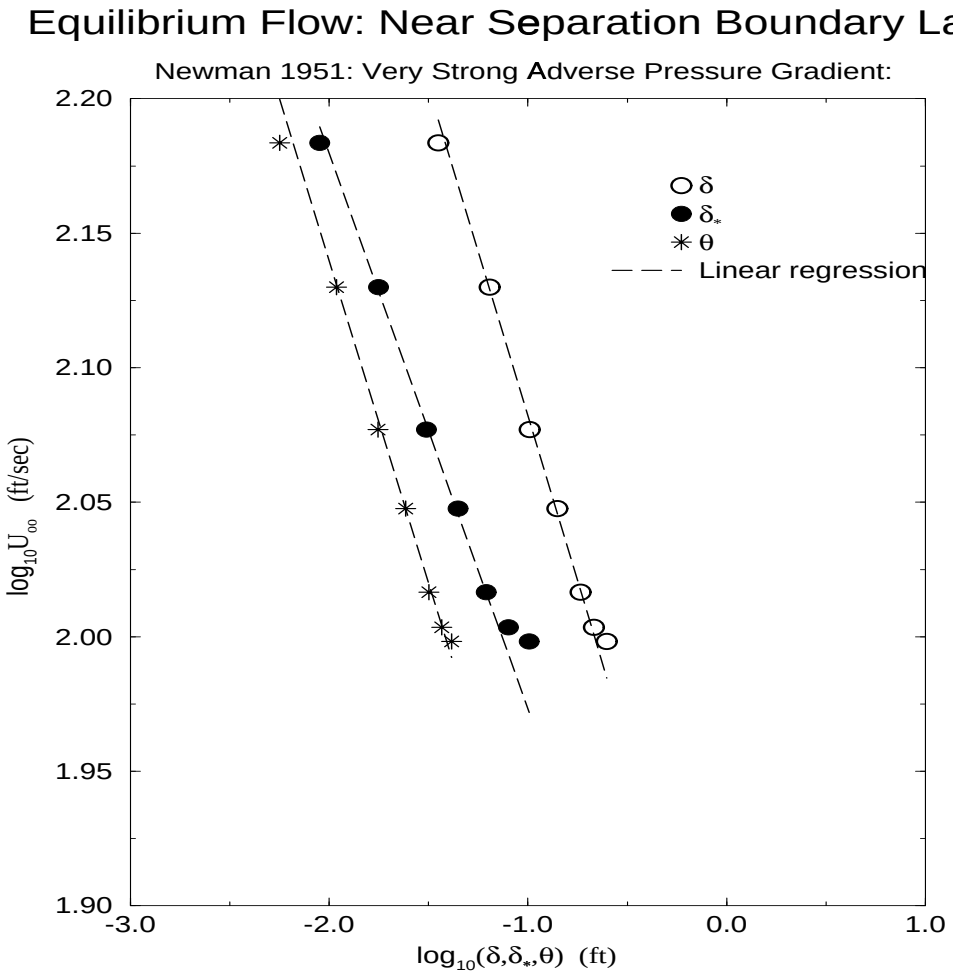

Figure 4.21: The log-log plot of U_∞ (ft/sec) vs. δ, δ_*, δ_* for the Newman 1951 data at very strong adverse pressure gradient.

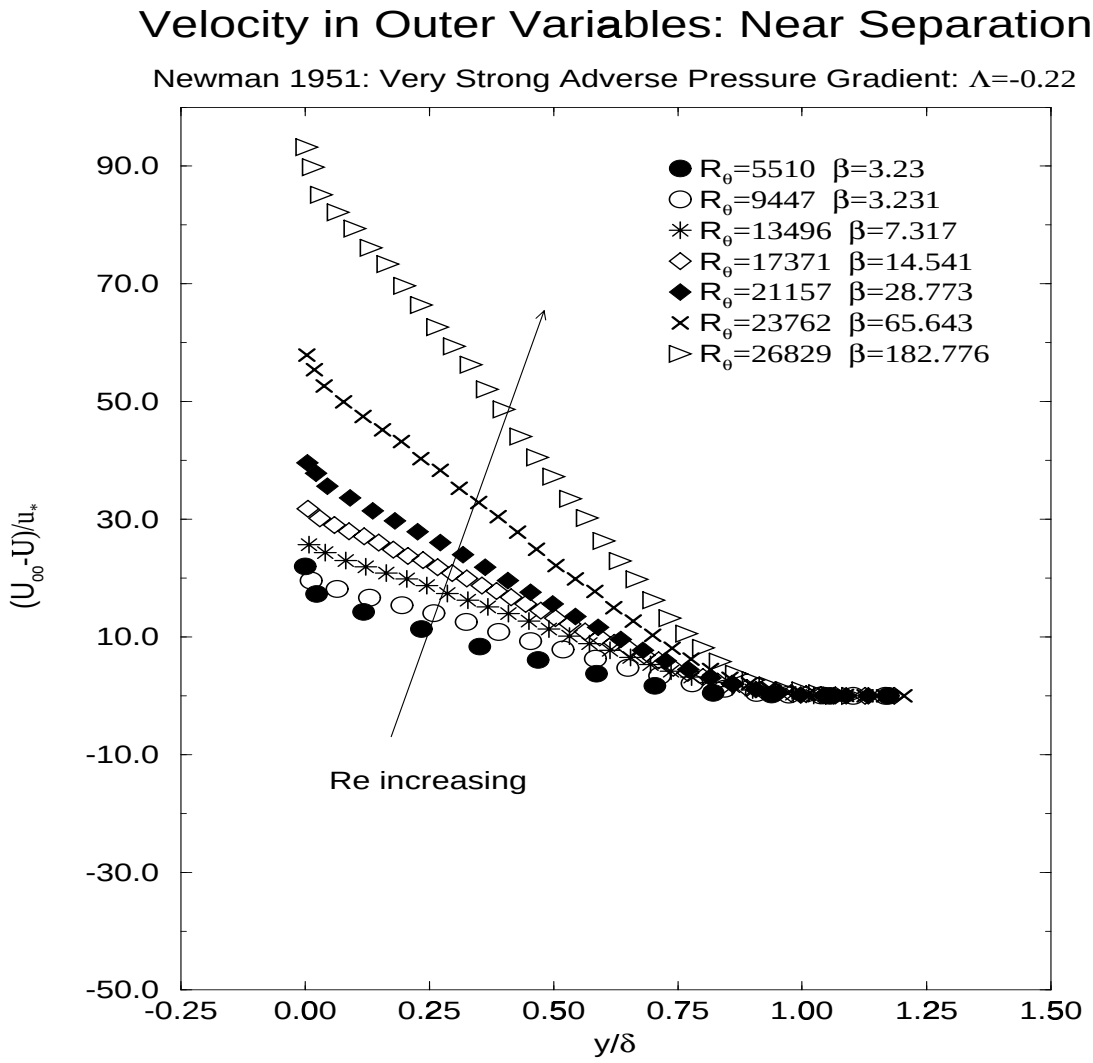

Figure 4.22: The velocity profiles in outer variables scaled with $U_{so} = u_*$ and δ for the Newman 1951 data at very strong adverse pressure gradient.

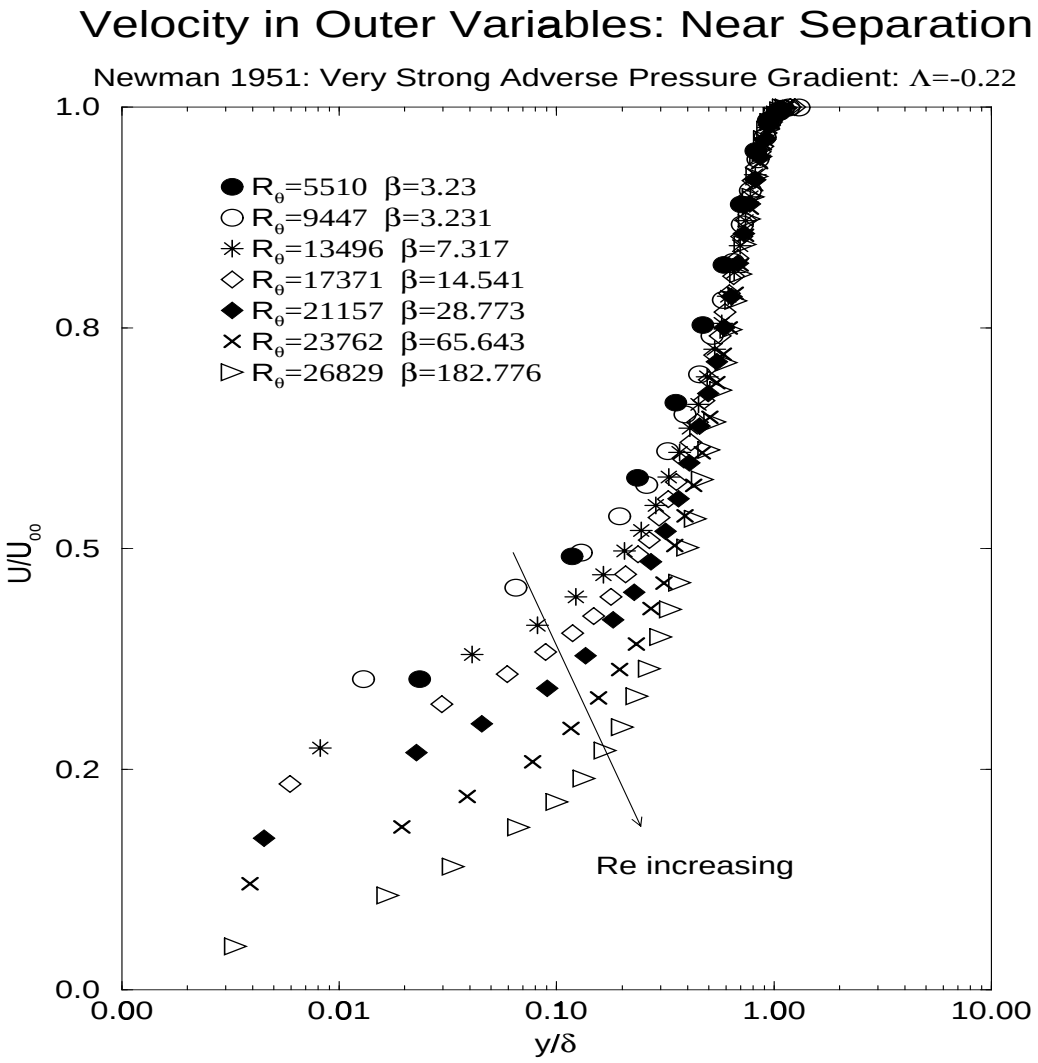

Figure 4.23: The velocity profiles in outer variables scaled with $U_{so} = U_\infty$ and δ for the Newman 1951 data at very strong adverse pressure gradient.

4.3.3 Moving Equilibrium Flows: $\Lambda = \Lambda(x)$

This is the category where most real flows with pressure gradient are classified since

$$\Lambda = \frac{\delta}{\rho U_\infty^2} \frac{1}{d\delta/dx} \frac{dP_\infty}{dx} \neq constant \tag{4.27}$$

As the name suggests these flows are equilibrium flows locally, but are in the process of moving from one equilibrium state to another as the external conditions change. The theory for equilibrium boundary layers set forth here applies to such cases. Several examples will be given in this section.

The first data is from Schubauer and Klebanoff 1947 ($1,412 \leq R_\theta \leq 76,711$). This data was acquired from a boundary layer on an large-airfoil like body, first with mild favorable pressure gradient, then a strong adverse pressure gradient with eventual separation. The log-log plot of U_∞ versus δ_*, θ is shown in Figure 4.24. Clearly there are three equilibrium regions where the $\Lambda \approx const.$ is the same for both length scales (δ_*, θ).

Another example where the flow is not in equilibrium is the boundary layer of a diverging channel with eventual separation (Ludweig and Tillman 1945). The log-log plot of U_∞ versus δ, δ_* and θ is shown in Figure 4.25. It is clear that the slope is not constant for any of the length scales, which leads to the conclusion that this flow is not in simple equilibrium. However, if the last two points of the data are considered to be a separate region (although c_f is still finite), then this flow has three regions where $\Lambda \approx const.$: The first corresponds to the region with a strong adverse pressure; the second is the transition toward separation; and for the third the flow is at a new equilibrium near separation ($c_f \to 0$). This shows clearly that the flow is locally in equilibrium, and as the external control imposed over the flow changes, the flow will continue to change until a new equilibrium is reached.

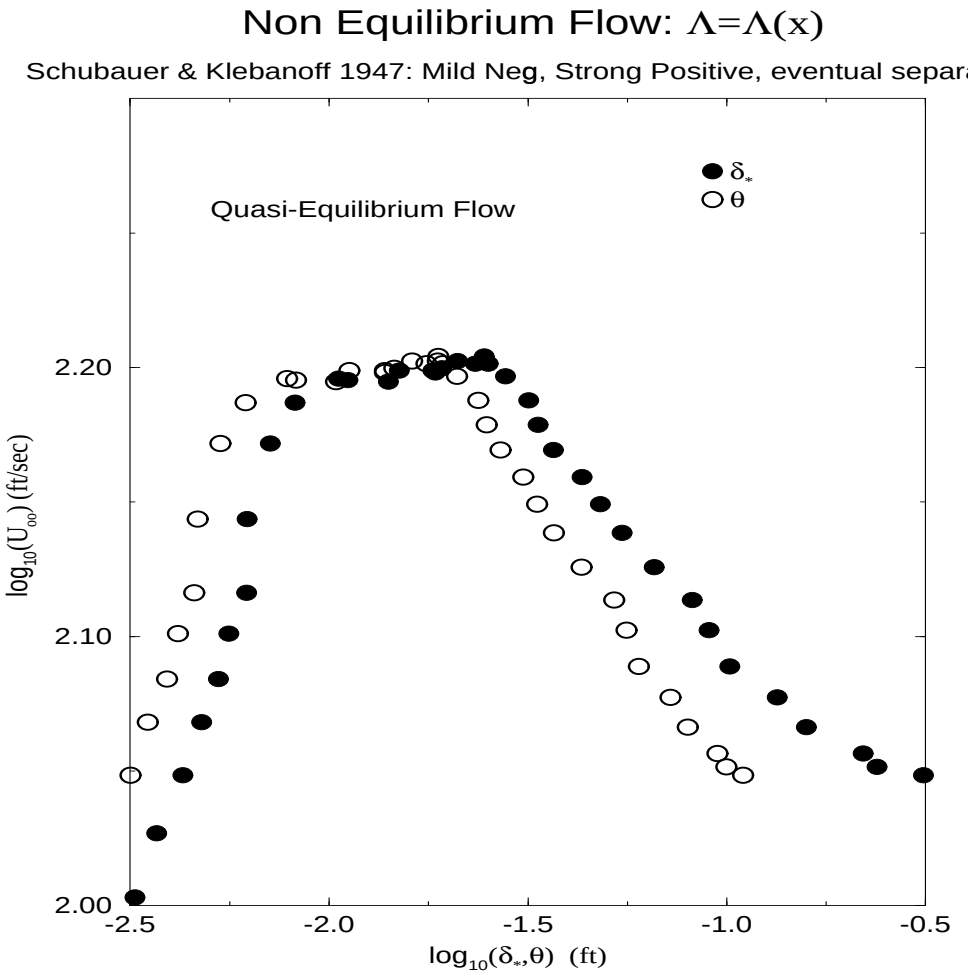

Q

Figure 4.24: The log-log plot of U_∞ (ft/sec) vs. δ_*, δ_* for the Schubauer and Klebanoff 1947 data in mild favorable pressure gradient then with a strong adverse pressure gradient with eventual separation.

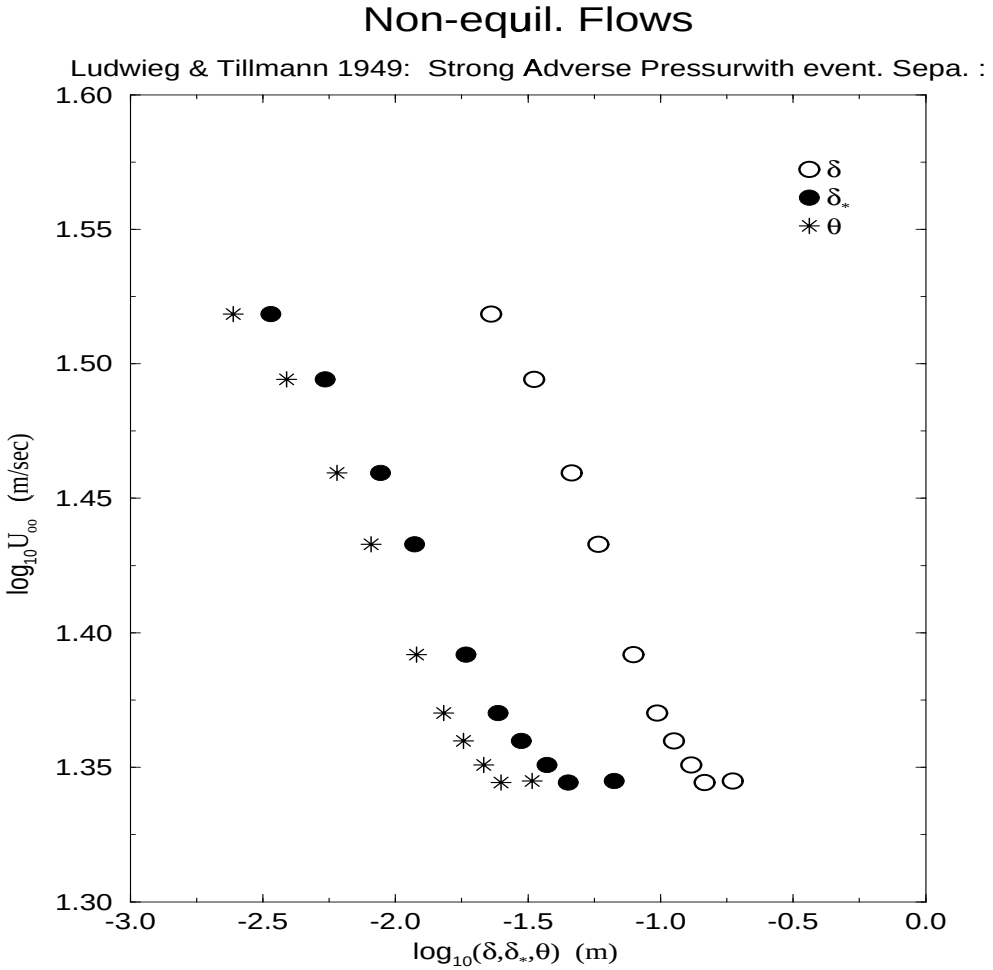

Figure 4.25: The log-log plot of U_∞ (ft/sec) vs. δ, δ_*, δ_* for the Ludweig and Tillmann 1949 data with a strong adverse pressure gradient with eventual separation.

The velocity profile scaled with U_∞ of the same experimental data is shown in Figure 4.26. Note that as the Reynolds number increases the collapse of the profiles moves closer to the wall toward what could be an asymptotic state, but since the pressure gradient keeps increasing downstream, the profiles adjust to a new equilibrium. The range in Reynolds number based on R_θ varies from 5,382, to 48,333. An important point that can only be obtained when the profiles are scaled this way is that as the adverse pressure gradient is increased in the flow, the wake or outer flow becomes more pronounced, at least relative to the overlap region.

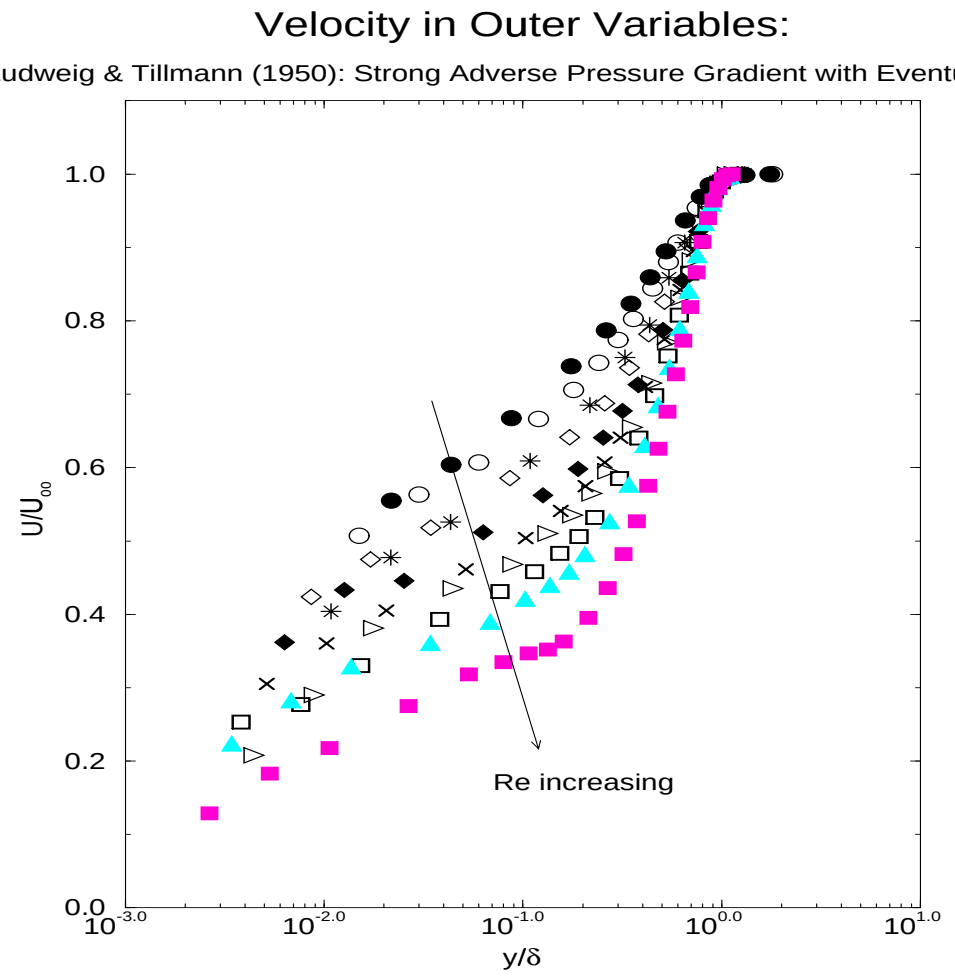

Figure 4.26: Velocity in outer variables scaled with U_∞ and δ for the Ludweig and Tillmann 1949 data with a strong adverse pressure gradient with eventual separation.

4.3.4 The Slow Approach to Equilibrium of the Inner Region

The objective of this section is to study how the boundary layer changes from one equilibrium state to another. Surprisingly, it will be seen to be the inner part of the boundary layer which lags the outer flow. The experimental data of Bradshaw 1965 and 1966 will be used to illustrate this effect on boundary layers with pressure gradient.

The first flow considered is that of Bradshaw 1965 ($24,984 \leq R_\theta \leq 30,217$) which was in equilibrium at moderate adverse pressure gradient, then the pressure gradient was abruptly decreased to zero. Figure 4.27 shows the equilibrium condition of U_∞ versus δ δ_* and θ. Note that the first three data points from top to bottom have the same slope implying that the flow is in equilibrium in this region, then the next four point from the bottom (left to right) have a zero slope which implies that $\Lambda = 0$ so that there is no pressure gradient in this region. Now the following question can be asked: Does this flow which is at zero pressure gradient behave in the same fashion as other zero pressure gradient flows?

To answer the question, the velocity profiles in outer variables scaled with U_∞ δ are plotted in Figure 4.28. Note how as the Reynolds number increases, the point of departure from the outer collapse moves outward, opposite to the expected behavior. However, even though the outer part of the last three profiles of Bradhsaw's data is consistent with the zero pressure gradient profiles of Smith/Walker at the same Reynolds number, the overlap and wall regions are not, although they are moving toward them. Note that $\Lambda = 0$ for both sets of data and the Reynolds number are about the same, so the profiles should be identical. Obviously the outer flow has begun to adjust to the new zero pressure gradient but the inner and overlap regions are lagging.

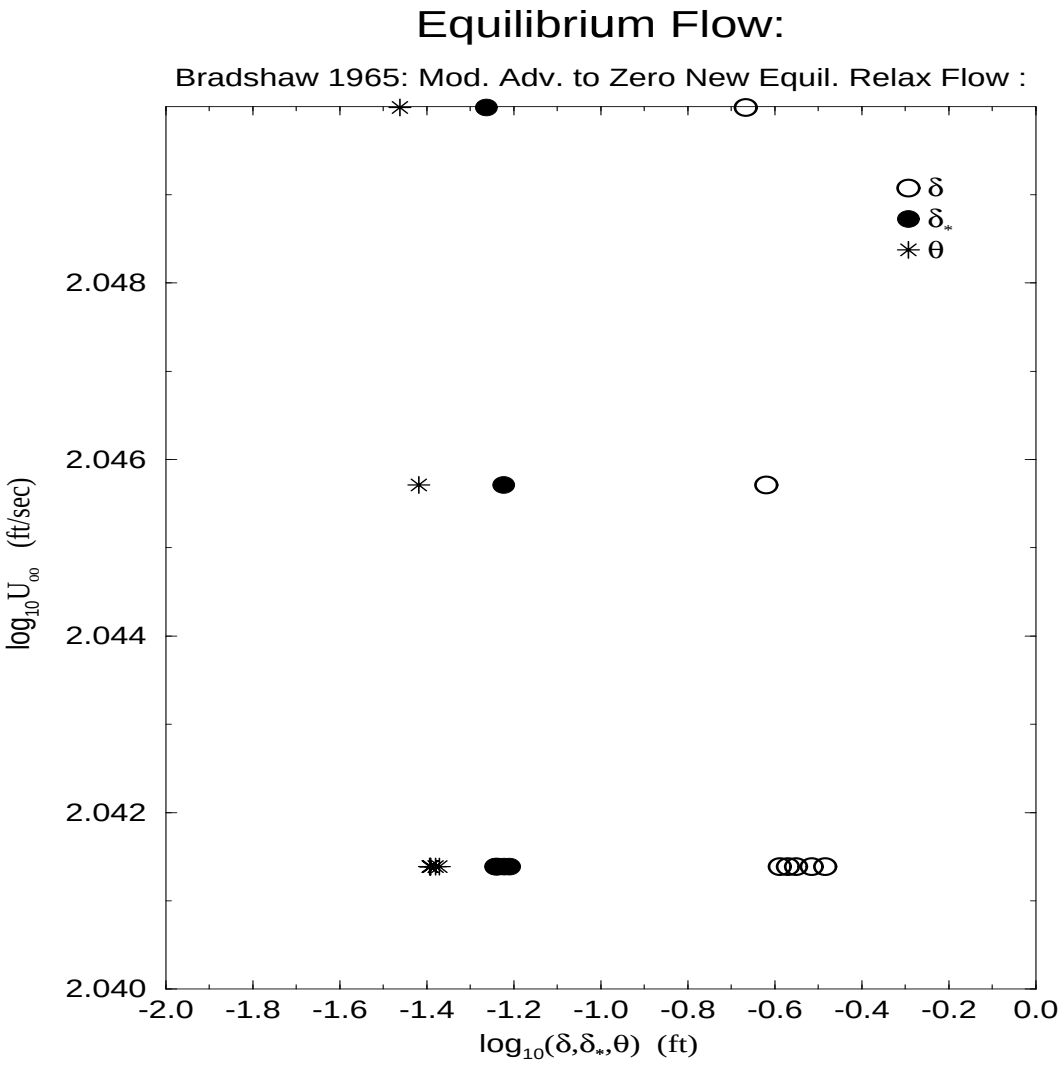

Figure 4.27: The log-log plot of U_∞ (ft/sec) vs. δ, δ_*, δ_* for the Bradshaw 1965 data. Equilibrium flow at moderate adverse pressure gradient, then the pressure gradient abruptly decreases to zero.

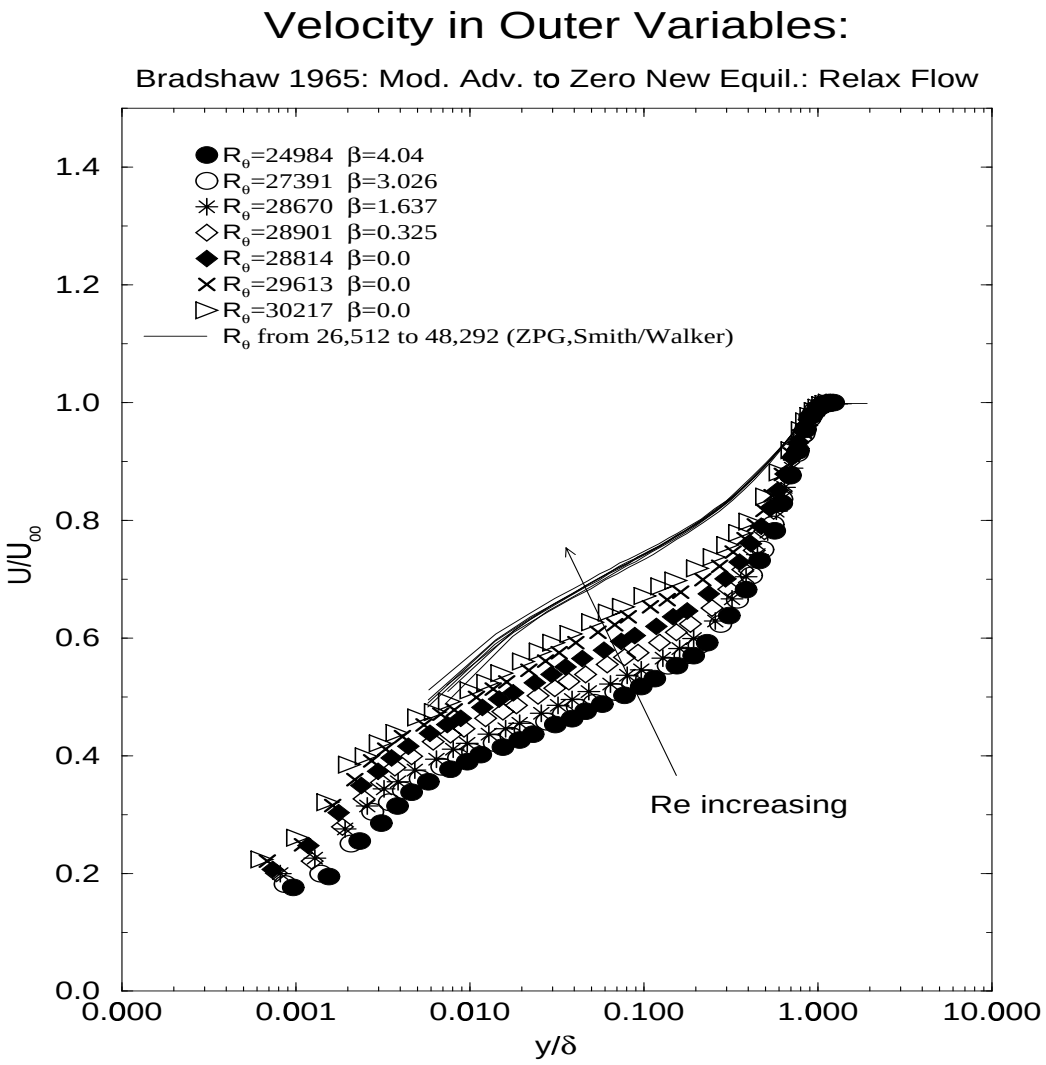

Figure 4.28: Velocity in outer variables scaled with U_∞ and δ for the Bradshaw 1965 data. Equilibrium flow at moderate adverse pressure gradient, then the pressure gradient abruptly decreases to zero.

In the next example, the data from Bradshaw 1966 is considered. In this particular experiment the flow was originally at zero-pressure gradient; then a moderate adverse pressure gradient was imposed on the flow. Figure 4.29 shows a log-log plot of U_∞ versus δ, δ_* θ. Obviously the flow is in equilibrium and Λ = constant. The velocity profile data scaled with U_∞ and δ are shown in Figure 4.30. Also shown is the Clauser's data for approximately the same conditions, but without the differing upstream history. Clearly Bradshaw's data is still changing toward a new equilibrium, even though the equilibrium condition is satisfied. Obviously the flow still has some memory of its past which was at zero pressure gradient. As in previous case considered, it is the inner flow which lags.

A question is raised by the observation above: How long does it take a flow to reach a state independent of its initial conditions or history? It will be seen in the next chapter that all of the effects of the pressure gradient show up in the outer parameter, C_o (or more properly C_{op}), at least as long as the flow is not near separation. *The inner flow is not affected directly, except by the value of* u_* *which is removed by the scaling in inner variables.* And the value of u_* is determined by the flux of momentum toward the wall imposed by the Reynolds stress in the outer flow. By arguments like those used for turbulence production in Chapter 2, it is possible to show that $D_{op} \sim 1/C_{op}$ (where D_{op} and C_{op} are the counterparts to C_o and D_o) since the inner parameters C_i and D_i are unaffected by the pressure gradient (v. Chapter 5). Thus the pressure gradient is reflected directly in the outer Reynolds stress scaling, but inversely to the velocity. If one argues that the turbulence can only adjust over several eddy turnover times to the new conditions, then the distance for this adjustment can be estimated as $\Delta x > U_\infty(\delta/u_*)$ where U_∞ is the convection velocity and δ/u_* is typical of the

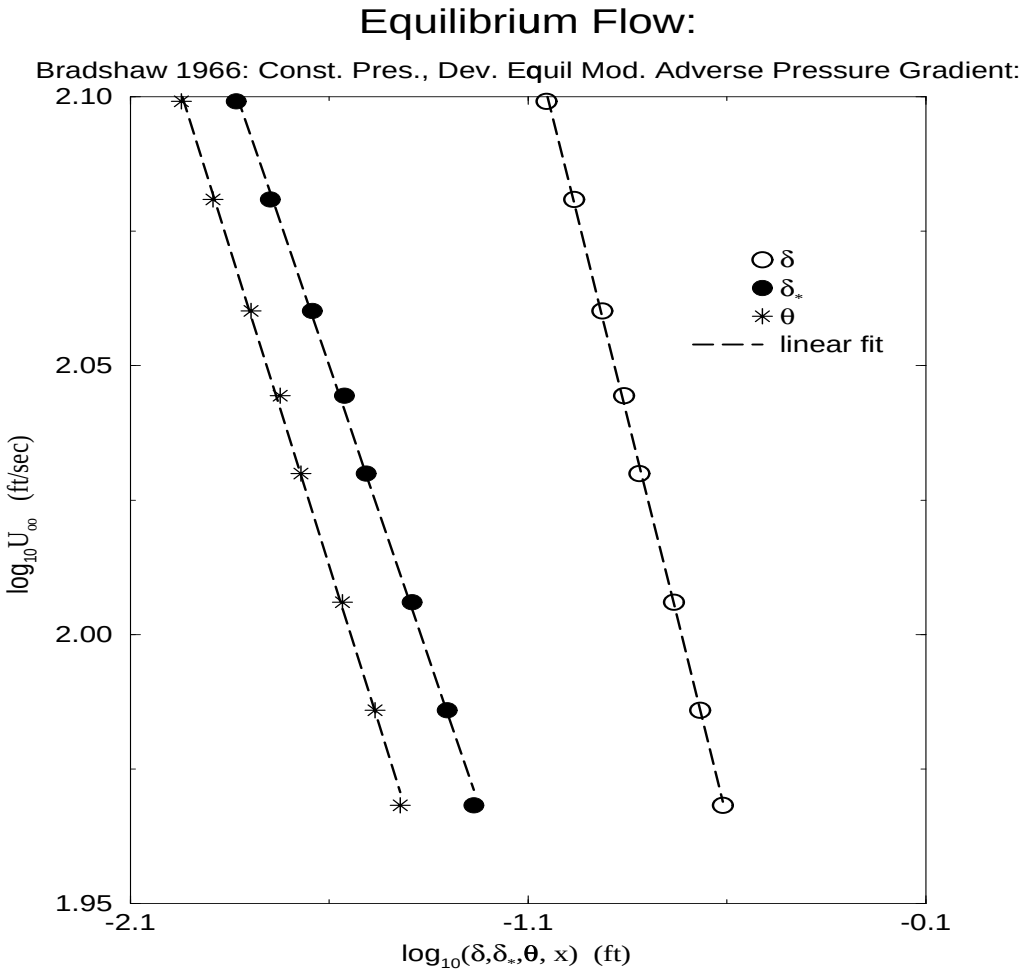

Figure 4.29: The log-log plot of U_∞ (ft/sec) vs. δ, δ_*, δ_* for the Bradshaw 1965 data. Flow at a zero pressure gradient then a moderate adverse pressure gradient is imposed on the flow.

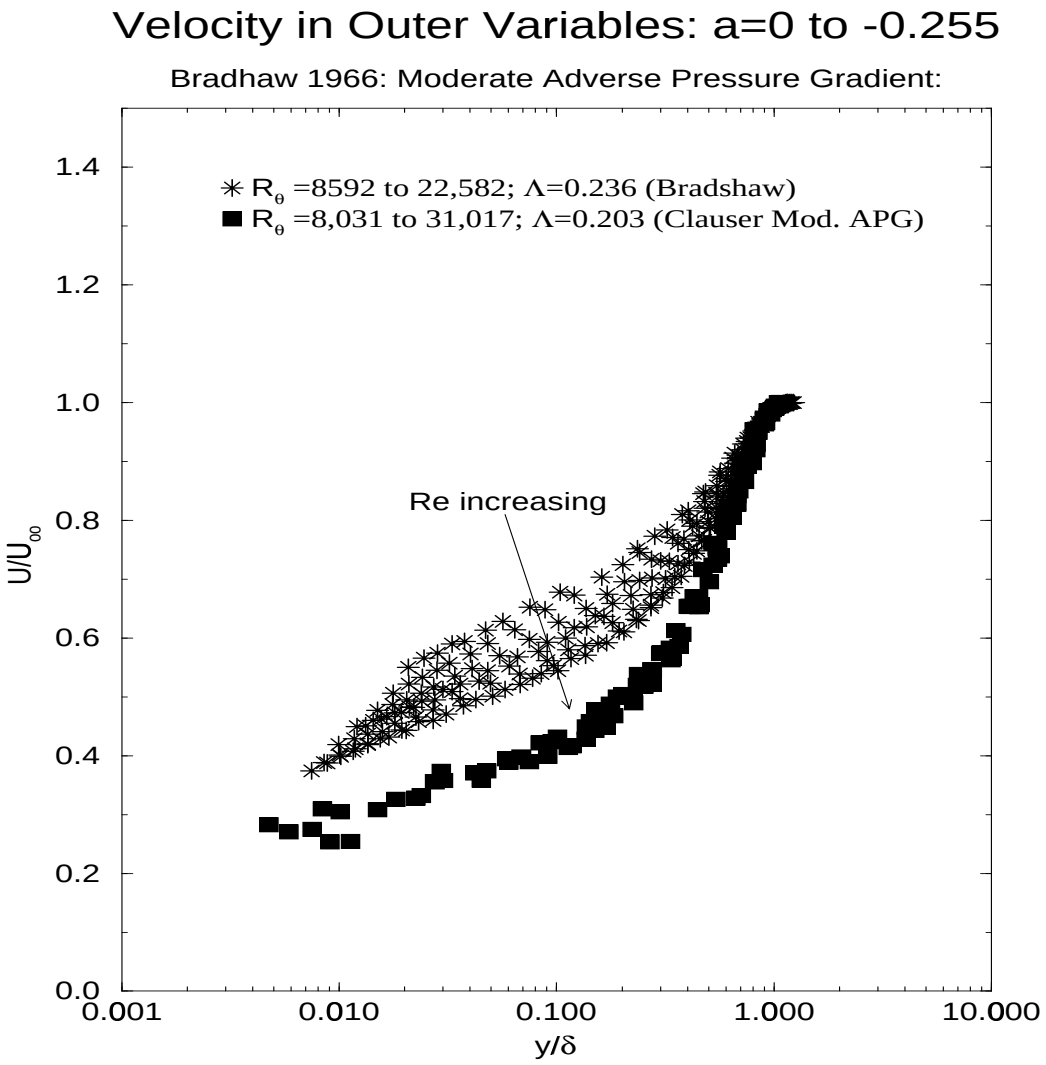

Figure 4.30: Velocity in outer variables scaled with U_∞ and δ for the Bradshaw 1965 data. Flow at a zero pressure gradient then a moderate adverse pressure gradient is imposed on the flow.

eddy turn over time. Obviously the outer flow responds more quickly because the external condition is directly imposed on it.

Chapter 5

PGBL: Inner and Overlap Regions

The Asymptotic Invariance Principle (AIP) and Near-Asymptotics is applied in this chapter to the inner boundary layer equations for pressure gradient boundary layers. The flow near separation is also considered.

5.1 Full Similarity of the Inner Equations

In keeping with the Asymptotic Invariance Principle set in previous chapters, solutions are sought which reduce to similarity solutions of the inner equations and boundary conditions (e.g., equation 1.3 in Chapter 1) in the limit of infinite Reynolds number (i.e., $\delta^+ \to \infty$). Solutions will be sought of the form

$$U = U_{si}(x) f_{ip\infty}(y^+, \Lambda) \tag{5.1}$$

$$-\overline{uv} = R_{si}(x) r_{ip\infty}(y^+, \Lambda) \tag{5.2}$$

where $y^+ = y/\eta(x)$ and Λ is the pressure gradient parameter defined in Chapter 4, i.e.,

$$\Lambda = \frac{\delta}{\rho U_\infty^2 d\delta/dx} \frac{dP_\infty}{dx} \tag{5.3}$$

The length scale $\eta = \eta(x)$ remains to be determined. Note that the subscript $ip\infty$ is used to distinguish the scaled velocity and Reynolds stress profiles, $f_{ip}(y^+, \delta^+, \Lambda)$ and $r_{ip}(y^+, \delta^+, \Lambda)$ which will be used later, from their limiting forms used here. Obviously f_{ip} and r_{ip} are dependent on δ^+ while $f_{ip\infty}$ and $r_{ip\infty}$ are not. Note that these solutions are less restrictive than the similarity forms used by Townsend 1956a,b, 1961 and Rotta 1962 in which the scaled velocity and Reynolds stress are the same in inner and outer variables (see Chapter 1).

Substitution into equation 1.4 and clearing terms yields to leading order in δ^+,

$$\left[\frac{u_*^2}{U_{si}^2}\right] = \left[\frac{R_{si}}{U_{si}^2}\right] r_{ip\infty} + \left[\frac{\nu}{\eta U_{si}}\right] f'_{ip\infty} - \left[\frac{\nu}{U_{si}^3}\frac{dP_\infty}{dx} y^+\right] \tag{5.4}$$

In the limit as $\delta^+ \to \infty$, the pressure gradient vanishes in the inner equation as long as Λ is finite (i.e., away from separation). Therefore, in this limit, the inner equation (for finite Λ) is exactly the same as for the zero pressure gradient boundary layer;

$$\left[\frac{u_*^2}{U_{si}^2}\right] = \left[\frac{R_{si}}{U_{si}^2}\right] r_{ip\infty} + \left[\frac{\nu}{\eta U_{si}}\right] f'_{ip\infty} \tag{5.5}$$

Thus, the velocity and length scales are the same as for zero pressure gradient boundary layer; i.e.,

$$\eta = \nu / U_{si} \tag{5.6}$$

$$U_{si} = u_* \tag{5.7}$$

$$R_{si} = U_{si}^2 \tag{5.8}$$

Using these equations in equation 5.4, the inner equation (retaining the pressure gradient for the moment) in similarity form reduces to,

$$1 = r_{i\infty} + f'_{i\infty} - \lambda y^+ \tag{5.9}$$

where

$$\lambda = \frac{\nu}{u_*^3}\frac{dP_\infty}{dx} \simeq \frac{\Lambda}{\delta^+} \tag{5.10}$$

As $\delta^+ \to \infty$, $\lambda \to 0$ (for finite Λ) and equation 5.9 reduces to the inner equation for zero pressure gradient boundary layer, i.e.,

$$1 = r_{i\infty} + f'_{i\infty} \tag{5.11}$$

For finite δ^+, it will be necessary to include δ^+ and Λ as arguments in the scaled inner profiles; obviously these should reduce to the zero pressure gradient results as $\Lambda \to 0$. Thus, as $\Lambda \to 0$,

$$\frac{U}{u_*} = f_{ip}(y^+, \delta^+, \Lambda) \to f_i(y^+, \delta^+) \tag{5.12}$$

$$-\frac{< uv >}{u_*^2} = r_{ip}(y^+, \delta^+, \Lambda) \to r_i(y^+, \delta^+) \tag{5.13}$$

where f_i and r_i are the functions for the zero pressure gradient derived in Chapters 2 and 3.

5.2 The Overlap Layer: An Application of Near-Asymptotics

It is obvious that (like the zero pressure gradient boundary layer discussed in Chapter 2) since both the outer and inner profiles are non-dimensional profiles with different scales and the ratio of the scales is Reynolds number dependent, then any region between the two similarity regimes cannot be Reynolds number independent, except possibly in the limit. Therefore both scaled forms of this solution, $f_{ip}(y^+; \delta^+; \Lambda)$ and $f_{op}(\overline{y}, \delta^+; \Lambda)$ respectively, represent the velocity everywhere, at least as long as the Reynolds number is finite. The following development is exactly analogous to the zero pressure gradient case, except for the parameter Λ. (The reader familiar with the analysis can skip the details and go directly to results, equations 5.24 and 5.25.)

As before, f_{ip} and f_{op} are quite unlike their limiting forms, $f_{i\infty}$ and $f_{o\infty}$, which are infinite Reynolds number solutions only for the inner and outer equations respectively. If f_{ip} and f_{op} are considered instead of $f_{ip\infty}$ and $f_{op\infty}$ (as is usually done), the problem of determining whether an overlap region exists is quite different from the usual asymptotic matching where infinite Reynolds number inner and outer solutions are extended and matched in an overlap region if one exists. Therefore, the objective here is *not* to see if f_{ip} and f_{op} overlap and match them if they do. It is rather to determine *whether the fact that these scaled finite Reynolds number solutions (to the whole flow) degenerate at infinite Reynolds number in different ways can be used to determine their functional forms in the common region they describe in the limit.*

There are several pieces of information about the two profiles which can be utilized without further assumptions. They are:

- First, since both inner and outer forms of the velocity profile must describe the flow everywhere as long as the ratio of length scales, $\delta^+ = \delta/\eta$, is finite, it follows that

$$1 + f_{op}(\overline{y}, \delta^+, \Lambda) = g_1(\delta^+) f_{ip}(y^+, \delta^+, \Lambda) \tag{5.14}$$

  where $g_1(\delta^+, \Lambda) = u_*/U_\infty$ since $U_\infty(1 + f_{op}) = u_* f_{ip}$ everywhere,

- Second, for finite values of δ^+, the velocity derivatives from both inner and outer forms of the velocity must also be the same everywhere. Differentiating equation 5.14 with respect to y at fixed δ^+ it follows that

$$\frac{\overline{y}}{1 + f_{op}} \frac{df_{op}}{d\overline{y}} = \frac{y^+}{f_{ip}} \frac{df_{ip}}{dy^+} \tag{5.15}$$

  for all values of δ^+ and y.

- Third, in the limit, both f_{op} and f_{ip} must become asymptotically independent of δ^+. Thus $f_{op}(\overline{y}, \delta^+, \Lambda) \rightarrow f_{o\infty}(\overline{y}, \Lambda)$ only and $f_{ip}(y^+, \delta^+, \Lambda) \rightarrow f_{ip\infty}(y^+, \Lambda)$ only as $\delta^+ \rightarrow \infty$, or otherwise full similarity is not possible which means that the velocity scales are not correct.

Now the problem is that *in the limit* as $\delta^+ \rightarrow \infty$, the outer form fails to account for the behavior close to the wall while the inner fails to describe the behavior away from it. The question then is: In this limit (as well as for all finite values approaching it) does there exist an "overlap" region where equation 5.14 is still valid? Since both δ and η are increasing with streamwise distance along the surface, this "overlap" region will not only increase in extent when measured in either inner or outer coordinates, it will move farther from the wall in actual physical variables.

As in Chapter 2, an intermediate variable $\tilde{y}$ can be introduced. The matching condition of equation 5.14 in terms of the intermediate variable, $\tilde{y}$, becomes,

$$1 + f_{op}(\tilde{y}{\delta^+}^{n-1}, \delta^+, \Lambda) = g_1(\delta^+, \Lambda) f_{ip}(\tilde{y}{\delta^+}^n, \delta^+, \Lambda) \tag{5.16}$$

where $\tilde{y}$ remain fixed in the limit as $\delta^+ \rightarrow \infty$ while $\overline{y} \rightarrow 0$ and $y^+ \rightarrow \infty$ and $0 < n < 1$. (The details can be found in chapter 2.)

Now equation 5.16 can be differentiated with respect to δ^+ *for fixed* $\tilde{y}$, the result is

$$\frac{\overline{y}}{1 + f_{op}} \frac{\partial (1 + f_{op})}{\partial \overline{y}}\Big|_{\delta^+} = \gamma_p(\delta^+, \Lambda) - \delta^+(S_{ip} - S_{op}) \tag{5.17}$$

where γ, S_{ip} and S_{op} are given as,

$$\gamma_p(\delta^+, \Lambda) = -\frac{\delta^+}{g_1} \frac{dg_1}{d\delta^+} \tag{5.18}$$

$$S_{ip}(\delta^+, y^+) \equiv \frac{1}{f_{ip}(y^+, \delta^+, \Lambda)} \frac{\partial f_{ip}(y^+, \delta^+, \Lambda)}{\partial \delta^+}\Big|_{y^+} \tag{5.19}$$

and

$$S_{op}(\delta^+, \overline{y}) \equiv \frac{1}{1 + f_{op}(\overline{y}, \delta^+, \Lambda)} \frac{\partial f_{op}(\overline{y}, \delta^+, \Lambda)}{\partial \delta^+}\Big|_{\overline{y}} \tag{5.20}$$

Now it is clear that if both

$$\delta^+ |S_{op}| << \gamma_p \tag{5.21}$$

and

$$\delta^+ |S_{ip}| << \gamma_p \tag{5.22}$$

then γ_p dominates. If $\gamma_p \rightarrow 0$, then the inequalities are still satisfied as long as the left hand side does so more rapidly than γ_p. Note that a much weaker condition can be applied which yields the same result, namely that both inner and outer scaled profiles have the same dependence on δ^+, i.e., $S_{ip} = S_{op}$ in the overlap range so γ_p is the only term remaining.

If these inequalities are satisfied over some range in y, then to leading order, equation 5.17 can be written as

$$\frac{\overline{y}}{1 + f_{op}^{(1)}} \frac{\partial (1 + f_{op}^{(1)})}{\partial \overline{y}}\Big|_{\delta^+} = \gamma_p(\delta^+, \Lambda) \tag{5.23}$$

The solution to equation 5.23 can be denoted as $f_{op}^{(1)}$ since it represents a first order approximation to f_{op}. It is *not*, however, simply the same as $f_{op\infty}$ because of the δ^+ dependence of γ_p, but reduces to it in the limit. Thus, by regrouping into the leading term all of the y-independent contributions, the method applied here has yielded a more general result than the customary expansion about infinite Reynolds number.

Equation 5.23 can be integrated analytically to yield,

$$\frac{U}{U_\infty} = 1 + f_{op}^{(1)}(\overline{y}, \delta^+, \Lambda) = C_{op}(\delta^+, \Lambda)\overline{y}^{\gamma_p(\delta^+,\Lambda)} \tag{5.24}$$

and

$$\frac{U}{u_*} = f_{ip}^{(1)}(y^+, \delta^+, \Lambda) = C_{ip}(\delta^+, \Lambda)y^{+\gamma_p(\delta^+,\Lambda)} \tag{5.25}$$

Thus the velocity profiles in inner and outer variables are **power law functions, exactly as for the zero pressure gradient case except for the presence of** Λ. The velocity parameters C_{ip}, C_{op} and γ_p must be asymptotically independent of Reynolds number, exactly as for zero pressure gradient boundary layer.

The relation between u_* and U_∞ can be obtained immediately from equation 5.14 as,

$$\sqrt{\frac{c_f}{2}} = \frac{u_*}{U_\infty} = g(\delta^+, \Lambda) = \frac{C_{op}(\delta^+, \Lambda)}{C_{ip}(\delta^+, \Lambda)}(\delta^+)^{-\gamma_p(\delta^+,\Lambda)} \tag{5.26}$$

Thus the friction law is also a power law entirely determined by the velocity parameters for the overlap region. However, equation 5.18 must also be satisfied. Substituting equation 5.26 into equation 5.18 implies that γ_p, C_{op}, and C_{ip} are constrained by

$$ln\delta^+ \frac{d\gamma_p}{d\delta^+} = \frac{d}{d\delta^+} ln\left[\frac{C_{op}}{C_{ip}}\right] \tag{5.27}$$

for all δ^+ and Λ.

As in Chapter 2 it is convenient to write the solution to equation 5.27 as

$$\frac{C_{op}}{C_{ip}} = exp[(\gamma_p - \gamma_{p\infty}) \ln \delta^+ + h_p] \tag{5.28}$$

where $h_p = h_p(\delta^+, \Lambda)$ remains to be determined, but must satisfy

$$\gamma_p - \gamma_{p\infty} = -\delta^+ \frac{dh_p}{d\delta^+} = -\frac{dh_p}{d \ln \delta^+} \tag{5.29}$$

It is easy to show that the condition that both $C_{op\infty}$ and $C_{ip\infty}$ be finite and non-zero requires that:

- *Either* C_{op}, C_{ip} and γ remain constant always,

or

- (i) $\gamma_p \rightarrow \gamma_{p\infty}$ faster than $1/\ln \delta^+$, and
- (ii) $h_p(\delta^+) \rightarrow h_{p\infty} = constant.$

It follows immediately that

$$\frac{C_{op\infty}}{C_{ip\infty}} = exp[h_{p\infty}] \tag{5.30}$$

Note that condition (i) together with equation 5.29 requires that $dh_p/d\ln\delta^+ \rightarrow 0$ faster than $1/\ln\delta^+$.

As $\Lambda \rightarrow 0$, the zero pressure gradient results must be recovered. Therefore, as $\Lambda \rightarrow 0$,

$$C_{op}(\delta^+, \Lambda) \rightarrow C_o(\delta^+) \tag{5.31}$$

$$C_{ip}(\delta^+, \Lambda) \rightarrow C_i(\delta^+) \tag{5.32}$$

$$\gamma_p(\delta^+, \Lambda) \rightarrow \gamma(\delta^+) \tag{5.33}$$

$$h_p(\delta^+, \Lambda) \rightarrow h(\delta^+) \tag{5.34}$$

5.3 Boundary Layer Not Near Separation ($\lambda << 1$)

It was shown earlier that as $\delta^+ \rightarrow \infty$, $\lambda \rightarrow 0$ if Λ is finite. Therefore, in this limit, the inner boundary layer is exactly the same as the zero pressure gradient boundary layer.

Figure 5.1 shows λ versus R_θ for most of the data which was considered in Chapter 4. [1] Note that λ is typically of order 10^{-3}, even for the relatively low Reynolds number

[1] The values for u_* were those cited by Coles 1968 using the Clauser method. These values will be challenged later, but the difference does not change the point being made here.

experiments.

Thus the inner solution for all pressure gradients is effectively the zero pressure gradient solution, at least away from separation. The reason for this is that $\lambda \simeq \Lambda/\delta^+$ in the limit as $\delta^+ \to \infty$. The absolute value of Λ is typically less than 0.3, at least as long as the flow is not near separation. On the other hand, $\delta^+ > 10^2$ always for turbulent boundary layers.

Thus it will appear that for flows not near separation, there is no influence at all of the externally imposed pressure gradient on the inner flow, *even for finite Reynolds number*. This can be seen another way by rewritting equation 5.9 so that the pressure gradient term is in outer variables; the result is,

$$1 \simeq r_{i\infty} + f'_{i\infty} - \Lambda\overline{y} \tag{5.35}$$

Since this equation is valid only for $\overline{y} < 0.1$ (due to the emergence of the convection terms in the outer flow), the last term is never greater than 0.1Λ. As long as the boundary layer is not near separation, $|\Lambda|$ is typically less than unity, so the direct pressure gradient contribution to the inner flow is negligible.

Therefore for all Reynolds number of interest, the inner boundary layer is effectively independent of Λ (or λ), and the zero pressure gradient results apply. As a consequence,

$$C_{ip}(\delta^+, \Lambda) \cong C_i(\delta^+) \tag{5.36}$$

$$\gamma_p(\delta^+, \Lambda) \cong \gamma(\delta^+) \tag{5.37}$$

as long as Λ is finite and δ^+ is large. Therefore, in this limit, only the outer parameter, C_{op} changes due to the effect of pressure gradient in the outer boundary layer.

So the only problem for the pressure gradient away from separation is to find C_{op}. But there is a constraint among C_{op}, C_{ip} and γ_p which using equation 5.36 and

equation 5.37 reduces to,

$$ln\delta^+ \frac{d\gamma}{d\delta^+} = \frac{d}{d\delta^+} ln\Big[\frac{C_{op}}{C_i}\Big] \tag{5.38}$$

Thus, whatever the dependence of C_{op} on Λ, it must not affect γ or C_i since they are independent of Λ in the limit as $\delta^+ \to \infty$ for finite Λ. Therefore, from equation 5.28, 5.29, 5.36, 5.37 and 5.38 it follows that

$$ln\frac{C_{op}}{C_i} = (\gamma_- \gamma_\infty) ln\delta^+ + h_p \tag{5.39}$$

and

$$(\gamma - \gamma_\infty) = -\frac{dh_p}{d(ln\delta^+)} \tag{5.40}$$

Since γ and C_i cannot be modified by h_p, it follows from equation 5.40 that the only way the pressure effect can enter in the solution for C_{op} is through an additive function of Λ only, say, Δh_p. Therefore,

$$h_p = h + \Delta h_p \tag{5.41}$$

where $h = h(\delta^+)$ only is the zero pressure gradient function and $\Delta h_p = \Delta h_p(\Lambda)$ only contains all the dependence on Λ.

It follows inmediately from equation 5.39 that,

$$\frac{C_{op}}{C_i} = \frac{C_{o\infty}}{C_{i\infty}} e^{\Delta h_p} exp\Big[(-ln\delta^+)\frac{dh}{dln\delta^+} + (h - h_\infty)\Big] \tag{5.42}$$

since $C_{o\infty}/C_{i\infty} = exp(h_\infty)$. Note that the argument of the exponential depends only on the $h - h_\infty$ for the zero pressure gradient turbulent boundary layer.

This equation can be written more conveniently as,

$$\frac{C_{op}}{C_i} = \frac{C_{o\infty}}{C_{i\infty}}\Big[1 + \Pi\Big] exp\Big[(-ln\delta^+ \frac{dh}{d(ln\delta^+)} + (h - h_\infty)\Big] \tag{5.43}$$

where

$$\Pi \equiv [e^{\Delta h_p} - 1]. \tag{5.44}$$

Thus all of the the Λ dependence is contained in $\Pi(\Lambda)$. Equation 5.43 can be rewritten as,

$$\frac{C_{op}}{C_{ip}} = \frac{C_o}{C_i}\Big[1 + \Pi\Big] \tag{5.45}$$

where C_o and C_i are the zero pressure gradient parameters for the same value of δ^+.

Thus, for finite Λ and large δ^+, the entire effect of the pressure gradient on the overlap region is reduced to a new additive parameter[2], Π, which is only a function of Λ. Therefore, all the results for the coefficients in the zero pressure gradient case can be used for the pressure gradient boundary layer with only one new unknown function of Λ, namely $\Pi(\Lambda)$.

The function $h - h_\infty$ was determined empirically in Chapter 2 to be given by $h - h_\infty = A/(ln\delta^+)^\alpha$. Substituting the function for h into equation 5.43 it follows,

$$\frac{C_{op}}{C_{ip}} = \frac{C_{o\infty}}{C_{i\infty}}\Big[1 + \Pi\Big] exp\Big[(1+\alpha)\frac{A}{(ln\delta^+)^\alpha}\Big] \tag{5.46}$$

The skin friction coefficient for pressure gradient boundary layer can inmediately, be obtained as

$$\frac{u_*}{U_\infty} = \frac{C_{o\infty}}{C_{i\infty}}[1 + \Pi]e^{-\gamma_\infty} exp\Big[(1+\alpha)\frac{A}{ln\delta^{+\alpha}}\Big] \tag{5.47}$$

It was determined in Chapter 3 that $C_{o\infty} = 0.897$, $C_{i\infty} = 55$, $\gamma = 0.0362$, $A = 2.90$ and $\alpha = 0.46$. Thus only Π needs to be determined as function of Λ to predict the skin friction in boundary layers with pressure gradient.

[2]This is not the same as Coles 1956 Π-parameter, although both atempt to account for pressure gradient effects

5.4 The Wake and Composite Velocity Profiles

It is possible to use the same composite velocity form proposed for the zero pressure gradient theory in the pressure gradient boundary layer. First, C_{op} must be substituted for C_o. And second, the linear term must be modified to account for the fact that the second derivative at the wall is non-zero because of the pressure gradient. In outer variables,

$$\begin{aligned}\frac{U}{U_\infty} &= (1-C_{op})\overline{y}\sin B\overline{y} + \frac{u_*}{U_\infty}\Big\{\Big[\overline{y}\delta^+ + \frac{1}{2}\lambda(\overline{y}\delta^+)^2\Big]exp[-d(\overline{y}\delta^+)^5] + \\ &\quad [C_i(\overline{y}\delta^+)^\gamma + C_{mi}(\overline{y}\delta^+)^{-1}][1-exp\{-d(\overline{y}\delta^+)^5\}] - C_i y^{+\gamma}\Big\} \qquad (5.48)\end{aligned}$$

where the only difference from zero pressure gradient[3] case is that $C_{op} = C_o + \Pi$ is used instead of C_o. Note that $C_o = C_o(\delta^+)$ only while $\Pi = \Pi(\Lambda)$ only. Thus both δ^+ and Λ must be known. The latter can be determined by iteration using the friction law (equation 5.47) with

$$\delta^+ = \frac{u_*}{U_\infty}\frac{\delta}{\theta}R_\theta \qquad (5.49)$$

where R_θ and δ/θ are known from the data.

The composite velocity in inner variables can be written as,

$$\begin{aligned}\frac{U}{u_*} &= \Big[C_i y^{+\gamma} + \frac{C_{mi}}{y^+}\Big]\Big[1-exp(-dy^{+5})\Big] \\ &+ \Big[y^+ + \frac{1}{2}\lambda y^{+2}\Big]exp(-dy^{+5}) + \Big[\frac{u_*}{U_\infty}\Big](1-C_{op})\frac{y^+}{\delta^+}sin(B\frac{y^+}{\delta^+}) \qquad (5.50)\end{aligned}$$

[3]Recall that for zero pressure gradient; $B = 2.03$, $C_{mi} = -37$ and $d = 2.0E-05$. These values apply also for the pressure gradient boundary layer.

5.5 The Inner Boundary Layer Near Separation

It was shown in Chapter 4 that at separation $\Lambda \equiv 1/(2+H)$ is the condition for equilibrium boundary layers at separation Thus, from the perspective of the scaling, at least, there is nothing particularly interesting for the outer flow. The inner flow, however, is much more interesting since the condition for negligibility of pressure gradient effects (i.e., $\lambda << 1$) is no longer satisfied. This situation was originally analyzed by Stratford 1959a,b and the scaling variables he proposed can be seen to fall nicely out of the similarity approach used here.

It is immediately obvious from equation 1.4 that u_* can not be a parameter in the separation limit since u_* it is zero in this limit (since $\tau_w/\rho = u_*^2 = 0$). Therefore, the viscous stress must be balanced by the pressure gradient alone. It follows inmediately from the similarity of the inner equations at separation that the velocity and length scales are given as,

$$U_{sep}(x) \equiv \frac{\nu}{\rho}\frac{dP_\infty}{dx} \tag{5.51}$$

and

$$\eta_{sep}(x) \equiv \frac{1}{\rho\nu}\frac{dP_\infty}{dx} \tag{5.52}$$

These, are of course, Stratford's variables.

Thus the velocity profile in the inner region is given by

$$U(x,y) = U_{sep}(x) f_{sep}(y/\eta_{sep}, \delta^+, \Lambda) \tag{5.53}$$

As before, Λ is the pressure gradient parameter. (Note that in the limit as the Reynolds number goes to infinity the above equation is independent of δ^+.)

Chapter 6

Turbulent Pipe and Channel Flows

In this chapter the scales and functions governing turbulent pipe and channel flows will be determined by employing similar ideas as in previous chapters [1]. It should be noted that because these flows are homogeneous in the x-direction the exact procedure applied to boundary layers to get the velocity scales can not be applied. But the equations of motion for the inner and outer flow can still be used to determine the velocity scales in inner and outer variables.

6.1 The Scaling Laws and the AIP

The streamwise momentum equation for a fully developed two-dimensional channel flow at high Reynolds number reduces to

$$0 = -\frac{1}{\rho}\frac{dP}{dx} + \frac{\partial}{\partial y}\left[- < uv > +\nu\frac{\partial U}{\partial y}\right] \tag{6.1}$$

Like the boundary layer, the viscous term is negligible everywhere but very near the wall, so that the core (or outer) flow in the limit of infinite Reynolds number is

[1] This chapter closely parallels George and Castillo 1996.

governed by

$$0 = -\frac{1}{\rho}\frac{dP}{dx} + \frac{\partial}{\partial y} - < uv > \tag{6.2}$$

In the limit of infinite Reynolds number, the inner layer is governed by

$$0 = \frac{\partial}{\partial y}\left[- < uv > + \nu \frac{\partial U}{\partial y} \right] \tag{6.3}$$

This can be integrated from the wall to obtain

$$u_*^2 = - < uv > + \nu \frac{\partial U}{\partial y} \tag{6.4}$$

where u_* is the friction velocity. It is obvious that the inner profile must scale with u_* and ν since these are the only parameters in the inner equations and boundary conditions. Hence, the only length scale is $\eta = \nu/u_*$, and there must be a law of the wall in which

$$\frac{U}{u_*} = f_{i\infty}(y^+) \tag{6.5}$$

where $y^+ = y/\eta$.

Because there is no imposed condition on the velocity, except at the wall, an outer scaling velocity must be sought from the parameters in the outer equation itself. Since there are only two, $-(1/\rho)dP/dx$, the externally imposed pressure gradient, and R the channel half-width, only a single velocity can be formed; namely,

$$U_o = \left(-\frac{R}{\rho}\frac{dP}{dx} \right)^{1/2} \tag{6.6}$$

Unlike the developing boundary layer, the channel flow is homogeneous in the streamwise direction, so there is an exact balance between the wall shear stress acting on the walls, and the net pressure force acting across the flow. This equilibrium requires that

$$u_*^2 = -\frac{R}{\rho}\frac{dP}{dx} \tag{6.7}$$

which is just the square of equation 6.6 above ; thus, $U_o = u_*$. Therefore, the outer scale velocity is also u_*, and the outer and inner velocity scales are the same. Since the only length scale is R, the velocity deficit relative to the centerline velocity, U_c, must be given by

$$\frac{U - U_c}{u_*} = f_{o\infty}(\overline{y}) \tag{6.8}$$

where $\overline{y} = y/R$. Thus channel and pipe flows are fundamentally different from boundary layer flows where asymptotic Reynolds number independence demands that the inner and outer scales for the mean velocity be different (see Chapter 2).

It is obvious that since the length scales governing the inner and outer equations are different, no single scaling law should be able to collapse data for the entire flow. Moreover, since the neglected terms in both the inner and outer equations above depend on the ratio of length scales (v. Tennekes and Lumley 1972), then neither set of scaling parameters will be able to perfectly collapse the data in either region at finite values of $R^+ = Ru_*/\nu$. The Asymptotic Invariance Principle of George 1995 states that the appropriate choices for scaling are those which lead to similarity solutions of the inner and outer equations separately in the limit for which those equations themselves are valid, namely $R^+ \to \infty$. Thus the appropriate inner and outer scaling laws for the velocity profile are

$$\frac{U}{u_*} = f_i(y^+, R^+) \tag{6.9}$$

and

$$\frac{U - U_c}{u_*} = f_o(\overline{y}, R^+) \tag{6.10}$$

where the outer velocity has been referenced to the velocity at the centerline, U_c, to avoid the necessity of accounting for the change over the inner layer. The only other difference from the boundary layer is that the outer length scale is some measure of the

width of the channel, say the half-width (or pipe radius), R. Note that both of these describe the *entire* velocity profile as long as $R^+ = u_* R/\nu$, the ratio of outer to inner length scales, is retained. This is because they represent the same solutions to the complete governing equations for given R^+, but have been simply scaled differently.

If the scaled profiles above are indeed proper scaling laws, then they should by the Asymptotic Invariance Principle (AIP) become asymptotically independent of R^+ in the limit of infinite Reynolds number; i.e.,

$$\begin{aligned} \lim f_i(y^+, R^+) &\rightarrow f_{i\infty}(y^+) \\ \lim f_o(\overline{y}, R^+) &\rightarrow f_{o\infty}(\overline{y}) \end{aligned}$$

as $R^+ \rightarrow \infty$. In fact, these limiting profiles should be solutions to the inner and outer equations respectively, which are themselves valid only in the infinite Reynolds number limit.

Figures 6.1 and 6.2 show the mean velocity profile data from the superpipe experiment (Zagarola 1996, see also Zagarola and Smits 1996) in both inner and outer variables. Note the excellent collapse very close to the wall ($y^+ < 100$) in inner variables and over the core region ($\overline{y} > 0.3$). Note also that the region of approximate collapse in inner variables (Figure 6.1) increases from the wall with increasing Reynolds number, as does the inward extent of the outer variable collapse (Figure 6.2). Finally note that the inner scaling does not collapse the data at all where the outer scaling collapses it best, and vice versa. Both the region of only approximate collapse and the region of no collapse at all are manifestations of the dependence of the scaled profiles on R^+ as argued above.

Unlike boundary layer measurements, the shear stress for the superpipe data can be independently determined from the pressure gradient alone. The close proximity

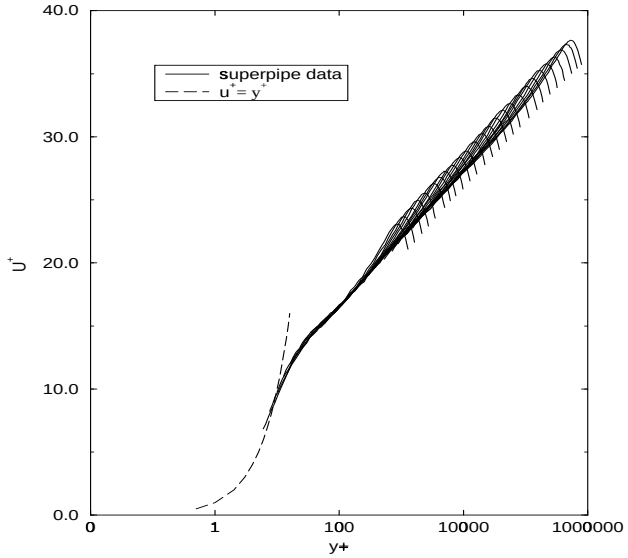

Figure 6.1: Velocity profiles in inner variables

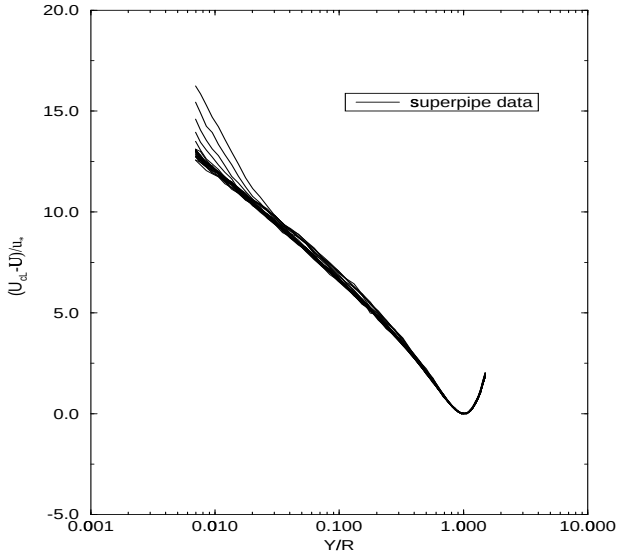

Figure 6.2: Velocity profiles in outer variables

of the data near the wall to the exact solution valid there ($u^+ = y^+$) gives considerable credibility to the velocity measurements, even without correction. The direct determination of the shear stress from the pressure drop down the pipe (without choosing it to collapse the 'log' layer which can only be assumed to collapse) is especially important since there is evidence of a lack of complete collapse of the data in Figure 6.1 outside of $y^+ = 10$, especially for the lowest Reynolds numbers. The lack of collapse is even more apparent for the outer scaling in Figure 6.2 inside of $\overline{y} \approx 0.3$ which includes all of the overlap region discussed below.

6.2 The Overlap Layer: Another Application of Near-Asymptotics

It is obvious that since the outer and inner profiles scale differently and the ratio of length scales is in fact the Reynolds number, then the region between the two similarity regimes cannot be Reynolds number independent, except possibly in the limit of infinite Reynolds number. The actual mean velocity profile at any finite Reynolds number, however, is the average of the instantaneous solutions to the Navier-Stokes equations and boundary conditions. And this profile, whether determined from a real flow by measurement, a DNS simulation, or not at all, exists, at least in principle, and is valid everywhere *regardless of how it is scaled.* Therefore both scaled forms of this solution, $f_i(y^+, R^+)$ and $f_o(\overline{y}, R^+)$ (equations 6.9 and 6.10 respectively), represent the velocity everywhere, at least as long as the Reynolds number is finite. In fact, the parameter R^+ uniquely labels the fanning out of the inner scaled profiles in the outer region and the outer scaled profiles near the wall in Figures 6.1 and 6.2.

Thus, f_i and f_o are quite unlike their limiting forms, $f_{i\infty}$ and $f_{o\infty}$, which are only

infinite Reynolds number solutions for the inner and outer equations respectively. If f_i and f_o are considered instead of $f_{i\infty}$ and $f_{o\infty}$ (as is usually done), the problem of determining whether an overlap region exists is quite different from the usual asymptotic matching where infinite Reynolds number inner and outer solutions are extended and matched in an overlap region if one exists. Therefore, the objective here is *not* to see if f_i and f_o overlap and match them if they do. Rather, it is rather to determine *whether the fact that these scaled finite Reynolds number solutions (to the whole flow) degenerate at infinite Reynolds number in different ways* can be used to determine their functional forms in the common region they describe in the limit. The methodology outlined below (termed *Near-Asymptotics*) is an extension of Intermediate Asymptotics (v. Barenblatt 1978), and is necessary because the traditional approach cannot account for the possibility of the matching parameter tending to zero, as might be the case.

The fact that analytical forms for these Reynolds number dependent solutions are not available, and they are only known *in principal* turns out not to be a significant handicap. There are several pieces of information about the two profiles which can be utilized without further assumptions. They are:

- First, since both inner and outer forms of the velocity profile must describe the flow everywhere as long as the ratio of length scales, $R^+ = R/\eta$, is finite, it follows from equations 6.9 and 6.10 that

$$\frac{1}{g(R^+)} + f_o(\overline{y}, R^+) = f_i(y^+, R^+) \tag{6.11}$$

  where $g(R^+)$ is defined by

$$g(R^+) \equiv u_*/U_c \tag{6.12}$$

- Second, for finite values of R^+, the velocity derivatives from both inner and

outer forms of the velocity must also be the same everywhere. It is easy to show that this implies that

$$\overline{y}\frac{\partial f_o}{\partial \overline{y}} = y^+\frac{\partial f_i}{\partial y^+} \tag{6.13}$$

for all values of R^+ and y.

- Third, as noted above, in the limit both f_o and f_i must become asymptotically independent of R^+; i.e., $f_o(\overline{y}, R^+) \rightarrow f_{o\infty}(\overline{y})$ and $f_i(y^+, R^+) \rightarrow f_{i\infty}(y^+)$ as $R^+ \rightarrow \infty$.

Now the problem is that *in the limit* as $R^+ \rightarrow \infty$, the outer form fails to account for the behavior close to the wall while the inner fails to describe the behavior away from it. The question then is: In this limit (as well as for all finite values approaching it) does there exist an "overlap" region where equation 6.11 is still valid? (Note that boundary layer flows are quite different from pipe and channel flows since the overlap layer in the latter remains at fixed distance from the wall for all x because of the streamwise homogeneity, as long as the external parameters are fixed, while in the former it moves away from the wall with increasing x.)

The question of whether there is a common region of validity can be investigated by examining how rapidly f_o and f_i are changing with R^+. The relative variation of f_i and f_o with Reynolds number can be related to their Taylor expansions about a fixed value of R^+; i.e.,

$$\frac{f_i(y^+; R^+ + \Delta R^+) - f_i(y^+; R^+)}{\Delta R^+ f_i(y^+, R^+)} \approx \frac{1}{f_i(y^+, R^+)}\frac{\partial f_i(y^+; R^+)}{\partial R^+}\Big|_{y^+} \equiv S_i(R^+, y^+) \tag{6.14}$$

and

$$\frac{f_o(\overline{y}; R^+ + \Delta R^+) - f_o(\overline{y}; R^+)}{\Delta R^+ f_o(\overline{y}, R^+)} \approx \frac{1}{f_o(\overline{y}, R^+)}\frac{\partial f_o(\overline{y}; R^+)}{\partial R^+}\Big|_{\overline{y}} \equiv S_o(R^+, \overline{y}) \tag{6.15}$$

Thus S_i and S_o are measures of the Reynolds number dependences of f_i and f_o respectively. Both vanish identically in the limit as $R^+ \to \infty$. If ${y^+}_{max}$ denotes a location where outer flow effects begin to be strongly felt on the inner scaled profile, then for $y^+ < {y^+}_{max}$, S_i should be much less than unity (or else the inner scaling is not very useful). Similarly, if $\overline{y}_{min}$ measures the location where viscous effects begin to be strongly felt (e.g., as the linear velocity region near the wall is approached), then S_o should be small for $\overline{y} > \overline{y}_{min}$. Obviously either S_i or S_o should increase as these limits are approached. Outside these limits, one or the other should increase dramatically.

The quantities S_i and S_o can, in fact, be used to provide a formal definition of an "overlap" region where both scaling laws are valid. Since S_i will increase drastically for large values of y for given R^+ and S_o will increase for small values of y, an "overlap" region exists only if there exists a region for which both S_i and S_o remain small simultaneously. In the following paragraphs, this condition will be used in conjunction with equation 6.11 to derive the functional form of the velocity in the overlap region *at finite Reynolds number*, hence the term 'Near-Asymptotics'. This is, of course, Intermediate Asymptotics, but at finite Reynolds numbers.

Because of the movement of the matched layer toward the wall with increasing R^+, it is convenient and necessary to introduce an intermediate variable $\tilde{y}$ which can be fixed in the overlap region all the way to the limit, regardless of what is happening in physical space (v. Cole and Kevorkian 1981). A definition of $\tilde{y}$ which accomplishes this is given by

$$\tilde{y} = y^+ {R^+}^{-n} \tag{6.16}$$

or

$$y^+ = \tilde{y} {R^+}^n \tag{6.17}$$

Since $\overline{y} = y^+/R^+$, it follows that

$$\overline{y} = \tilde{y}{R^+}^{n-1} \tag{6.18}$$

For all values of n satisfying $0 < n < 1$, $\tilde{y}$ can remain fixed in the limit as $R^+ \to \infty$ while $\overline{y} \to 0$ and $y^+ \to \infty$. Substituting these into equation 6.11 yields the matching condition on the velocity in terms of the intermediate variable as

$$\frac{1}{g(R^+)} + f_o({R^+}^{n-1}\tilde{y}, R^+) = f_i({R^+}^{n}\tilde{y}, R^+) \tag{6.19}$$

Now equation 6.19 can be differentiated with respect to R^+ *for fixed* $\tilde{y}$ to yield equations which explicitly include S_i and S_o. The result after some manipulation is

$$\overline{y}\left(\frac{\partial f_o}{\partial \overline{y}}\right)_{R^+} = \frac{1}{\kappa} - R^+[S_i(y^+, R^+)f_i(y^+, R^+) - S_o(\overline{y}, R^+)f_o(\overline{y}, R^+)] \tag{6.20}$$

where

$$\frac{1}{\kappa(R^+)} \equiv -\frac{R^+}{g^2}\frac{dg}{dR^+} = \frac{d(1/g)}{d\ln R^+} \tag{6.21}$$

Note that the first term on the right hand side of equation 6.20 is at most a function of R^+ alone, while the second term contains all of the residual y-dependence.

Now it is clear that if both

$$R^+|S_o|f_o << 1/\kappa \tag{6.22}$$

and

$$R^+|S_i|f_i << 1/\kappa \tag{6.23}$$

then the first term on the right-hand side of equation 6.20 dominates. Even if $1/\kappa \to 0$, the inequalities are still satisfied as long as the left hand side does so more rapidly than $1/\kappa$. Note that a much weaker condition can be applied which yields the same result; namely that both inner and outer scaled profiles have the same dependence

on R^+, i.e., $S_i f_i = S_o f_o$ in the overlap range so $1/\kappa$ is the only term remaining. If these inequalities are satisfied over some range in y, then to leading order, equation 6.20 can be written as

$$\overline{y}\frac{\partial f_o}{\partial \overline{y}} = \frac{1}{\kappa} \tag{6.24}$$

The solution to equation 6.24 can be denoted as $f_o^{(1)}$ since it represents a first order approximations to f_o. It is *not*, however, simply the same as $f_{o\infty}$ because of the R^+ dependence of $1/\kappa$, but reduces to it in the limit. Thus, by regrouping into the leading term all of the y-independent contributions, the method applied here has yielded a more general result than the customary expansion about infinite Reynolds number. (It is also easy to see why the usual matching of infinite Reynolds number inner and outer solutions will not work if the limiting value of $1/\kappa$ is zero.)

From equations 6.13 and 6.24, it follows that

$$y^+\frac{\partial f_i}{\partial y^+} = \frac{1}{\kappa} \tag{6.25}$$

An interesting feature of these first order solutions is that the inequalities given by equations 6.22 and 6.23 determine the limits of validity of both equations 6.24 and 6.25 since either S_o or S_i will be large outside the overlap region. Clearly the extent of this region will increase as the Reynolds number (or R^+) increases.

Equations 6.24 and 6.25 can be readily integrated to yield (to leading order)

$$f_o^{(1)}(\overline{y}, R^+) = \frac{1}{\kappa(R^+)} ln\overline{y} + B_o(R^+) \tag{6.26}$$

and

$$f_i^{(1)}(y^+, R^+) = \frac{1}{\kappa(R^+)} lny^+ + B_i(R^+) \tag{6.27}$$

In the remainder of this Chapter, the superscript '(1)' will be dropped; however it is these first order solutions that are being referred to unless otherwise stated. Thus

the velocity profiles in the overlap are logarithmic, but with parameters which are Reynolds number dependent.

The parameters $1/\kappa$, B_i and B_o must themselves be asymptotically constant since the equations to which they are solutions are themselves Reynolds number independent in the limit (the AIP). Moreover, the limiting values, κ_∞, $B_{i\infty}$, and $B_{o\infty}$ cannot all be zero, or else the solutions themselves are trivial. In fact, in the limit of infinite Reynolds number the energy balance in the overlap range reduces to production equals dissipation; i.e.,

$$\epsilon^+ = \frac{du^+}{dy^+} = \frac{1}{\kappa y^+} \tag{6.28}$$

Also the local energy dissipation rate ϵ^+, must be finite and non-zero (v. Frisch 1995). It follows that $1/\kappa_\infty$ must be finite and non-zero, consistent with the Millikan 1938 assumption. It will be shown below that these conditions severely restrict the possible Reynolds number dependencies for the parameters.

The relation between u_* and U_c follows immediately from equation 6.11; i.e.,

$$\frac{1}{g(R^+)} = \frac{1}{\kappa(R^+)} lnR^+ + [B_i(R^+) - B_o(R^+)] \tag{6.29}$$

Thus the friction law is entirely determined by the velocity parameters for the overlap region. However, equation 6.21 must also be satisfied. Substituting equation 6.29 into equation 6.21 implies that κ, B_i, and B_o are constrained by

$$lnR^+ \frac{d(1/\kappa)}{dR^+} = -\frac{d(B_i - B_o)}{dR^+} \tag{6.30}$$

Equation 6.30 is exactly the criterion for the neglected terms in equation 6.20 to vanish identically (i.e., $S_i f_i - S_o f_o \equiv 0$). Therefore the solution represented by equations 6.26 – 6.30 is, indeed, the first order solution for the velocity profile in the overlap layer at *finite*, but large, Reynolds number. Clearly when y^+ is too big or $\overline{y}$

is too small for a given value of R^+, the inequalities of equation 6.22 and 6.23 cannot be satisfied. Since all the derivatives with respect to R^+ must vanish as $R^+ \to \infty$ (the A.I.P.), the inner range of the outer overlap solution is unbounded in the limit, as is the outer range of the inner.

Thus the velocity profile in the overlap layer is logarithmic, *but* with parameters which depend on Reynolds number, R^+. The functions $\kappa(R^+)$, $B_i(R^+)$ and $B_o(R^+)$ must be determined either empirically or from a closure model for the turbulence. Regardless of how they are determined, the results must be consistent with equation 6.30.

6.3 A Solution for the Reynolds Number Dependence

It is convenient to transform equation 6.30 using

$$H(R^+) = (\frac{1}{\kappa} - \frac{1}{\kappa_\infty}) \ln R^+ + (B_i - B_o) \tag{6.31}$$

where $H = H(R^+)$ remains to be determined. It is easy to show that if $H(R^+)$ satisfies

$$\frac{1}{\kappa} - \frac{1}{\kappa_\infty} = \frac{dH}{d \ln R^+} \tag{6.32}$$

then equation 6.30 is satisfied. It follows immediately that

$$\frac{1}{g} = \frac{U_c}{u_*} = \frac{1}{\kappa_\infty} \ln R^+ + H(R^+) \tag{6.33}$$

Thus the Reynolds number dependence of $H(R^+)$ determines that of both κ and $B_i - B_o$.

It is easy to show that the condition that both $B_{i\infty}$ and $B_{o\infty}$ be finite and non-zero requires that:

- *Either* B_i, B_o and κ remain constant always;

or

- (i) $1/\kappa \to 1/\kappa_\infty$ faster than $1/\ln R^+$, and
- (ii) $H(R^+) \to H_\infty = constant.$

Obviously from equation 6.31,

$$H_\infty = B_{i\infty} - B_{o\infty} \tag{6.34}$$

An empirical choice for $H(R^+) - H_\infty$ satisfying these conditions is suggested by the boundary layer results of Chapter 3; it is,

$$H(R+) - H_\infty = \frac{A}{[\ln R^+]^\alpha} \tag{6.35}$$

Note that conditions (i) and (ii) above imply that $\alpha > 0$.

Using this in equation 6.33 yields

$$\frac{U_c}{u_*} = \frac{1}{\kappa_\infty} \ln R^+ + [B_{i\infty} - B_{o\infty}] + \frac{A}{[\ln R^+]^\alpha} \tag{6.36}$$

As $R^+ \to \infty$ this reduces to the classical solution of Millikan 1938.

The Reynolds number variation of $1/\kappa$ and $B_i - B_o$ can be immediately obtained from equations 6.31, 6.32 and 6.35 as

$$\frac{1}{\kappa} - \frac{1}{\kappa_\infty} = \frac{-\alpha A}{(\ln R^+)^{1+\alpha}} \tag{6.37}$$

and

$$(B_i - B_o) - (B_{i\infty} - B_{o\infty}) = \frac{(1+\alpha)A}{(\ln R^+)^\alpha} \tag{6.38}$$

Figures 6.3 and 6.4 show the friction data of the superpipe experiment of Zagarola and Smits (1996). Careful scrutiny reveals that the data do not fall on a straight line,

so a simple logarithmic friction law with constant coefficients does not describe all the data. Figure 6.4 also shows two curves: The first represents a regression fit of equation 6.36 (also shown on Figure 6.3), while the second shows only the asymptotic log form of equation 6.36.

The former provides an excellent fit to the data for *all* Reynolds numbers and asymptotes exactly to the latter, but only at much higher Reynolds numbers. The differences although slight are very important since they entirely determine (or reflect) the Reynolds number dependence of the parameters $1/\kappa$, B_i and B_o. The latter will be seen later to be especially sensitive to this dependence.

Since, the data U_c/u_* is known with excellent accuracy for the superpipe experiment, it is possible to use this information to determine $1/\kappa_\infty$, $B_{i\infty} - B_{o\infty}$, A and α. The optimization problem is given below as:

- Objective Function:

$$\sum_{i=1}^{26} \frac{c_{f_{data}}}{c_{f_{thr}}} - 1 \tag{6.39}$$

  where $c_f = 2u_*^2/U_\infty^2$.

- Design Variables: $1/\kappa_\infty$, $(B_{i\infty} - B_{o\infty})$, A, α

The goal is to determine the design variables to minimize the objective function.

The values obtained for the friction law parameters are $\kappa_\infty = 0.447$, $B_{i\infty} - B_{o\infty} = 8.45$, while those describing the Reynolds number dependence are $A = -0.668$ and $\alpha = 0.441$. Note that the values of $B_{i\infty}$ and $B_{o\infty}$ cannot be determined individually from the friction data, only their difference. The values of κ_∞ and $B_{i\infty} - B_{o\infty}$ differ only slightly from the values determined by Zagarola (1996) (0.44 and 7.8 respectively) using the velocity profiles alone and assuming that the asymptotic state had been

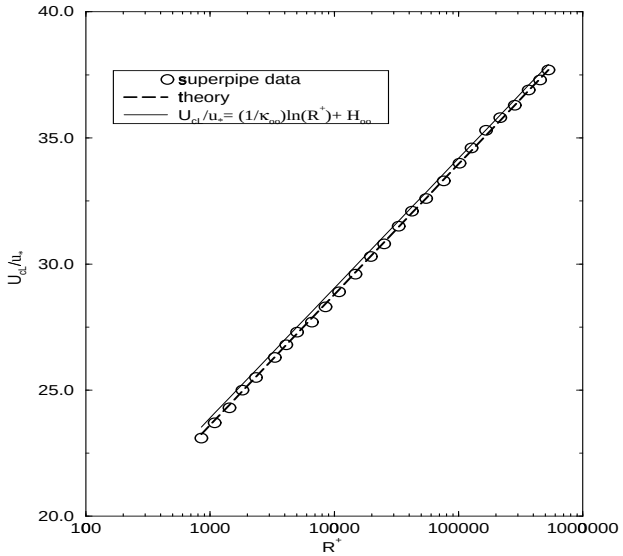

Figure 6.3: Variation of U_c/u_* with $R^+ = Ru_*/\nu$: linear-linear plot

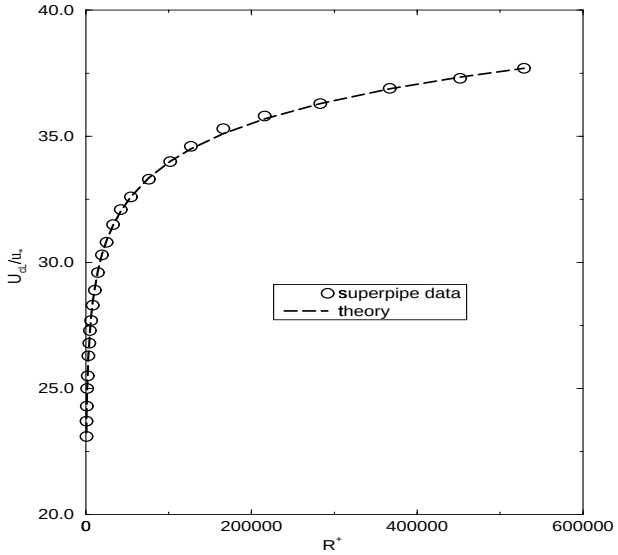

Figure 6.4: Variation of U_c/u_* with $R^+ = Ru_*/\nu$: log-log plot

reached. All the parameters are remarkably independent of the particular range of data utilized.

For the boundary layer the friction data were not as reliable as those reported here, so that the functional form of H had to be inferred after a variety of attempts to describe the variation of the exponent in a power law description of the velocity profile in the overlap region. Interestingly, the value for α obtained here is almost exactly the value obtained for the boundary layer data (0.461 versus 0.44). In view of the differing definitions of the length scales, the physical significance of this, if any, is not yet clear.

6.4 Is the Superpipe Rough?

Barenblatt 1996 claimed that the data by Zagarola and Smit (1996) does not accurately represent a smooth pipe, and claimed that there was evidence of surface roughness present in the last fifteen profiles. The primary reason for this contention is that the superpipe data were not in agreement with his theory (Barenblatt 1993). The fact is that even dropping last fifteen points in the data does not change the coefficients for the present theory. This suggests strongly that the data are in fact a smooth curve, uncontaminated by roughness, and that the proposed form of H properly captures the shape of the Reynolds number dependence. Table 6.1

shows how little the coefficients change as the higher Reynolds number data points are successively omitted from the regression analysis.

Barenblatts's claim was based on the failure of the superpipe data to agree in his power law theory. Obviously the analysis presented here does not accept the applicability of power laws to pipe and channel flows. Moreover, it was pointed out

Number of points	$1/\kappa_\infty$	$B_{i\infty} - B_{o\infty}$	A	α
26	2.235	8.454	-0.668	0.441
24	2.235	8.453	-0.668	0.441
21	2.235	8.454	-0.668	0.441
16	2.232	8.464	-0.627	0.449
11	2.230	8.482	-0.653	0.456

Table 6.1: Effect of dropping the highest Reynolds number data on determination of parameters. The number of data points retained beginning from the lowest Re is given in the leftmost column.

in Chapter 2 that Barenblatt's theory is inconsistent with asymptotic similarity of the inner and outer equations for boundary layers. The same is true for pipe and channel flows since the parameters must also be asymptotically constant and finite, whether power law or log law. Hence it is not surprising that there is a problem when Barenblatt attempts to describe data at higher Reynolds numbers than at which the parameters were originally determined (i.e., the data of Nikuradse 1932).

6.5 The Effect of Reynolds Number on the Overlap Range

The parameters established for the friction law will be used below to calculate the values of κ, B_i and B_o for each Reynolds number of the superpipe data. Only either of the B's need be established from the experiments since their difference is known from equation 6.31. Before carrying out a detailed comparison with the velocity data, however, it is is useful to first consider exactly which region of the flow is being described by the overlap profiles. Also of interest is the question of how large the Reynolds number must be before the flow begins to show the characteristics of the asymptotic state. Much of this section parallels the boundary layer discussions of

Chapter 2, but is included here for completeness.

The overlap layer identified in the preceding sections can be related directly to the averaged equations for the mean flow and the Reynolds stresses. From about $y^+ > 10$ to 20 approximately, out to about the center of the flow, the averaged momentum equation is given approximately by

$$0 = -\frac{\partial < uv >}{\partial y} - \frac{1}{\rho}\frac{dP}{dx} \tag{6.40}$$

It has no explicit Reynolds number dependence; and the Reynolds shear stress is drops linearly all the way to the center of the flow. Inside about $\overline{y} = 0.1$, however, the Reynolds shear stress is nearly constant. In fact, at infinite Reynolds number the pressure gradient term vanishes identically and the mean momentum equation reduces to

$$0 = -\frac{\partial < uv >}{\partial y} \tag{6.41}$$

At finite (but large) Reynolds numbers this region is similar to the developing boundary layer where the Reynolds stress is effectively constant. Obviously it is reasonable to expect the overlap region to more or less correspond to this constant stress layer.

Even when there is a region of reasonably constant Reynolds stress, however, this is not the entire story because of the Reynolds number dependence of $- < uv >$ itself. And it is this weak Reynolds number dependence which is the reason that κ, B_i, and B_o are only asymptotically constant. The origin of this weak Reynolds number dependence (which is well-known to turbulence modelers) can be seen by considering the Reynolds transport equations. For the same region, $y^+ > 10$ to 20, the viscous diffusion terms are negligible (as in the mean momentum equation), so

the equations reduce approximately to (Tennekes and Lumley 1972),

$$0 = -(< p\frac{\partial u_i}{\partial x_k} > + < p\frac{\partial u_k}{\partial x_i} >) - \left[< u_i u_2 > \frac{\partial U_k}{\partial x_2} + < u_k u_2 > \frac{\partial U_i}{\partial x_2} \right] - \frac{\partial < u_i u_k u_2 >}{\partial x_2} - \epsilon_{ik} \tag{6.42}$$

where $U_i = U\delta_{i1}$. Thus viscosity does not appear directly in any of the single point equations governing this region, nor does it appear in those governing the outer boundary layer.

In spite of the above, however, viscosity can be shown to play a crucial role in at least a portion of the constant stress layer, even at infinite Reynolds number. The reason is that the *scales of motion* at which the dissipation, ϵ_{ik}, actually takes place depend on the *local* turbulence Reynolds number, $R_t = q^4/\nu\epsilon$. For $R_t > 1000$ approximately, the energy dissipation is nearly completely controlled by the large energetic scales of motion. These are effectively inviscid, but control the energy transfer through non-linear interactions (the energy cascade) to the much smaller viscous scales where the actual dissipation occurs (v. Tennekes and Lumley 1972). When this is the case, the dissipation is nearly isotropic so $\epsilon_{ik} \approx 2\epsilon\delta_{ik}$. Moreover, ϵ can be approximated by the infinite Reynolds number relation: $\epsilon \sim q^3/L$ where L is a scale characteristic of the energy-containing eddies. The coefficient has a weak Reynolds number dependence, but is asymptotically constant. Thus, the Reynolds stress equations are effectively inviscid, but only exactly so in the limit. Note that in this limit the Reynolds shear stress has no dissipation at all, i.e., $\epsilon_{12} = 0$.

At very low turbulence Reynolds number, however, the dissipative and energy-containing ranges nearly overlap, and so the latter (which also produce the Reynolds shear stress) feels directly the influence of viscosity. In this limit, the energy and dissipative scales are about the same, so the dissipation is more reasonably estimated by $\epsilon \sim \nu q^2/L^2$, where the constant of proportionality is of order 10. The dissipation

tensor, ϵ_{ik} is anisotropic and ϵ_{12}, in particular, is non-zero (Launder 1993). (Hanjalic and Launder 1972, for example, take $\epsilon_{12} = (- < u_1 u_2 > /q^2)\epsilon$.)

For turbulence Reynolds numbers between these two limits, the dissipation will show characteristics of both limits, gradually making a transition from $\epsilon \sim \nu q^2/L^2$ to $\epsilon \sim q^3/L$ as R_t increases. Thus the Reynolds stresses themselves will feel directly this, and will show a strong Reynolds number dependence. Obviously, in order to establish when (if at all) parts of the flow become Reynolds number independent, it is necessary to determine how the local turbulence Reynolds number varies downstream and across flow.

Over the outer boundary layer (which is most of it), $L \approx R/2$ and $q \approx 3u_*$. So when $R^+ > 7,000$, the dissipation in the outer flow is effectively inviscid. Above this value the mean and turbulence quantities in the core region of the flow should show little Reynolds number dependence, This is indeed the case as illustrated by Figure 2. The outer region can, of course, not be entirely Reynolds number independent, except in the limit, and this residual dependence manifests itself in the overlap layer in the slow variations of κ and B_o, for example.

The near wall region is considerably more interesting since in it the scales governing the energy-containing eddies are constrained by the proximity of the wall. Hence, the turbulence Reynolds number, R_t, depends on the distance from the wall, y. In fact, $R_t \sim y^+$ with a coefficient of about 3; so, in effect, y^+ is the turbulence Reynolds number. Because of this, two things are immediately obvious:

- First, as the Reynolds number increases more and more of the pipe (in outer variables) will become effectively inviscid and will be governed by the inviscid dissipation relation. And correspondingly, the mean and turbulence quantities in the overlap layer will become Reynolds number independent, albeit very

slowly. Clearly these limiting values cannot be reached until the entire overlap layer is governed by the infinite Reynolds number dissipation relation and its coefficient has reached the limiting value. Obviously this can happen only when there is a substantial range satisfying $y^+ > 300$ and for which the mean convection terms are negligible, typically $\overline{y} < 0.1$. Thus the asymptotic limits are realized only when $300\nu/u_* << 0.1R$ or $R^+ >> 3000$. Therefore the overlap layer below approximately $R^+ = 30,000$ should display a Reynolds number dependence, not only in κ, B, and B_1, but correspondingly in the behavior of $< u^2 >$, $< uv >$, etc.

- Second, there will always be a *MESOLAYER* [2], below about $y^+ \approx 300$ in which the dissipation can *never* assume the character of a high Reynolds number flow, no matter how high the Reynolds number becomes. This is because the dissipation (and Reynolds stress as well) can never become independent of viscosity — even though the mean momentum equation itself is inviscid above $y^+ \approx 20$! This fact is well-known to turbulence modelers (v. Hanjalic and Launder 1972), but the consequences for similarity theory and asymptotic analyses do not seem to have been noticed previously. It is particularly important for experimentalists who have routinely tried to apply asymptotic formulas to data from to this region, wrongly believing the mesolayer to be the overlap region.

Thus the constant stress layer is really four separate regions, each having their own unique character. The overlap layer ($y^+ > 300$, $\overline{y} < 0.1$) obtained in the preceding section which is nearly inviscid; an 'in-between layer' or mesolayer ($10 < y^+ < 300$) in which the viscous stresses are negligible, but in which viscosity acts directly on the

[2] This appropriates a term from Long 1976 (see also Long and Chen 1982) who argued strongly for its existence, but from entirely different physical and scaling arguments which we find untenable. Nonetheless, despite the skepticism which greeted his ideas, Long's instincts were correct.

turbulence scales producing the Reynolds stresses; a buffer layer ($5 < y^+ < 10$) where the Reynolds stress and viscous stress both act directly on the mean flow; and the real viscous sublayer, the linear region near the wall ($y^+ < 5$) where the viscous stresses dominate. And of these four regions, the overlap layer will be the *last* to appear as the flow develops or as the Reynolds number is increased. *Thus, the overlap layer will be the most difficult to identify at the modest Reynolds numbers of most laboratory experiments.* Identification will be easier if the properties of the mesolayer are known, and accordingly a model for it is presented in the next section.

6.6 The Mesolayer

Using the same ideas as for the zero pressure gradient mesolayer it is possible to construct a mesolayer model for the pipe and channel flows. It follows that,

$$\frac{du^+}{dy^+} = \left(\frac{c_1}{c_3}\right)\left(\frac{q}{u_*}\right) y^{+-1} + \left(\frac{c_2}{c_3}\right) y^{+-2} \tag{6.43}$$

Note that it is the factor q/u_* which determines whether the first term on the right hand side integrates to a logarithm or a power law (or something else). For boundary layer flows this was shown have shown to depend on a power of y^+, consistent with the power law velocity profile. Pipe and channel flows, however, show a logarithmic dependence for all quantities. If the additive constant in the logarithm dominates so that q/u_* itself is nearly constant, then the first term yields the logarithmic overlap profile derived earlier *plus* an additional term due to the low local Reynolds number; i.e.,

$$u^+ = [\frac{1}{\kappa}\ln + B_i] + C_{mi} y^{+-1} \tag{6.44}$$

where the parameters c_1, c_2 and c_3 have been collected into $1/\kappa$, B_i and C_{mi}. Note that the second term is unaffected by the behavior of q/u_*; hence there is reason to hope that it may be the same for all wall-bounded flows. (Note that equation 6.44 can also be derived using only the overlap characteristics without reference to an eddy viscosity model.)

Thus the additional contribution of the mesolayer to the velocity profile (in inner variables) is $C_{mi}y^{+-1}$. The parameter C_{mi} must be negative and should be nearly constant. For the boundary layer profiles it appears that this is indeed the case and $C_{mi} \approx -37$. This value will be used in the next section without any attempt to optimize it for the pipe flow data. It is important to note that because of the relative values of B_i and C_{mi}, there is no region where the second term dominates, at least where the assumptions are valid. Therefore there will be no y^{+-1}-layer, only a modified log region. Moreover, because of this, the first term in equation 6.44 will be clearly visible only when the second is negligible. Since this is not the case for many of the low and moderate Reynolds number experiments, it will not be possible to even identify the parameters B_i, B_o, and κ for most of the data *without first accounting for the mesolayer contribution.*

Equation 6.44 can be expressed in outer variables as

$$\frac{U - U_c}{u_*} = \frac{1}{\kappa} \ln R^+ + B_o + \frac{C_{mo}}{\overline{y}} \tag{6.45}$$

where

$$C_{mo} = C_{mi} R^{+-1} \tag{6.46}$$

Obviously if C_{mi} is constant, C_{mo} is not.

Before leaving this section it might be noted that it should be possible to calculate values for the parameters using the values for c_1, c_2 and c_3 from the many turbulence

models which have determined them. Unfortunately, all have been chosen to conform to the old log law, and at distances from the wall which are well inside the mesolayer defined here (e.g., Reynolds 1976). If the above arguments are indeed correct, then these model constants should be re-evaluated.

6.7 The Velocity Data

Now that the approximate region of validity of the overlap solution has been established as $300 < y^+ < 0.1R^+$ it is possible to test the theoretical profiles and the proposed model for the Reynolds number dependence. If they are correct, only an independent determination of either B_i or B_o is necessary to completely specify the profile, the rest of the parameters having been determined from the friction data. Also it should be possible to determine whether the proposed mesolayer model is reasonable, at least for those data sets where data are available below $y^+ = 300$.

For all of the data sets it appears $B_i = 6.50$ is nearly optimal (at least for values of $R^+ < 850$, the lowest available from the superpipe experiment), so that for the remainder of this paper it will be assumed that $B_i = B_{i\infty}$. This value is very close to the value of 6.3 determined by Zagarola and Smits (1996) by assuming κ fixed at 0.44. Since the difference, $B_{i\infty} - B_{o\infty} = 8.45$, was established from the friction data, it follows immediately that $B_{o\infty} = -1.95$. The constancy of B_i implies that it is B_o which shows all the Reynolds number dependence of the difference given by equation 6.38.

Figures 6.5 and 6.6 show the theoretical variation of $1/\kappa$ and B_o with Reynolds number (equations 6.31 and 6.32). Clearly both converge very slowly to their asymptotic values. This slow approach has far more relative effect on B_o than it does on

$1/\kappa$, however, since B_o has achieved only 85% of its asymptotic value at $R^+ = 10^5$. The observed variation of $1/\kappa$ and B_o and the constancy of B_i can be contrasted with the boundary layer results of Chapter 3 in which C_o, the outer coefficient was nearly constant while the power exponent γ and the inner coefficient C_i varied over the entire range of Reynolds numbers available.

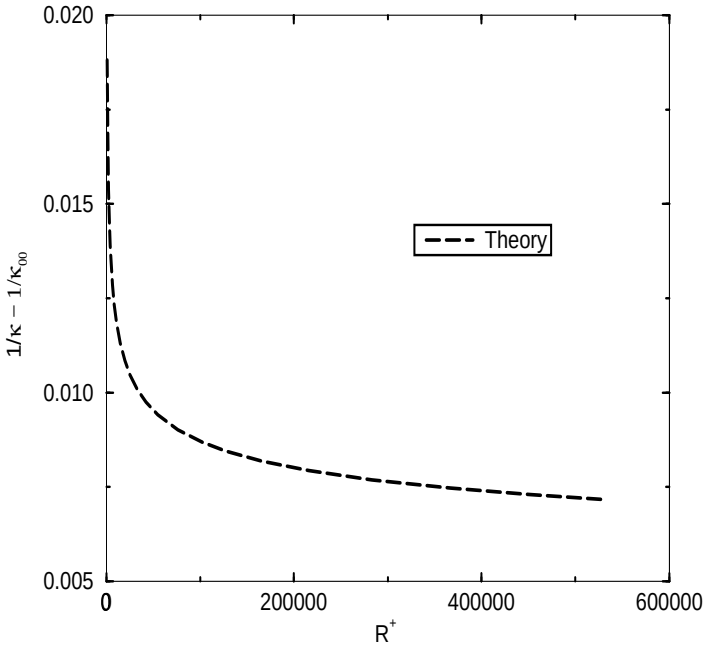

Figure 6.5: Variation of $1/\kappa - 1/\kappa_\infty$ with R^+, $\kappa_\infty = 0.447$

The relative behavior of B_o and B_i means that the outer profile scaling shows more variation with Reynolds number in the overlap region than does the inner where only κ varies. This undoubtedly explains a great deal of the problems historically in establishing what $B_{o\infty}$ is and in determining whether the outer scaling is correct. And it might also explain the conclusion of Zagarola and Smits (1996) that a different scale

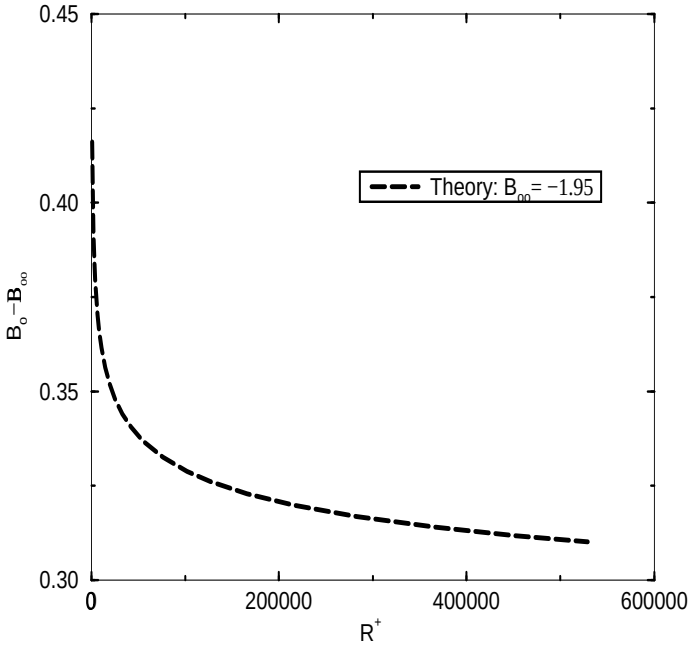

Figure 6.6: Variation of $B_o - B_{o\infty}$ with R^+, $B_{o\infty} = 8.50$

for the outer flow is required, especially if attention is focussed on the overlap region instead of the core region of the flow.

Figures 6.7 and 6.8 show representation of the velocity profiles of the superpipe data in inner and outer variables respectively, together with the overlap solution using equations 6.26 and 6.27 and the model equations 6.37 and 6.38. The vertical lines on each profile show the suggested bounds for the mesolayer model ($30 < y^+ < 300$ or $30/R^+ < \overline{y} < 300/R^+$) and the overlap region ($300 < y^+ < 0.1R^+$ or $300/R^+ < \overline{y} < 0.1$). Note that because of the varying Reynolds number, the limits depending on R^+ are different for each profile. As noted above, the boundary layer value for the mesolayer parameter of $C_{mi} = -37$ was used.

The overlap plus mesolayer solution provides an excellent fit to the data from $70 < y^+ < 0.1R^+$ for the entire range of Reynolds numbers available. The mesolayer

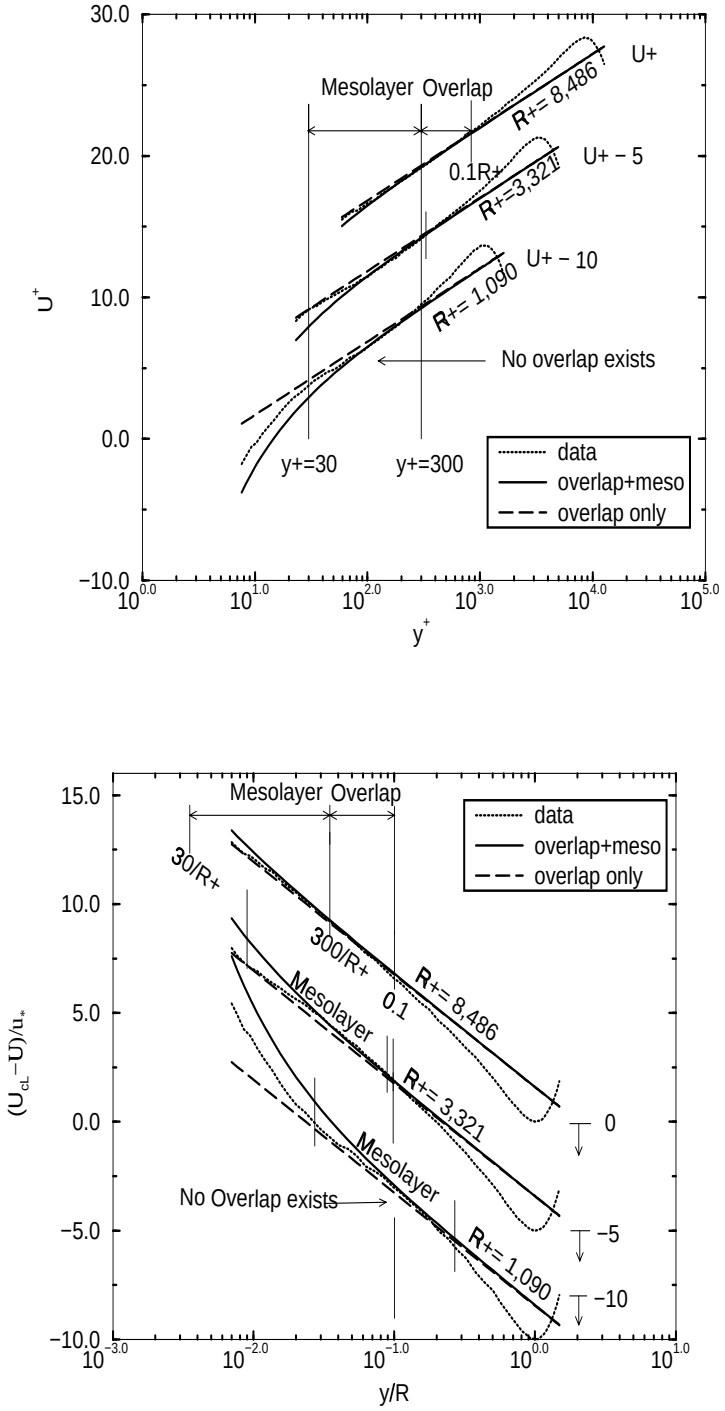

Figure 6.7: Inner and outer profiles at relatively low Reynolds number

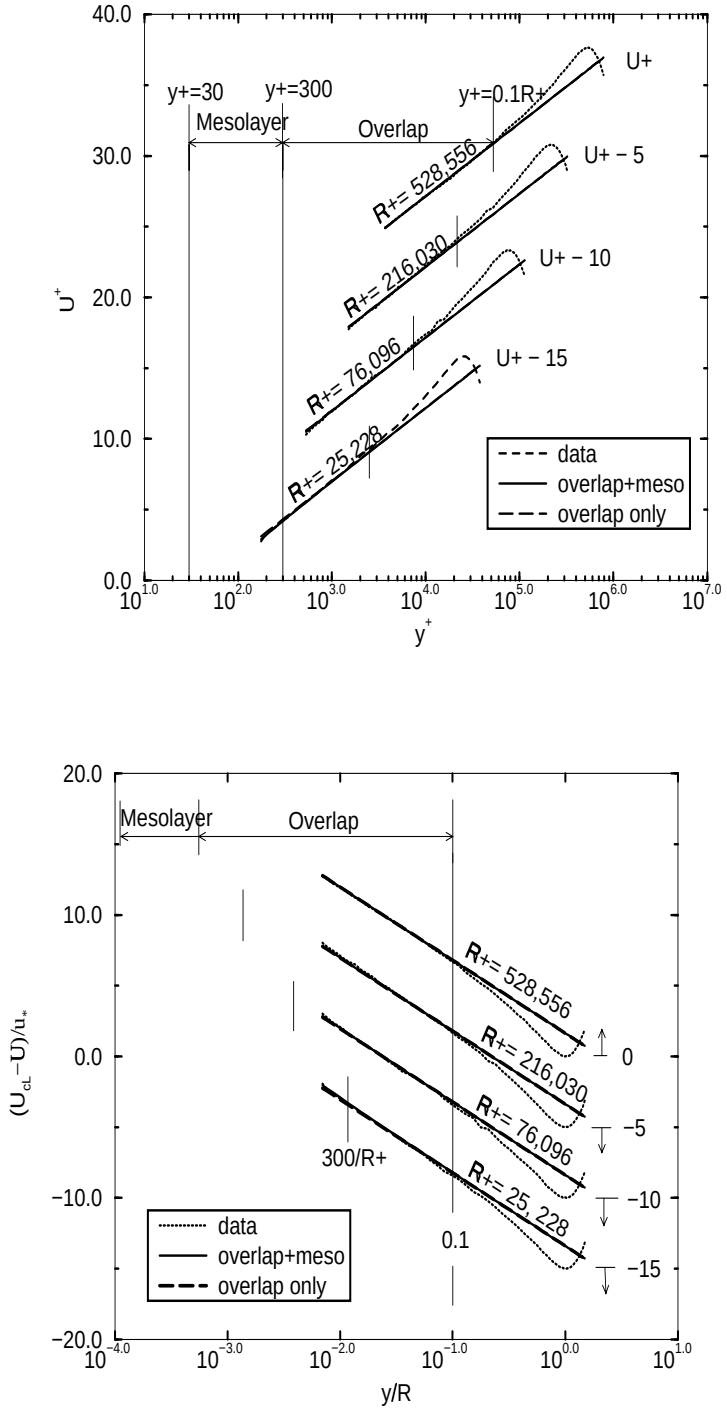

Figure 6.8: Inner and outer profiles at relatively high Reynolds number

term captures well the point of departure from the overlap solution, as well as the deviations from it below $y^+ = 300$, even for the lowest Reynolds number where there is no overlap region at all. It does not, however, describe the profile down to $y^+ = 30$ as expected, since the velocity data bend away from the overlap plus mesolayer solution back to the overlap solution alone below about $y^+ = 80 - 90$. This may indicate that the lower limit on the proposed mesolayer model is higher than believed, or it may simply represent a problem with the data used here which were not corrected for the various sources of error near the peak in the turbulence intensity (Smits, private communication). The corrections which were applied by Zagarola (1996) to some of the data were primarily important below $y^+ = 100$ and move the data close to the mesolayer/overlap result. The excellent agreement for $100 < y^+ < 300$, however, suggests that both the form of the mesolayer model and the boundary layer value for C_{mi} are essentially correct. The agreement between experiment and theory is particularly gratifying in view of the fact that the velocity data were only used to establish B_i, the remaining parameters having been entirely determined by the friction data.

It is easy to see how the deviations from the log law due to the mesolayer could be viewed as a separate and distinct region. For example, Zagarola and Smits (1996) argue that the region $50 < y^+ < 500$ is described by a 1/7 power law with a coefficient of 8.7, and not the logarithmic profile (with constant coefficients) which fits the inner solution between $500 < y^+ < 0.1R^+$. If a power law is fitted to data generated by the overlap plus mesolayer profile proposed herein using the constants determined above, it produces almost exactly the same 1/7-power and 8.7 coefficient over the same range. Thus it is clear that the same phenomenon is being described.

6.8 Summary

In summary, the streamwise homogeneity of pipe and channel flows has been seen to dictate logarithmic profiles. Thus these flows are fundamentally different from boundary layer flows which exhibit power law behavior. Near-Asymptotics has also been applied to these flows, and yields results which are in excellent agreement with the superpipe experiment over the entire range of Reynolds numbers.

The theory of Millikan 1938 was found to be essentially correct, and is obtained as a limiting condition. The experiments, however, do not reach this limit, not even the Princeton Superpipe experiment for which $10^3 < R^+ < 5{\times}10^5$. As a consequence, the finite Reynolds number aspects of the theory proposed here are essential to understanding the experiments, and to determining from them what the limiting values of the parameters κ, B_o and B_i might be. The data show that B_i is constant at 6.50 to within the experimental error. The values of κ and B_o, and especially the latter, continue to vary for all Reynolds numbers of the experiments. Their asymptotic values have been estimated as 0.447 and -1.95 respectively.

Chapter 7

Summary and Conclusions

A new theory has been set forth for boundary layers (with and without pressure gradient) and for channel and pipe flows using an Asymptotic Invariance Principle and Near–Asymptotics. The equations of motion for these flows in the inner and outer regions become asymptotically independent of the Reynolds number in the limit of infinite Reynolds number. In this limit (and only in this limit), these inner and outer equations admit to similarity solutions. These similarity solutions are used to determine the profiles for boundary layers and channel and pipe flows at finite Reynolds number. The fact that similarity solutions are strictly valid only for infinite Reynolds number means that *no scaling 'law' can work perfectly at finite Reynolds numbers*. Moreover, only the proposed scaling can be Reynolds number invariant in the limit.

The outer boundary layer is found to be governed by a different scaling law in the case of boundary layers with zero and non-zero pressure gradient than has been commonly believed. In particular, the velocity deficit in the outer layer scales as $(U - U_\infty)/U_\infty$. (To satisfy Galilean invariance, U_∞ can be replaced by the difference

between the free stream velocity and the velocity at the surface.) The Reynolds shear stress in the outer layer, on the other hand, scales with $U_\infty^2 d\delta/dx$ which to first order is u_*^2, so that the outer layer is governed by two velocity scales. The classical inner scaling laws using u_* and ν were found to be consistent with the similarity analysis, except that their region of applicability is less than previously believed.

In addition for boundary layers with pressure gradient it was found that an equilibrium flow is one with $\Lambda = (\delta/\rho U_\infty^2)(1/d\delta/dx)dP_\infty/dx = constant$ from which it follows that the boundary layer thickness (δ) follows the imposed pressure gradient over the boundary layer (i.e., $\delta \sim U_\infty^\Lambda$). The new definition for equilibrium boundary layers proves to be more satisfactory than the old definition of Clauser. In particular, most flows that were believed not to be equilibrium flows according to the Clauser definition were in equilibrium when the new definition is used. In addition the new theory for boundary layers with pressure gradient also applies locally for non-equilibrium flows.

Near-Asymptotics was used to examine how the inner and outer scaled velocity profiles in the overlap region behave for finite Reynolds number. The velocity in the overlap layer for boundary layers was shown to exhibit power law behavior, i.e., for zero pressure gradient: $U/u_* = C_i y^{+\gamma}$ and $U/U_\infty = C_o \overline{y}^\gamma$. The parameters C_o, C_i and γ are Reynolds number dependent, and only asymptotically constant. For the pressure gradient case: $U/u_* = C_{ip} y^{+\gamma}_p$ and $U/U_\infty = C_{op} \overline{y}^\gamma_p$. Thus, unlike earlier theories, the overlap region is not Reynolds number invariant in either inner or outer variables, except in the infinite Reynolds number limit. The friction law was also shown to be of power law form; in particular, $u_*/U_\infty = (C_{op}/C_{ip})(R^+)^{-\gamma_p}$. It was found that the velocity parameters in inner variables for the pressure gradient case are the same as those for the zero pressure gradient case even at finite Reynolds number

(i.e., $C_{ip} = C_i$, $\gamma_p = \gamma$) as long as the flow is not near separation. Therefore, only one new parameter [$\Pi = \Pi(\Lambda)$ only] is needed for the pressure gradient boundary layer to determine the skin friction, the mean velocity profile for the entire boundary layer at finite Reynolds number, the boundary layer parameters and even the Reynolds shear stress at finite Reynolds number.

For the cases of channel and pipe flows, the velocity profiles are logarithmic as in the traditional theory, but with coefficients that are Reynolds number dependent contrary to the classical theory. Again, these velocity parameters are independent of Reynolds number only in the limit as Reynolds number goes to infinity.

New scaling laws for some of the turbulence moments were derived from similarity considerations of the turbulence Reynolds stress equations for boundary layers. For the turbulence quantities in the outer boundary layer to be asymptotically independent of Reynolds number, it was shown to be necessary that the asymptotic growth rate of the boundary layer be constant (i.e., $d\delta/dx = \text{constant}$). A consequence of this is that the friction coefficient must be asymptotically constant. It was not clear from the theory or the data available whether zero was an acceptable value of this constant, or whether the power exponent was itself asymptotically zero. The requirement for a finite energy dissipation rate in the limit appears to resolve this question by requiring that the power exponent be asymptotically non-zero, so then the friction coefficient must be asymptotically zero. (Similar arguments were presented for channel and pipe flows). Regardless, arguments were presented that these limits are reached well beyond the Reynolds number range of existing experiments, i.e., $R_\theta > 10^5$.

By considering the role of viscosity in the single point and two point Reynolds stress equations, it was argued that there exists a *Mesolayer* in the region approximately defined by $10 < y^+ < 300$. In this region the overlap solutions *alone* do not

apply because the *local* turbulence Reynolds number is too low. A simple turbulence model, valid in the range approximately $30 < y^+ < 0.1\delta^+$, was used to derive a correction to the overlap velocity profile given in inner variables by C_{mi}/y^+ (where, from the data, $C_{mi} \approx -37$). This term only modifies the power law (or the log law in the case of channel and pipe flows) but never dominates it, so there is no separate y^{-1} layer. Even so, because of the mesolayer, the overlap region does not even begin to evolve as a distinct region until $R_\theta \sim 10^4$ since, below this value there is no region satisfying $300 < y^+ < 0.1\delta^+$, a necessary condition for an overlap to exists. The model was also applied to boundary layer with pressure gradient and channel and pipe flows. In both cases the same constant as in zero pressure gradient case was obtained. In view of the simplicity of the model, better approximations to the mesolayer contribution are probably possible.

The theory was shown to be in general agreement with the bulk of the experimental data. From a single empirical relationship, $h = A/(\ln R^+)^\alpha$, determined from the data, both the power, γ and the ratio C_o/C_i could be calculated analytically from a constraint relationship between γ and C_o/C_i. The asymptotic value of $C_o = 0.897$ is achieved in the experiments at about $R_\theta \sim 3 \times 10^3$, so beyond this, the variation of C_i is known, to within the accuracy and extent of the data. Thus the variation with Reynolds number of all the boundary layer parameters are known, and the shear stress as well. The asymptotic values of $\gamma_\infty = 0.0362$ and $C_{i\infty} = 55$ are achieved at Reynolds numbers well beyond the range of the data. It is likely that the precise values for these parameters will change as better experiments become available. These results also applied for the pressure gradient boundary layer except that C_{op} needs to be determined as function of Λ, the similarity parameter. Equations for the Reynolds number dependence of B_i, B_o and κ are also obtained for pipe and channel flows. The

asymptotic values of these are: $B_{i\infty} = 6.5$, $B_{o\infty} = -1.95$, $\kappa_\infty = 0.447$. For channel and pipe flows the same functions for H applies, but the coefficient for A is different. The value for α is the same for boundary layers and pipe flows.

The introduction of empiricism for the Reynolds number dependence of γ or κ, the function $h(\delta^+)$ or $H(R^+)$, *at the very end of the analysis* must be contrasted with the traditional theory where the empiricism appears at the very first step with the *assumption* of a velocity deficit law on which all subsequent arguments depend. It seems likely that even this relationship can be determined from symmetry considerations in the future. It is clear, however, that the proposed form for $h(\delta^+)$ can not be exactly right since the constants A and α depend on the definition of δ. An intriguing and invariant possibility is the $h = A'/(\ln \delta^+/\delta_o^+)^{\alpha'}$ where δ_o^+ is determined in some way by the initial (or upstream) conditions. There is some evidence from the boundary layer experiments for such a weak dependence on upstream conditions (e.g., the imperfect overlap of the skin friction, the integral boundary layer parameters, and even the values of γ, C_o and C_i between the Smith/Walker and Purtell experiments), but it was not possible to quantify it in the present study.

The power law dependence of the matched region derived here (for boundary layers only) was suggested by Barenblatt (1978, 1993) from very different considerations. Unlike Barenblatt's inferences, however, the theory here suggests that pipe and channel flows will not show this behavior, and in fact the new theory allows a clear distinction to be made between the pipe or channel flows, and boundary layers (Chapter 6). Since the former must satisfy the homogeneous integral momentum equation, the pressure gradient and wall shear stress are not independent, and thus only one can enter the scaling (contrary to the assumption of Tennekes 1968, see also Tennekes and Lumley 1972). As a consequence, u_* is the correct scaling velocity for

the core region and Millikan's analysis of it is correct. Thus the pipe is governed by a log law, while the zero pressure-gradient boundary layer is governed by a power law.

It appears that the streamwise homogeneity of the pipe or channel flows dictates log layers, while the inhomogeneity of the boundary layer dictates power laws. Moreover, the Reynolds number of the flow does not change with downstream distance for the pipe/channel, but it evolves continuously in the boundary layer. As a consequence, the overlap and mesolayer regions for the boundary layer are slowly moving away from the wall in physical variables, and the distance from the wall alone cannot characterize variations within it as for the pipe/channel. Prandtl's hypothesis that y, the distance from the wall, is the only length scale in the matched layer is thus only an approximation for boundary layers, while it is an exact asymptotic limit for pipe and channel flows.

That the boundary layer is only weakly inhomogeneous accounts for the fact that the log results have been close enough to be rationalized as correct. It is clear from the above that the wall layers of boundary layers and pipe/channel flows must be fundamentally different, however close they might be in practice. Because of the long period of time (more than 60 years) the log law theory has been believed to apply to turbulent boundary layers, it is natural to expect some resistance to any new theory which challenges it, no matter how well reasoned or argued. Part of the reason for acceptance of the old theory is that it has been believed to have been more or less consistent with the experimental velocity data which seemed to exhibit a logarithmic region. (Other philosophical reasons have arisen to justify it, like the principle of Reynolds number invariance, but it is the data itself which has been at the root of the faith.) It is, therefore, incumbent on any new theory to not only be internally consistent, but to explain how so many could have been so wrong for so

long in believing the old. The dissertation has attempted to do both. At the very least, it is hoped that a strong motivation has been provided for a new generation of experiments over the entire range of Reynolds numbers.

Bibliography

[1] Abrahamsson, H. private communication (1996).

[2] Abramowitz, M. and Stegun I.A. *Handbook of Mathematical Functions.* Dover, New York (1965).

[3] Balint, J-L., Wallace, J.M. and Vukoslavcevic, P. The velocity and vorticity vector fields of a turbulent boundary layer. Part 2. Statistical properties. *J. Fluid Mech.*, **228**, 53–86 (1991).

[4] Barenblatt, G.I. *Similarity, Self-similarity, and Intermediate Asymptotics.* Plenum, New York (1978).

[5] Barenblatt, G.I. Scaling laws for fully developed shear flow. Part I, Basic hypotheses and analysis. *J. Fluid Mech.*, **248**, 513–520 (1993).

[6] Bell, J.B. *Heat Transfer to Turbulent Boundary Layers in Pressure Gradients.* M.S. Thesis, Univ. Melbourne (1966).

[7] Blackwelder, R. Presentation at the Symposium on Turbulence, Asilomar Conference Center. Monterey, CA (1993).

[8] Blackwelder, R.F. and Haridonitis J.H. Scaling of the bursting frequency in turbulent boundary layers. *J. Fluid Mech.*, **132**, 87–103 (1983).

[9] Bradshaw, P. and Ferriss, D. The response of a retarded equilibrium turbulent boundary layer to the sudden removal of pressure gradient. NPL Aero. Rep. 1145 (1965).

[10] Bradshaw, P. The turbulence structure of equilibrium boundary layers. NPL Aero. Rep. 1184 (1966).

[11] Bradshaw, P. The response of a constant-pressure turbulent boundary layer to the sudden application of an adverse pressure gradient. NPL Aero. Rep. 1219 (1967).

[12] Bradshaw, P., Launder, B. and Lumley, J.L. CTTM, AIAA 91 - 0215 (1991).

[13] Bradshaw, P. Turbulence: The Chief Outstanding Difficulty of Our Subject. 3rd Stewartson Mem. Lecture,*Symp. on Numerical and Physical Aspects of Aerodynamic Flows*, Long Beach, CA (1992).

[14] Bradshaw, P. and Huang, G.P. The Law of the Wall in Turbulent Flows. *Osborne Reynolds Anniversary Symposium*, Univ. Manchester (1995).

[15] Bush, W.B. and Fendell, F.E. Asymptotic Analysis of Turbulent Channel and Boundary Layer Flow. *J. Fluid Mech.*, **56**, 657–681 (1974).

[16] Cebecci, T. and Smith, A.M.O. *Analysis of Turbulent Boundary Layers*. Academic Press, New York (1974).

[17] Clauser, F.H. The turbulent boundary layer. *Adv. Appl. Mech.*, IV, 1-51 (1954).

[18] Clauser, F.H. Turbulent boundary layers in adverse pressure gradients. *J. Aeron. Sci.*, **21**, 91–108 (1954).

[19] Cole, J.D. and Kevorkian *Perturbation Methods in Applied Mathematics*. Springer, New York (1981).

[20] Coles, D.C. The Law of the Wake in Turbulent Boundary Layers. *J. Fluid Mech.*, **1**, 191–226 (1956).

[21] Coles, D.C. The Turbulent Boundary Layer in a Compressible Fluid, Rand Report R-403-PR (1962).

[22] Coles, D.C. in Kline, et al., 1968 AFOSR-IFP-Stanford Conf. Computation Turbulent Boundary Layers. Stanford U., Dept. Mech. Engr., Palo Alto, CA (1968).

[23] Erm, L.P. and Joubert, P.N. Low Reynolds number turbulent boundary layers *J. Fluid Mech.*, **230**, 1–44 (1991).

[24] Fernholz, H.H., Krause, E., Nockermann, M., and Schober, M. Comparative measurements in the canonical boundary layer at $Re_{\delta_2} < 6 \times 10^4$ on the wall of the German-Dutch windtunnel. *Phys.Fluids*, **7**, 1275–1281 (1995).

[25] Frisch, U. *Turbulence: The Legacy of A.N. Kolmogorov*. Cambridge University Press (1995).

[26] Gad-el-Hak, M. and Bandyopadhyay, P.R. Reynolds Number Effects in Wall-Bounded Flows. *Applied Mech. Rev.*, **47**, 307–3365 (1994).

[27] George, W.K. and Capp, S.C. A Theory for Natural Convection Boundary Layers Next to Heated Vertical Surfaces. *Int. J. Heat and Mass Transfer, 22*, 813-826 (1979).

[28] George, W.K. Self-Preservation of Turbulent Flows and Its Relation to Initial Conditions and Coherent Structures. in *Advances in Turbulence* (George and Arndt, eds.), 39–73, Hemisphere, New York (1989).

[29] George, W.K. and Hussein, H.J. Locally Axisymmetric Turbulence. *J. Fluid Mech.*, **233**, 1–23 (1991).

[30] George, W.K., Knecht, P. and Castillo, L. The Zero-Pressure Gradient Boundary Layer Revisited, *13th Symposium on Turbulence* (Reed, X.B., ed.), Rolla, MO (1992).

[31] George, W.K. and Castillo, L. Boundary Layers with Pressure Gradient: Another Look at the Equilibrium Boundary Layer. *Near Wall Turbulent Flows*, (So, R.M.C. et al. editors), 901–910, Elsevier, New York (1993).

[32] George, W.K. Some New Ideas for Similarity of Turbulent Shear Flows. *Proc. ICHMT Symposium on Turbulence, Heat and Mass Transfer, Lisbon*, Hanjalic and Pereira, eds., Elsevier, Amsterdam (1995).

[33] Hama, F.R. Boundary-Layer Characteristics for Smooth and Rough Surfaces. *Trans. Soc. Nav. Archt. Marine Engrs.*, **62**, 333–358 (1954).

[34] Hanjalic, K. and Launder B.E. Contribution towards a Reynolds stress closure for low-Reynolds number turbulence, J. Fluid Mech., xxxx (xxxx).

[35] Herring, H. and Norbury, J. Some experiments on equilibrium turbulent boundary layers in favourable pressure gradients. *J. Fluid Mech.*, **27**, 541–549 (1967).

[36] Hinze, J.O. *Turbulence*, McGraw Hill, New York (1975).

[37] von Karman, T. Mechanische Ähnlichkeit und Turbulenz. *Nachr. Ges. Wiss.*, Göttingen, pp 68 (1930).

[38] Karlsson, R. Eriksson, J, and Persson, J. An Experimental Study of a two-dimensional Plane Turbulent Wall Jet. Rept VU-S 93:B36, Vattenfall Utveckling, Alvekarleby, Sweden (1993).

[39] von Kempf, G. Weitere Reibungsergebnisse an ebenen glatten und rauhen Flächen. Hydrodynamische Probleme des Schiffsantriebs, vol. 1, 74-82 (1932).

[40] King, W.F. private communication (1993)

[41] Klewicki, J.C. Ph.D. dissertation. Michigan State U. (1989).

[42] Klewicki, J.C. and Falco, R.E. On accurately measuring statistics associated with small-scale structure in turbulent boundary layers using hot-wire probes. *J. Fluid Mech.*, **219**, 119–142 (1990).

[43] Klewicki, J.C. and Falco, R.E. Effects of Reynolds Number on Turbulent Boundary Layer Statistics. submitted for publication.

[44] Kline, S.J., Reynolds, W.C., Schraub, F.A. and Rundstatler, P.W. The Structure of Turbulent Boundary Layers. *J. Fluid Mech.*, **30**, 4, 741–773 (1967).

[45] Knecht, P. An Investigation of the Matched Layer in a Turbulent Boundary Layer with Zero Pressure Gradient, M.S. Thesis, Dept. Mech. & Aerosp. Eng., SUNY at Buffalo, Buffalo, NY (1990).

[46] Long, R.R. Presentation at Naval Hydrodynamics Meeting. Washington, D.C., June 1976.

[47] Long, R.R. and Chen, T.-C. Experimental Evidence for the Existence of the 'Mesolayer' in Turbulent Systems. *J. Fluid Mech.*, **105**, 19–59 (1981).

[48] Ludwig, H. and Tillmannn, W. *Ing.-Arch.*,**17**, 288-299 (1949); translated as: "Investigations of the wall shearing stress in turbulent boundary layers," NACA TM 1285 (1950).

[49] Monin, A.S. and Yaglom, A.M. *Statistical Fluid Mechanics*. MIT Press, Cambridge, MA (1971).

[50] Moses, H.L. The behavior of turbulent boundary layers in adverse pressure gradients. MIT Gas Turbine Lab. Rep. No. 73 (1964).

[51] Millikan, C.M. A critical discussion of turbulent flows in channels and circular tubes. *Proc. 5th Int. Congr. Appl. Mech.*, 386–392, Wiley, New York (1938).

[52] Murlis, J.T. and Bradshaw, P. *J. Fluid Mech.*, **122**, 13 (1982).

[53] Nagib, H. and Hites, M. High Reynolds Number Boundary-Layer Measurements in the NDF. AIAA 95-0786, 33rd Aero. Sci. Mtg., Reno, (1995).

[54] Newman, B.G. Some contributions to the study of the turbulent boundary layer near separation. Aust. Dept. Supply Rep. ACA-53 (1951).

[55] Panton, R. Scaling Turbulent Wall Layers. *J. Fluids Engr.*, **112**, 425–432 (year??).

[56] Perry, A. Turbulent boundary layers in decreasing adverse pressure gradients. *J. Fluid Mech.*, **26**, 481–506 (1966).

[57] Perry, A.E. and Abell, C.J. *J. Fluid Mech.*, **67**, 257 (1975).

[58] Prandtl, L. Zur Turbulenten Strömung in Rohren und längs Platten, *Ergeb. Aerod. Versuch Göttingen*, IV Lieferung, 18 (1932).

[59] Purtell, L.P., Klebanoff, P.S. and Buckley, F.T. Turbulent Boundary Layer at Low Reynolds Number. *Phys. Fluids*, **24**, 802–811 (1981).

[60] Reynolds, W.C. Computation of Turbulent Flows. *Ann. Rev. of Fluid Mech.*, **8**, 183–208 (1976)

[61] Schubauer, G.B. and Klebanoff, P. Investigation of Separation of the Turbulent Boundary Layer. NACA TN 2213 (1950), NACA TR 1030 (1951).

[62] Schubauer, G.B. and Spangenberg, W.G. Forced Mixing in boundary layers. *J. Fluid Mech.*, **8**, 10–32 (1960)

[63] Schultz-Grunow, F. New Frictional Resistance Law for Smooth Plates, NACA Tech. Mem. 986 (transl. from Neues Reibungswiderstandsgesetz fuer glatte Platten. *Luftfahrtforsch.*, 17, 8, 239–246, 1940), (1941).

[64] Simpson, R.L. Characteristics of turbulent boundary layers at low reynolds number with and without transpiration. *J. Fluid Mech.*, **42**, 769–802 (1970).

[65] Smith, R.W. *Effect of Reynolds Number on the Stucture of Turbulent Boundary Layers*. Ph.D. Diss., Princeton U. (1994).

[66] Smith, D.W. and Walker, J.H. Skin-friction measurements in incompressible flow. NACA Rept. R 26 (1959).

[67] Spalart, P.R. Direct simulation of a turbulent boundary layer up to $R_\theta = 1410$. *J. Fluid Mech.*, **187**, 61–98 (1988).

[68] Stanton, T.E. and Pannell, J.R. Similarity of motion in relation to the surface friction of fluids. *Phil. Trans. Roy. Soc. A*, **214**, p.199 (year??).

[69] Stratford, B.S. *J. Fluid Mech.*, **5**, 1 (1959).

[70] Stratford, B.S. *J. Fluid Mech.*, **5**, 17 (1959).

[71] Tennekes, H. and Lumley, J.L. *A First Course in Turbulence*. MIT Press, Cambridge, MA (1972).

[72] Tennekes, H. Outline of a Second-Order Theory of Turbulent Pipe Flow. *AIAA Jour.*, **6**, 1735–1740 (1968).

[73] Townsend, A.A. *The Structure of Turbulent Shear Flow*. Cambridge University Press, London (1956).

[74] Townsend, A.A. *J. Fluid Mech.*, **1**, 561 (1956).

[75] Van Dyke, M. *Perturbation Methods in Fluid Mechanics*. Parabolic Press, Stanford, CA (1964).

[76] Zagorola, M.V. Ph.D Dissertation, Princeton U. (1996).

[77] Zagorola, M.V. and Smits, A.J. Scaling of the mean velocity profile for turbulent pipe flow. Draft document (1996).

Bibliography